Fakultät für Medizin der Technischen Universität München

Hepatitis B virus core protein SUMOyaltion represents a novel functional switch for cccDNA generation

Samuel Hofmann

Vollständiger Abruck der von der Fakultät für Medizin der Technischen Universität München zur Erlangung des akademischen Grades eines

Doktors der Naturwissenschaften (Dr. rer. nat.)

genehmigten Dissertation.

Vorsitzender: Prof. Dr. Dirk H. Busch

Prüfende/-r der Dissertation:

1. Prof. Dr. Sabrina Schreiner

2. Prof. Dr. Percy A. Knolle

3. Prof. Dr. Maura Dandri-Petersen

Die Dissertation wurde am 07.06.2021 bei der Technischen Universität München eingereicht und durch die Fakultät für Medizin am 15.03.2022 angenommen.

Table of contents

Table of contents

Abbreviations

A	
A	Adenine
A	Alanine
AML1	Acute myeloid leukemia 1
APL	Acute promyelocytic leukemia
APS	Ammonium persulfate
ARD	Arginine rich domain
ATCC	American Type Culture Collection
ATM	Ataxia telangiectasia mutated
ATP	Adenosine triphosphate
ATR	Ataxia telangiectasis and Rad3-related
B	
BAF200	BRG1-associated factor 200
Bp	Basepair
BLM	Bloom syndrome protein
BSA	Bovine serum albumin
C	
C	Cytosine
C	Cysteine
cDNA	Complementary DNA
cccDNA	Covalentyl closed circular DNA
CDK	Cyclin dependent kinase
CHB	Chronic hepatitis B virus infection
ChIP	Chromatin immunoprecipitation
CHK2	Serins/threonine-protein kinase checkpoint kinase 2
CMV	Cytomegalovirus
co-IP	Co-immunoprecipitation
CpAM	Core protein allosteric modulator
CTD	C-terminal domain
CTL	Control
CRE	Cyclic AMP response element
CSK	Cytoskeleton
D	
d	Day
D	Aspartic acid
Dapi	4',6-Diamidine-2'-phenylindole dihydrochloride

Daxx	Death domain-associated protein6
ddH$_2$O	Double distilled water
DDR	DNA damage response
DHBV	Duck hepatitis B virus
DMEM	Dulbecco's modified eagle's medium
DMSO	Dimethyl sulfoxide
DNA	Desoxyribonucleic acid
DNase	Desoxyribonuclease
dNTP	Deoxynucleotide
dsDNA	Double stranded DNA
DR	Direct repeat
E	
E	Glutamic acid
E2F1	Transcription factor E2F1
E.coli	*Escherichia coli*
ECL	Enhanced chemiluminescence
ECMV	Encephalomyocarditis virus
EDTA	Ethylenediaminetetraacetic acid
eGFP	Enhanced green fluorescent protein
EGFR	Epidermal growth factor receptor
ELISA	Enzyme linked immunosorbent assay
Enh	Enhancer
F	
F	Phenylalanine
FCS	Fetal calf serum
FEN1	Flap endonuclease 1
Fwd	Forward
G	
G	Guanine
G	Glycine
g	Gravitational constant
G418	Geneticin 418
GA	Ginkgolic acid
GAPD	Glyceraldehyde-3-phosphate dehydrogenase
GE	Genomic equivalent
GFP	Green fluorescent protein
H	
h	Hour

H	Histidine
HA	Haemagglutinin
HAdV	Human adenovirus
HBV	Hepatitis B virus
HBVdb	Hepatitis B virus database
HBeAg	Hepatitis B virus e antigen
HBsAg	Hepatitis B virus surface antigen
HBx	Hepatitis B virus X protein
HCC	Hepatocellular carcinoma
HEPES	(4-(2-hydroxyethyl)-1-piperazineethanesulfonic acid
HF	High fidelity
HIPK2	Homeodomain-interacting protein kinase 2
His	Histidine
HIV-1	Human immunodeficiency virus type 1
HRP	Horseradish peroxidase
HSP	Heatshock protein
Hus1	Checkpoint protein Hus1
HSV-1	Herpes simplex virus 1
I	
I	Isoleucine
ICP0	HHV infected cell polypeptide 0
IF	Immunofluorescence
IFITM1	Interferon-induced transmembrane protein 1
IFN	Interferon
IP	Immunoprecipitation
K	
K	Lysine
kb	Kilobases
kDa	Kilodalton
L	
l	Liter
L	Leucine
L	Large HBsAg
LB	Lysogeny broth
M	
M	Molar
M	Methionine
M	Middle HBsAg

mAb	Monoclonal antibody
mg	Milligramm
µg	Microgramm
MHC	Major histocompatibility complex
min	Minute
ml	Milliliter
µl	Microliter
mm	Millimeter
µm	Micrometer
mM	Millimolar
µM	Micromolar
MNase	Micrococcal nuclease
MOI	Multiplicity of infection
MOPS	3-(-N-Morpholino)propanesulfonic acid
M-PBS	PBS containing skim milk powder
M-PBS-T	PBS-T containing skim milk powder
mRNA	Messenger ribonucleic acid
MRN	Mre11, Rad50, Nbs1 complex
MTOC	Microtubuli organizing center
N	
N	Asparagine
NAbs	Neutralizing antibodies
NAGE	Native agarose gel electrophoresis
NC	Nitrocellulose
ND10	Nuclear domain 10
Nedd4	Neural precursor cell expressed developmentally downregulated protein 4
NES	Nuclear export signal
ng	Nanogramm
NIRF	Np95/ICBP90-like RING finger protein
NLS	Nuclear localization signal
nm	Nanometer
NP40	Nonidet-P40
NPC	Nuclear pore complex
NTA	Nitrilotriacetic acid
NTCP	Sodium taurocholate co-transporting polypeptide
NTD	N-terminal domain
Nup	Nucleoporin
O	

OD$_{600}$	Optical density at 600nm
ORF	Open reading frame
P	
P	Proline
P	HBV polymerase
pAb	Polyclonal antibody
PAGE	Polyacrylamide gel electrophoresis
PBS	Phosphate buffered saline
PBS-T	Phosphate buffered saline, 0.1% (V/V) Tween-20
PCNA	Proliferating cell nuclear antigen
PCR	Polymerase chain reaction
PDB	Protein database
PDP2	Pyruvate dehydrogenase phosphatase catalytic subunit 2
PEG	Polyethylene glycol
PF	Protein free
PFA	Paraformaldehyde
PEI	Polyethylenimine
PF	Protein free
pgRNA	Pregenomic RNA
p.i.	Post infection
Pin1	Peptidyl-prolyl cis-trans isomerase NIMA interacting 1
PK	Protein kinase
PKC	Protein kinase C
PLK1	Polo-like kinase
PML	Promyelocytic leukemia
PML-NB	PML nuclear body
PMSF	Phenylmethylsulfonyl fluoride
POD	PML oncogenic domain
Pol	Polymerase
PP1	Serine/threonine protein phosphatase
PP2A	Serine/threonine protein phosphatase 2 alpha subunit
PRMT5	Protein arginine N-methyltransferase 5
PRNP	Major prion protein P
p.t.	Post transfection
PTM	Posttranslational modification
PTPN3	Tyrosine protein phosphatase non-receptor type 3
PU.1	Transcription factor PU.1
PVDF	Polyvinylidene fluoride

Q	
Q	Glutamine
qPCR	Quantitative PCR
R	
R	Arginine
RARA	Retinoic acid receptor α
RBCC	RING, B box, coiled coil motif
rcDNA	Relaxed circular DNA
Rev	Reverse
RFC	Replication factor C complex
RNA	Ribonucleic acid
RNase	Ribonuclease
RING	Really interesting new gene
RIPA	Radio-immunoprecipitation
rpm	Rounds per minute
RT	Room temperature Reverse transcriptase
S	
s	Second
S	Serine
S	Small HBsAg
S100A10	S100 calcium binding protein A10
SAE	SUMO activating enzyme
SamHD1	Sterila alpha miotif and histidine-aspartic domain containing protein 1
SCM	SUMO conjugation motif
SDS	Sodium dodecylsulfate
SENP	SUMO specific protease
shRNA	Short hairpin RNA
SIM	SUMO interaction motif
Smc	Structural maintenance of chromosomes
Sp100	Speckled protein 100
SRPK	Serine/arginine rich protein specific kinase
SRSF10	Serine/arginine rich splicing factor 10
SSC	Saline sodium citrate
SUMO	Small ubiquitin related modifier
Su	SUMO
SUZ12	Suppressor of zeste 12 protein homolog
T	

T	Thymidine
T	Threonine
T	Tetrahedron
TBE	Tris/boric acid/EDTA
TBS-BG	Tris-buffered saline-BSA, glycine buffer
TDP	Tyrosyl-DNA phosphodiesterase
TEMED	Tetramethylethylenediamine
TERT	Telomerase reverse transcriptase
TFB-I	Transformation buffer I
TFB-II	Transformation buffer II
TGS	Tris/Glycine/SDS buffer
Tip60	60kDa Tat-interactive protein
Top	Topoisomerase
TOPBP1	Toposiomerase binding protein 1
TP	Terminal protein
TRF1	Telomeric repeat binding factor 1
TRIM	Tripartite motif
Tris	Tris(hydroxymethyl)aminomethane
U	
U	Unit
U	Uracil
Uba2	SUMO activating enzyme subunit 2
Ubc9	SUMO-conjugating enzyme ubiquitin carrier protein 9
V	
V	Valine
V	Volume
VA-RNA	Virus associated RNA
VSV	Vesicular stomatitis virus
VZV	Varizella zoster virus
W	
w	Weigth
W	Tryptophane
WRN	Werner syndrome ATP-dependent helicase
Wt	Wild type
Y	
Y	Tyrosine
Z	
ZNF198	Zinc finger MYM-type protein 2

Abstract

Hepatitis B virus (HBV) infection is still one of the major threats to global health. Over 257 million people worldwide are chronically infected, despite the broad availability of an effective prophylactic vaccine. The key to a curative treatment of chronic HBV is the nuclear episomal persistence reservoir of the virus, the covalently closed circular DNA (cccDNA), which is not targeted by current therapeutic approaches. The cccDNA is generated from a protein- and RNA-linked incomplete precursor, the relaxed circular DNA (rcDNA), in a process involving several proteins of the host cell DNA damage response (DDR). The molecular pathway, however, is not yet fully understood. During HBV life cycle, the HBV core protein takes over a variety of functions, including nuclear import of the rcDNA and promotion of cccDNA maintenance as well as transcriptional activity. The multitude of HBV core protein activities are tightly regulated by posttranslational modifications (PTMs), including phosphorylation and acetylation.

Here, we report SUMO (small ubiquitin related modifier) modification as novel PTM acting as functional switch in HBV core protein regulation. SUMO PTM of HBV core protein monomers within mature HBV capsids induces disruption of HBV capsids in the nuclear basket of the nuclear pore complex as shown by *in silico* and *in vitro* SUMOylation studies. This indicates HBV core SUMOylation as the missing link in the nuclear entry process during HBV infection. Using SUMOylation deficient mutants of HBV core protein, we could prove that SUMO2 PTM of this viral protein mediates nuclear localization. More precisely, it recruits HBV core to promyelocytic leukemia nuclear bodies (PML-NBs), which are hotspots of the host cell DDR and regulated by SUMOylation. HBV core association to PML-NBs is especially based on PML isoforms I and II. PML-NB association regulates cccDNA formation from its rcDNA precursor in a process which is critically dependent on PML-II and -VI.

In proof-of-concept experiments using the *pan*-SUMOylation inhibitor ginkgolic acid we could show that inhibition of the host cellular SUMOylation machinery impairs efficient HBV replication on several levels, including nuclear entry as well as PML association of HBV core, and efficient cccDNA formation.

Our work highlights the novel role of PML-NBs and SUMO PTM in the regulation of HBV nuclear entry as well as rc- to cccDNA conversion and provides promising new targets for inhibiting the formation of the HBV persistence reservoir.

Zusammenfassung

Infektionen mit Hepatitis B Virus (HBV) stellen eine wesentliche Gefahr für die Weltgesundheit dar. Trotz der breiten Verfügbarkeit eines effektiven präventiven Impfstoffes leiden weltweit über 257 Millionen Menschen an einer chronischen HBV Infektion. Die cccDNA (*covalently closed circular DNA*) liegt episomal im Kern infizierter Zellen vor und stellt das Persistenzreservoir des Virus dar. Diese ist der Schlüssel für eine vollständige Heilung, wird jedoch von derzeitigen Therapieansätzen nicht direkt adressiert. Die cccDNA wird von mehreren DDR (*DNA damage response*) Proteinen der Wirtszelle aus der nicht kompletten, Protein- und RNA-gebundenen rcDNA (*relaxed circular DNA*) hergestellt. Der genaue Prozess ist jedoch noch nicht vollständig erforscht und verstanden. Das HBV Core Protein übernimmt eine Vielzahl an Aufgaben während der HBV Infektion und ist am Import der rcDNA in den Kern beteiligt. Zudem fördert es die Stabilität und transkriptionelle Aktivität der cccDNA. Die Vielfalt der Funktionen, die das HBV Core Protein annimmt, ist strikt über posttranslationale Modifikationen (PTM) wie Phosphorylierung und Acetylierung reguliert.

In dieser Arbeit wird die Modifikation mit SUMO (*small ubiquitin related modifier*) als neue PTM beschrieben, die einen funktionalen Schalter der HBV Core Protein Aufgaben darstellt. Durch *in silico* und *in vitro* SUMOylierungs-Experimente konnte gezeigt werden, dass SUMO PTM von HBV Core Protein Monomeren innerhalb des maturierten Capsids die Auflösung des HBV Capsids im nukleären Korb des Kernporenkomplexes induziert. Die Modifikation des HBV Core Proteins mit SUMO stellt somit das fehlende Bindeglied im Kernimport während der HBV Infektion dar. Durch Mutanten, die nicht mehr SUMO modifiziert werden können, konnten wir zeigen, dass SUMO2 PTM des viralen Proteins nicht nur für den Import in den Kern, sondern auch für die Assoziation mit PML-NBs (*promyelocytic leukemia nuclear bodies*) verantwortlich ist. PML-NBs sind Hotspots für die DDR der Wirtszelle und werden selbst über SUMOylierung reguliert. HBV Core interagiert hierbei insbesondere mit den PML Isoformen I und II. Die Assoziation von HBV Core zu PML-NBs reguliert weiterhin die Bildung der cccDNA aus der rcDNA, wobei PML-II und -VI eine kritische Rolle spielen.

Globale Inhibierung der zellulären SUMOylierung durch den *pan*-SUMO Inhibitor Ginkgolsäure beeinträchtigte eine effiziente HBV Replikation auf mehreren Ebenen, einschließlich des nukleären Imports und der PML Assoziation von HBV Core und der cccDNA Bildung, was als Konzeptnachweis diente.

Zusammenfassend hebt unsere Arbeit die Rolle von PML-NBs und SUMOylierung für den Kernimport und die Konversion von rc- zu cccDNA während der HBV Replikation hervor und bietet neue Ansätze zur Inhibierung der Bildung des HBV Persistenzreservoirs.

1. Introduction

1.1 Hepatitis B virus

1.1.1 Classificaiton, pathogenesis and epidemiology

Hepatitis B virus (HBV) is the prototypic member of the *hepadnaviridae* family of small hepatotropic enveloped DNA viruses (*1, 2*). Traces of HBV infection were found by discovery of HBV surface antigens (HBsAg) in aboriginal Australians in 1967, followed by the first description of the infectious HBV virus particle, which was named "Dane particle" after its discoverer, three years later (*3, 4*). The *hepadnaviridae* group is characterized by a narrow organ- and host tropism, as well as a related organization of their genomic DNA (*5-7*). The family of *hepadnaviridae* is further subgrouped into two genera, *orthohepadnaviriade*, infecting mammals, and *avihepadnaviridae*, which infect birds (*8, 9*). Prominent examples for mammalian *orthohepadnaviridae* are the human hepatitis B virus HBV, the woodchuck hepatitis virus and the woolly monkey hepatitis B virus (*1, 2, 10, 11*). An example for *avihepadnaviridae* is the duck hepatitis B virus (DHBV) (*12*). *Hepadnaviridae* replicate their DNA genome via an intermediate RNA form, which is why they belong to the group of para-retroviruses (*13*).

Human HBV comprises ten different genotypes A-J, which differ in at least 8% of their complete genomic sequence. Each genotype can be further grouped into the subtypes ayw, ayr, adw and adr, yielding in a total of 40 subgenotypes (*14*). The divergent genotypes are differentially distributed throughout the world (*14*). Genotype A is preferentially found in Northwest Europe, North America, and Africa. Genotype B and C are dominant in East Asia and Far East countries, whereas genotype D is spread worldwide (*15, 16*). Genotype E is primarily found in West Africa, F in Central and South America and genotype G is widespread in Turkey, France, Canada, Vietnam, Germany, and America. The most recently discovered genotype J is solely found in Japan (*15, 17, 18*).

An effective prophylactive vaccine was first introduced in 1982 and since then lead to a strong global decline in HBV infections. However, still 257 million people worldwide suffer from chronic HBV (CHB) infection. CHB is characterized by sustained presence of HBsAg in the blood of infected patients for over 6 months (*19-27*). In total, approximately 2 billion individuals were subject to HBV infection. CHB leads to an increased risk for the development of liver cirrhosis, fibrosis, and hepatocellular carcinoma (HCC), one of the leading causes of cancer related death (*28-31*). As a consequence, around 887000 people die annually due to

CHB related diseases (*21*). HBV infection *per se* is not cytopathic for the infected cell populations, however, liver damage is inflicted by the host immune reaction (*2, 32-37*).

The worldwide prevalence is highly variable. The highest prevalence is observed in the Western Pacific region and the African region, with 6.2% and 6.1% of the population carrying a chronic HBV infection. CHB prevalence in the Eastern Mediterranean region is 3.3%, followed by 2.0% in South East Asia and 1.6% in the European region (*21*). HBV is primarily transmitted from mother to child during childbirth, by exposure to infected blood or body fluids or by sexual contact. Additionally, HBV particles can remain intact and infectious for several weeks on moist surfaces (*38-40*). Two thirds of infected adults show asymptomatic courses of infection. One third develops symptomatic acute infection and between 0.5-1% develop fulminant hepatitis, leading to liver failure (*20, 41, 42*). Only 5-10% of HBV infected adults transmit to CHB, whereas this proportion is significantly higher in children of five years with 30-50% and even more severe in infants, where 90% of infections lead to CHB (*38, 43, 44*). The chronically HBV infected population is not only at risk of developing severe disease progressions but also suffers from personal pressure due to community stigma and discrimination caused by their, at the moment incurable, disease (*45*).

Currently approved therapeutic strategies for the treatment of HBV infections are only able to limit HBV replication, block sustained HBV infection or relieve the symptoms, but fail at completely curing the patient. PEGylated interferon (IFN) α is used to reconstitute the exhausted antiviral immune response of the host. This treatment is often supplemented by additional therapy using nucleos(t)ide analogues, including entecavir, telbivudine, lamivudine, adefovir, and tenofovir (*46-48*). Novel treatment approaches include the interference with HBV nucleocapsid assembly using core protein allosteric modulators (CpAMs). These compounds either prevent or accelerate nucleocapsid assembly, leading to abberant capsid structures (*48, 49*). Further strategies aim at inhibiting entry of HBV into the host hepatocyte (*50-54*). However, none of the approaches outlined above is able to directly affect the covalently closed circular DNA (cccDNA), which is the persistence reservoir of the virus and considered as the "holy grail" for a functional cure (*48*).

1.1.2 Virion structure and genome organization

The mature HBV virion, or "Dane particle", consists of a lipid bilayer, which is hijacked from the infected host cell, decorated with the large (L), middle (M) and small (S) HBV surface antigens (HBsAg). The complete virion has a size of approximately 42nm (*7, 42, 55-57*). The envelope harbors the icosahedral nucleocapsid with a diameter of 32-36nm composed of 120 (T=4 symmetry) or, in rare cases, 90 (T=3 symmetry) HBV core protein dimers (*58, 59*). Inside

the HBV nucleocapsid, the small partially double stranded and 3.2kb long relaxed circular DNA (rcDNA) genome is present (7, 42). A schematic representation of the HBV virion, as well as electron microscopy pictures of Dane particles are shown in figure 1.
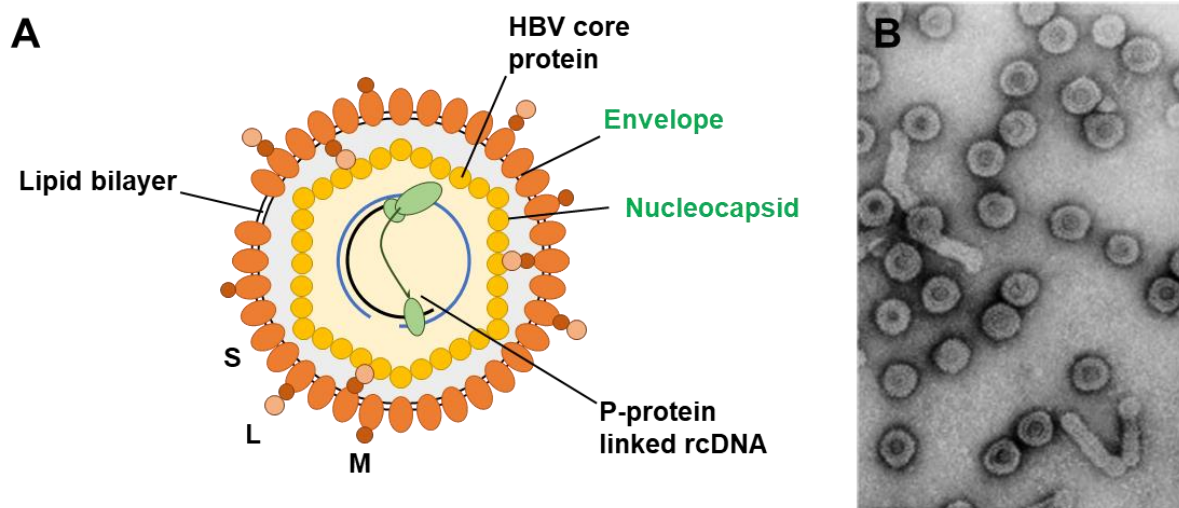
Figure 1: Structure of HBV Dane particles. A Schematic representation of the HBV virion. S, M and L HBsAg are embedded in a lipid bilayer generating the envelope. The nucleocapsid is composed of 240 HBV core proteins and harbors the incomplete polymerase (P) and RNA linked rcDNA (adapted from (7, 60)). **B** Cryo electron micrographs of HBV particles (61).

The rcDNA (-) strand is harboring overlength terminal redundancies and its 5' end is covalently bound to the TP domain of the HBV polymerase by a tyrosyl-DNA phosphodiester bond. The (+) strand is incomplete with a gap of several hundreds of nucleotides and a capped RNA primer at its 5' end (1, 62, 63). A schematic representation of the HBV rcDNA showing the arrangement of the open reading frames (ORFs), expressed mRNAs, and enhancer regions is shown in figure 2. The HBV genome is compactly organized with four overlapping ORFs and every nucleotide encodes at least one protein (5, 7, 42, 64-67). In addition to the ORFs, the rcDNA contains several regulatory elements, including the direct repeats (DR) 1 and 2, as well as the transcriptional enhancer regions I and II (EnhI and EnhII) (7, 65, 68-73). Transcription of the HBV ORFs occurs from the cccDNA which is generated from the rcDNA in a multi-step process (see chapter 1.1.4) and leads to the expression of four different mRNAs (60, 74-77). The longest mRNA is the 3.5kb pregenomic RNA (pgRNA), which encodes the secreted HBeAg, the HBV core protein and the HBV polymerase. Furthermore, two 2.4kb and 2.1kb mRNAs, expressing S, M and L HBsAg, and a 0.7kb transcript, leading to HBx expression, are transcribed (1, 5, 7, 63-67, 78). The molecular functions of the HBV core protein during the HBV replication cycle will be outlined in detail in chapters 1.1.5.1, 1.1.5.2 and 1.1.5.3. HBeAg is secreted after extensive posttranslational processing and is proposed to have immune-modulatory functions (78-83). The structural S, M and L HBsAg share the same carboxyterminal domain S, while M additionally contains PreS2 and L contains PreS1 and

PreS2 in addition to S (*56, 57*). S, M and L HBsAg are translated at the rough endoplasmic reticulum and undergo the host cell secretory pathway to either envelope rcDNA containing or empty nucleocapsids. Additionally, they are secreted as empty subviral particles (*7, 13, 84-90*). The HBV polymerase is essential to viral replication and consists of three functional domains. These are the terminal protein (TP), the ribonuclease H (RNase H) domain and the reverse transcriptase (RT) domain, which are separated by a flexible spacer (*91, 92*). The small multifunctional non-structural HBx protein promotes permissive cccDNA transcription and counteracts repressive factors of the host cell (*93-96*).
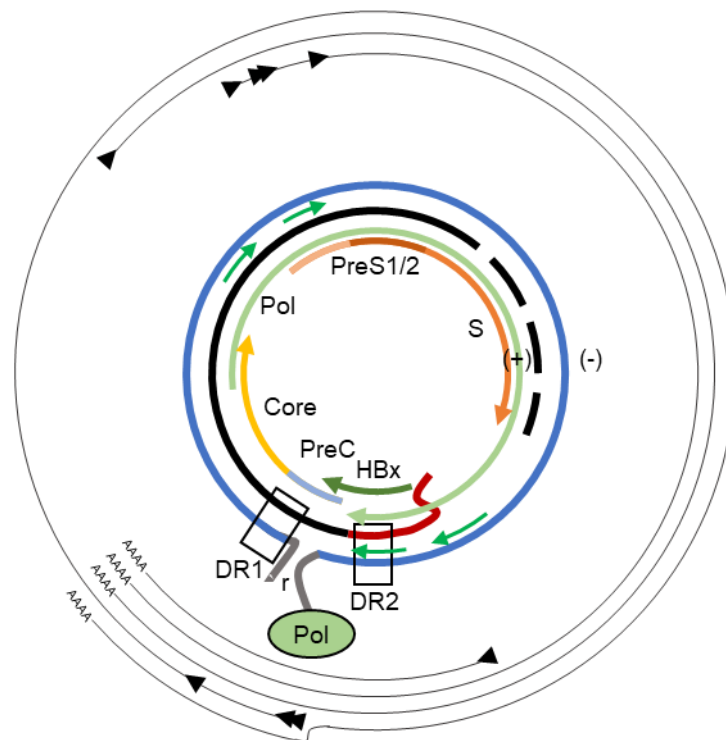
Figure 2: Overview of HBV rcDNA organization. The outer lines represent viral transcripts. Transcriptional start sites are denoted as arrowheads. The polymerase (Pol) linked (-) strand with terminal redundancies (r) is shown in blue, the RNA bound incomplete (+) strand in black. Small green arrows show promoter sequences. Direct repeats DR1 and DR2 are indicated as black boxes. Protein coding overlapping ORFs are shown in the center. Note that the template for transcription is the cccDNA. Additional details are given in the text. PreC: Pre-core (adapted from (*7, 60*)).

1.1.3 Replication cycle

The primary sites of HBV infection are differentiated hepatocytes. Viral attachment is initiated by low-affinity interactions of Dane particles with heparan sulfate proteoglycans (HSPG) on the host cell (see figure 3 [1]). This is followed by binding of the myristoylated L HBsAg PreS1 domain to the cognate receptor, the sodium taurocholate co-transporting polypeptide (NTCP) and the co-receptor epidermal growth factor receptor (EGFR) (see figure 3 [2]) (*97-102*). The virus is taken up by receptor mediated endocytosis (see figure 3 [3]). To release the rcDNA containing mature HBV capsid, the endosomal membrane fuses with the viral envelope (see figure 3 [4, 5]) (*102*). The C-terminal domain of the HBV core protein, which contains the

nuclear localization signal (NLS) necessary for nuclear import, is exposed from the interior of the nucleocapsid. Only then, the capsid is transported to the nuclear pore complex (see figure 3 [6]), where it disassembles by a not yet identified trigger and releases the rcDNA into the nucleus (see figure 3 [7]) (*103-113*). The rcDNA is subsequently repaired by enzymes of the host cell DNA damage response (DDR) to yield in the cccDNA, which is subsequently chromatinized by histones and non-histone proteins (see figure 3 [8, 9]) (*63, 71, 74, 75, 95, 107, 114-120*). The process of cccDNA generation will be described in detail in chapter 1.1.4. The cccDNA remains as an episome in the host cell nucleus and serves as template for viral mRNA transcription. This leads to expression of the subgenomic mRNAs and the pgRNA, mediated by the host RNA polymerase II (see figure 3 [10]). Viral mRNAs are exported from the nucleus and translated (see figure 3 [11, 12]) (*2, 7, 121-124*). The pgRNA is transcribed into HBV core protein, polymerase, and the HBeAg, which is secreted after extensive posttranslational cleavage (see figure 3 [12]) (*65, 78-83, 125-128*). The viral polymerase binds to an ε-sequence of pgRNA. The polymerase-pgRNA complex is subsequently recognized and packaged by HBV core protein and nucleocapsids assemble around pgRNA and polymerase (see figure 3 [13]) (*6, 76, 123, 129*). The nucleocapsid then actively participates in reverse transcription of pgRNA and provides a closed environment for rcDNA synthesis (*130, 131*). Completion of rcDNA synthesis within newly formed capsids induces capsid maturation. Subequently, the matured capsids are enveloped by HBsAg at the endoplasmic reticulum and secreted via multivesicular bodies (see figure 3 [14a, 15]). Besides rcDNA containing mature capsids, also empty nucleocapsids are enveloped and secreted, as well as empty subviral particles consisting of HBsAg and host cell lipid membranes (see figure 3 [15]) (*7, 13, 84-90, 106*). Alternatively, mature rcDNA containing capsids can be transported back to the nucleus to establish a stable pool of nuclear cccDNA, ensuring HBV persistence (see figure 3 [14b]) (*75, 132, 133*). However, the biological relevance of this nuclear re-shuttling of mature capsids during HBV infection is still under debate (*134*).

RcDNA is generated from the pgRNA in a strictly regulated reverse transcription mechanism, including three template switches (*6, 7*). Reverse transcription is initiated by binding of the polymerase to the 5' ε-sequence of pgRNA. The TP domain serves as protein primer and is covalently bound to the nascent (-) strand DNA by a tyrosyl-DNA-phosphodiester bond (*7, 42, 65, 76, 132, 135-139*). After synthesis of a small amount of nucleotides, the (-) strand together with the polymerase is transferred to DR1 at the 3' end of pgRNA (first template switch), followed by complete (-) strand synthesis and degradation of the pgRNA by the RNase H activity of the viral polymerase (*7, 42, 65, 76, 140, 141*). A small 5' capped proportion

of the pgRNA, which includes DR1, remains after RNase H digestion and serves as RNA primer for (+) strand synthesis (*7, 140, 142-146*).
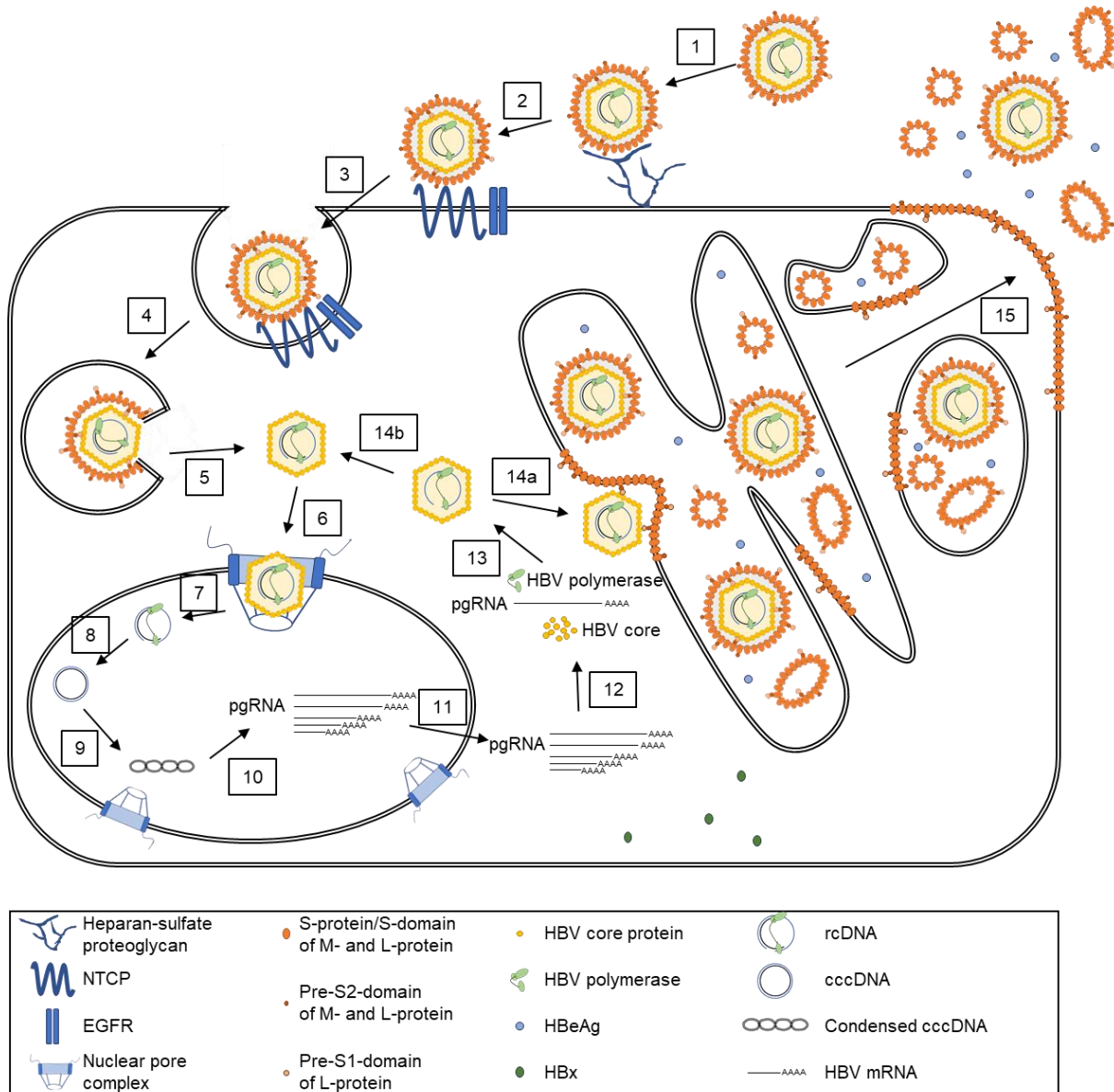
Figure 3: HBV replication cycle. Details are given in the text (adapted from (*147*))

The RNA primer anneals to DR2 at the 5' end of the (-) strand (second template switch) to start (+) strand synthesis (*7, 70, 140, 142, 144*). In the progression of (+) strand synthesis, the (-) strand circularizes to enable the third template switch, leading to the generation of the rcDNA. The (+) strand is not synthesized completely but lacks a region of hundreds of nucleotides, which is probably due to the limited supply of desoxynucleotide-triphosphates (dNTPs) within the enclosed mature capsid (*2, 6, 7, 70, 143*). If the second template switch fails, a ds linear HBV DNA is formed, which can be converted into a cccDNA-like molecule or is integrated into the host DNA. It can be template for viral protein expression, but does not support formation of infectious virions (*62, 148-150*).

1.1.4 Generation of cccDNA as the key to viral persistence

For cccDNA synthesis, rcDNA containing mature HBV capsids, which either occur from infection or *de novo* capsid formation, are transported to the nucleus. Therefore, the HBV core protein in the nucleocapsid needs to undergo a series of until now poorly characterized changes, which lead to an exposition of its NLS for binding of importins and release of the rcDNA into the nucleus (*105, 107, 108, 110, 111, 151-155*). The rcDNA, which contains single strand gaps, terminal redundancies, as well as RNA- and protein adducts, is probably recognized and repaired by proteins of the host cell DDR (*7, 62, 107, 156-159*). The rcDNA undergoes several enzymatic reactions as shown in figure 4. First, removal of the viral polymerase, which is covalently bound to the 5' end of the (-) strand (*160, 161*), and of the RNA primer on the (+) strand, is necessary (*114*). This is followed by removal of the terminal redundancies of the (-) strand (*162*). Next, repair of the incomplete (+) strand (*163-165*) and ligation of the (-) and (+) strand are needed to form complete cccDNA (*166*).

For the removal of the viral polymerase in the first step, two enzymes are proposed to be involved. Tyrosyl-DNA phosphodiesterase 2 (TDP2), which removes 5' bound topoisomerase 2 (Top2) during DNA replication, was shown to be able to cleave polymerases from rcDNA in *in vitro* studies using DHBV and HBV rcDNA (*160, 161, 167, 168*). Short-hairpin RNA (shRNA) mediated depletion of TDP2 delays cccDNA formation (*160*). The exact impact and the question if TDP2 is crucial for cccDNA formation, however, are still under debate, as a complete knockout of TDP2 during infection in HepG2-NTCP cells does not affect cccDNA formation (*161*). Another possible candidate for the formation of protein free (PF) rcDNA is the flap endonuclease 1 (FEN1), which removes 5'-flap structures of Okazaki fragments during cellular DNA replication (*74, 105, 157, 162, 169*). It was shown that FEN1 does not only remove the polymerase from the rcDNA, but also the terminal redundancies in the (-) strand (*162*). The enzyme which is envolved in the removal of the RNA primer from the (+) strand is, until now, not identified (*114*). The host polymerases necessary for filling up the gap in the (+) strand of the rcDNA are different in the first round of cccDNA generation during infection and the intracellular amplification pathway. For generation of the first cccDNA molecules from incoming virions during HBV infection in HepG2-NTCP cells, polymerases κ and λ are necessary (*163*), whereas polymerases α, δ and ε play a role in the intracellular amplification pathway in the HBV producing HepAD38 cell line (*164*). Further enzymes involved in cccDNA generation are Top1 and Top2, which are probably necessary during circularization of the cccDNA to reduce torsion. They are involved in *de novo* synthesis during infection and in the intracellular amplification pathway (*165*). Finally, DNA ligases 1 and 2 are proposed to ligate the strands to yield in cccDNA (*166*). SamHD1 was thought to have a general antiviral activity

by depletion of the cellular dNTP pool. It is, however, also supposed to play a role during the early steps of cccDNA formation, maybe by acting as a scaffolding protein (*170*).
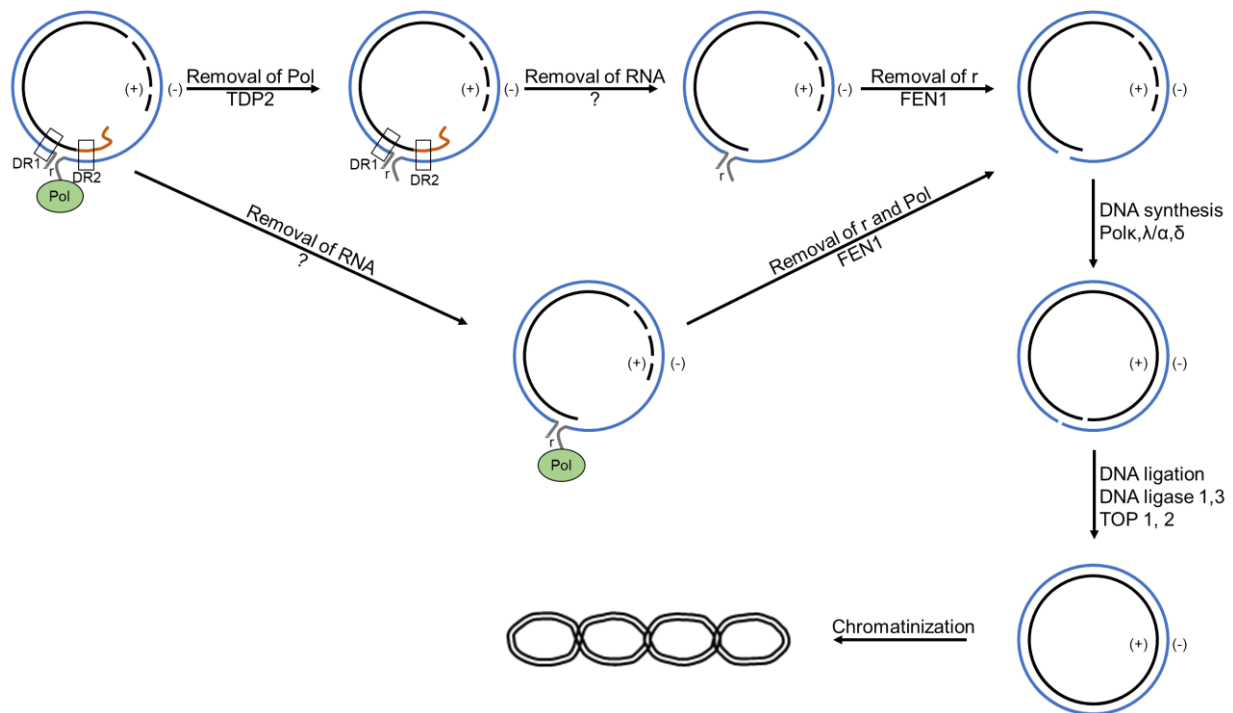
Figure 4: Mechanism of cccDNA formation from rcDNA. cccDNA generation includes removal of the viral polymerase, the terminal redundancies and the RNA primer, completion of the (+) strand by DNA synthesis, and ligation of the strands. Further details are given in the text (adapted from (*63*)).

More recently, using a synthetic rcDNA and cell extracts depleted for specific DDR factors, Wei and Ploss could identify five core factors being both necessary and sufficient to promote cccDNA formation in a cell free system. These factors included and confirmed the already above mentioned polymerase δ, FEN1, and DNA ligase 1 and added the proliferating cell nuclear antigen (PCNA) as well as the replication factor C complex (RFC) (*171*). The cccDNA in the host cell nucleus is strongly chromatinized and contact with histone and non-histone proteins of the virus and the host regulates viral transcription (*71, 115, 120, 158*). Chromatinization occurs already at the rcDNA and during the repair progress (*117, 120*). The organization and interplay of the host DDR factors involved in cccDNA formation still remains elusive. However, recent studies suggest the involvement of the ataxia telangiectasia and Rad3-related (ATR) pathway in regulation of cccDNA formation (*172*).

1.1.5 HBV core protein

1.1.5.1 Role throughout the viral life cycle

The HBV core protein is a 21kDa protein with 183 to 185 amino acids, depending on the HBV genotype (*173-181*). It consists of a N-terminal domain (NTD) (aa 1-140) being necessary and sufficient for formation of HBV capsids, a flexible linker domain (141-149) and a C-terminal,

arginine rich domain (CTD/ARD) with several features (see figure 5 C). Besides its role in formation of viral capsids, the HBV core protein has a wide plethora of functions in the HBV replication cycle, including subcellular trafficking, release of the rcDNA genome into the nucleus, RNA metabolism, capsid assembly, and reverse transcription (*108, 110, 173, 176, 178, 180-184*). The NTD is, besides capsid formation, involved in packaging of the pgRNA, followed by rcDNA synthesis by reverse transcription, virion secretion, but also cccDNA formation (*130, 154, 155, 182, 185-188*). The CTD is highly phosphorylated at several serine and one threonine residue and takes part in the regulation of capsid assembly, packaging of pgRNA and reverse transcription to generate rcDNA, as well as nuclear import (*103, 113, 175, 182-185, 189-194*). Besides the four arginine-rich stretches (ARDI-IV), the CTD also contains a NLS, as well as a nuclear export signal (NES) (*195, 196*).
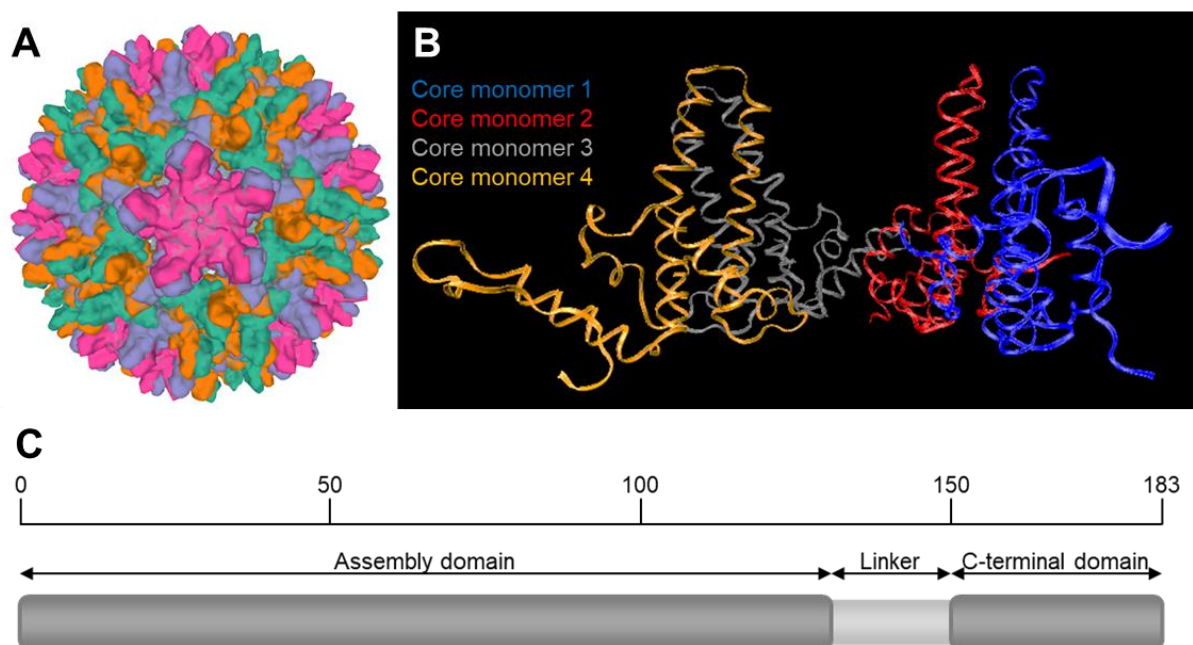
Figure 5: The HBV core protein. A, B Representation of the HBV capsid structure **A** and structure of a dimer of HBV core protein dimers as the asymmetric unit of T=4 capsids **B** based on (*197*). **C** Schematic representation of the HBV core protein amino acid sequence. HBV core protein consists of an N-terminal assembly domain (amino acids 1-140), a flexible linker (amino acids 141-149) and a C-terminal, arginine rich domain (150-183).

HBV capsid assembly

HBV core protein consists of five α-helices. Helices 1, 2, and 5 build up the hydrophobic core, while helices 3 and 4 protrude from the hydrophobic core (see figure 5 B) (*198-200*). The HBV core protein self-assembles into HBV capsids with a diameter of 32-36nm, which have pores of 1.2-2.5nm (see figure 5 A) (*58, 59, 198, 201-203*). Usually, capsids consisting of 120 HBV core protein dimers with a T=4 symmetry are formed. However, also formation of smaller capsids containing 90 core protein dimers and a T=3 symmetry is observed (*58, 59*). Assembly proceeds via different intermediates. In a first step, two HBV core protein monomers form a

dimeric structure by reciprocal interactions. These require helices 3 and 4, which form the characteristic spike (see figure 5 B). Trimers of dimers are then formed by interactions within helix 5 and the downstream proline-rich loop (see figure 5 B) (*198, 204, 205*). Finally, capsids assemble from intermediate semiclosed capsids, mostly consisting of 40 dimers (*206*).

Nucleic acid association

The CTD has a total of 16 arginine residues clustered in four ARDs I-IV (*173, 207*). Due to its highly basic nature and its structural flexibility, the CTD is suggested to function as a nucleic acid chaperone (*182, 197, 208, 209*). Nucleic acid chaperones are characterized by their ability to bind and catalyze structural rearrangements within nucleic acids without the need of ATP hydrolysis (*210*). Indeed, it was shown that the CTD regulates the reverse transcription of pgRNA into rcDNA by pgRNA binding, using the first two arginines of ARDI and by supporting the template switch during rcDNA formation using ARDII-IV (*175, 182, 207, 209, 211-213*). Additionally, the assembled HBV capsid provides a defined and closed environment for reverse transcription (*130, 131*).

A small proportion of the HBV core protein is associated with the nuclear cccDNA during infection, mediated by the histone-tail like CTD and especially by ARDIII and IV (*71, 117, 158, 207, 214, 215*). HBV core regulates cccDNA chromatin organization and alters the nucleosome spacings (*117, 214*). It is preferentially associated with the CpG island 2 plus 3 and enhances pre-core promoter activity by increasing the binding of NF-κB upstream of EnhII (*215, 216*).

Nuclear entry and localization of HBV core

For nuclear entry, the HBV core protein CTD is crucial, as it harbors the NLS, which is recognized by cellular importin α and β proteins (*109, 195, 217, 218*). Therefore, the CTD must undergo structural changes to be released from the inner lumen of the HBV capsid to its surface. This only occurs in mature rcDNA containing nucleocapsids (*219*). HBV capsids are then transported to the nucleus where they directly interact with nucleoporin (Nup) 153 and are stalled in the nuclear basket (*111, 113*). There, the capsids dissociate to dimers by an, until now, unknown trigger and release the rcDNA into the nucleus (*107-113*). Currently discussed mechanisms of HBV capsid disassembly include interaction of mature capsids with Nup153 and phosphorylation of HBV core proteins within the capsid (*108, 111, 183, 184*).

HBV core protein can show both, nuclear and cytoplasmic localization, whereby the distribution of the core protein depends on its phosphorylation status (*103, 110, 220, 221*),

HBV replication and assembly (*221-225*), as well as cell cycle stages (*103, 226*). The HBV core protein can shuttle rapidly between cytoplasm and the nucleus (*195*).

Mutational analysis of HBV core protein functions

HBV core protein functions in terms of formation of HBV capsids and capsid envelopment were extensively studied by mutagenesis. Using alanine mutations, it was shown that residues L60, L95, K96, F97 and I126 are necessary for interaction of HBV core with L HBsAg. They are therefore crucial for generation of enveloped viral particles, but do not interfere with formation of HBV capsids (*188, 227-230*). In contrast, residues I126, V124, W125, R127, and Y132 are supposed to be indispensable for formation of HBV capsids (*204, 231-233*). Interestingly, mutations which affect capsid envelopment, but still support formation of rcDNA containing HBV capsids, induce higher cccDNA levels. This was shown for L95A and K96A and is proposed to be caused by enhanced nuclear recycling of secretion deficient mature capsids. Another explanation could be capsid destabilization by the smaller amino acid side chain (L95A and K96A) or loss of a positive charge in the HBV capsid (K96A) (*154*).

1.1.5.2 HBV core protein interactions with host cellular proteins

Until now, little is known about the interactions of HBV core protein with host cellular proteins (*121*). Some proteins of the host were shown to interact with HBV core protein and act on formation of mature HBV capsids (*234, 235*). Nucleophosmin binds HBV core directly and aids in capsid formation and the assembly steps (*236*). Another host factor, which supports HBV capsid formation by interaction with HBV core, is HSP90 (*234*). Additionally, HBV core association with γ-2-adaptin and Nedd4 is necessary for efficient HBV particle release (*237, 238*). Recently, interactions of phosphorylated HBV core protein with Pin1 were shown to interfere with lysosomal HBV core protein degradation (*239, 240*). In contrast, interaction of HBV core with HSP40 destabilizes HBV capsids and accelerates HBV core protein degradation by the proteasome, with the E3 ubiquitin ligase NIRF being implicated in HBV core protein decay (*241, 242*). HBV core further interacts with factors which enhance HBV replication like filamin B or the nuclear export factor NXF1/p15 (*196, 243*), or interfere with efficient HBV infection, like PTPN3 and SRSF10 (*244-246*). HBV core protein is also implicated in regulation of host cellular gene expression and binds to promoters of over 3000 host genes (*247*). Here, HBV core enhances CRE-mediated transcription (*248*), inhibits transcription of p53 by interfering with E2F1 binding to p53 promoter sequences (*96*), or ensures survival of infected hepatocytes by repressing the promoter activity of the human death receptor 5 (*249*). HBV core also interferes with efficient innate antiviral immunity in infected host cells by interaction with BAF200, which deregulates IFITM1 and inhibits IFNα induced innate immunity

(*48*). Importantly, HBV core interacts and co-localizes with promyelocytic leukemia (PML) nuclear bodies (NB) in HBV producing cell lines, which were challenged with DNA damaging agents (*250*). In line with a possible PML-NB association, a recent proteomics screen suggested SUMO2/3 and 4 as interaction partners of HBV core (*246*). The biological function as well as the molecular background of these interactions, however, is currently unknown.

1.1.5.3 Posttranslational modifications of HBV core

The HBV core protein is subject to a wide variety of posttranslational modifications (PTMs), regulating its activity in the course of infection (*183-185, 190, 193, 251-254*).

Phosphorylation

During packaging of pgRNA inside the HBV capsid, the virus needs to retain electrostatic homeostasis between core proteins and the pgRNA (*213*). Therefore, the HBV core protein harbors three major (S155, S162 and S170) and four minor (T160, S168, S176, S178) phosphorylation sites within its CTD, which are dynamically regulated (*178, 183-186, 189, 190, 193, 194, 212, 251-253, 255-258*). CTD phosphorylation at all seven phosphorylation sites can yield up to $2*7*240 = 3360$ negative charges within the nucleocapsid, which can regulate the homeostasis together with the 16 arginines in the ARD, providing $16*240 = 3840$ positive charges (*259*). CTD phosphorylation occurs early during assembly of HBV capsids and is thought to prevent unspecific binding and packaging of host mRNAs (*90, 212, 213, 255*). HBV core protein then recognizes the complex of the viral polymerase bound to the pgRNA, probably by preferred sequences in the pgRNA, and packaging of the pgRNA induces dephosphorylation of HBV core (*258, 260, 261*). Further dephosphorylation of the CTD might occur during rcDNA synthesis, as the negative charge within the HBV capsid increases with increasing length of the (+) strand (*183, 184, 213, 251*). CTD dephosphorylation is additionally involved in its presentation on the capsid surface, where the CTD protrudes through the pores in the HBV capsid (*219*). HBV core re-phosphorylation is supposed to occur during HBV infection. Re-phosphorylation of HBV core was shown to be necessary for targeting of HBV capsids to the NPC and also for destabilization of capsids prior to disassembly at the NPC (*155, 189*). In line with this, HBV core phosphorylation might also affect subcellular localization (*103, 110, 220, 221*).

A recent study by Luo et al. showed that besides the CTD, also the NTD of HBV core protein is phosphorylated at two conserved residues, namely S44 and S49 (*155*). Mutations of both serine residues to alanine indicate that NTD phosphorylation has no role in regulation of HBV core protein expression levels, formation of HBV capsids and pgRNA packaging, subsequent synthesis of rcDNA within the capsid, as well as secretion of progeny virions (*155*). For

cccDNA formation, however, a severe defect was observed. These findings indicate a role of NTD phosphorylation in HBV capsid disassembly and cccDNA formation, probably by destabilizing the HBV capsid (*155*). In line with this hypothesis, mutation of S44 and S49 to glutamic acid, which acts as phosphomimic, destabilizes HBV capsid structures and increases cccDNA formation (*155*). NTD phosphorylation alone, however, was not sufficient to initiate disassembly. Probably, further factors are necessary to direct HBV capsid disruption at the NPC and nuclear entry (*155*).

Phosphorylation of NTD and CTD are highly dynamic and show a mutual regulation. Phosphorylation of several sites in the NTD and CTD enhances phosphorylation at other sites, indicating a cooperative or sequential phosphorylation in the HBV core protein. These findings might also explain the different roles that some phosphorylation sites take during virus replication (*155, 190, 193, 253, 255, 262*). Additionally, CTD phosphorylation is regulated by the flexible linker domain in the HBV core protein (*131*).

Several kinases were shown to regulate HBV core protein phosphorylation, including the cell cycle regulated kinases CDK2 and PLK1, SRPK1 and 2, PKC as well as GAPD-PK. These kinases probably share redundant functions in HBV core phosphorylation (*256, 262-266*). CDK2 was shown to be co-packaged into HBV nucleocapsids and might be involved in initiation of disassembly by destabilization of the capsid due to NTD re-phosphorylation (*155, 263*). It is proposed that CDK2 activity within the capsid is regulated by dNTP deprivation during rcDNA synthesis, yielding an inactive CDK2 in enveloped viral particles. Reactivation occurs after uncoating, when ATP can enter the capsid again via the pores within the capsid structure (*2, 6, 7, 70, 143, 155*).

Dephosphorylation of HBV core CTD and NTD is regulated by the cellular phosphatases PP2A, PDP2 and PP1. PP2A binds to the linker domain of HBV core and stresses the importance of the linker in dynamic regulation of HBV core protein phosphorylation and therefore the functional switch of HBV core protein (*131, 267*). PDP2 is able to dephosphorylate T160 and S162 in the HBV core protein CTD and might play a role in regulation of pgRNA packaging by CTD dephosphorylation (*240*). PP1 dephosphorylates HBV core proteins during pgRNA packaging and is co-packaged into newly formed HBV capsids. Together with the also co-packaged kinase CDK2, these two proteins might contribute to the dynamical phosphorylation, dephosphorylation and re-phosphorylation of HBV core proteins during infection (*155, 268*).

Ubiquitinylation

HBV core protein harbours six possible sites for ubiquitinylation or ubiquitin like PTMs, including K7, S44, S49, T67, K96, and S157 (*254, 269*). While Garcia et al. showed that mutation of K7 and K96 into arginine residues does not alter release of newly produced viral particles and reported no evidence of HBV core protein ubiquitinylation (*269*), a newer study by Langerovà et al. demonstrated ubiquitinylation of HBV core protein, preferentially by K29 linked poly-ubiquitinylation (*270*). By mutation of K7 and K96 to arginine, they could identify K7 as the primary site for ubiquitinylation and that even HBV core protein lacking K7 and K96 is still ubiquitinylated, probably at one of the additional sites for ubiquitin PTM (S44, S49, T67 or S157) (*270*).

Methylation

A further PTM regulating HBV core protein function and localization is arginine methylation. HBV core protein is methylated by PRMT5. Symmetrical dimethylation results in nuclear localization, while monomethylation induces transport to the cytoplasm (*254*). Additionally, PRMT5 binding to HBV core protein and subsequent arginine methylation decreases HBV replicaton, probably by induction of an epigenetically repressive state of the cccDNA (*254, 271*).

1.2 PML nuclear bodies and SUMOylation

1.2.1 The SUMOylation pathway

The small ubiquitin-related modifier SUMO comprises the five different isoforms SUMO1 to SUMO5, having a size of 11kDa (*272-274*). SUMO2 and SUMO3 share over 95% sequence homology, which makes them hard to distinguish, and which is the reason they are often referred to as SUMO2/3. In contrast, SUMO1 has only 50% sequence homology to SUMO2/3 (*275, 276*). SUMO4 and SUMO5 are still subject to controversial discussions, as they might represent pseudogenes of the other SUMO isoforms and their expression is not extensively characterized yet (*274, 277, 278*). They share several similar characteristics with ubiquitin, such as their tertiary structure, 18% of their sequence, and also the three-step conjugation pathway (see figure 6), which is why they belong to the group of ubiquitin-like proteins (*273, 279-281*).

SUMO proteins are expressed as immature precursors. Maturation is mediated by proteolytic processing by SUMO specific endopeptidases (SENPs), which release the C-terminal di-glycine motif necessary for SUMO conjugation (*282*). SUMO proteins are then activated by

the SUMO activating enzymes (SAE) Aos1 and Uba2 in a process that involves ATP hydrolysis and formation of a thioester bond between the SAEs and SUMO (*283*).
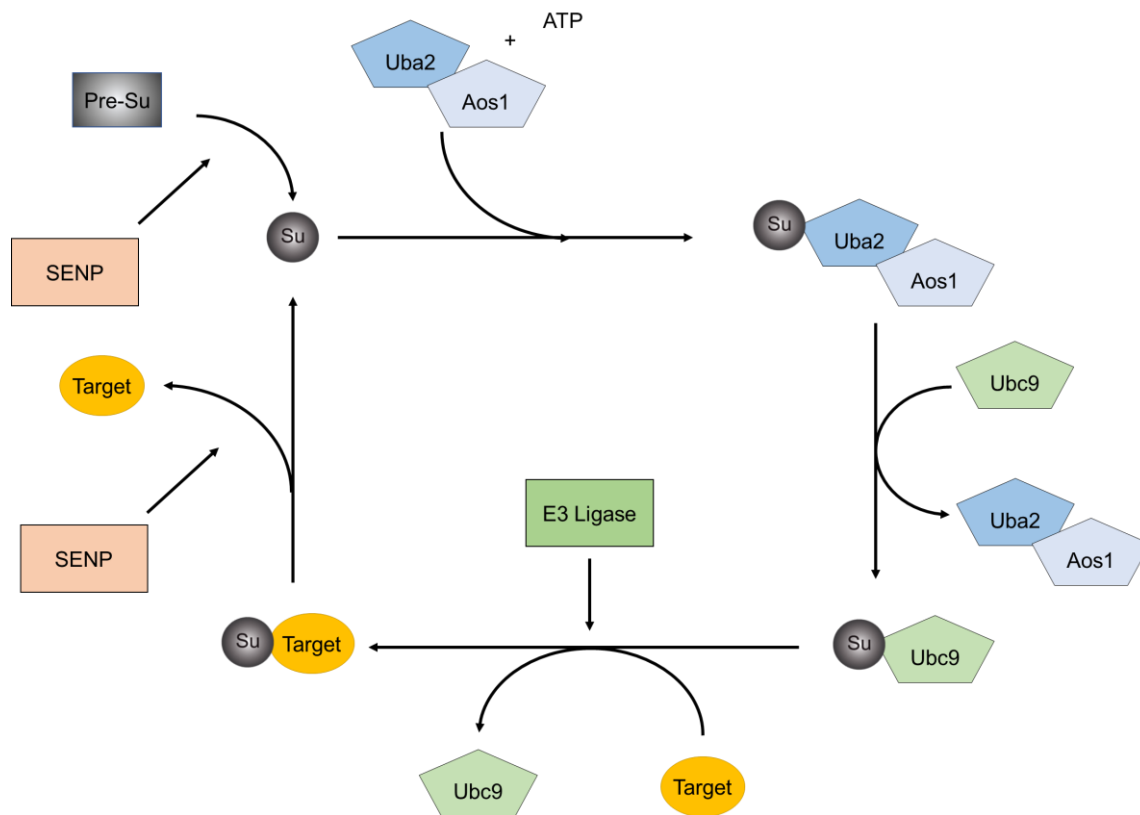
Figure 6: Schematic representation of the SUMOylation pathway. SUMO precursor proteins are matured by SENPs and activated by Uba2 and Aos1 in an ATP dependent mechanism. SUMO is transferred to Ubc9 and subsequently conjugated to its cognate target protein. DeSUMOylation is mediated by SENPs. Pre-Su: SUMO precursor, Su: SUMO (adapted from (*284*)).

Activated SUMO proteins are then covalently transferred to Ubc9, again via a thioester bond, which is the, until now, only identified SUMO E2 conjugating enzyme. Eventually, SUMO is conjugated to its target protein by formation of an ε-amide bond between the C-terminal di-glycine motif of SUMO and a lysine residue within the target protein in a process mediated by SUMO E3 ligases (*283-286*). SUMOylation preferentially occurs at a lysine residue present in a so-called "SUMO conjugation motif" (SCM) ψKxE/D, where ψ represents a large hydrophobic resiude and x can be an arbitrary amino acid. However, also lysine residues in non-consensus motifs can be SUMO modified (*272-274, 283-287*). SENPs do not only have the ability to mediate maturation of SUMO precursors, but also harbor the activity to reverse SUMOylation by cleavage of the ε-amide bond between SUMO and the target protein. This makes SUMO PTM a dynamic and reversible process (*282*).

SUMOylation can also occur internally in SUMO2/3 at lysine residue K11, leading to the formation of SUMO chains of different length (*276, 288, 289*). Proteins which are not SUMOylated at a SCM can also interact with the SUMO PTM pathway and SUMO modified

proteins, based on an intrinsic SUMO interacting motif (SIM), by undergoing non-covalent SUMO-SIM interactions (*290, 291*). SUMOylation is strongly associated with other PTMs including phosphorylation, acetylation, and methylation of target proteins (*292, 293*). Noteworthy is the interplay between phosphorylation and SUMOylation, as several publications could show that phosphorylation is a prerequisite for efficient subsequent SUMOylation of target proteins (*294-298*).

Key cellular processes and signalling pathways regulated by protein SUMOylation are for example differentiation, transcriptional regulation, but also the host cell DNA damage response (*280, 281, 299-304*). This is mainly achieved by affecting protein stability and degradation, protein interactions by SUMO-SIM association, changes in conformation as well as enzymatic activities, and subcellular localization of target proteins (*305, 306*). SUMOylation is often associated with localization to and interaction with promyelocytic leukemia (PML) nuclear bodies (NBs). Most enzymes of the host SUMO conjugation and deconjugation pathways are localizing to PML-NBs. PML-NB associated proteins either carry SCM or SIM motifs, which is why PML-NBs are suggested to be hotspots for SUMO PTM (*284, 305, 307-311*).

1.2.2 PML-NB organization and composition

PML-NBs, also known as nuclear domain 10 (ND10) or PML oncogenic domains (PODs), are spherical multi-protein complexes residing in the nuclear matrix of mammalian cells. They appear at a frequency of 2-30 PML-NBs per cell and have a size of 0.2-1µm (*284, 312-318*). The eponymous component of PML-NBs, the PML protein, was first described in a malignant form of leukemia, the acute promyelocytic leukemia (APL). APL is characterized by a fusion of the PML encoding gene to retinoic acid receptor α (RARA) caused by a chromosomal translocation (*319-321*). PML is generally assumed to act as a tumor suppressor protein due to its deregulation in several human cancer types (*322, 323*). Besides the PML protein, PML-NBs harbor the constitutively present factors SUMO1 and SUMO2/3, the isoforms A, B, C and HMG of the speckled protein 100 (Sp100), as well as Daxx (*324, 325*). PML builds together with Sp100 and SUMO the outer shell of the PML-NB (*310, 324*).

Expression of the *pml* gene yields seven PML isoforms, PML-I to PML-VII, due to differential splicing of the nine exons. PML-I to PML-VI are nuclear isoforms that orchestrate the formation of PML-NBs, while PML-VII is the only cytoplasmic PML isoform, as it lacks the NLS. (*313, 326-328*). All nuclear PML isoforms share the N-terminal exons 1-6. These harbor the characteristic tripartite motif (TRIM), also referred to as RBCC motif, consisting of a really

interesting new gene (RING) domain, two B boxes B1 and B2 and a coiled-coil domain (see figure 7) (*313, 325, 326*).
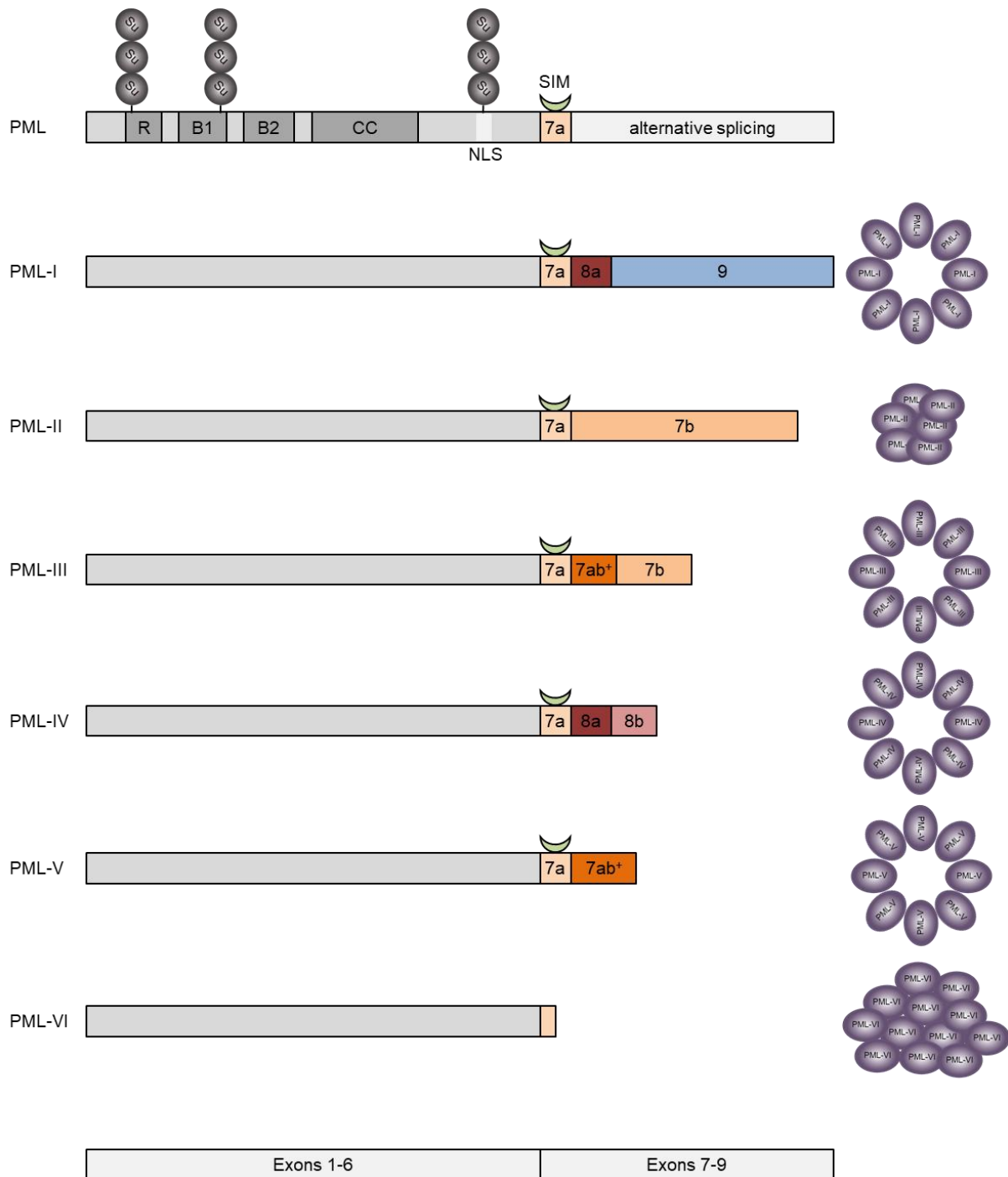
Figure 7: PML protein isoforms. Schematic representation of the nuclear PML isoforms PML-I to PML-VI. All PML isoforms share exons 1-6 in their N-terminal domain, while the unique C-terminal domain is generated from extensive differential splicing of exons 7-9. The distribution of PML proteins in PML-NBs formed by only one single PML isoform as determined by super resolution microscopy is depicted on the right. R: RING domain, B: B-box, CC: Coiled coil, Su: SUMO, SIM: SUMO interacting motif, NLS: Nuclear localization signal (adapted from (*310, 329*))

Exons 1-6 also encode three SCM sites at K65, K160, and K490, which are extensively modified by SUMOylation, and a NLS, mediating nuclear localization of PML-I to PML-VI.

Poly-SUMOylation of PML is proposed to play a role in PML-NB formation and integrity (*305, 306, 324, 330-333*). PML is further subject to PTMs including ubiquitinylation, phosphorylation, and acetylation, which might be involved in fine-tuning of PML-NB function (*334*). The nuclear PML isoforms PML-I to PML-VI differ in their C-terminal domains generated as result of alternative splicing of exons 7-9. PML-I to PML-V are especially characterized by the presence of a SIM motif in exon 7a, which is absent in PML-VI (see figure 7). The differences in the C-terminus of the PML isoforms probably also mediate isoform-specific functions and protein-protein interactions (*313, 326, 335*).

PML-I specifically interacts with the transcription factor acute myeloid leukemia 1 (AML1) and stimulates myeloid cell differentiation by targeting specific chromosome translocations during AML (*336*). In infection with herpes simplex virus 1 (HSV-1), PML-I is directly interacting with ICP0 and subsequently degraded, independently of SUMOylation (*337, 338*).

PML-II extensively interacts with proteins of human adenovirus (HAdV). During HAdV infection, PML-II is directly bound by the viral E4orf3 protein, leading to re-organization of PML-NBs into so called "track-like structures" (*339, 340*). Additionally, PML-II enhances transcriptional activity of the E1A-13S protein, which is necessary for efficient adenoviral gene expression (*341*).

PML-III is especially relevant during centrosome duplication, where it localizes to the centrosome and regulates Aurora A kinase activity (*342*). Other cellular interactions of PML-III include p53 and TIP60 (*343, 344*). PML-III overexpression interferes with efficient replication of several DNA and RNA viruses, including for example influenza A or vesicular stomatitis virus (VSV) (*345*).

There are various interactions of PML-IV with cellular factors, including telomerase reverse transcriptase (TERT), telomeric repeat binding factor 1 (TRF1) and PU.1 (*346, 347*). PML-IV interaction with p53 induces apoptosis, senescence and is supposed to play a role in DDR regulation (*348-350*). PML-IV is additionally able to destabilize c-Myc, which inhibits uncontrolled proliferation and induces differentiation (*351*). PML-IV also has antiviral capacity and interferes with efficient replication of varizella zoster virus (VZV), rabies virus, and encephalomyocarditis virus (EMCV) (*352-354*).

PML-V is supposed to be the major scaffolding protein of PML-NBs and recruits PML-NB components Daxx and Sp100 (*355, 356*). During adenoviral infection, PML-V together with PML-IV are necessary for efficient SUMOylation of p53 by the early adenoviral protein E1B-55K (*357*).

PML-VI only carries a small proportion of exon 7a and lacks the SIM motif. In contrast to the other nuclear PML isoforms, PML-VI is resistant to degradation induced by arsenic trioxide (*358*).

Besides differences in their interaction partners, PML isoforms also differ in their localization when they form PML-NBs in absence of other PML isoforms. Super resolution microscopy could show a ring like distribution of PML-I, -III, -IV and -V, while PML-II localized in small, solid dots and PML-VI formed larger accumulations (see figure 7) (*329*).
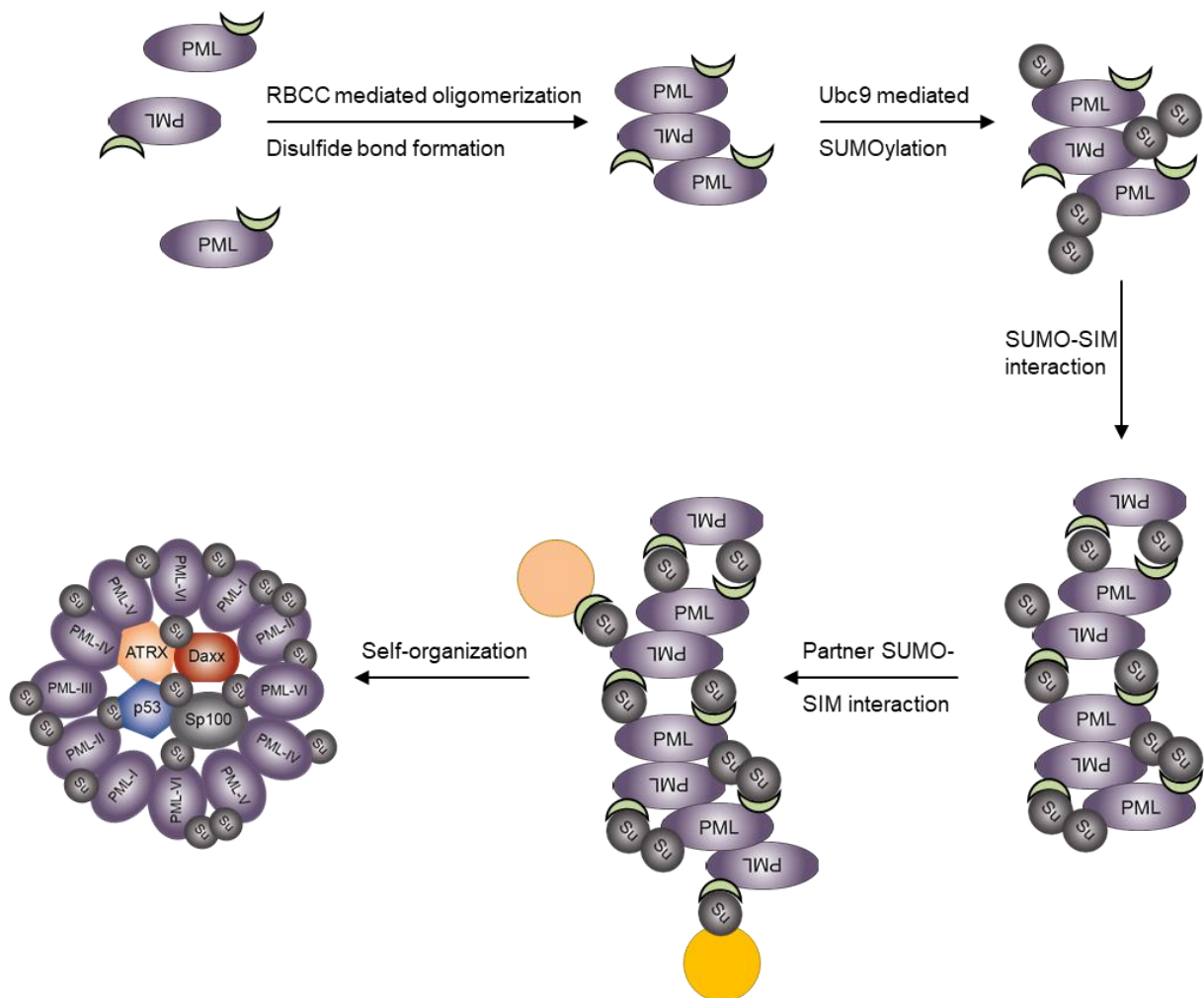
Figure 8: PML-NB biogenesis. PML-NB formation initiates with non-covalent RBCC mediated dimerization followed by covalent linkage via disulfide bonds. Ubc9 poly-SUMOylates PML proteins within smaller oligomers, which further assemble based on SUMO-SIM interactions. PML-NB partner proteins are then recruited via additional SUMO-SIM interactions and self-organization leads to formation of the typical dot-like PML-NB. Su: SUMO (adapted from (*310*)).

Formation of PML-NBs occurs in multiple steps and is initiated by non-covalent dimerization of PML proteins via their common RBCC motif as well as formation of covalent disulfide bonds. PML proteins are then SUMOylated by Ubc9 and further self-assemble by SUMO-SIM interactions. Recruitment of partner proteins, which is also regulated by SUMO-SIM

interactions, is followed by self-organization into the typical dot like shape of PML-NBs (see figure 8) (*305, 306, 324, 359-361*).

Several hundreds of different proteins localize to PML-NBs and their composition, which regulates the function, is depending on cell type, cell cycle stages, and the cellular stress response (*315, 316*). PML-NBs can participate in regulation of a variety of cellular processes, including replication, apoptosis and senescence, transcriptional regulation and epigenetic silencing, protein PTM, localization and degradation, antiviral defense, as well as DNA damage response (*318, 345, 359, 362-369*). Many proteins involved in host SUMOylation and deSUMOylation are present in PML-NBs. Additionally, localization to PML-NBs is preferentially regulated by SUMO-SIM interactions. Due to these observations, it is suggested that PML-NBs regulate the afore mentioned functions by serving as hubs and scaffold for the recruitment of essential proteins, especially via SUMO-SIM interactions (*284, 305, 307-311, 359, 370*).

PML-NBs can be considered as model system for phase separation in liquid-liquid interfaces. The scaffold of the condensed droplet consisting of SUMO and PML is generated by RBCC mediated interactions and SUMO-SIM association between different SUMO modified PML proteins (*371-373*). The composition of PML-NBs is then dynamically regulated by changing the SUMO status of the scaffolding PML proteins. DeSUMOylation of PML results in enhanced recruitment of SUMOylated interactor proteins, and increased SUMOylation of PML leads to preferential recruitment of SIM-containing proteins (*372*). Besides SUMOylation and deSUMOylation of the scaffold protein PML and the interactor proteins, PML-NB composition can also be regulated by phosphorylation of SIMs, which increases their affinity for SUMOylated proteins (*372, 374-377*).

1.2.3 PML-NBs and SUMOylation: Implications in the host DNA damage response

PML-NBs show extensive interplay with the DNA damage response. Upon DNA damage, PML proteins are phosphorylated by the DNA damage activated kinases ATM, ATR, CHK2 or HIPK2 and accumulate at sites of DNA damage within the host genome. There, they act as molecular hubs for the regulation of the DDR, mostly by recruitment of DDR factors like TOPBP1, BLM, WRN or the MRN complex. These associations are often based on SUMO-SIM interactions (*318, 367-369, 378, 379*). In line with these observations, several proteins known to be involved in cccDNA generation are either interacting with PML-NBs or are SUMO modified.

TDP2, which might be involved in removal of the HBV polymerase bound to the 5' end of the (-) strand (*160, 161, 167, 168*), localizes to PML-NBs, probably mediated by its internal SIM

motif (*167, 380-382*). FEN1 is supposed to cleave the viral polymerase as well as the terminal redundancies of the (-) strand (*162, 171*) and is modified by SUMO1 and SUMO2/3 PTM. FEN1 SUMOylation regulates its association to the Rad9-Rad1-Hus1 complex, which is localized in alternative lengthening of telomeres PML-NBs (*318, 383-385*). Of the DNA polymerases involved in cccDNA generation (*163, 164, 171*), Polymerase δ interacts with BLM, a protein present in PML-NBs (*378, 386*), and SUMO2 modification of Polymerase λ promotes its recruitment to damaged dsDNA (*385, 387*). In addition, DNA polymerase α (*385*) as well as DNA ligase 1 are SUMO2 modified, the latter being involved in ligation of the DNA strands after repair (*166, 171, 385*). Top1 and Top2, necessary to reduce torsional stress on cccDNA during circularization (*165*), are both targeted and regulated by SUMO PTM (*388-391*). Top1 SUMOylation induces recruitment from nucleoli into the nucleoplasm (*388*), while SUMO modification of Top2 mediates relocalization to centromeric structures during mitosis and cohesion of sister chromatids (*389, 390*). PCNA, recently shown to be involved in cccDNA generation (*171*), localizes to PML-NBs during S-phase or DNA damage and is present in alternative lengthening of telomeres PML-NBs (*392-394*). PCNA activity is dynamically regulated by SUMOylation (*391, 395-401*) and PCNA recruitment to alternative lengthening of telomeres PML-NBs also depends on its SUMO status (*399*). SUMO1 modification of PCNA is crucial for resolving of stalled replication forks by the error-free template switch pathway (*400*). Additionally, PCNA SUMO2 PTM is involved in chromatin remodeling during transcription-replication conflicts (*401*).

1.2.4 Role of PML-NBs during viral infection

Expression of key PML-NB components PML, Daxx and Sp100 is inducible by interferons and may impair efficient viral replication, which is why PML-NBs are suggested to harbor a general antiviral capacity (*345, 402-405*). In line with this hypothesis, several DNA and RNA viruses express early viral proteins that disrupt PML-NBs and interfere with PML-NB function, including HAdV, herpesviruses, or rabies virus (*345, 405, 406*). However, further studies suggest that PML-NBs do not only harbor antiviral activity, but also recruit proteins, which are beneficial for viral infection. This is based on the observation that the incoming genomes of several nuclear replicating viruses associate with PML-NBs as initial site of transcription, suggesting a dual role for PML-NBs during viral infections (*345, 405, 406*).

During HBV infection, several interactions of viral proteins with PML and PML-NB components are observerd. HBV polymerase localizes to PML-NBs dependent on interaction with S100A10. These findings suggest a possible role of PML in HBV replication, however, the underlying function is not clear (*407*). Chung and Tsai showed an association of the HBV core protein to PML in HBV producing cell lines during stress induced by DNA damage and

suggest a positive effect of the interaction on HBV replication. The exact molecular mechanism and the biological function of this association is not known yet (*250*). Another HBV interaction with PML-NB proteins enhancing viral replication is the association of speckled protein 110kDa with HBx to promote HBV transcriptional activity (*408*). Besides these proviral factors, also anti-HBV activities are present in PML-NBs. PML-NB factors SUZ12 and ZNF198 interfere with HBV replication, probably due to their function in chromatin remodeling complexes. HBx expression reduces SUZ12 and ZNF198 protein levels and rescues HBV transcription (*409-413*). The structural maintenance of chromosomes 5/6 (Smc5/6) complex associated with PML-NBs restricts HBV transcription. This interference with efficient viral gene expression is counteracted by HBx mediated degradation of the Smc5/6 complex (*94, 414*). In a recent study using the DHBV model system, a general suppressive role of PML and other IFN induced genes in cccDNA transcription and an association with cccDNA was observed (*415*). Further studies in mice showed that high HBsAg levels induce a loss of PML expression in the liver and coincide with enhanced chromosome breaks, indicating a link of HBsAg induced loss of PML with HBV mediated tumorigenesis (*416, 417*). Taken together, PML and PML-NB components have a dual role in the HBV replication cycle and show interaction with several HBV proteins, but the knowledge on the biological function and the regulation of these interactions is scarce.

2. Aim of the study

Chronic HBV infection is still a major threat to global health. This is due to the stable nature of the epsiomal cccDNA, the HBV persistence reservoir, which is considered to be the key for a functional cure (*48*). A deeper understanding of the molecular mechanism and regulation of cccDNA generation from the incoming incomplete and damaged rcDNA by proteins of the host cell DDR (see chapter 1.1.4) is of crucial interest to find novel targets for the development of antiviral therapies. PML-NBs emerged in the recent years as molecular hub for the host cell DDR (see chapter 1.2.3) and show a plethora of interactions with HBV proteins. However, the exact function of these interactions remains elusive (see chapter 1.2.4).

Based on these observations, we formed the hypothesis that PML-NBs act as regulator of the DDR in cccDNA formation and that this regulation is based on SUMO PTM. The HBV core protein is highly relevant during cccDNA formation (see chapter 1.1.5.1) and subject to a variety of PTMs (see chapter 1.1.5.3). Therefore, the overall aim of this thesis was to unravel the impact of HBV core protein SUMO PTM and PML-NB association on formation of the HBV persistence reservoir, the cccDNA.

The first question addressed was, if the HBV core protein was posttranslationally modified by SUMOylation and associated to PML-NBs. After confirmation of HBV core SUMOylation and a SUMO dependent association with PML-NBs during transfection and infection, the aim of the second part was to determine the impact of HBV core protein SUMOylation on cccDNA generation and nuclear entry of viral particles. To address this question, a plasmid-based HBV replicon system was used. As PML-NBs serve as hub for the recruitment of several hundreds of proteins (see chapter 1.2.2), we further aimed at narrowing the possible candidates involved in cccDNA formation by generation of HepG2-NTCP-K7 based cell lines with expression of single PML isoforms. As proof-of-concept, inhibition of SUMOylation during early phases of HBV infection was used to restrict nuclear entry of HBV capsids and therefore cccDNA formation. Taken together, this work aimed at elucidating early steps of the HBV replication cycle leading to cccDNA formation in order to suggest novel therapeutic approaches for HBV infections.

3. Materials and Methods

3.1 Materials

3.1.1 Laboratory equipment

Table 1: Laboratory equipment used in this dissertation

Equipment	Manufacturer
AGFA Curix 60	AGFA, Mortsel, Belgium
Avanti JE centrifuge	Beckman Coulter, München, Germany
Axiovert 200M microscope	Zeiss, Oberkochen, Germany
Biometra Multigel	Analytik Jena, Jena, Germany
Biometra Minigel Twin	Analytik Jena, Jena, Germany
Biometra Standard Power Pack P25 T	Analytik Jena, Jena, Germany
Bio-Rad ChemiDoc MP Imaging System	Bio-Rad, München, Germany
Bio-Rad Universal Hood II Gel Doc	Bio-Rad, München, Germany
Bio-Rad PowerPac 3000	Bio-Rad, München, Germany
Bio-Rad Trans Blot Cell	Bio-Rad, München, Germany
Bioruptor plus	Diagenode, Seraing, Belgium
BRAND AccuJet Pro	Sigma Aldrich, Darmstadt, Germany
ChemiDoc MP Imaging System	Bio-Rad, München, Germany
Eppendorf Biophotometer 6131	Eppendorf, Hamburg, Germany
Eppendorf Concentrator 5301	Eppendorf, Hamburg, Germany
Eppendorf Mastercycler	Eppendorf, Hamburg, Germany
Eppendorf 5427 R centrifuge	Eppendorf, Hamburg, Germany
Eppendorf 5702 centrifuge	Eppendorf, Hamburg, Germany
Eppendorf Research Plus 0.1-2.5µl pipette	Eppendorf, Hamburg, Germany
Eppendorf Research Plus 0.5-10µl pipette	Eppendorf, Hamburg, Germany
Eppendorf Research Plus 10-100µl pipette	Eppendorf, Hamburg, Germany
Eppendorf Research Plus 20-200µl pipette	Eppendorf, Hamburg, Germany
Eppendorf Research Plus 100-1000µl pipette	Eppendorf, Hamburg, Germany
FiveEasy Plus FEP20 pH-Meter	Mettler Toledo, Fürstenfeldbruck, Germany
Hera cell 150 CO_2 incubator	Thermo Scientific, Dreieich, Germany
Heraeus HB 2448	Heraeus, Hanau, Germany
Heraeus Biofuge pico	Thermo Scientific, Dreieich, Germany
Heraeus Fresco 21 tabletop centrifuge	Thermo Scientific, Dreieich, Germany
Heraeus Megafuge 40	Thermo Scientific, Dreieich, Germany
Heraeus Herafreeze HFU 568 Basic	Thermo Scientific, Dreieich, Germany
Improved Neubauer chamber	Laboroptik, Lancing, UK
Incubation Shaker Multitron Standard	Infors HT, Bottmingen, Switzerland

3. Materials and Methods

Incubator	Memmert, Büchenbach, Germany
LSM980 Inverted Laser Scanning Microscope	Zeiss, Oberkochen, Germany
LightCycler 480 II	Roche, Mannheim, Germany
Mr. Frosty freezig container	Thermo Scientific, Dreieich, Germany
Mulitgel electrophoresis chamber	Analytik Jena, Jena, Germany
Multiron incubation shaker	Infors HT, Bottmingen, Switzerland
Nanodrop 2000c	Thermo Scientific, Dreieich, Germany
Orbital shaker	GFL, Burgwedel, Germany
PerfectBlu Wide Format Gel System Maxi ExW	VWR International, Darmstadt, Germany
Pipetboy acu 2	Integra, Zizers, Switzerland
Primo vert light microscope	Zeiss, Oberkochen, Germany
qTOWER^3	Analytik Jena, Jena, Germany
Rotina 420 R centrifuge	Hettich Zentrifugen, Tuttlingen, Germany
Rotixa 50 RS centrifuge	Hettich Zentrifugen, Tuttlingen, Germany
Smart Spec Plus spectrophotometer	Bio-Rad, München, Germany
Sonifier 450	Branson, Dietzenbach, Germany
Test Tube Rotating Shaker 3025	GFL, Burgwedel, Germany
TE62 Transfer Tank	Serwa Electrophoresis, Heidelberg, Germany
Thermomixer comfort	Eppendorf, Hamburg, Germany
Trans-Blot Electrophoretic Transfer Cell System	Bio-Rad, München, Germany
Vacusafe laboratory vacuum pump	Integra, Zizers, Switzerland
Vortex-Genie 2T	Scientific industries, Bohemia, NY, US

3.1.2 Chemicals and media

Table 2: Chemicals, media and enzymes used in this dissertation

Substance	Supplier
10x Antarctic phosphatase reaction buffer	New England BioLabs, Frankfurt a.M., Germany
2-Propanol	Carl Roth, Karlsruhe, Germany
30% acrylamide/bisacrylamide mixture	Carl Roth, Karlsruhe, Germany
6x DNA loading dye	New England BioLabs, Frankfurt a.M., Germany
Agarose	Biozym, Hessisch Oldendorf, Germany
Ampicillin	Sigma-Aldrich, Darmstadt, Germany
Antarctic phosphatase	New England BioLabs, Frankfurt a.M., Germany
Aprotinin	Sigma-Aldrich, Darmstadt, Germany
Ammonium persulfate (APS)	Carl Roth, Karlsruhe, Germany
Bovine serum albumin (BSA)	Thermo Scientific, Dreieich, Germany
Boric acid	Sigma-Aldrich, Darmstadt, Germany
Bradford reagent	Bio-Rad, München, Germany

Bromophenol blue	Carl Roth, Karlsruhe, Germany
Buffer 3.1	New England BioLabs, Frankfurt a.M., Germany
Buffer 4	New England BioLabs, Frankfurt a.M., Germany
$CaCl_2$	Sigma-Aldrich, Darmstadt, Germany
Chloroform	Carl Roth, Karlsruhe, Germany
Collagen R solution, 0.2%, sterile	Serwa Electrophoresis, Heidelberg, Germany
CutSmart buffer	New England BioLabs, Frankfurt a.M., Germany
4',6-Diamidin-2-phenylindol (Dapi)	Sigma-Aldrich, Darmstadt, Germany
Developing solution	Tetenal, Norderstedt, Germany
Dimethyl sulfoxide (DMSO) ≥ 99.5%	Carl Roth, Karlsruhe, Germany
DNase I	Carl Roth, Karlsruhe, Germany
dNTP mix (100mM)	New England BioLabs, Frankfurt a.M., Germany
Dulbecco's modified eagle's medium D6429	Sigma-Aldrich, Darmstadt, Germany
Dulbecco's modified eagle's medium D5671	Sigma-Aldrich, Darmstadt, Germany
DpnI	New England BioLabs, Frankfurt a.M., Germany
EcoRI-HF	New England BioLabs, Frankfurt a.M., Germany
Ethylenediaminetetraacetic acid (EDTA)	Carl Roth, Karlsruhe, Germany
Ethanol	Carl Roth, Karlsruhe, Germany
Ethidium bromide	Sigma-Aldrich, Darmstadt, Germany
Fetal calf serum (FCS)	Biochrom, Berlin, Germany
Fixation solution	Tetenal, Norderstedt, Germany
Geneticin (G) 418 disulfate salt solution 50mg/ml	Sigma-Aldrich, Darmstadt, Germany
Ginkgolic Acid (15:1)	Sigma-Aldrich, Darmstadt, Germany
Glycerol	AppliChem, Darmstadt, Germany
Glycine	AppliChem, Darmstadt, Germany
Guanidine hydrochloride	AppliChem, Darmstadt, Germany
H_2O_2, 30% solution	Sigma-Aldrich, Darmstadt, Germany
HCl	Carl Roth, Karlsruhe, Germany
HEPES	Sigma-Aldrich, Darmstadt, Germany
Hydrocortisone-21-hemisuccinate	Sigma-Aldrich, Darmstadt, Germany
Imidazole	AppliChem, Darmstadt, Germany
Insulin from bovine pancreas	Sigma-Aldrich, Darmstadt, Germany
Iodacetamide	Sigma-Aldrich, Darmstadt, Germany
Kanamycin	Sigma-Aldrich, Darmstadt, Germany
KCl	Carl Roth, Karlsruhe, Germany
KoAc	Sigma-Aldrich, Darmstadt, Germany
Leupeptin	Sigma-Aldrich, Darmstadt, Germany
Luminol sodium salt	Sigma-Aldrich, Darmstadt, Germany
L-glutamine solution, 200mM	Sigma-Aldrich, Darmstadt, Germany

3. Materials and Methods

Methanol	Carl Roth, Karlsruhe, Germany
MEM Non-essential amino acids (100x)	Sigma-Aldrich, Darmstadt, Germany
$MgCl_2$	Carl Roth, Karlsruhe, Germany
$MnCl_2$	Sigma-Aldrich, Darmstadt, Germany
MOPS	Sigma-Aldrich, Darmstadt, Germany
Mowiol 4-88	Carl Roth, Karlsruhe, Germany
Na_2HPO_4	AppliChem, Darmstadt, Germany
NaCl	Carl Roth, Karlsruhe, Germany
NaH_2PO_4	AppliChem, Darmstadt, Germany
NcoI	New England BioLabs, Frankfurt a.M., Germany
N-ethylmaleimide	Sigma-Aldrich, Darmstadt, Germany
NiNTA resin	Thermo Scientific, Dreieich, Germany
Nonidet-P40 (NP40)	Carl Roth, Karlsruhe, Germany
p-Coumaric acid	Sigma-Aldrich, Darmstadt, Germany
Paraformaldehyde (PFA)	Carl Roth, Karlsruhe, Germany
PageRuler prestained protein ladded plus	Fermentas/Thermo Scientific, Dreieich, Germany
Pansorbin	Calbiochem, Bad Soden, Germany
Penicillin/streptomycin	Sigma-Aldrich, Darmstadt, Germany
Pepstatin	Sigma-Aldrich, Darmstadt, Germany
PfuUltra II Fusion 10 x Reaction buffer	Agilent Technologies, Santa Clara, CA, US
PfuUltra II Fusion HS DNA Polymerase	Agilent Technologies, Santa Clara, CA, US
Phenol/chloroform/isoamyl alcohol (25:24:1)	Sigma-Aldrich, Darmstadt, Germany
Phenylmethylsolfonyl fluoride (PMSF)	Sigma-Aldrich, Darmstadt, Germany
Phosphate buffered saline (PBS)	Biochrom, Berlin, Germany
Polyethylene imine (PEI)	Sigma-Aldrich, Darmstadt, Germany
Polyethyleneglycol 8000 (PEG8000)	Promega, Madison, WI, USA
Proteinase K	Carl Roth, Karlsruhe, Germany
Puromycin, 10mg/ml	Thermo Scientific, Dreieich, Germany
RbCl	Sigma-Aldrich, Darmstadt, Germany
RNase A	Carl Roth, Karlsruhe, Germany
Sepharose A beads	Sigma-Aldrich, Darmstadt, Germany
Skim milk powder	Sigma-Aldrich, Darmstadt, Germany
Sodium acetate	Carl Roth, Karlsruhe, Germany
Sodium azide	AppliChem, Darmstadt, Germany
Sodium deoxycholate	Carl Roth, Karlsruhe, Germany
Sodium dodecylsulfate (SDS)	Carl Roth, Karlsruhe, Germany
Sodiumacetate	Sigma-Aldrich, Darmstadt, Germany
Sodium pyruvate, 100mM	Thermo Scientific, Dreieich, Germany
T4 DNA ligase	Roche, Basel, Switzerland

T4 DNA Ligation buffer, 10 x conc.	Roche, Basel, Switzerland
T4 Polynucleotide kinase	Roche, Basel, Switzerland
T5 exonuclease	New England BioLabs, Frankfurt a.M., Germany
TEMED	AppliChem, Darmstadt, Germany
Tris(hydroxymethyl)aminomethane (Tris)	Carl Roth, Karlsruhe, Germany
Triton X-100	AppliChem, Darmstadt, Germany
TRIzol	Thermo Scientific, Dreieich, Germany
Trypsin/EDTA	Sigma-Aldrich, Darmstadt, Germany
Trypan blue solution	Thermo Scientific, Dreieich, Germany
Tween-20	AppliChem, Darmstadt, Germany
TRIzol Reagent	Sigma-Aldrich, Darmstadt, Germany
Urea	AppliChem, Darmstadt, Germany
XhoI	New England BioLabs, Frankfurt a.M., Germany
β-mercaptoethanol	AppliChem, Darmstadt, Germany

3.1.3 Disposable laboratory equipment

Table 3: Disposable laboratory equipment used in this dissertation

Equipment	Manufacturer
0.2µm sterile filter	Merck Millipore, Darmstadt, Germany
0.45µm sterile filter	Merck Millipore, Darmstadt, Germany
1.8ml CryoPure tubes 72.379	Nunc/Thermo Scientific, Dreieich, Germany
1.5 ml Eppendorf tubes	Sarstedt, Nümbrecht, Germany
100mm cell culture plates 83.3902	Sarstedt, Nümbrecht, Germany
150mm cell culture plates 83.3903	Sarstedt, Nümbrecht, Germany
12mm cover slides	Hartenstein, Würzburg, Germany
12-well plates F 83.3921	Sarstedt, Nümbrecht, Germany
15ml falcon tubes 62.554.502	Sarstedt, Nümbrecht, Germany
2ml Eppendorf tubes	Sarstedt, Nümbrecht, Germany
5ml polypropylene tubes Falcon 2059	Corning, Berlin, Germany
50ml falcon tubes 62.547.254	Sarstedt, Nümbrecht, Germany
6-well plates 83.3920	Sarstedt, Nümbrecht, Germany
Cell scraper 39cm	Sarstedt, Nümbrecht, Germany
Filter Tips 1000µl 70.762.211	Sarstedt, Nümbrecht, Germany
Filter Tips 200µl 70.760.212	Sarstedt, Nümbrecht, Germany
Filter Tips 20µl 70.760.213	Sarstedt, Nümbrecht, Germany
Filter Tips 10µl 70.1116.210	Sarstedt, Nümbrecht, Germany
Greiner CELLSTAR serological pipette, 5ml	Sigma-Aldrich, Darmstadt, Germany
Greiner CELLSTAR serological pipette, 10ml	Sigma-Aldrich, Darmstadt, Germany

Greiner CELLSTAR serological pipette, 25ml	Sigma-Aldrich, Darmstadt, Germany
Greiner CELLSTAR aspiration pipette	Sigma-Aldrich, Darmstadt, Germany
Microscope slides	Hartenstein, Würzburg, Germany
Nitrocellulose membranes, 0.2µm, Amersham Protran	GE Healthcare, Solingen, Germany
Nitrocellulose membranes, 0.45µm, Amersham Protran	GE Healthcare, Solingen, Germany
PVDF membranes, 0.2µm	Hartenstein, Würzburg, Germany
qPCR plates, 96 well	4titude, Berlin, Germany
qPCR 96 well 0.2ml 8-transformer plate	Biozym, Hessisch Oldendorf, Germany
qPCR lid Transformer Cap Strip plate	Biozym, Hessisch Oldendorf, Germany
Semi-micro cuvette 10mm 67.742	Sarstedt, Nümbrecht, Germany
Whatman blotting paper, 460x570mm, 195g/m^2	Hartenstein, Würzburg, Germany
X-ray films	CEA

3.1.4 Commercial kits

Table 4: Commercial kits used in this dissertation

Kit	Manufacturer
NucleoSpin Tissue	Macherey Nagel, Düren, Germany
LightCycler 480 SYBR Green I Master	Roche, Basel, Switzerland
Luna Universal qPCR Master Mix	New England BioLabs, Frankfurt a.M., Germany
CUT&RUN Assay Kit	Cell Signaling Technology, Frankfurt a.M., Germany
DNA Purification Buffers and Spin Columns (ChIP, CUT&RUN)	Cell Signaling Technology, Frankfurt a.M., Germany
Promega Reverse Transcription System	Promega, Madison, WI, USA
QIAGEN Plasmid Maxi Kit	QIAGEN, Hilden, Germany
SureBeads Magnetic Beads with Protein A or G	Bio-Rad, München, Germany

3.1.5 Software and databases

Table 5: Softwares and databases used in this dissertation

Software	Source	Purpose
Adobe Reader XI	Adobe, Munich, Germany	Processing of PDF files
CLC Sequence Viewer 6	CLC Bio, Aarhus, Denmark	Sequence analysis
Clustal Omega	(418)	Sequence alignments

Endnote X8	Thomson Reuters, New York City, USA	Organization of literature
Excel 2016	Microsoft, Albuquerque, NM, USA	Calculations and data processing
FiJi	(*419*)	Analysis of immunofluorescence data, analysis of signal intensities
FileMaker Pro 14	Claris, Cupertino, CA, USA	Management of group database
GPS-SUMO 1.0	(*420*)	Prediction of SCMs and SIMs
GraphPad PRISM 5	GraphPad, San Diego, CA, USA	Statistical analysis
HBV database	(*421*)	Source for HBV genome sequence data
LightCycler 480 Software	Roche, Basel, Switzerland	Analysis of qPCR data
PDB	Open Source (RCSB)	Source for protein structure data
PowerPoint 2016	Microsoft, Albuquerque, NM, USA	Data processing and presentation
PubMed	Open Source (NCBI)	Literature database, open source tools for sequence analysis
Quantity One	Bio-Rad, München, Germany	Analysis of agarose gels
qPCRsoft	Analytik Jena, Jena, Germany	Analysis of qPCR data
Serial Cloner	Serial Basics	Sequence analysis, generation of plasmid cards
Swiss Model	Open Source online tool (*422*)	Modeling of SCM mutant HBV core protein structures
Volocity	Quorum Technologies Puslinch, O, USA	Acquistion and processing of fluorescence microscopy pictures (Nikon TiE microscope)
Word 2016	Microsoft, Albuquerque, NM, USA	Text processing
VMD molecular graphics viewer	(*423*)	Processing and visualization of protein structures
ZDOCK Server	(*424*)	*In silico* docking studies with protein structures
Zeiss Zen 3.2 blue	Zeiss, Oberkochen, Germany	Acquistion and processing of fluorescence microscopy pictures (Zeiss LSM980 microscope)

3.1.6 Bacterial strains

Table 6: Bacterial strains used in this dissertation

Bacterial strain	Characteristics	Reference
Escherichia coli DH5α	supE44, ΔlacU169, (φ80dlacZΔM15), hsdR17, recA1, endA1, gyrA96, thi-1, relA1	(425)

3.1.7 Human cell lines

Table 7: Human cell lines used in this dissertation

Database No.	Cell line	Characteristics	Reference
1	HepaRG *parental*	Human hepatoma cells able to differentiate into hepatocyte-like and biliary cells, susceptible to HBV infection	(426); ATCC
8	HEK293-T	Human embryonic kidney cell line, immortalized by HAdV-C5 infeciton and integration of the HAdV-C5 E1 region. Expressing SV-40 large T antigen	(427); ATCC
12	HepaRG *SUMO2*	HepaRG cell line with stable expression of His$_6$-tagged SUMO-2	(428), Prof. Ron Hay, University of Dundee
20	HepaRG *His/HA*	HepaRG cell line with stable expression of His$_6$-HA as control for HepaRG *SUMO2*	(428), Prof. Ron Hay, University of Dundee
49	HepaRG *shCTL*	HepaRG cells with stable expression of control shRNA	This work
51	HepaRG *shPML*	HepaRG cells with stable shRNA mediated depletion of all PML isoforms (shRNA: 5'-AGATGCAGCTGTATCCAAG-3')	This work, (429)
64	HepG2-NTCP-K7	Human hepatoma cells with stable overexpression of human NTCP receptor, susceptible to HBV infection	(133), Prof. Ulrike Protzer, Technical University Munich
110	HepG2 *shCTL*	HepG2-NTCP-K7 cells with stable expression of control shRNA	This work
74	HepG2 *shPML*	HepG2-NTCP-K7 cells with stable shRNA mediated depletion of all PML isoforms (shRNA: 5'-AGATGCAGCTGTATCCAAG-3')	This work, (429)
43	HepG2 *PML-I*	HepG2 *shPML* cells stably expressing shRNA resistant GFP-PML-I	This work, (338)

44	HepG2 *PML-II*	HepG2 *shPML* cells stably expressing shRNA resistant GFP-PML-II	This work, (*338*)
45	HepG2 *PML-III*	HepG2 *shPML* cells stably expressing shRNA resistant GFP-PML-III	This work, (*338*)
46	HepG2 *PML-IV*	HepG2 *shPML* cells stably expressing shRNA resistant GFP-PML-IV	This work, (*338*)
47	HepG2 *PML-V*	HepG2 *shPML* cells stably expressing shRNA resistant GFP-PML-V	This work, (*338*)
48	HepG2 *PML-VI*	HepG2 *shPML* cells stably expressing shRNA resistant GFP-PML-VI	This work, (*338*)

5.1.8 Primer

Primers were obtained from Metabion (Planegg, Germany)

Table 8: Primer used in this dissertation

Database No.	Primer	Sequence (5'-3')
104	qPCR-PRNP fwd	TGCTGGGAAGTGCCATGAG
105	qPCR-PRNP rev	CGGTGCATGTTTTCACGATAGTA
106	qPCR-cccDNA 971 fwd	GCCTATTGATTGGAAAGTATGT
107	qPCR-cccDNA 2010 rev	AGCTGAGGCGGTATCTA
108	qPCR-HBV-comp 465 fwd	GTTGCCCGTTTGTCCTCTAATTC
109	qPCR-HBV-comp 564 rev	GGAGGGATACATAGAGGTTCCTTGA
197	qPCR-GAPDH fwd	CATCCTGGGCTACACTGA
198	qPCR-GAPDH rev	TTGACAAAGTGGTCGTTG
340	qPCR-PML fwd	GCTGCCAGCAATGCCAGCAATGCCAGG
341	qPCR-PML rev	GCAGCGGGTGCACACAGC
424	HBV core K7R rev	GGGTCGATGTCCATGAATTC
425	HBV core K7R fwd	TTATAGAGAATTTGGAGCTACTGTGGAG
426	HBV core K96R rev	TAGGCCCATATTAGTGTTGAC
428	HBV core K96R fwd	AGGTTCAGGCAACTCTTGTGG
469	Sequencing_CMV fwd	GGTAGGCGTGTACGGTGG
917	HBV-ChIP 254-428 fwd	TCGTGGTGGACTTCTCTCAA
918	HBV ChIP 254-428 rev	TGAGGCATAGCAGCAGGAT
919	HBV ChIP 462-562 fwd	GTTGCCCGTTTGTCCTCTAATTC
920	HBV ChIP 462-562 rev	GGAGGGATACATAGAGGTTCCTTGA
921	HBV ChIP 1089-1154 fwd	GCTTTCACTTTCTCGCCAAC
922	HBV ChIP 1089-1154 rev	AACGGGGTAAAGGTTCAGGT
923	HBV ChIP 1305-1438 fwd	AGCAGGTCTGGAGCAAACAT
924	HBV ChIP 1305-1438 rev	GACGGGACGTAAACAAAGGA

925	HBV ChIP 1581-1693 fwd	GTGCACTTCGCTTCACCTCT
926	HBV ChIP 1581-1693 rev	GGTCGTTGACATTGCAGAGA
927	HBV ChIP 1901-2054 fwd	GCATGGACATCGACCCTTAT
928	HBV ChIP 1901-2054 rev	TGAGGTGAACAATGCTCAGG
929	HBV ChIP 2112-2297 fwd	CTGGGTGGGTGTTAATTTGG
930	HBV ChIP 2112-2297 rev	TAAGCTGGAGGAGTGCGAAT
931	HBV ChIP 2279-2392 fwd	TTCGCACTCCTCCAGCTTAT
932	HBV ChIP 2279-2392 rev	GAGGCGAGGGAGTTCTTCTT
933	HBV ChIP 2983-3133 fwd	ACAAGGTAGGAGCTGGAGCA
934	HBV ChIP 2983-3133 rev	GTAGGCTGCCTTCCTGTCTG

3.1.9 Plasmids

Table 9: Vectors and recombinant plasmids used in this dissertation

Database No.	Plasmid	Description	Reference
V18	pcDNA-HA-Eco-if (pcDNA-HA)	Empty pcDNA vector with HA-tag, EcoRI restricition site in frame to start codon of HA-tag	Group database
L1	pCMV-VSV-G	Plasmid encoding VSV-G antigen, for generation of lentiviral particles	(*430*)
L2	pMDLg-pRRE	Plasmid encoding HIV Gag, integrase, Pol and Rev responsive element, for generation of lentiviral particles	(*431*)
L3	pRSV-rev	Plasmid encoding HIV Rev, for generation of lentiviral particles	(*431*)
SH3	pLKO-shPML	Plasmid encoding a shRNA directed against all human PML isoforms and a puromycin resistance (shRNA: 5'-AGATGCAGCTGTATCCAAG-3')	(*429*), Prof. Roger Everett, University of Glasgow
SH14	pLKO-shCTL	Plasmid encoding a scrambled control shRNA and a puromycin resistance	Sigma-Aldrich, Darmstadt, Germany
P73	pLKO-GFP-PML-I	Lentiviral plasmid encoding shRNA resistant PML isoform I with N-terminal GFP-tag and a G418 resistance	(*338*), Prof. Roger Everett, University of Glasgow

P74	pLKO-GFP-PML-II	Lentiviral plasmid encoding shRNA resistant PML isoform II with N-terminal GFP-tag and a G418 resistance	(*338*), Prof. Roger Everett, University of Glasgow
P75	pLKO-GFP-PML-III	Lentiviral plasmid encoding shRNA resistant PML isoform III with N-terminal GFP-tag and a G418 resistance	(*338*), Prof. Roger Everett, University of Glasgow
P76	pLKO-GFP-PML-IV	Lentiviral plasmid encoding shRNA resistant PML isoform IV with N-terminal GFP-tag and a G418 resistance	(*338*), Prof. Roger Everett, University of Glasgow
P77	pLKO-GFP-PML-V	Lentiviral plasmid encoding shRNA resistant PML isoform V with N-terminal GFP-tag and a G418 resistance	(*338*), Prof. Roger Everett, University of Glasgow
P78	pLKO-GFP-PML-VI	Lentiviral plasmid encoding shRNA resistant PML isoform VI with N-terminal GFP-tag and a G418 resistance	(*338*), Prof. Roger Everett, University of Glasgow
P567	pHBc	Plasmid coding for HBV core protein, subtype ayw, genotype D	Prof. Ulrike Protzer, Technical University Munich
P512	pcore-HA *wt*	pcDNA-HA based plasmid coding for *wt* HBV core-HA, subtype ayw, genotype D with an N-terminal HA-tag	This work
P513	pcore-HA *Δscm1*	pcDNA-HA based plasmid coding for *Δscm1* (K7R) HBV core-HA, subtype ayw, genotype D with an N-terminal HA-tag	This work
P515	pcore-HA *Δscm2*	pcDNA-HA based plasmid coding for *Δscm2* (K96R) HBV core-HA, subtype ayw, genotype D with an N-terminal HA-tag	This work
P516	pcore-HA *Δscm1/2*	pcDNA-HA based plasmid coding for *Δscm1/2* (K7R, K96R) HBV core-HA, subtype ayw, genotype D with an N-terminal HA-tag	This work

P674	pHBV1.1 *wt*	Plasmid encoding a 1.1x copy of a *wt* HBV genome, subtype ayw, genotype D, controlled by HCMV promoter	(*182*), Prof. Ulrike Protzer, Technical University Munich
P675	pHBV1.1 *Δscm1*	Plasmid encoding a 1.1x copy of a *Δscm1* (K7R) HBV genome, subtype ayw, genotype D, controlled by HCMV promoter	This work
P676	pHBV1.1 *Δscm2*	Plasmid encoding a 1.1x copy of a *Δscm2* (K96R) HBV genome, subtype ayw, genotype D, controlled by HCMV promoter	This work
P677	pHBV1.1 *Δscm1/2*	Plasmid encoding a 1.1x copy of a *Δscm1/2* (K7R, K96R) HBV genome, subtype ayw, genotype D, controlled by HCMV promoter	This work

3.1.10 Antibodies

Table 10: Primary antibodies used in this dissertation

Database No.	Antibody	Properties	Supplier	Dilution
17	PML (sc-966)	Mouse monoclonal anti-PML antibody	Santa Cruz, Heidelberg, Germany	Western Blot: 1:1000 IF: 1:200
21	HA	Rat polyclonal anti-HA antibody	MAB, Helmholtz Zentrum Munich, Germany	Western Blot: 1:10 IF: 1:10 IP: 1µl/IP
39	GFP (ab290)	Rabbit polyclonal anti-GFP antibody	Abcam, Cambridge MA, USA	Western Blot: 1:2000 IF: 1:500 IP: 0.2µl/IP
41	6-His	Mouse monoclonal anti-His$_6$ antibody	Clontech/Takara, Göteborg, Sweden	Western Blot: 1:5000 IF: /
60	HBV core (8C9)	Mouse monoclonal anti-HBV core antibody	MAB, Helmholtz Zentrum Munich, Germany	Western Blot: 1:2 IF: /
61	β-Actin (NC-15)	Mouse monoclonal anti-β-Actin antibody	Sigmal Aldrich, Hamburg, Germany	Western Blot: 1:5000 IF: /

67	HBV core (sc-23945)	Mouse monoclonal anti-HBV core antibody	Santa Cruz, Heidelberg, Germany	Western Blot: / IF: 1:100
133	SUMO2/3 (ab81371)	Mouse monoclonal anti-SUMO2/3 antibody	Abcam, Cambridge MA, USA	Western Blot: 1:2000 IF: /
140	PML (ab72137)	Rabbit polyclonal anti PML antibody	Abcam, Cambridge MA, USA	Western Blot: 1:2000 IF: 1:200
177	HBV capsid (B0586)	Rabbit polyclonal anti HBV capsid antibody	DAKO/Agilent, Frankfurt a.M., Germany	Western Blot: 1:10000 IF: 1:10000

Table 11: Secondary antibodies for western blots used in this dissertation

Antibody	Properties	Supplier	Dilution
HRP-anti-mouse	Horseradish peroxidase conjugated goat-anti-mouse antibody	Dianova, Hamburg, Germany	1:10000
HRP-anti-rabbit	Horseradish peroxidase conjugated goat-anti-rabbit antibody	Dianova, Hamburg, Germany	1:10000
HRP-anti-rat	Horseradish peroxidase conjugated goat-anti-rat antibody	Dianova, Hamburg, Germany	1:10000
IRDye 800CW anti-rabbit	IRDye 800 CW conjugated goat-anti-rabbit antibody	LI-COR Biotechnology, Bad Homburg, Germany	1:10000

Table 12: Secondary antibodies for IF stainings used in this dissertation

Antibody	Properties	Supplier	Dilution
488-anti-mouse	Alexa-488 conjugated goat-anti-mouse antibody	Thermo Scientific, Dreieich, Germany	1:200
488-anti-rabbit	Alexa-488 conjugated goat-anti-rabbit antibody	Thermo Scientific, Dreieich, Germany	1:200
488-anti-rat	Alexa-488 conjugated goat-anti-rat antibody	Thermo Scientific, Dreieich, Germany	1:200
647-anti-mouse	Alexa-647 conjugated goat-anti-mouse antibody	Dianova, Hamburg, Germany	1:200
647-anti-rabbit	Alexa-647 conjugated goat-anti-rabbit antibody	Dianova, Hamburg, Germany	1:200
647-anti-rat	Alexa-647 conjugated goat-anti-rat antibody	Dianova, Hamburg, Germany	1.200

3.1.11 Viruses

Table 13: Viruses used in this dissertation

Virus	*Properties*	*Reference*
HBV	*Wild type* hepatitis B virus, serotype ayw, genotype D, isolated from supernatants of HepG2.2.15 cells	Prof. Ulrike Protzer, Technical University Munich
HBV *wt*	*Wild type* hepatitis B virus, serotype ayw, genotype D, isolated from supernatants of pHBV1.1 *wt* transfected cells according to 3.2.2.1	(*182*), Prof. Ulrike Protzer, Technical University Munich
HBV *Δscm1*	Hepatitis B virus harboring a K7R mutation in the HBV core protein, serotype ayw, genotype D, isolated from supernatants of pHBV1.1 *Δscm1* transfected cells according to 3.2.2.1	This work
HBV *Δscm2*	Hepatitis B virus harboring a K96R mutation in the HBV core protein, serotype ayw, genotype D, isolated from supernatants of pHBV1.1 *Δscm2* transfected cells according to 3.2.2.1	This work
HBV *Δscm1/2*	Hepatitis B virus harboring K7R and K96R mutations in the HBV core protein, serotype ayw, genotype D, isolated from supernatants of pHBV1.1 *Δscm1/2* transfected cells according to 3.2.2.1	This work

3.2 Methods

3.2.1 Cell culture

3.2.1.1 Maintenance of human cell lines

All cell lines were cultured as adherent monolayers on 150mm dishes at 37°C and 5% CO_2 in a Hera cell 150 CO_2 incubator. Cells were handled under sterile conditions and frequently tested for mycoplasma contamination. HepaRG cell lines were grown in DMEM (D6429) medium supplemented with 10% FCS, 5µg/ml of bovine insulin, 0.5µM hydrocortisone, 100U/ml of penicillin, and 100µg/ml of streptomycin. For the lentiviral transduced HepaRG *shCTL* and HepaRG *shPML* cell lines, additionally 2µg/ml of puromycin were added. For HepG2-NTCP-K7 cells and HepG2-NTCP-K7 based cell lines (HepG2 *shCTL*, HepG2 *shPML*, HepG2 *PML-I*, HepG2 *PML-II*, HepG2 *PML-III*, HepG2 *PML-IV*, HepG2 *PML-V*, and HepG2 *PML-VI*) all tissue culture dishes were coated with a 0.002% (V/V) solution of collagen in PBS. HepG2-NTCP-K7 cells were maintained in DMEM (D5671) supplemented with 10% FCS, 2mM L-glutamine, 1mM sodium pyruvate, 1mM non-essential amino acids, 100U/ml of penicillin, and 100µg/ml of streptomycin. For the HepG2-NTCP-K7 based cell lines HepG2 *shCTL* and HepG2 *shPML*, 2µg/ml of puromycin and for HepG2 *PML-I*, HepG2 *PML-II*, HepG2 *PML-III*, HepG2 *PML-IV*, HepG2 *PML-V*, and HepG2 *PML-VI*, 2µg/ml of puromycin and 2mg/ml of G418 were added to the medium. HEK293-T cells were grown in in DMEM (D6429) medium supplemented with 10% FCS, 100U/ml of penicillin, and 100µg/ml of streptomycin.

Thawing of cells

Frozen cells were thawed and resuspended in 10ml of corresponding medium. Cells were centrifuged at 2000rpm and room temperature (RT) for 3 min (Heraeus Megafuge 40) and the supernatant was discarded. The cell pellet was resuspended in 15ml of the corresponding medium and distributed on a 150mm plate.

Passaging of cells

To avoid death of cells due to overgrowth and starvation, cells were passaged once or twice a week. For passaging, the medium was removed and the cells were washed once with PBS. Cells were detached using 3ml of trypsin/EDTA and incubation for 5-10min at 37°C and 5% CO_2. Trypsin was inactivated and the cells were resuspended by addition of 7ml of the corresponding medium. The cells were transferred into falcon tubes and pelleted by centrifugation at 2000rpm and RT for 3min (Heraeus Megafuge 40). The supernatant was discarded and the pellet was resuspended in an appropriate amount of the corresponding

medium. Resuspended cells were either distributed on new plates for propagation (ratio 1:2-1:10) or counted using an improved Neubauer chamber for seeding for experiments as outlined in 3.2.1.2.

Freezing of cells

For long-term storage of cell lines, cells from 150mm plates were treated as described above, resuspended in a mixture of 10% (V/V) DMSO in FCS and transferred to cryotubes. Cells were frozen in a Mr Frosty freezing container at -80°C. After at least 5h, the cells were removed from the freezing container and stored at -80°C or in liquid nitrogen.

3.2.1.2 Seeding for experiments

For experiments, cells were treated as described above. The pellet was resuspended in 10 ml respective medium per 150mm dish and the cell count per ml was determined using an improved Neubauer chamber as follows:

$$Cell\ count\ \left(\frac{cells}{ml}\right) = Counted\ cells\ *\ 10^4$$

For HepaRG cells and HepaRG based cell lines, $2*10^5$ cells were seeded in 12 well plates, $4*10^5$ in 6 well plates, and $4*10^6$ in 100mm dishes. HepG2-NTCP-K7 and HepG2-NTCP-K7 based cell lines were seeded at $6*10^5$ cells/well in 12 well plates, $1.2*10^6$ cells/well in 6 well plates, and $8*10^6$ cells/dish in 100mm dishes. If cells were used for immunofluorescence stainings, a 12mm round glass coverslide was added to the tissue culture dishes prior to seeding. HEK293-T cells were seeded at $6*10^6$ cells/dish in 100mm dishes.

3.2.1.3 Transient transfection

Cells for transient transfection were seeded 24h prior to transfection as outlined in 3.2.1.2. Transient transfection of plasmid DNA was performed using linear 25kDa polyethyleneimine (PEI). PEI was dissolved in ddH$_2$O and NaOH at a concentration of 1mg/ml. The pH was adjusted to 7.3 with HCl (Mettler Toledo FiveEasy Plus FEP20 pH-Meter) and the solution was sterile filtered using a 0.45µm filter. Aliquots were stored at -80°C. For transfection, 10µg prewarmed (37°C) PEI per 1µg of transfected DNA was transferred to 2ml Eppendorf tubes. 2ml prewarmed (37°C) DMEM medium without supplements were added and the solution was mixed, briefly vortexed (Vortex-Genie 2T), centrifuged (Heraeus Fresco 21) and incubated for 15-20min at RT. The medium of the cells was removed, changed to DMEM medium without supplements and the transfection mixture was added to the cells. After 3h, the transfection mixture was replaced by corresponding medium with supplements. Depending on the experiment, the cells were harvested after 48h or 8d, with medium exchange every two days.

3.2.1.4 Generation of lentiviral particles

For generation of lentiviral particles, HEK293-T cells were seeded 24h prior to transfection as outlined in 3.2.1.2. Cells were transfected using PEI as described in 3.2.1.3 with 3µg of the corresponding lentiviral plasmid, encoding either an shRNA targeting PML (shPML, No. SH3, 5'-AGATGCAGCTGTATCCAAG-3'), a scambled control shRNA (shCTL, No. SH14), or eGFP-tagged, shRNA resistant PML isoforms I-VI (GFP-PML-I to -VI, No. P73-P78). In addition, 0.75µg of the helper plasmids pMDLg-pRRE and pRSV-rev, encoding HIV polymerase, integrase, Gag as well as Rev, and 1.5µg of the helper plasmid pCMV-VSV-G, encoding the vesicular stomatitis virus (VSV) G-antigen, were co-transfected. After 6-8h of incubation, the transfection mixture was replaced by DMEM medium (D6429) supplemented with 10% FCS, 100U/ml of penicillin, 100µg/ml of streptomycin, and 20mM of HEPES buffer. 72h post transfection (p.t.), the cells were harvested. Cell debris was removed by 10min centrifugation at 2000rpm and RT (Heraeus Megafuge 40). The lentivirus-containing supernatant was sterile filtered using a 0.45µm filter and aliquoted. Aliquots were immediately frozen in liquid nitrogen and stored at -80°C.

3.2.1.5 Generation of stable cell lines by lentiviral transduction

Stable cell lines were generated by lentiviral transduction, followed by selection using a suitable antibiotic. Cells were seeded in 12 well plates as described in 3.2.1.2 at 24h prior to transduction. For lentiviral transduction, the medium of the cells was removed and replaced by corresponding DMEM medium without supplements. 200-1000µl of lentivirus stock solution were added and the cells were incubated for 6h. The lentivirus was removed and the cells were incubated in corresponding medium with supplements for 20h. For selection of transduced cells, 2µg/ml puromycin for the shRNA targeting PML (shPML, No. SH3) and the scambled control shRNA (shCTL, No. SH14), or 2mg/ml G418 for eGFP-tagged shRNA resistant PML isoforms I-VI (GFP-PML-I -VI, No. P73-P78) were added to the medium. During the selection process, the medium was changed daily. Cell lines generated by lentiviral transduction were verified by immunofluorescence staining (see chapter 3.2.3.6) and western blot (see chapter 3.2.3.5). Depletion of PML expression by shRNA was further analyzed by mRNA extraction and qPCR. Therefore, HepG2 *shCTL* and HepG2 *shPML* were harvested by centrifugation at 8000rpm and RT for 3min (Heraeus Fresco 21). The supernatant was discarded and the cell pellet was washed once in 1ml PBS by resuspension and centrifugation at 8000rpm and RT for 3min (Heraeus Fresco 21). The supernatant was removed and the cells were resuspended in 400µl of TRIzol reagent. 200µl of chloroform was added and the samples were vortexed for 15s (Vortex-Genie 2T) prior to centrifugation at 14000rpm and 10°C for 15min (Heraeus Fresco 21). The aqueous mRNA containing phase was transferred into a fresh

---

1.5ml Eppendorf tube and precipitated by addition of 600µl isopropanol, followed by centrifugation at 14000rpm and 10°C for 15min (Heraeus Fresco 21). The supernatant was discarded and the pellet was washed by addition of 400µl of 75% (V/V) ethanol an centrifugation at 14000 rpm and RT for 10min (Heraeus Fresco 21). The mRNA pellet was dried at 42°C for 5min (Eppendorf Thermomixer comfort) and resuspended in 40µl ddH$_2$O. RNA concentration was determined using a NanoDrop 2000c spectrophotometer. For cDNA synthesis, 1000µg of mRNA were subjected to the Promega reverse transcription system according to table 14 and incubated at 42°C for 45min (Eppendorf Thermomixer comfort). The reaction was stopped by incubation at 95°C for 5min (Eppendorf Thermomixer comfort) and qPCR for PML gene expression (Primers No. 340 and 341) and GAPDH (Primers No. 197 and 198) as control were prepared and run according to tables 15 and 16. Expression levels were analyzed using the $2^{-\Delta\Delta Ct}$ method.

Table 14: Setup for cDNA synthesis

MgCl$_2$	4µl
10x RT buffer	2µl
dNTP mix	2µl
Oligo dT/random primer	1µl
RNAsin	0.5µl
AMV reverse transcriptase	0.7µl
mRNA template	1000ng
ddH$_2$O	Ad 20µl

Table 15: qPCR setup for determination of mRNA levels

Primer fwd (20µM)	0.5µl
Primer rev (20µM)	0.5µl
qPCR master mix (2x)	5µl
cDNA	4µl

Table 16: Cycling conditions for determination of mRNA levels

Denaturation	95°C	600s		
Amplification	95°C	30s	40x	
	62°C	30s		
	72°C	30s		Acquisition
Melting curve	65°C			
	95°C	Continuous		Acquisition

3.2.2 Hepatitis B virus

3.2.2.1 PEG precipitation of HBV

For isolation of crude HBV stocks from supernatans of pHBV1.1 transfected cells, HepaRG cells were seeded in 100mm tissue culture dishes 24h prior to transfection as described in 3.2.1.2. The cells were transfected with 10µg of either pHBV1.1 *wt*, pHBV1.1 *Δscm1*, pHBV1.1 *Δscm2*, or pHBV1.1 *Δscm1/2* accodring to 3.2.1.3. The medium of transfected cells was collected at days 3, 6 and 9 p.t. and stored at 4°C. For polyethylene glycol (PEG) precipitation of HBV virions, the cell debris was removed by centrifugation at 2000rpm and RT for 5 min (Heraeus Megafuge 40). The supernatant was transferred into a fresh falcon tube and 0.33 volumes of a 30% (w/V) PEG8000 solution in 1.5M NaCl were added. Virions were precipitated over night by rotation at 4°C (GFL 3025 spinning shaker). Samples were centrifuged at 4500rpm and 4°C for 30min (Hettich Rotina 420R). The supernatant was discarded and samples were again centrifuged at 4500rpm and 4°C for 15min (Hettich Rotina 420R). The remaining supernatant was aspirated and the pellet was covered in 0.01 volumes of PBS over night at 4°C. The pellet was resuspended, transferred into a fresh 1.5ml Eppendorf tube and centrifuged at 12000xg and 4°C (Heraeus Fresco 21). The virion containing supernatant was transferred to a fresh 1.5ml Eppendorf tube and stored at -80°C. Relative amount of virions was assumed based on native agarose gel electrophoresis (NAGE) as described in 3.2.2.4.

3.2.2.2 HBV infection

For HBV infection, HepG2-NTCP-K7 cells, or HepG2-NTCP-K7 based cell lines were seeded as outlined in 3.2.1.2. After 24h of cultivation, cells were differentiated for 2d by addition of corresponding medium supplemented with 2.5% (V/V) DMSO. HBV infection was performed 3d post seeding in corresponding medium containing 2.5% (V/V) DMSO and 4% (w/V) PEG8000. For 6 well plates, 1ml of inoculum was used and 0.5ml for 12 well plates. Cells were infected with multiplicities of infection (MOI) between 200 and 1000 genomic equivalents (GE) per cell (GE/cell), depending on the experiment. As uninfected mock control, cells were incubated in corresponding medium containing 2.5% (V/V) DMSO and 4% (w/V) PEG8000 without addition of virus. The respective necessary volume of virus stock solution based on the viral titer and the seeded cell count was determined as follows:

$$Volume_{Vius\ Stock} = \frac{Cell\ count * MOI\ (\frac{GE}{cell})}{Virus\ titer\ (\frac{GE}{ml})}$$

After 20h of incubation, the inoculum was removed and cells were washed twice in PBS. Cells were further cultivated in corresponding medium supplemented with 2.5% DMSO for up to 7d, with medium exchange every two days.

3.2.2.3 Determination of HBV DNA

For determination of complete HBV DNA and cccDNA from pHBV1.1 transfected HepaRG or HepaRG based cells, or HBV infected HepG2-NTCP-K7 and HepG2-NTCP-K7 based cell lines, the MachereyNagel NucleoSpin Tissue Kit was used. The cells were washed once with PBS, covered with 200µl of buffer T1 and incubated for 5-10min at 37°C. The lysed cells were scraped off the wells, transferred to a fresh 1.5ml Eppendorf tube and 25µl of proteinase K were added. Samples were incubated for 1-3h at 56°C and 800rpm (Eppendorf Thermomixer comfort). For complete lysis, 200µl buffer B3 were added and samples were incubated for 10min at 70°C and 800rpm (Eppendorf Thermomixer comfort). 210µl of 100% ethanol were added, the samples were transferred to NucleoSpin Tissue Columns and centrifuged at 11000xg and RT for 1min (Heraeus Fresco 21). The column was transferred to a fresh collection tube and washed with 500µl buffer BW by centrifugation at 11000xg and RT for 1min (Heraeus Fresco 21). The flow through was discarded and the column was washed with 600µl buffer B5 by centrifugation at 11000xg and RT for 1min (Heraeus Fresco 21). The flow through was discarded and the column was dried by centrifugation at 11000xg and RT for 2min (Heraeus Fresco 21). For elution, the column was transferred to a fresh 1.5ml Eppendorf tube and DNA was eluted by addition of 100µl of prewarmed (70°C) buffer BE, incubation for 5min and centrifugation at 11000xg and RT for 1min (Heraeus Fresco 21). The eluted DNA was stored at -20°C until further analysis.

Complete HBV DNA and PRNP were determined by quantitative polymerase chain reaction (qPCR) using the conditions shown in tables 17 and 18. Primers No. 108 and 109 were used for determination of complete HBV DNA and primers No. 104 and 105 for PRNP.

Table 17: qPCR setup for complete HBV DNA and PRNP

Primer fwd (20µM)	0.5µl
Primer rev (20µM)	0.5µl
qPCR master mix (2x)	5µl
Template DNA	4µl

3. Materials and Methods

Table 18: Cycling conditions for complete HBV DNA and PRNP qPCR

Denaturation	95°C	300s		
Amplification	95°C	25s	40x	
	60°C	10s		
	72°C	30s		Acquisition
Melting curve	65°C			
	95°C	Continuous		Acquisition

Prior to determination of cccDNA by qPCR, rcDNA and incomplete replication intermediates were removed by digestion of non-circular DNA by T5 exonuclease treatment as follows:

Table 19: T5 exonuclease treatment setup

Template DNA	8.5µl
NEB buffer 4 (10x)	1µl
T5 exonuclease	0.5µl

Samples were incubated at 37°C for 30min followed by inactivation of the T5 exonuclease at 99°C for 5min (Eppendorf Mastercycler). Samples were diluted with 30µl of ddH$_2$O and subjected to qPCR determination of cccDNA using primers No.106 and 107 and the following cycling conditions:

Table 20: qPCR setup for cccDNA

Primer fwd (20µM)	0.5µl
Primer rev (20µM)	0.5µl
qPCR master mix (2x)	5µl
Template DNA	4µl

Table 21: Cycling conditions for cccDNA qPCR

Denaturation	95°C	600s		
Amplification	95°C	15s	40x	
	60°C	5s		
	72°C	45s		
	88	2s		Acquisition
Melting curve	65°C			
	95°C	Continuous		Acquisition

qPCR reactions were either run using the qPCR master mix LightCycler 480 SYBR Green I Master and the LightCycler 480 II (figure 18, figure 19) or using Luna Universal qPCR master mix and the qTower^3 (figure 36, figure 28, figure 41).

3.2.2.4 Native agarose gel electrophoresis

To assess HBV nucleocapsid formation and stability, native agarose gel electrophoresis (NAGE) was performed. Either recombinantly expressed and purified nucleocapsids, which were a kind gift of Prof. Dr. Michael Nassal (Univiersity Hospital Freiburg), were used or HBV nucleocapsids were isolated from pHBV1.1 transfected HepaRG cells as follows. Cells were washed twice with ice cold PBS 8 days post transfection (d.p.t.), covered with 400μl of NP40 lysis buffer, scraped off the wells and transferred to a 1.5ml Eppendorf tube. Samples were incubated on ice for 10min and the nuclei were pelleted by centrifugation at 12000xg and 4°C for 15 min (Heraeus Fresco 21). The supernatant was transferred to a fresh 1.5ml Eppendorf tube and stored at -20°C.

Samples were mixed with 6x NAGE loading dye prior to agarose gel electrophoresis. Agarose gels with concentrations of 1.2% (w/V) agarose in TBE (Tris/boric acid/EDTA) buffer were prepared and run in TBE buffer at 90V for 1-2h (VWR PerfectBlu Wide Format Gel System Maxi ExW, Bio-Rad PowerPac 3000). The capsids were then transferred to 0.2μm nitrocellulose membranes by capillary transfer using 10x SSC buffer over night. Following the transfer, the membrane was washed in PBS containing 0.1% Tween-20 (PBS-T) and blocked in 5% skim milk powder in PBS (5% M-PBS) for 1h at RT (GFL orbital shaker). The membrane was washed three times in PBS-T and incubated in primary antibody raised against HBV nucleocapsids (DAKO B0586) diluted 1:10000 in PBS-T for 5h to over night at 4°C (GFL orbital shaker). The membrane was washed three times with PBS-T and incubated for at least 2h in 3% skim milk powder in PBS-T (3% M-PBS-T) supplemented with a 1:10000 dilution of anti-rabbit secondary antibody coupled to either horseradish peroxidase (HRP) (figure 17, figure 30 A) or IRDye 800CW (figure 30 B, NAGE) (GFL orbital shaker). The mebrane was washed three times with PBS-T and signals were detected using ECL solution and X-ray films for blots incubated with HRP coupled secondary antibodies (AGFA Curix 60) or using a Bio-Rad ChemiDoc MP imaging system for membranes incubated with IRDye 800CW coupled secondary antibodies. For deveopling with ECL solution, 10ml of ECL A were mixed with 100μl of ECL B and 10μl of a 30% (V/V) H_2O_2 solution. Signal density was determined using *FiJi* (*419*).

For determination of HBV core protein levels in the preparations, samples were mixed with 2xLaemmli buffer and incubated at 95°C for 5min before separation by denaturing

sodiumdodecylsulfate polyacrylamide gel electrophoresis (SDS-PAGE) and western blot as described in 3.2.3.4 and 3.2.3.5.

Table 22: Composition of NP40 lysis buffer for NAGE

Tris-HCl, pH 8.0	50mM
NaCl	100mM
EDTA	1mM
NP40	1% (V/V)

Table 23: Composition of 6x NAGE loading dye

Glycerol	50% (V/V)
Bromophenol blue	0.1% (w/V)

Table 24: Composition of TBE buffer

Tris-HCl, pH 7.6	0.13mM
Boric acid	45mM
EDTA	2.5mM

Table 25: Composition of ECL A

Tris-HCl	100mM
Luminol sodium salt	250mg/ml

Table 26: Composition of ECL B

p-Coumaric acid	1.25mg/ml
Dissolved in DMSO	

Table 27: Composition of 2xLaemmli buffer

Tris-HCl, pH 6.8	100mM
Glycerol	20% (V/V)
SDS	4% (w/V)
Bromophenol blue	0.2% (w/V)
β-mercaptoehanol	1.5% (V/V)

3.2.2.5 CUT&RUN assay

For determination of host cell protein binding to HBV DNA, the Cell Signaling Technologies CUT&RUN assay kit was used. 10µl of convacalin A beads per reaction were transferred to a fresh 1.5ml Eppendorf tube and 100µl of convacalin A bead activation buffer per reaction was added. The tube was placed on a magnetic rack for 1min and the supernatant was removed. The convacalin A beads were washed two times in 100µl convacalin A bead activation buffer per reaction by resuspension, followed by magnetization of beads for 1min on a magnetic rack and removal of the supernatant. The convacalin A beads were resuspended in 10µl of convacalin A bead activation buffer per reaction and stored on ice until further use. HepG2-NTCP-K7 cells were infected with HBV at a MOI of 1000 GE/cell as described in 3.2.2.2 and harvested 7 days post infection (d.p.i.). Therefore, the cells were washed two times with PBS, scraped off the wells, transferred to a 1.5ml Eppendorf tube and centrifuged at 600xg and RT for 3min (Heraeus Fresco 21). The supernatant was discarded and cells were washed twice in 1ml of washing buffer supplemented with spermidine and protease inhibitors by

resuspension, centrifugation at 600xg and RT for 3min (Heraeus Fresco 21), and removal of the supernatant. For each reaction, 300000 cells were used and cells were permeabilized with 150% of the recommended volume of digitonin. Washed cells were resuspended in 100µl of washing buffer supplemented with spermidine and protease inhibitors per reaction, 100µl were transferred to a fresh 1.5ml Eppendorf tube, and stored on ice until further processing as input sample. 10µl of activated convacalin A beads per reaction were added to the samples and the cells were rotated at RT for 5min (GFL 3025 spinning shaker). The samples were centrifuged at 100xg and RT for 30s (Heraeus Fresco 21) and placed on a magnetic rack. The supernatant was removed and the cells were resuspended in 100µl antibody binding buffer per reaction supplemented with spermidine, protease inhibitors, and digitonin. For each reaction, 100µl were transferred into a fresh 1.5ml Eppendorf tube. For binding of the primary antibody, 0.6µl of rabbit anti-PML antibody ab72137 were added. As positive control 2µl of Tri-methyl-histone H3 antibody and as negative control 5µl of rabbit DA1E IgG isotype control were used. Both control antibodies were included in the CUT&RUN assay kit. Samples were rotated for 2h at 4°C (GFL 3025 spinning shaker). Samples were centrifuged at 100xg and RT for 30s (Heraeus Fresco 21) and placed on a magnetic rack. The supernatant was removed and the cells were resuspended in 1ml of digitonin buffer supplemented with spermidine, protease inhibitors, and digitonin. The samples were placed on a magnetic rack and the supernatant was discarded. The cells were resuspended in 50µl of digitonin buffer supplemented with spermidine, protease inhibitors, digitonin, and 1.5µl of pAG-MNase and rotated for 1h at 4°C (GFL 3025 spinning shaker). The samples were centrifuged at 100xg and RT for 30s (Heraeus Fresco 21), and placed on a magnetic rack. The supernatant was removed and the cells were washed two times in 1ml of digitonin buffer supplemented with spermidine, protease inhibitors, and digitonin. For digestion of DNA, the samples were resuspended in 150µl digitonin buffer supplemented with spermidine, protease inhibitors, and digitonin and 3µl of cold calcium chloride was added to the samples. Samples were incubated at 4°C for 30min and the digestion was stopped by addition of 150µl stop buffer supplemented with digitonin and RNAse A. For diffusion of the DNA, the samples were incubated at 37°C for 30min (Eppendorf Thermomixer comfort). Samples were centrifuged at 16000xg and 4°C for 2min (Heraeus Fresco 21) and the tubes were placed on a magnetic rack for 1min. The supernatant containing the enriched DNA was transferred into a fresh 1.5ml Eppendorf tube and stored on ice until DNA purification.

For preparation of the input DNA sample, 200µl of DNA extraction buffer supplemented with proteinase K and RNAse A were added to the cells and incubated at 55°C and 400rpm for 1h (Eppendorf Thermomixer comfort). The tubes were cooled on ice prior to chromatin shearing

using a 30s on/30s off interval for 5 cycles at low output (Bioruptor plus). The lysates were clarified by centrifugation at 16000xg and 4°C for 10min (Heraeus Fresco 21) and the supernatant was transferred into a fresh 1.5ml Eppendorf tube.

The input samples, as well as the enriched DNA from the CUT&RUN assay were further purified using Cell Signaling Technologies DNA purification buffers and spin columns. 1.5ml of DNA binding buffer were added to each sample and the complete samples were loaded on DNA spin columns in steps of 600μl by centrifugation at 16000xg and RT for 30s (Heraeus Fresco 21). The column was washed by addition of 750μl of DNA wash buffer and centrifugation at 16000xg and RT for 30s (Heraeus Fresco 21). The flow through was discarded and the column was dried by centrifugation at 16000xg and RT for 30s (Heraeus Fresco 21). The column was transferred into a fresh 1.5ml Eppendorf tube and the DNA was eluted by addition of 50μl DNA elution buffer and centrifugation at 16000xg and RT for 30s (Heraeus Fresco 21). After elution, the DNA was diluted with 50μl ddH$_2$O and stored at -20°C until analysis by qPCR.

For qPCR analysis, the following parameters were used:

Table 28: qPCR setup for CUT&RUN

Primer fwd (20μM)	0.5μl
Primer rev (20μM)	0.5μl
qPCR master mix (2x)	5μl
Template DNA	4μl

Table 29: Cycling parameters for CUT&RUN qPCR

Denaturation	95°C	180s		
Amplification	95°C	15s	45x	
	60°C	60s		Acquisition
Melting curve	65°C			
	95°C	Continuous		Acquisition

qPCR reactions were run using Luna Universal qPCR master mix and the qTower[3]. As positive control, primers for human Rpl30 were used, which were included in the CUT&RUN Assay Kit. For determination of HBV DNA, primers No. 917-934 were used.

3.2.2.6 Ginkgolic acid treatment

For inhibition of SUMOylation, ginkgolic acid (15:1) was used. Ginkgolic acid (GA) was dissolved in DMSO to a stock solution of 20mM and stored at -20°C. For inhibition of SUMOylation during HBV infection, ginkgolic acid was added to differentiated HepG2-NTCP-K7 cells 8h prior to infection and during infection at concentrations of 10µM and 15µM. As control, DMSO treated cells were used. Total time of ginkgolic acid treatment was 24h.

3.2.3 Protein biochemistry methods

3.2.3.1 Whole-cell protein lysates

For analysis of protein levels, whole-cell protein lysates were prepared using radio-immunoprecipitation assay (RIPA) lysis buffer. Cells were harvested by scraping them off the tissue culture dishes using a cell scraper and transferred into 15ml or 50ml falcon tubes. Cells were pelleted by centrifugation at 2000rpm and RT for 3min (Heraeus Megafuge 40). The supernatant was removed and the cells were resuspended in 5ml of PBS. The cells were centrifuged at 2000rpm and RT for 3min (Heraeus Megafuge 40), supernatant was removed, and the pellet was stored at -20°C until lysis.

For lysis, the pellet was resuspended in a volume of 100-1000µl of RIPA lysis buffer supplemented with 0.2mM PMSF, 1mg/ml pepstatin, 20mg/ml leupetin, 5mg/ml aprotinin, and 25mM iodoacetamide and N-ethylmaleimide, depending on the size of the pellet. Lysates were incubated on ice for 30min and vortexed every 10min (Vortex-Genie 2T). For improved lysis, the samples were sonicated for 30s in a precooled Sonifier 450 (80% output, 0.8 pulses/s, 40 pulses). After homogenization, cell debris was removed by centrifugation at 11000rpm and 4°C for 3 min (Heraeus Fresco 21). The supernatant was transferred to a fresh 1.5ml Eppendorf tube and the total protein concentration was determined using the Bradford method. 1µl of lysate was transferred into a 10mm microcuvette containing 800µl ddH$_2$O. 200µl of Bradford reagent was added, the samples were mixed and measured in a Smart spec plus spectrophotometer. As standard curve, BSA dilutions at concentrations of 1, 2, 4, 8, and 16µg/µl were used. Samples were diluted with ddH$_2$O and 5xLaemmli buffer was added to reach a final protein concentration of 5µg/µl. The samples were heated to 95°C for 3min (Eppendorf Thermomixer comfort) and stored at -20°C until further analysis by SDS-PAGE (see chapter 3.2.3.4) and western blot (see chapter 3.2.3.5).

3. Materials and Methods

Table 30: Composition of RIPA buffer

Tris-HCl, pH 8.0	50mM
NaCl	150mM
EDTA	5mM
NP40	1% (V/V)
SDS	0.1% (w/V)
Sodium deoxycholate	0.1% (w/V)

Table 31: Composition of 5xLaemmli buffer

Tris-HCl, pH 6.8	250mM
Gylcerol	50% (V/V)
SDS	10% (w/V)
Bromophenol blue	0.5% (w/V)
β-mercaptoehanol	3.75% (V/V)

3.2.3.2 Co-immunoprecipitation

For determination of protein-protein interactions, co-immunoprecipitation (co-IP) assays were performed. Lysates were prepared as described in 3.2.3.3 and 2000-3000µg of protein lysate were subjected to pre-clearing with pansorbin to reduce background caused by unspecific binding of proteins. Per reaction, 30µl pansorbin were transferred to a 1.5ml Eppendorf tube and centrifuged at 6000rpm and 4°C for 3min (Heraeus Fresco 21). The supernatant was removed and the pellet was washed twice by resuspension in 1ml of RIPA buffer and centrifugation at 6000rpm and 4°C for 3min (Heraeus Fresco 21). Pansorbin was resuspended in 100µl RIPA buffer per reaction and 100µl pansorbin were added to the prepared lysate. The lysates were rotated for 30min at 4°C (GFL 3025 spinning shaker). Pansorbin was pelleted by centrifugation at 6000rpm and 4°C for 3min (Heraeus Fresco 21). The pre-cleared lysate was then subjected to co-immunoprecipitation using either sepharose beads loaded with protein A (figure 9 A, figure 16) or magnetic beads loaded with protein A (figure 23, IP-GFP) or protein G (figure 23, IP-HA).

Co-immunoprecipitation using sepharose A beads

For co-IP assays using sepharose A beads, 3mg of sepharose A beads per reaction were transferred into a 1.5ml Eppendorf tube and 1ml of RIPA buffer was added. The beads were rotated at 4°C for 20min (GFL 3025 spinning shaker), centrifuged at 600rpm and 4°C for 3min (Heraeus Fresco 21) and the supernatant was discarded. Sepharose A beads were washed twice by resuspension in 1ml of RIPA buffer and centrifugation at 6000rpm and 4°C for 3min (Heraeus Fresco 21). For coupling of antibodies, the sepharose A beads were resuspended in 1ml of RIPA buffer and the respective volume of primary antibody was added (see table 10). The beads were rotated for 30min at 4°C (GFL 3025 spinning shaker), centrifuged at 6000rpm and 4°C for 3min (Heraeus Fresco 21), and washed two times using 1ml of RIPA buffer and centrifugation at 6000rpm and 4°C for 3min (Heraeus Fresco 21) to remove unbound antibody. The sepharose A beads were resuspended in 100µl of RIPA buffer per reaction and 100µl were transferred to the pre-cleared lysates. The lysates were rotated with

the sepharose A beads for 1h at 4°C (GFL 3025 spinning shaker). After incubation, the beads were centrifuged at 6000rpm and 4°C for 3min (Heraeus Fresco 21) and the supernatant was discarded. Beads were washed two times using 1ml of RIPA buffer and centrifugation at 6000rpm and 4°C for 3min (Heraeus Fresco 21). To elute the proteins, 20µl of 2xLaemmli buffer were added and the samples were heated to 95°C for 5min (Eppendorf Thermomixer comfort). Samples were stored at -20°C until analysis by SDS-PAGE (see chapter 3.2.3.4) and western blot (see chapter 3.2.3.5). Prior to loading to the SDS-PAGE, the sepharose A beads were pelleted by centrifugation at 14000rpm and RT for 5min (Heraeus Fresco 21).

Co-immunoprecipitation using magnetic beads

For co-IP assays using magnetic beads, 50µl of magnetic beads per reaction were transferred to a fresh 1.5ml Eppendorf tube and placed on a magnetic rack for 1min. The supernatant was removed and the beads were washed twice with 1ml RIPA buffer, by magnetization and removal of the supernatant. For binding of the primary antibody, the beads were resuspended in 1ml of RIPA buffer, the respective volume of primary antibody was added (see table 10) and the beads were rotated at 4°C for 30min (GFL 3025 spinning shaker). The beads were placed on a magnetic rack and the supernatant was removed. Beads were washed twice with 1ml of RIPA buffer followed by magnetization and removal of the supernatant. The magnetic beads were resuspended in 100µl RIPA buffer per reaction, 100µl were added to the pre-cleared lysate, and the samples were rotated for 1h at 4°C (GFL 3025 spinning shaker). The samples were placed on a magnetic rack and the supernatant was removed. Beads were washed twice with 1ml of RIPA buffer followed by magnetization and removal of the supernatant. The bound proteins were eluted by addition of 20µl of 2xLaemmli and incubation at 95°C for 5min (Eppendorf Thermomixer comfort). The samples were briefly centrifuged (Heraeus Fresco 21) and placed on a magnetic rack. The eluate was transferred to a fresh 1.5ml Eppendorf tube and stored at -20°C until further analysis by SDS-PAGE (see chapter 3.2.3.4) and western blot (see chapter 3.2.3.5).

3.2.3.3 Determination of protein SUMOylation by nickel charged nitrilotriacetic acid resin precipitation

Protein SUMOylation in HepaRG *SUMO2* cells was determined using nickel charged nitrilotriacetic acid resin (NiNTA) precipitation. Transfected HepaRG *SUMO2* and HepaRG *His/HA* cells as control were harvested by scraping the cells off the tissue culture dishes using a cell scraper. The cells were transferred into 15ml falcon tubes and pelleted by centrifugation at 2000rpm and RT for 3min (Heraeus Megafuge 40). The supernatant was removed and the pellet was resuspended in 10ml of PBS. 1ml of the cell suspension was transferred to a fresh

1.5ml Eppendorf tube and centrifuged at 8000rpm and RT for 3min (Heraeus Fresco 21). The supernatant was discarded and the cells were processed as input sample as described in 3.2.3.1. The cell suspension in the falcon tubes was centrifuged at 2000rpm and RT for 3min (Heraeus Megafuge 40) and the supernatant was removed. The pellet was resuspended in 5ml of NiNTA buffer B1 and stored at -80°C.

Prior to the NiNTA precipitation, samples were thawed on ice and homogenized by three times 10s sonication in a precooled Sonifier 450 (80% output, 0.8 pulses/s, 40 pulses). Per reaction, 30µl of NiNTA resin were transferred to a fresh 1.5ml Eppendorf tube and centrifuged at 6000rpm and RT for 3min (Heraeus Fresco 21). The supernatant was removed and the resin was washed twice by resuspension in 1ml of NiNTA B1 buffer, centrifugation at 6000rpm and RT for 3min (Heraeus Fresco 21), and aspiration of the supernatant. The NiNTA resin was resuspended in 100µl NiNTA buffer B1 per reaction, 100µl were added to each sample, and the samples were rotated over night at 4°C (GFL 3025 spinning shaker). Samples were centrifuged at 4500rpm (Hettich Rotina 420R). The supernatant was discarded, the resin was resuspended in 1ml of NiNTA buffer B1, transferred to a fresh 1.5ml Eppendorf tube, and centrifuged at 6000rpm and RT for 3min (Heraeus Fresco 21). The supernatant was discarded, the resin was resuspended in 1ml of NiNTA buffer B2, and centrifuged at 6000rpm and RT for 3min (Heraeus Fresco 21). The supernatant was discarded and the resin was washed twice by resuspension in 1ml of NiNTA buffer B3, centrifugation at 6000rpm and RT for 3min (Heraeus Fresco 21), and removal of the supernatant. His_6-SUMO2 modified proteins were eluted by addition of 20µl of elution buffer, incubation for 10min at RT followed by 95°C for 3min (Eppendorf Thermomixer comfort). The samples were stored at -20°C until analysis by SDS-PAGE (see chapter 3.2.3.4) and western blot (see chapter 3.2.3.5). Prior to loading to SDS gels, the samples were centrifuged at 14000rpm and RT for 5min (Heraeus Fresco 21).

Table 32: Composition of NiNTA buffer B1

Guanidine hydrochloride	6M
NaH_2PO_4	100mM
Na_2HPO_4	
Tris-HCl, pH 8.0	10mM
Imidazole	20mM
β-mercaptoehanol	5mM

Table 33: Composition of NiNTA buffer B2

Urea	8M
NaH_2PO_4	100mM
Na_2HPO_4	
Tris-HCl, pH 8.0	10mM
Imidazole	20mM
β-mercaptoehanol	5mM

3. Materials and Methods

Table 34: Composition of NiNTA buffer B3

Urea	8M
NaH$_2$PO$_4$	100mM
Na$_2$HPO$_4$	
Tris-HCl, pH 6.3	10mM
Imidazole	20mM
β-mercaptoehanol	5mM

Table 35: Composition of NiNTA elution buffer

Tris-HCl, pH 6.3	150mM
Imidazole	200mM
SDS	0.1% (w/V)
Glycerol	30% (V/V)
Bromophenol blue	0.01% (w/V)
β-mercaptoehanol	720mM

3.2.3.4 SDS-PAGE

For protein analysis, protein lysates were subjected to SDS-PAGE and separated by their molecular weight. SDS gels were prepared according to tables 33-36 (Biometra Multigel) and run in TGS buffer at 15mA per gel for 1-2h, until the running front containing the bromophenol blue loading dye ran out (Multigel electrophoresis chamber, Biometra Standard Power Pack P25 T). For assignment of the respective molecular weights, the PageRuler prestained protein ladder plus was used.

Table 36: Composition of 10% stacking gels

30% Acrylamide/bisacrylamide	34% (V/V)
Tris-HCl, pH 8.0	250mM
SDS	0.1% (w/V)
APS	0.1% (w/V)
TEMED	0.6% (V/V)

Table 37: Composition of 12% stacking gels

30% Acrylamide/bisacrylamide	40% (V/V)
Tris-HCl, pH 8.0	250mM
SDS	0.1% (w/V)
APS	0.1% (w/V)
TEMED	0.6% (V/V)

Table 38: Composition of 15% stacking gels

30% Acrylamide/bisacrylamide	50% (V/V)
Tris-HCl, pH 8.0	250mM
SDS	0.1% (w/V)
APS	0.1% (w/V)
TEMED	0.6% (V/V)

Table 39: Composition of 5% collecting gels

30% Acrylamide/bisacrylamide	17% (V/V)
Tris-HCl, pH 6.3	120mM
SDS	0.1% (w/V)
APS	0.1% (w/V)
TEMED	0.6% (V/V)

Table 40: Composition of TGS running buffer

Tris	25mM
Glycine	200mM
SDS	0.1% (w/V)

3.2.3.5 Western Blot

After separation of protein lysates by their molecular weight using SDS-PAGE, the proteins were transferred to 0.2µm nitrocellulose membranes for analysis of SUMO2, His and HBV core, or 0.45µm nitrocellulose membranes for PML, GFP and β-Actin by western blot. Membranes and gels were assembled between four layers of whatman paper soaked in Towbin transfer buffer and proteins were transferred at 400mA for 90min in Towbin transfer buffer (Bio-Rad Trans Blot Cell, Bio-Rad PowerPac 3000). Following the transfer, the membrane was blocked in 5% M-PBS for 1h at RT (GFL orbital shaker). The membrane was washed three times in PBS-T and incubated in respective primary antibody diluted in PBS-T over night at 4°C (see table 10) (GFL orbital shaker). The membrane was washed three times with PBS-T and incubated for at least 2h in 3% M-PBS-T supplemented with a 1:10000 dilution of corresponding secondary antibody coupled to HRP (GFL orbital shaker). The mebrane was washed three times with PBS-T and signals were detected using ECL solution and X-ray films (AGFA Curix 60). For deveopling with ECL solution, 10ml of ECL A were mixed with 100µl of ECL B and 10µl of a 30% (V/V) H_2O_2 solution. Signal density was determined using _FiJi_ (_419_).

Table 41: Composition of Towbin transfer buffer

Tris	25mM
Glycine	200mM
Methanol	20% (V/V)
SDS	0.05% (w/V)

3.2.3.6 Immunofluorescence

To detect protein localization by immunofluorescence stainings, cells seeded on 12mm coverslides were fixed using 4% PFA in PBS. Therefore, the medium was removed and the cells were washed once with PBS. Cells were covered with 4% PFA in PBS and incubated for 15min at RT. The PFA solution was aspirated and the cells were washed twice with PBS. The PBS was removed, 1ml of PBS was added and the cells were stored at 4°C until further analysis. Depending on the experimental setup, a washout of the soluble protein fraction using a cytoskeleton (CSK) buffer was preformed prior to fixation (protocol adapted from (_432_)). For the CSK wash, the cells were overlayed with CSK buffer and incubated on ice for 5min. The CSK buffer was removed and the cells were fixed with 4% PFA in PBS as described above. Fixed cells were permeabilized by incubation in 0.5% (V/V) Triton X-100 in H_2O for 5min and washed once in TBS-BG (Tris-buffered saline-BSA, glycine). To avoid background signals by unspecific binding of the antibody, the coverslides were blocked using TBS-BG buffer for

30min at RT followed by incubation of the coverslides in a mixture of two primary antibodies diluted in PBS (see table 10) for 1h at RT or over night at 4°C. After incubation in primary antibody, the coverslides were wased three times in PBS-T and incubated in the respective secondary antibodies diluted 1:200 in PBS. For a nuclear staining, Dapi was added in a dilution of 1:200. Coverslides were incubated in the secondary antibody mixture for 2h at RT and washed three times in PBS-T. Coverslides were mounted on microscope slides using Mowiol 4-88 and dried over night at room temperature. Dried slides were stored at 4°C until analysis. Pictures were either taken using a Nikon TiE confocal laser scanning microscope and the *Volocity* software (figure 9, figure 10, figure 11, figure 15, figure 31, figure 32, figure 35) or a Zeiss LSM980 laser scanning microscope and the *Zeiss Zen 3.2 blue* software (figure 21, figure 22, figure 24, figure 26, figure 38). Analysis of co-localization by Pearson correlation coefficient was performed using *FiJi* (*419*).

Table 42: Composition of CSK buffer

HEPES, pH 6.8	10mM
NaCl	100mM
Sucrose	300mM
$MgCl_2$	3mM
EDTA	2mM
Triton X-100	0.5% (V/V)

Table 43: Composition of TBS-BG buffer

Tris-HCl, pH 7.6	20mM
NaCl	137mM
KCl	3mM
$MgCl_2$	1.5mM
Tween-20	0.05% (V/V)
Sodium azide	0.05% (w/V)
Glycine	5% (w/V)
BSA	5% (w/V)

Table 44: Composition of Mowiol 4-88

Glycerol	6g
Mowiol 4-88	2.4g
0.2M Tris-HCl, pH 8.5	12ml
ddH_2O	6ml

3.2.3.7 In vitro SUMOylation assay

Effects of SUMOylation on HBV nucleocapsids was determined using the Abcam *In vitro* SUMOylation assay system. Therefore, equal amounts of *wt* and *Δscm1/2* nucleocapsids, which were kindly provided by Prof. Dr. Michael Nassal (University Hospital Freiburg), were used in a reaction mixture as shown in table 42. As control, either Mg-ATP (figure 30 A) or SUMO1-3 (figure 30 B) were replaced by ddH_2O. Samples were incubated at 37°C for 1h (Eppendorf Thermomixer comfort). The samples were subsequently split and half of the

volume was supplemented with 2x NAGE loading buffer and subjected to NAGE as described in 3.2.2.4. The other half of the volume was mixed with 2xLaemmli buffer, incubated at 95°C for 5min (Eppendorf Thermomixer comfort) and analyzed by SDS-PAGE and western blot as outlined in 3.2.3.4 and 3.2.3.5.

Table 45: Setup for *in vitro* SUMOylation assay

Target protein	0.06µg
10x Buffer	2µl
Mg-ATP	1µl
SUMO E1 enzyme	1µl
SUMO E2 enzyme	1µl
SUMO1	0.5µl
SUMO2	0.5µl
SUMO3	0.5µl

3.2.4 Bacterial culture

3.2.4.1 Maintenance of bacterial cells

Escherichia coli (*E. coli*) DH5α were maintained in LB medium. DH5α strains transformed with plasmid DNA were grown under selective pressure of the respective antibiotic, which was either ampicillin at 100µg/ml or kanamycin at 50µg/ml. Solid cultures from transformed bacteria or stored glycerol stocks were plated on LB-agar plates and incubated at 37°C in a Memmert incubator. Liquid cultures for mini preparations (5ml culture volume) or maxi preparations (500ml culture volume) of plasmid DNA were inoculated with a single colony from solid cultures and incubated at 37°C and 150-180rpm (Multitron standard incubation shaker). To prepare bacterial strains for longterm storage, 5ml of a dense liquid culture were harvested by centrifugation at 4000rpm and RT for 5 min (Heraeus Rotina 420R). The medium was discarded and the bacteria were resuspended in 1ml of a 1:1 (V/V) mixture of LB-medium and 87% glycerol. The bacterial suspension was transferred to cryotubes and stored at -80°C as glycerol stocks.

Table 46: Composition of LB-medium

Trypton	10g/l
Yeast extract	5g/l
NaCl	5g/l

Table 47: Composition of LB-agar

Trypton	10g/l
Yeast extract	5g/l
NaCl	5g/l
Agar	15g/l

3.2.4.2 Generation of chemically competent E. coli DH5α

For preparation of chemically competent *E. coli* DH5α, the rubidium chloride method was used. Bacteria were streaked out from a glycerol stock on a LB-agar plate without antibiotics and incubated at 37°C over night (Memmert incubator). One colony was used to inoculate 10ml LB-medium which were incubated over night at 37°C and 180rpm (Multitron standard incubation shaker). The next day, 200ml of LB-medium were inoculated with 2ml of the over night culture and incubated at 37°C and 180rpm (Multitron standard incubation shaker) until a density (OD_{600}) of 0.43 was reached. OD_{600} was determined using a Smart spec plus spectrophotometer. The culture was cooled down in an ice-waterbath for 20min to stop growth of the bacteria, transferred to 50ml falcon tubes, and harvested by centrifugation at 3000rpm and 4°C for 5min (Heraeus Rotina 420R). The supernatant was discarded, the pellets were resuspended and pooled in 15ml TFBI buffer, and centrifuged at 3000rpm and 4°C for 5min (Heraeus Rotina 420R). The supernatant was discarded, the pellets were resuspended and pooled in 4ml TFBII buffer, and 100μl aliquots were transferred in precooled 1.5ml Eppendorf tubes. The aliquots were frozen in liquid nitrogen and stored at -80°C.

Table 48: Composition of TFBI buffer

Glycerol	15% (w/V)
$CaCl_2$	10mM
KOAc	30mM
$RbCl_2$	100mM
$MnCl_2$	50mM
	pH 5.8

Table 49: Composition of TFBII buffer

Glycerol	15% (w/V)
MOPS, pH 7.0	10mM
$CaCl_2$	75mM
$RbCl_2$	10mM

3.2.4.3 Transformation

For transformation of plasmid DNA, chemically competent DH5α were thawed on ice. 10μl of ligation or 50ng of plasmid DNA were transferred into a 5ml polypropylene tube. The chemically competent DH5α were resuspended, added to the DNA, and incubated on ice for 30min. Uptake of the plasmid DNA into the chemically competent bacteria was triggered by heatshock at 42°C for 30s in a waterbath. The bacteria were briefly cooled on ice, 1ml of LB-medium was added, and the culture was incubated at 37°C and 150-180rpm (Multitron standard incubation shaker). The suspension was plated on LB-agar plates containing the respective antibiotic and incubated at 37°C over night (Memmert incubator).

3.2.5 Molecular biology methods

3.2.5.1 Restriction digest

The coding sequence of the HBV core protein was isolated from pHBc (No. P567) by restriction digest with EcoRI-HF and XhoI. Therefore, 5µg of pHBc were supplemented with 2.5µl of each restrictrion enzyme, 10µl of Cutsmart buffer, and the mixture was incubated in a total volume of 100µl at 37°C and 300rpm for 2-3h (Eppendorf Thermomixer comfort). The respective destination vector pcDNA-HA (No. V18) was treated equally. The digested DNA was supplemented with 6x DNA loading dye, loaded on a preparative agarose gel, and separated by agarose gel electrophoresis as described in 3.2.5.2.

To determine insertion of the HBV core protein coding region in pcDNA-HA to generate pcore-HA, a control digest of DNA generated from mini preparations as described in 3.2.5.6 was performed. The isolated plasmid DNA from the mini preparation was dissolved in 17.5µl of ddH$_2$O, supplemented with 1µl of NEB buffer 3.1 and 0.5µl of NcoI, and incubated at 37°C and 300rpm for 2-3h (Eppendorf Thermomixer comfort). The digested DNA was supplemented with 6x DNA loading dye, loaded on an analytical agarose gel, and analyzed as described in 3.2.5.2.

3.2.5.2 Agarose gel electrophoresis

For agarose gel electrophoresis, 0.6% (w/V) agarose gels in TBE buffer were prepared. For preparative agarose gels, TBE buffer was supplemented with 1mM guanosine. As DNA stain, ethidium bromide at a final concentration of 0.5µg/ml was used. Samples were separated on agarose gels at 100-120V for 2-3h (VWR PerfectBlu Wide Format Gel System Maxi ExW, Bio-Rad PowerPac 3000) and a 1kb ladder was used for assignment of bands. Bands of interest were analyzed using the Universal Hood II Gel Doc station and *Quantity One* software for analytical agarose gels, and UV light at 366nm for preparative agarose gels.

3.2.5.3 Isolation of DNA from agarose gels

Bands of interest were determined as described in 3.2.5.2, cut out of the preparative agarose gel, minced, and transferred into a 1.5ml Eppendorf tube. DNA was extracted by centrifugation at 20000rpm and 10°C for 90min (Beckman-Coulter Avanti JE) and the DNA containing supernatant was transferred into a fresh 1.5ml Eppendorf tube. The DNA was precipitated by addition of 0.9 volumes of 2-propanol and 0.1 volume of 3M sodium acetate and centrifugation at 14800rpm and 10°C for 10min (Heraeus Fresco 21). The supernatant was discarded and the pellet was washed by addition of 400µl of 70% (V/V) EtOH and centrifugation at 14800rpm and 10°C for 5min (Heraeus Fresco 21). The supernatant was removed and the DNA containing pellet was dried at 42°C for 5min (Eppendorf Thermomixer

comfort). The DNA pellet was dissolved in an appropriate amount of 10mM Tris-HCl, pH 8.0 and stored at 4°C until further use.

3.2.5.4 Ligation

For ligation, the amount of DNA from the HBV core protein coding region and the pcDNA-HA vector backbone were estimated by analytical agarose gel electrophoresis as described in 3.2.5.2. Ligation reactions were performed with a 1:7 ratio of vector:insert in a total volume of 21µl containing 2µl of 10x DNA ligation buffer and 1µl of T4 DNA ligase and incubated over night at 13°C (Eppendorf Thermomixer comfort). About 1h prior to the transformation of the ligation reaction into chemically competent DH5α as described in 3.2.4.3, the temperature was increased to 37°C. Colonies were picked and cultivated for mini preparation as described in 3.2.4.1 and mini preparation was performed as outlined in 3.2.5.6. Positive clones were identified by control digest according to 3.2.5.1 and sequencing as described in 3.2.5.6.

3.2.5.5 Mutagenesis by inverse PCR

To generate pcore-HA *Δscm1* (No. P513), pcore-HA *Δscm2* (No. P515), pHBV1.1 *Δscm1* (No. P675) and pHBV1.1 *Δscm2* (No. P676), point mutations were introduced into pcore-HA *wt* (No. P512) and pHBV1.1 *wt* (No. P674) by inverse PCR using the following conditions (Eppendorf MasterCycler):

Table 50: Setup for mutagenesis by inverse PCR

Template DNA	50ng
Primer fwd	125ng
Primer rev	125ng
dNTP mix	2µl
PfuUltra II Fusion 10x buffer	5µl
PfuUltra II Fusion DNA polymerase	2µl
ddH$_2$O	Ad 50µl

Table 51: Cycling conditions for mutagenesis by inverse PCR

Denaturation	95°C	120s	
Amplification	95°C	60s	27x
	55°C	60s	
	72°C	180s	
Final elongation	68°C	600s	
	10°C	Continuous	

For generation of pcore-HA $\Delta scm1/2$ (No. P516) and pHBV1.1 $\Delta scm1/2$ (No. P677), pcore-HA $\Delta scm1$ (No. P513) and pHBV1.1 $\Delta scm1$ (No. P675) were used as template, respectively. Primers used for the mutagenesis were No. 424 and 425 ($\Delta scm1$) and No. 426 and 428 ($\Delta scm2$).

After the PCR based mutagenesis, the template was removed by DpnI digest. Therefore, the PCR mixture was supplemented with 10µl of Cutsmart buffer and 1µl of DpnI, filled up to a total volume of 100µl with ddH$_2$O, and incubated at 37°C for 1h (Eppendorf Thermomixer comfort). The reaction was stopped by incubation at 95°C for 5min (Eppendorf Thermomixer comfort), the DNA was supplemented with 6x DNA loading dye, and run on a preparative agarose gel as described in 3.2.5.2. The band of interest was isolated as outlined in 3.2.5.3 and the amount of DNA was estimated by analytical agarose gel electrophoresis as described in 3.2.5.2. A suitable amount of DNA was phosphorylated by addition of 2µl of 10x DNA ligation buffer and 1µl of T4 polynucleotide kinase, and incubation in a total volume of 20µl at 37°C for 1h (Eppendorf Thermomixer comfort). For ligation, 2µl of 10x DNA ligation buffer and 1µl of T4 DNA ligase were added, and the ligation was incubated at 13°C (Eppendorf Thermomixer comfort) over night in a total volume of 40µl. About 1h prior to the transformation of the ligation reaction into chemically competent DH5α as described in 3.2.4.3, the temperature was increased to 37°C. Colonies were picked and cultivated for mini preparation as described in 3.2.4.1 and mini preparation was performed as outlined in 3.2.5.6. Positive clones were identified by control digest according to 3.2.5.1 and sequencing as described in 3.2.5.6.

3.2.5.6 Preparation of plasmid DNA

Bacterial liquid cultures for mini and maxi preparation of plasmid DNA were prepared according to 3.2.4.1.

Mini preparation

Plasmid DNA mini preparations for identification of positive clones after molecular cloning or mutagenesis were performed using the P1, P2 and P3 buffers included in the QIAGEN Plasmid Maxi Kit. For each preparation, 200-1000µl of a bacterial liquid culture were transferred to a 1.5ml Eppendorf tube and harvested by centrifugation at 14800rpm and 10°C for 3min (Heraeus Fresco 21). The supernatant was discarded and the pellet was resuspended in 300µl buffer P1. Lysis was induced by addition of 300µl buffer P2 and the samples were mixed by inversion. Cell debris and proteins were precipitated by addition of 300µl buffer P3, the samples were mixed by inversion, and centrifuged at 14800rpm and 10°C for 10min (Heraeus Fresco 21). 800µl of the DNA containing supernatant were transferred to a fresh

1.5ml Eppendorf tube, precipitated as described in 3.2.5.3, and dried for 10min at 42°C (Eppendorf Concentrator 5301). DNA pellets were dissolved in 17.5µl ddH$_2$O and a control digest was performed according to 3.2.5.1.

Maxi preparation

Plasmid DNA for transient transfection was isolated using the QIAGEN Plasmid Maxi Kit from 500ml of bacterial liquid culture. In brief, the bacterial cultures were harvested by centrifugation at 4500rpm and 10°C for 20min (Heraeus Rotixa 50 RS). The pellet was resuspended in 10ml of buffer P1, 10ml of buffer P2 were added, and the cells were lysed by inversion. Lysis was stopped by addition of 10ml buffer P3 and inversion. The samples were centrifuged at 4500rpm and 10°C for 20min (Heraeus Rotina 420R) and the supernatant was transferred to an anion-exchange column, which was equilibrated with 5ml of buffer QBT. The column was washed twice with one column volume of buffer QC and the DNA was eluted using 15ml QF buffer. The DNA in the eluate was precipitated by addition of 12.5ml 2-propanol and centrifugation at 4500rpm and 10°C for 90min (Heraeus Rotina 420R). The supernatant was discarded and the DNA was washed once by addition of 5ml of 70% (V/V) EtOH and centrifugation at 4500rpm and 10°C for 10min (Heraeus Rotina 420R). The supernatant was discarded and the DNA was dried at RT. The DNA pellet was dissolved in a suitable volume of 10mM Tris-HCl, pH 8.0 and concentration was measured using a NanoDrop 2000c spectrophotometer.

All plasmids were verified by sequencing performed by Eurofins genomics. For sequencing, 1µg of DNA and 30pmol of primer No. 469 were diluted with ddH$_2$O to a total volume of 17µl.

3.2.6 *In silico* methods

3.2.6.1 In silico prediction of SCMs

In silico prediction of SCMs within the HBV core protein was performed using *GPS SUMO1.0* software (*420*). Consensus coding sequences of HBV core protein for genotypes A-H were retrieved from the *HBV database* (HBVdb) (*421*) and alignments were performed using *ClustalOmega* (*418*).

3.2.6.2 In silico modeling of HBV core protein SCM mutant structures

Effects of lysine to arginine mutations in HBV core protein on HBV nucleocapsid structure were determined by *in silico* modeling of the structure of HBV core protein K7R, K96R and K7/96R using *Swiss Model*, based on the tetrameric structure of HBV core protein (PDB: 3J2V) (*197*). Predicted structures were visualized using *VMD-Visual Molecular Dynamics* software and superimposed to the original HBV core tetrameric structure (*423*).

3.2.6.3 In silico modeling of HBV core protein SUMOylation

To asses the impact of HBV core protein SUMOylation on HBV capsid structure, *in silico* docking of the structure of SUMO2 (PDB: 2CHK_2) (*433*) to HBV core in HBV core protein tetramers (PDB: 3J2V) (*197*) was performed using the *ZDOCK Server* (*424*). Predicted structures were visualized using *VMD-Visual Molecular Dynamics* software and superimposed to the original HBV core tetrameric structure (*423*).

4. Results

4.1 HBV core protein is recruited to PML-NBs

Previous studies showed an association of the HBV core protein with PML-NBs during DNA damage in HBV producing cell lines with an integrated HBV genome (*250*). To first determine the interaction of HBV core protein with PML-NBs, independently of other viral proteins or nucleic acids, the HBV core coding sequence of genotype D subtype ayw was cloned into pcDNA-HA to enable HBV core protein expression with a N-terminal HA-tag. pcore-HA *wt* was transfected in HepaRG cells and the interaction of HBV core protein and PML was determined by immunoprecipitation using anti-HA antibodies and subsequent western blot analysis. The input showed expression of HA-tagged HBV core protein in pcore-HA *wt* transfected HepaRG cells (see figure 9 A, input, lane 2) and presence of HBV core protein did not alter PML steady state levels (see figure 9 A, input, lane 1, 2). In the immunoprecipitation, a co-precipitation of PML in the samples transfected with pcore-HA *wt* was observed, indicating an interaction between HBV core and PML during transfection (see figure 9 A, IP-HA, lane 2). PML did hereby not run in distinct bands but showed a more smeary running behaviour, which might be indicative of PML PTM (see figure 9 A, IP-HA, lane 2) (*434*).

These data were further confirmed using immunofluorescence analysis of the same cells. Co-staining of HA-tagged HBV core protein and PML confirmed the data of the immunoprecipitation. The overexpressed HA-tagged HBV core protein was found to localize in discrete dot-like structures with a distinct and almost exclusive co-localization with PML-NBs (see figure 9 B, panels f-h, j-l).
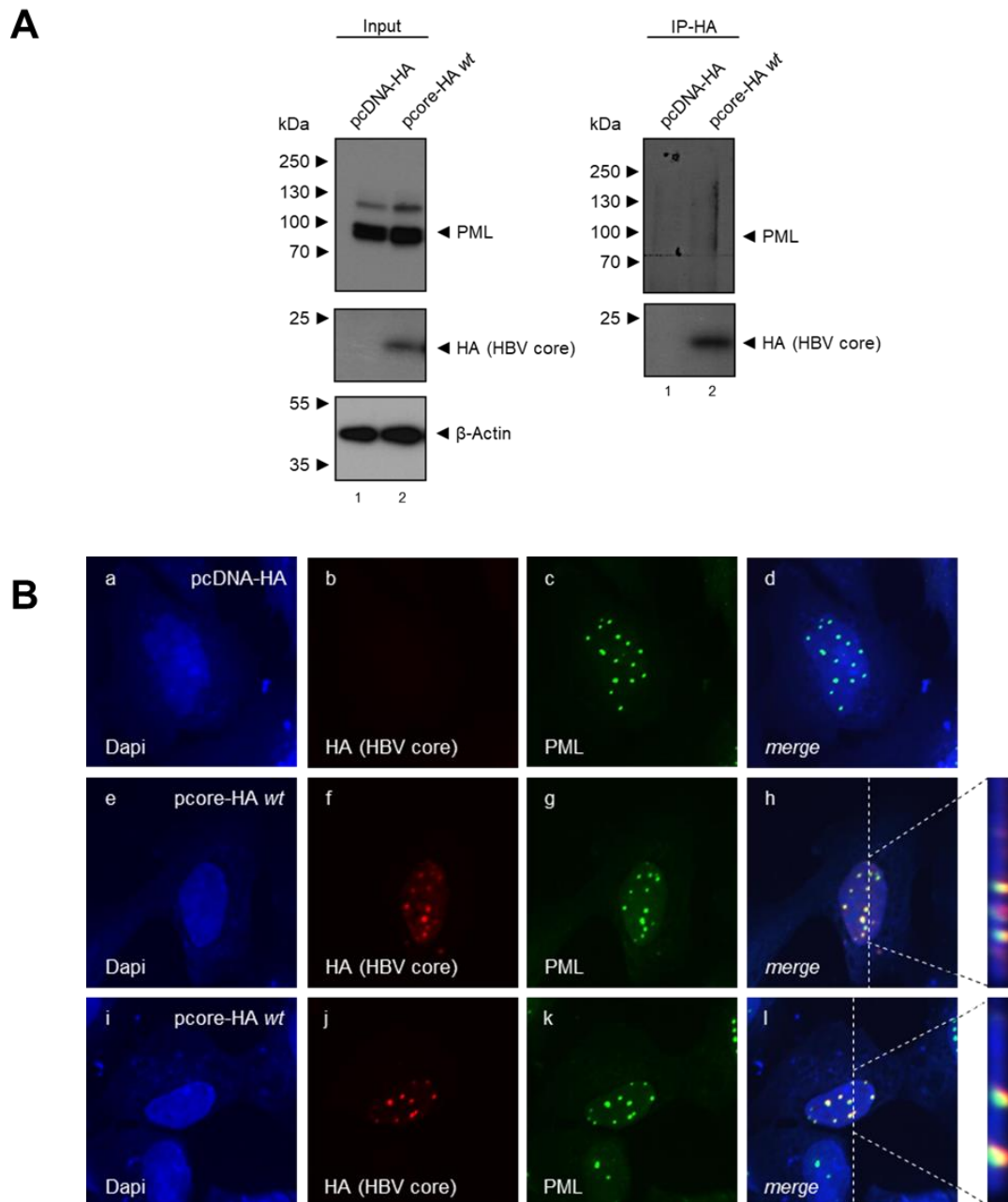
Figure 9: HBV core protein interacts with PML during transfection. A, B HepaRG cells were transfected with 10µg of pcore-HA (**A** lane 2, **B** panels e-l) or empty vector pcDNA-HA (**A** lane 1, **B** panels a-d). **A** Whole-cell protein lysates were prepared 48h post transfection and immunoprecipitation using an anti-HA antibody (3F10) was performed. Protein lysates and immunoprecipitation were analyzed by SDS-PAGE and western blot using anti-PML (NB100-59787), anti-HA (3F10) and anti-β-Actin (AC-15) antibodies. Molecular weights are depicted on the left, respective proteins are indicated on the right of each blot. Data are representative for two independent biological replicates. **B** Transfected cells were fixed with 4% PFA at 48h post transfection and double stained with anti-PML (NB100-59787) and anti-HA (3F10) antibodies. Primary antibodies were detected using Alexa 488 (green, PML) and Alexa 647 (red, HA) conjugated secondary antibodies and the nuclei were co-stained using Dapi. Pictures and Z-stacks were taken using a Nikon TiE laser scanning microscope. Representative images for at least 40 cells from two independent biological replicates are shown.

During infection, HBV core protein distribution was reported to be different, with a diffuse localization in the nucleus, as well as in the cytoplasm, which further depends on HBV core protein phosphorylation status, HBV replication and the cell cycle stage (*103, 110, 195, 220-226*). Therefore, to assess association of HBV core protein with PML during infection, differentiated HepG2-NTCP-K7 cells were infected with HBV and immunofluorescence stainings were performed 7d.p.i.. In line with previous observations, a diffuse localization of HBV core protein was observed by staining with an antibody, which recognizes assembled HBV capsids or capsid intermediates (see figure 10, panels f-h, j-l), or a linear epitope within the HBV core protein (see figure 11, panels f-h, j-l). No specific co-localization with PML-NBs could be observed in both cases.

PML-NBs are stably residing in the nuclear matrix of mammalian cells (*284, 312-318*). Pre-extraction of cells with CSK buffer prior to fixation removes soluble proteins and leaves the insoluble protein fraction, including proteins of the cytoskeleton and also nuclear matrix associated proteins. CSK pre-extraction is therefore feasible to reduce diffuse background stainings in immunofluorescence (*341, 432*). CSK treatment of HBV infected HepG2-NTCP-K7 cells at 7d.p.i. before fixation and IF staining resulted in a distinct dot-like nuclear distribution of HBV core protein stained by antibodies detecting assembled HBV capsids and capsid intermediates or a linear epitope within HBV core protein (see figure 10, panels r-t, v-x, figure 11, panels r-t, v-x). In contrast to the results obtained without prior CSK treatment (see figure 10, panels f-h, j-l, figure 11, panels f-h, j-l) those nuclear HBV core protein accumulations co-localized with PML-NBs (see figure 10, panels r-t, v-x, figure 11, panels r-t, v-x).
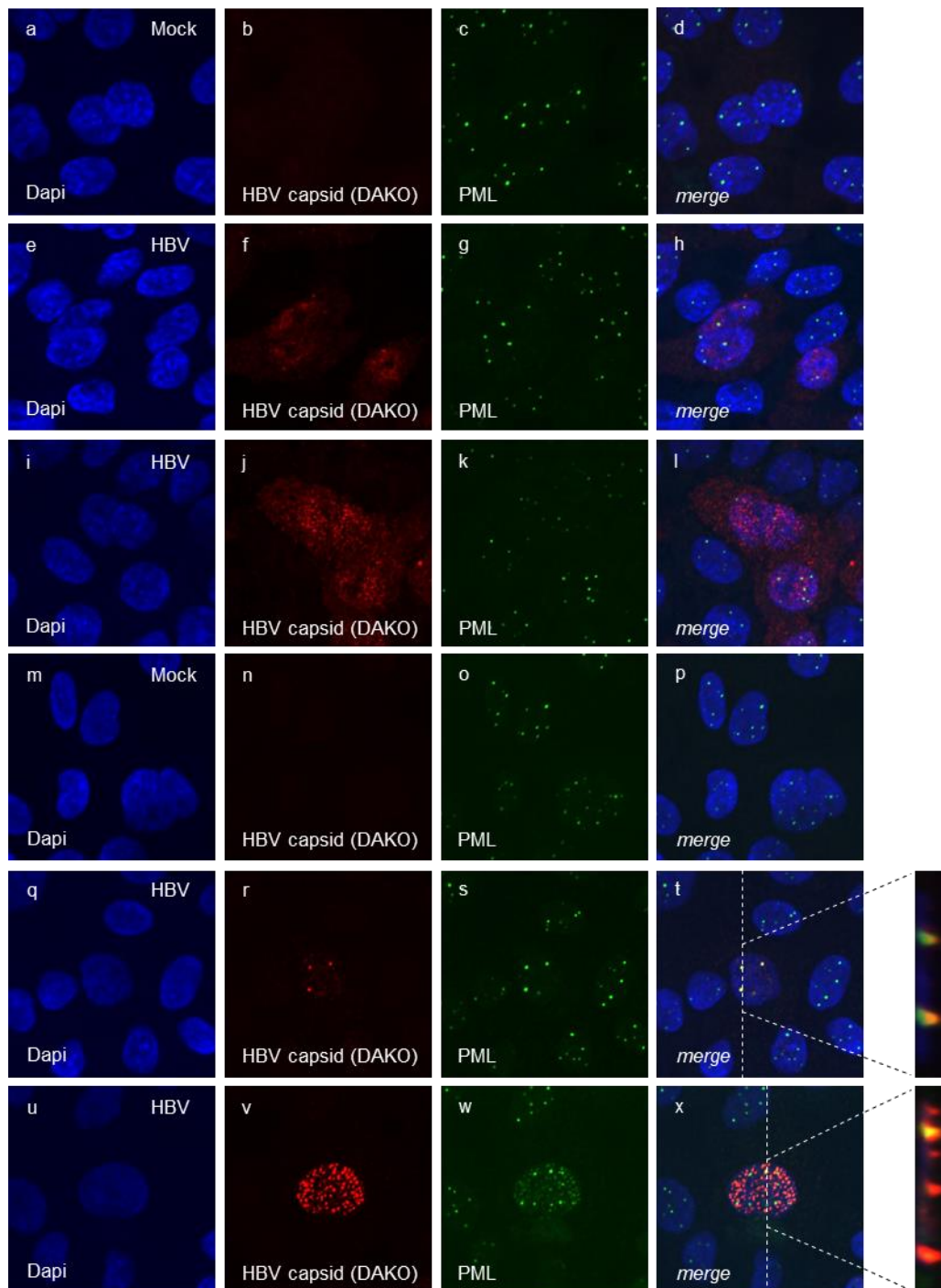
Figure 10: HBV capsids and capsid intermediates associate with PML-NBs during HBV infection. HepG2-NTCP-K7 cells were differentiated by addition of 2.5% DMSO for 2d. Cells were infected with HBV at a MOI of 400 GE/cell and fixed with 4% PFA at 7d.p.i.. Cells in panels m-x were pre-extracted by incubation in CSK buffer prior to fixation. All cells were stained using anti-PML (sc-966) and anti-HBV capsid (DAKO B0586) antibodies. Primary antibodies were detected using Alexa 488 (green, PML) and Alexa 647 (red, HBV capsid) conjugated secondary antibodies and the nuclei were co-stained using Dapi. Pictures and Z-stacks were taken using a Nikon TiE laser scanning microscope. Images are representative for at least 30 mock and infected cells without CSK treatment and at least 20 mock and infected cells with CSK treatment.

Figure 11: HBV core protein associates with PML-NBs during HBV infection. HepG2-NTCP-K7 cells were differentiated by addition of 2.5% DMSO for 2d. Cells were infected with HBV at a MOI of 400 GE/cell and fixed with 4% PFA at 7d.p.i.. Cells in panels m-x were pre-extracted by incubation in CSK buffer prior to fixation. All cells were stained using anti-PML (NB100-59787) and anti-HBV core (sc-23945) antibodies. Primary antibodies were detected using Alexa 488 (green, PML) and Alexa 647 (red, HBV core) conjugated secondary antibodies and the nuclei were co-stained using Dapi. Pictures and Z-stacks were taken using a Nikon TiE laser scanning microscope. Images are representative for at least 30 mock and infected cells without CSK treatment and at least 20 mock and infected cells with CSK treatment.

Hereby, not all PML-NBs were occupied by co-localizing HBV core protein staining, but HBV core protein rather localized to specific PML-NBs (see figure 10, panels r-t, v-x, figure 11, panels r-t, v-x). Further analysis revealed that a mean of 50% of PML-NBs were able to recruit HBV core protein. These findings indicated preferential association of HBV core protein with specific PML-NBs (see figure 12). Taken together, these findings confirmed an association of HBV core protein with PML-NBs and expanded the previous published data by showing HBV core protein-PML interaction in absence of further viral factors during transfection (see figure 9) and also during HBV infection of differentiated HepG2-NTCP-K7 cells (see figure 10, figure 11).
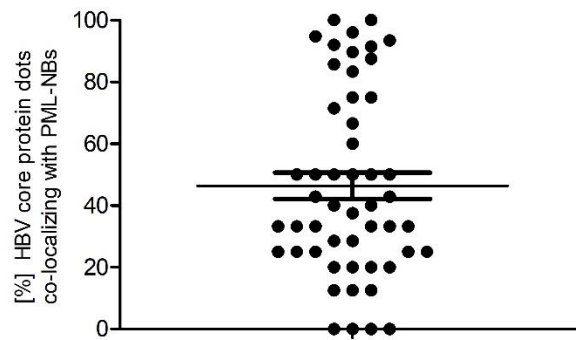
Figure 12: HBV core protein associates with specific PML-NBs during infection. HBV core protein dots co-localizing with PML from data shown in figures 10 and 11 were counted and visualized as [%] HBV core protein dots co-localizing with PML-NBs using GraphPad *PRISM5*.

4.2 HBV core protein is subject to SUMO PTM and SUMOylation regulates PML association of the viral factor

PML-NBs are supposed to be cellular hotspots for regulative SUMOylation and interaction, as well as recruitment to PML-NBs is mediated by SUMO-SIM interactions (*284, 305, 307-311*). Due to the association of HBV core protein with PML-NBs during transfection and infection (see chapter 4.1), the question arose if HBV core protein is modulated by SUMO PTM. Therefore, *in silico* prediction of possible SCMs within the HBV core protein sequence using the program *GPS SUMO1.0* (*420*) was performed. Indeed, both HBV core protein lysine residues K7 and K96 in the NTD were predicted to be SUMO conjugation motives (SCM1 and SCM2). Alignment of the amino acid sequences of HBV core proteins from genotypes A-H showed that SCM1 and SCM2 were highly conserved between all major HBV genotypes (see figure 13 A, C). SCM1 was present in the globular domain of the HBV core protein structure, while SCM2 localized to the spike (see figure 13 B).

To confirm SUMOylation of HBV core and the identity of the *in silico* predicted SCMs, both sites were mutated to arginine residues either individually (pcore-HA *Δscm1* and pcore-HA *Δscm2*) or both together (pcore-HA *Δscm1/2*) using PCR based mutagenesis. HepaRG cells overexpressing His$_6$-tagged SUMO2 (HepaRG *SUMO2*) and HepaRG *His/HA*, expressing a His$_6$-HA-tag as control, were transfected with the vectors encoding HA-tagged *wt* (see figure 14 A, lanes 2, 7), *Δscm1* (see figure 14 A, lanes 3, 8), *Δscm2* (see figure 14 A, lanes 4, 9), or *Δscm1/2* (see figure 14 A, lanes 5, 10) HBV core protein. Lysates were prepared under denaturing conditions and SUMOylation of HBV core protein was analyzed by NiNTA precipitation. Consistently with the presence of two predicted SCMs (see figure 13), SUMO PTM of *wt* HBV with SUMO2 could be confirmed (see 14 A, NiNTA lane 2, figure 14 B). SUMO2 modification of HA-tagged HBV core protein *Δscm1* (see figure 14 A, NiNTA lane 3, figure 14 B) and *Δscm2* (see figure 14 A, NiNTA lane 4, figure 14 B) mutants was severely reduced to 30% of *wt* core-HA SUMO PTM. Consequently, SUMOylation of the double SCM mutant HBV core protein *Δscm1/2* (see figure 14 A, NiNTA lane 5, figure 14 B) was completely abrogated, despite higher steady state expression levels compared to the *wt* HBV core protein (see figure 14 A, input lane 2, 5). In contrast to HBV core protein *Δscm2* and *Δscm1/2*, *Δscm1* showed lower steady state expression levels compared to the *wt* HBV core protein (see figure 14 A, input lanes 2-5)

4. Results

A

```
                                           SCM1
HBV Genotype A   ------------MDIDPYKEFGATVELLSFLPSDFFPSVRDLLDTASALYREALESPEHC    48
HBV Genotype B   ------------MDIDPYKEFGASVELLSFLPSDFFPSIRDLLDTASALYREALESPEHC    48
HBV Genotype C   ------------MDIDPYKEFGASVELLSFLPSDFFPSIRDLLDTASALYREALESPEHC    48
HBV Genotype D   ------------MDIDPYKEFGATVELLSFLPSDFFPSVRDLLDTASALYREALESPEHC    48
HBV Genotype E   ------------MDIDPYKEFGATVELLSFLPSDFFPSVRDLLDTASALYRDALESPEHC    48
HBV Genotype F   ------------MDIDPYKEFGASVELLSFLPSDFFPSVRDLLDTASALYRDALESPEHC    48
HBV Genotype G   MDRTTLPYGLFGLDIDPYKEFGATVELLSFLPSDFFPSVRDLLDTASALYRESLESSDHC    60
HBV Genotype H   ------------MDIDPYKEFGASVELLSFLPSDFFPSVRDLLDTASALYRDALESPEHC    48
                             :*********:***************:***********::*** :**
                                                                SCM2
HBV Genotype A   SPHHTALRQAILCWGELMTLATWVGNNLEDPASRDLVVNYVNTNMGLKIRQLLWFHISCL   108
HBV Genotype B   SPHHTALRQAILCWGELMNLATWVGSNLEDPASRELVVSYVNVNMGLKIRQLLWFHISCL   108
HBV Genotype C   SPHHTALRQAILCWGELMNLATWVGSNLEDPASRELVVSYVNVNMGLKIRQLLWFHISCL   108
HBV Genotype D   SPHHTALRQAILCWGELMTLATWVGGNLEDPASRDLVVSYVNTNMGLKFRQLLWFHISCL   108
HBV Genotype E   SPHHTALRQAILCWGELMTLATWVGVNLEDPASRDLVVSYVNTNMGLKFRQLLWFHISCL   108
HBV Genotype F   TPNHTALRQAILCWGELMTLASWVGNNLEDPAARDLVVNYVNTNMGLKIRQLLWFHISCL   108
HBV Genotype G   SPHHTALRQAILCWGELMTLATWVGNNLEDPASRDLVVNYVNTNMGLKIRQLLWFHISCL   120
HBV Genotype H   TPNHTALRQAILCWGELMTLASWVGNNLEDPAARDLVVNYVNTNMGLKIRQLLWFHISCL   108
                 :*:***************.**:*** ******:*:***.***.*****:***********

HBV Genotype A   TFGRETVLEYLVSFGVWIRTPPAYRPPNAPILSTLPETTVVRRRDRGRSPRRRTPSPRRR   168
HBV Genotype B   TFGRETVLEYLVSFGVWIRTPPAYRPPNAPILSTLPETTVVRR--RGRSPRRRTPSPRRR   166
HBV Genotype C   TFGRETVLEYLVSFGVWIRTPPAYRPPNAPILSTLPETTVVRR--RGRSPRRRTPSPRRR   166
HBV Genotype D   TFGRETVLEYLVSFGVWIRTPPAYRPPNAPILSTLPETTVVRR--RGRSPRRRTPSPRRR   166
HBV Genotype E   TFGRETVIEYLVSFGVWIRTPPAYRPPNAPILSTLPENTVVRR--RGRSPRRRTPSPRRR   166
HBV Genotype F   TFGRETVLEYLVSFGVWIRTPPAYRPPNAPILSTLPETTVVRR--RGRSPRRRTPSPRRR   166
HBV Genotype G   TFGRETVLEYLVSFGVWIRTPPAYRPPNAPILSTLPETTVVRR--RGRSPRRRTPSPRRR   178
HBV Genotype H   TFGRETVLEYLVSFGVWIRTPPAYRPPNAPILSTLPETTVVRQ--RGRAPRRRTPSPRRR   166
                 *******:*************************************.****: ***:***********
```

```
HBV Genotype A   RSQSPRRRRSQSRESQC  185
HBV Genotype B   RSQSPRRRRSQSRESQC  183
HBV Genotype C   RSQSPRRRRSQSRESQC  183
HBV Genotype D   RSQSPRRRRSQSRESQC  183
HBV Genotype E   RSQSPRRRRSQSPASQC  183
HBV Genotype F   RSQSPRRRRSQSPASQC  183
HBV Genotype G   RSQSPRRRRSASPASQC  195
HBV Genotype H   RSQSPRRRRSQSPASQC  183
                 **********.*  ***
```

B Core monomer 1 / Core monomer 2 / Core monomer 3 / Core monomer 4 / K7 (SCM1) / K96 (SCM2)

C

```
0        50        100       150   183
```

Assembly domain | Linker | C-terminal domain

5-Y**K**EF-10 **HBV core SCM1 (K7)**   94-L**K**I/FR-99 **HBV core SCM2 (K96)**

Figure 13: HBV core protein carries two highly conserved SCMs in its NTD. A HBV core protein consensus amino acid sequences of genotypes A-H were retrieved from the *HBV database* (HBVdb) (*421*) and multiple sequence alignments were performed using the *Clustal Omega* online tool (*418*). SCMs within the HBV core sequence were identified using *GPS SUMO1.0* (*420, 435*). The lysine residues are marked in red, the highly conserved SCMs in green. **B** SCM1 (yellow) and SCM2 (green) are highlighted in the asymmetric tetrameric unit of T=4 capsids based on (*197*). **C** Schematic representation of the HBV core protein. SCM1 and SCM2 within the NTD are highlighted.

The impact of HBV core protein SUMOylation on its association with PML-NBs was subsequently determined using immunofluorescence microscopy in HepaRG cells transfected with expression vectors for either *wt*, *Δscm1*, *Δscm2*, or *Δscm1/2* HA-tagged HBV core protein. For *wt* HBV core protein, the association with PML-NBs could be confirmed

70

by an efficient and distinct co-localization of the PML staining with HA-tagged HBV core protein (see figure 15 A, panels f-h, j-l). This co-localization between HBV core protein and PML was found to be less efficient in cells transfected with the single SCM mutants of the HBV core protein *Δscm1* (see figure 15 A, panels n-p, r-t) or *Δscm2* (see figure 15 A, panels v-x, z-ab). PML co-localization was further and more severely reduced for the double SCM mutant *Δscm1/2* HBV core protein (see figure 15 A, panels ad-af, ai-ak).
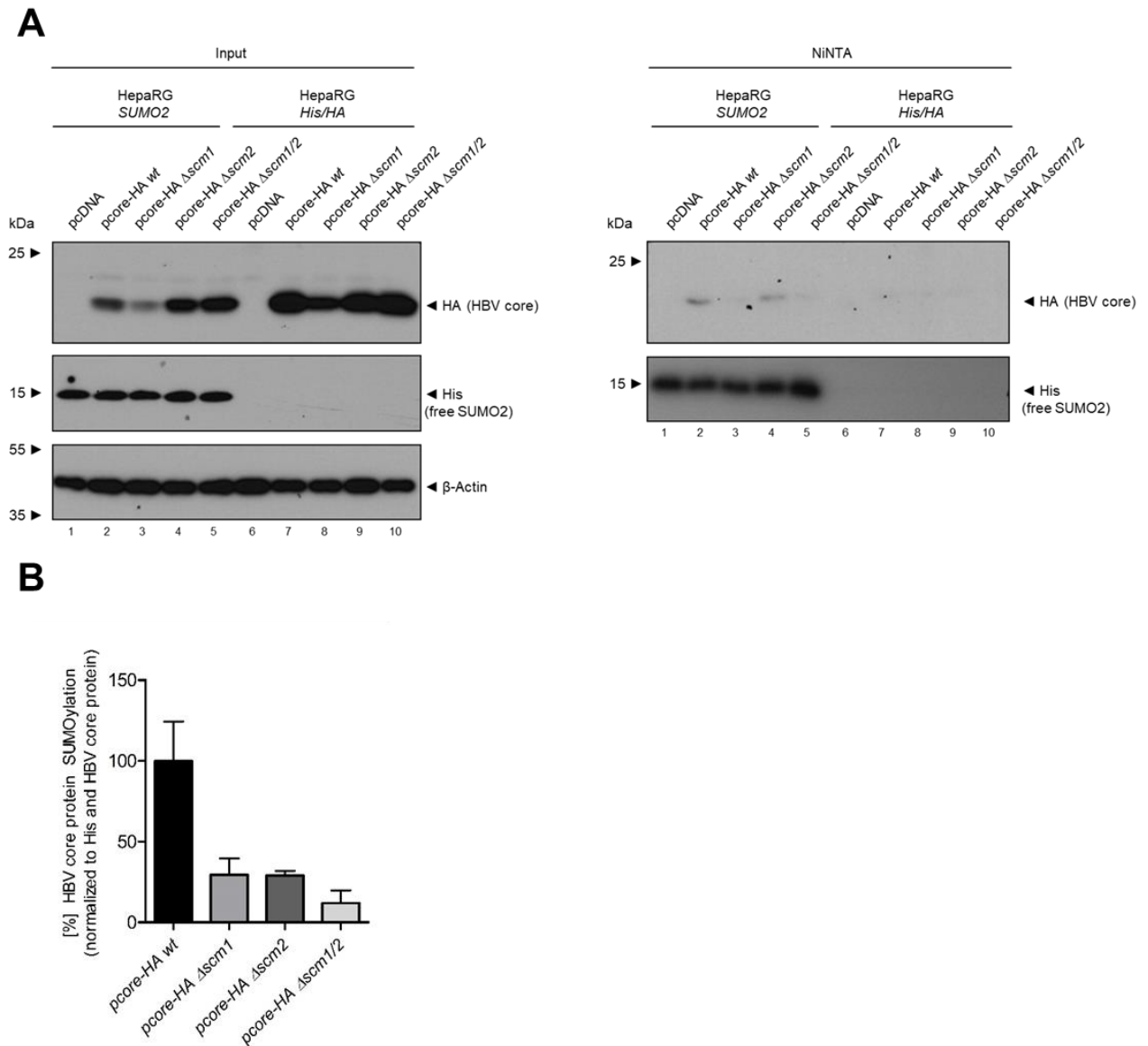
Figure 14 HBV core protein is SUMO2 modified at SCM1 and SCM2. A, B HepaRG *SUMO2* cells stably overexpressing His$_6$-tagged SUMO2 and HepaRG *His/HA* control cells were transfected with 10µg of pcore-HA *wt* (lanes 2, 7), *Δscm1* (lanes 3, 8), *Δscm2* (lanes 4, 9), or *Δscm1/2* (lanes 5, 10), harvested 48h post transfection and lysed under denaturing conditions. His$_6$-SUMO2 modified proteins were precipitated using NiNTA resin and NiNTA purified proteins, as well as whole-cell protein lysates were analyzed by SDS-PAGE and western blot. Proteins of interest were detected using anti-HA (3F10), anti-His$_6$ (6-His) and anti-β-Actin (AC-15) antibodies. Molecular weights are depicted on the left, respective proteins are indicated on the right of each blot. **B** Western blot signals were analyzed by densitrometry using *FiJi* (version 1.45s). Signals for SUMOylated HBV core protein were normalized to free SUMO2 and input HBV core protein. The graph was visualized using GraphPad *PRISM5*. Data are representative for two independent biological replicates.

4. Results

This reduction in co-localization was further confirmed by determination of the Pearson correlation coefficient, which was significantly decreased for HBV core *Δscm1*, *Δscm2*, or *Δscm1/2* compared to the *wt* protein (see figure 15 B).
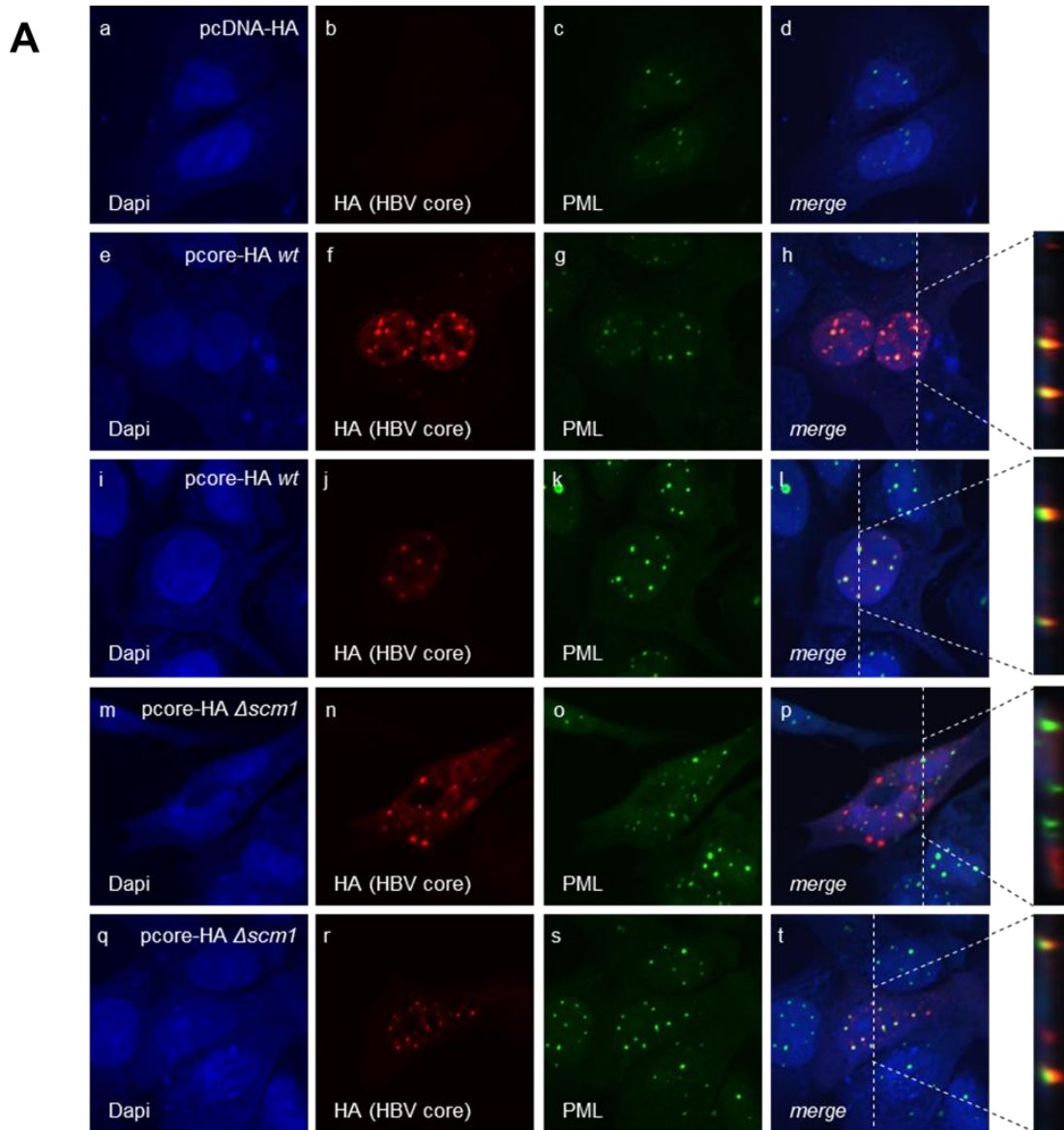
Figure 15: HBV core protein SUMOylation is a prerequisite for efficient PML-NB association. **A, B** HepaRG cells were transfected with 10µg of pcore-HA *wt* (**A** panels e-l), *Δscm1* (**A** panels m-t), *Δscm2* (**A** panels u-ab), *Δscm1/2* (**A** panels ac-ak), or pcDNA-HA empty vector control (**A** panels a-d). Cells were fixed with 4% PFA at 48h post transfection and and double stained with anti-PML (NB100-59787) and anti-HA (3F10) antibodies. Primary antibodies were detected using Alexa 488 (green, PML) and Alexa 647 (red, HA) conjugated secondary antibodies and the nuclei were co-stained using Dapi. Pictures and Z-stacks were taken using a Nikon TiE laser scanning microscope. Representative images for at least 40 cells from two independent biological replicates are shown. **B** Pearson correlation coefficient for co-localization of HA (HBV core) and PML for at least 40 cells from two independent biological replicates were calculated using *FiJi* (version 1.45s) and visualized using GraphPad *PRISM5*. Statistical significance was calculated using Oneway ANOVA and Dunn's post test. n.s.: not significant, *: $p<0.05$, **: $p<0.01$, ***: $p<0.001$

A (cont.)
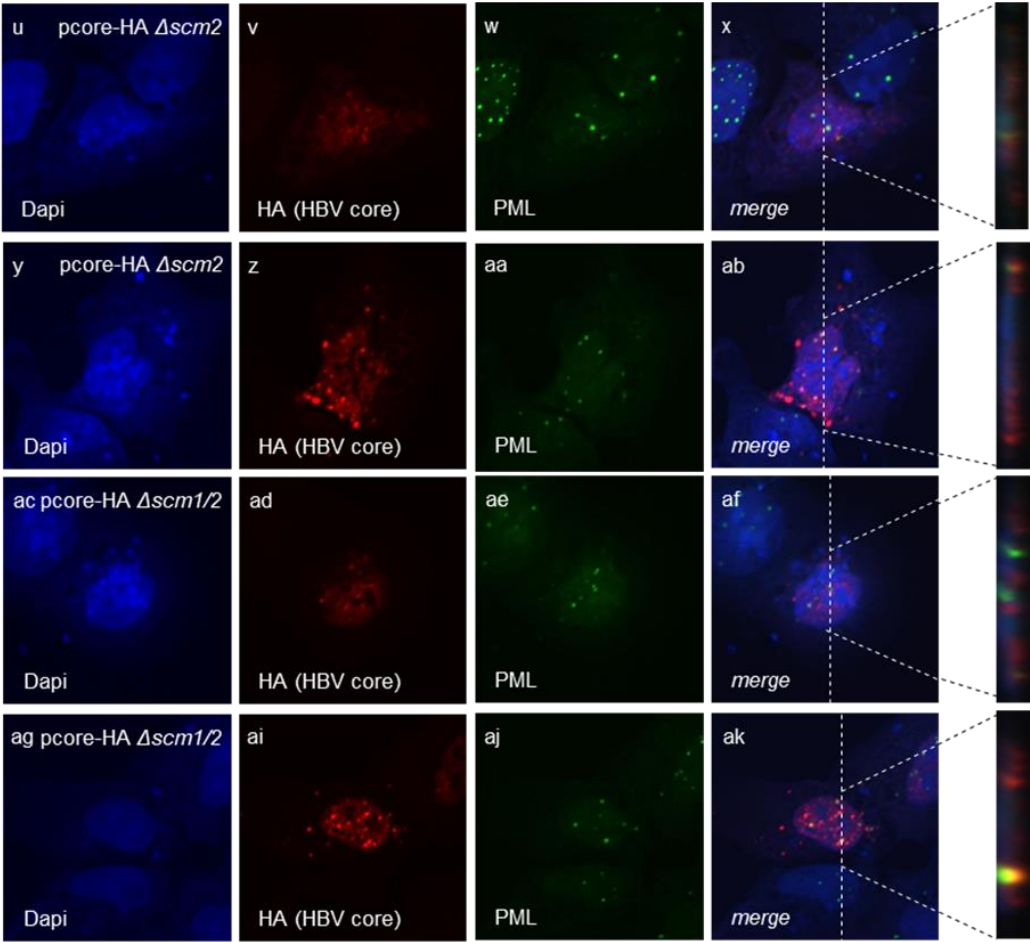
B
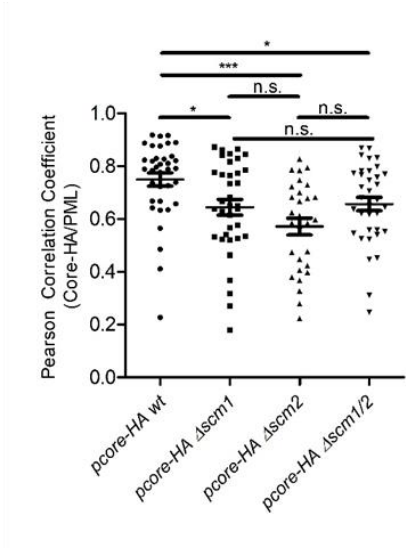
Figure 15 (continued): HBV core protein SUMOylation is a prerequisite for efficient PML-NB association.

To further confirm the requirement of HBV core protein SUMOylation for its interaction with PML-NBs, HepaRG cells were transfected with plasmids encoding either *wt* or the double SCM mutant *Δscm1/2* HA-tagged HBV core protein and whole-cell protein lysates were analyzed by immunoprecipitation using an anti-HA antibody. The data confirmed the previous findings (see chapter 4.1) as *wt* HA-tagged HBV core protein co-precipitated PML (see figure 16 A, IP-HA, lane 2, figure 16 B), while HBV core *Δscm1/2* had lost the ability to interact with PML protein (see figure 16 A, IP-HA, lane 3, figure 16 B). These findings altogether indicated that HBV core protein SUMOylation acted as key mediator for the core protein-PML interaction and recruitment of HBV core protein to PML-NBs.
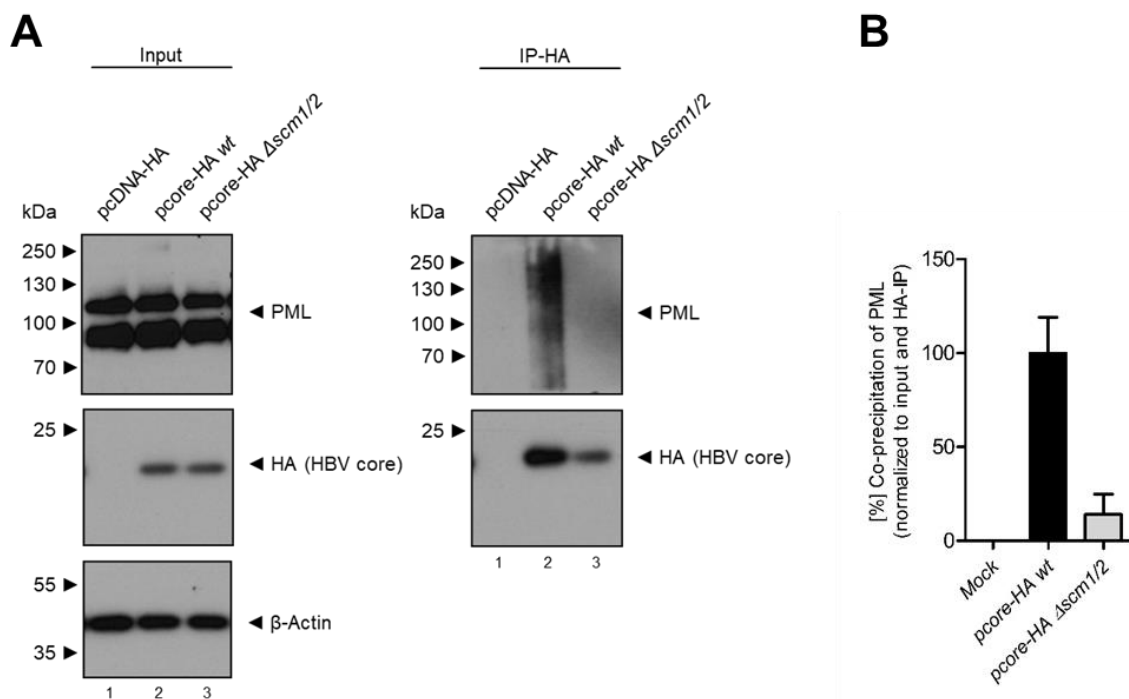
Figure 16: HBV core protein SUMOylation is essential for its interaction with PML. A, B HepaRG cells were transfected with 10µg of pcore-HA *wt* (**A** lane 2), *Δscm1/2* (**A** lane 3), or pcDNA-HA empty vector control (**A** lane 1). **A** Whole-cell protein lysates were prepared 48h post transfection and immunoprecipitation using an anti-HA antibody (3F10) was performed. Protein lysates and immunoprecipitation were analyzed by SDS-PAGE and western blot using anti-PML (NB100-59787), anti-HA (3F10) and anti-β-Actin (AC-15) antibodies. Molecular weights are depicted on the left, respective proteins are indicated on the right of each blot. **B** Western blot signals were analyzed by densitrometry using *FiJi* (version 1.45s). Signals for co-precipitated PML protein were normalized to PML input and precipitated and input HBV core protein. The graph was visualized using GraphPad *PRISM5*. Data are representative for two independent biological replicates.

4.3 HBV core protein SUMOylation enhances HBV replication

The impact of HBV core protein SUMOylation on HBV replication and cccDNA was further determined using a plasmid-based HBV replicon system, which harbors a 1.1 times copy of the HBV genome expressed under control of a constitutively active CMV promoter (pHBV1.1 *wt*).
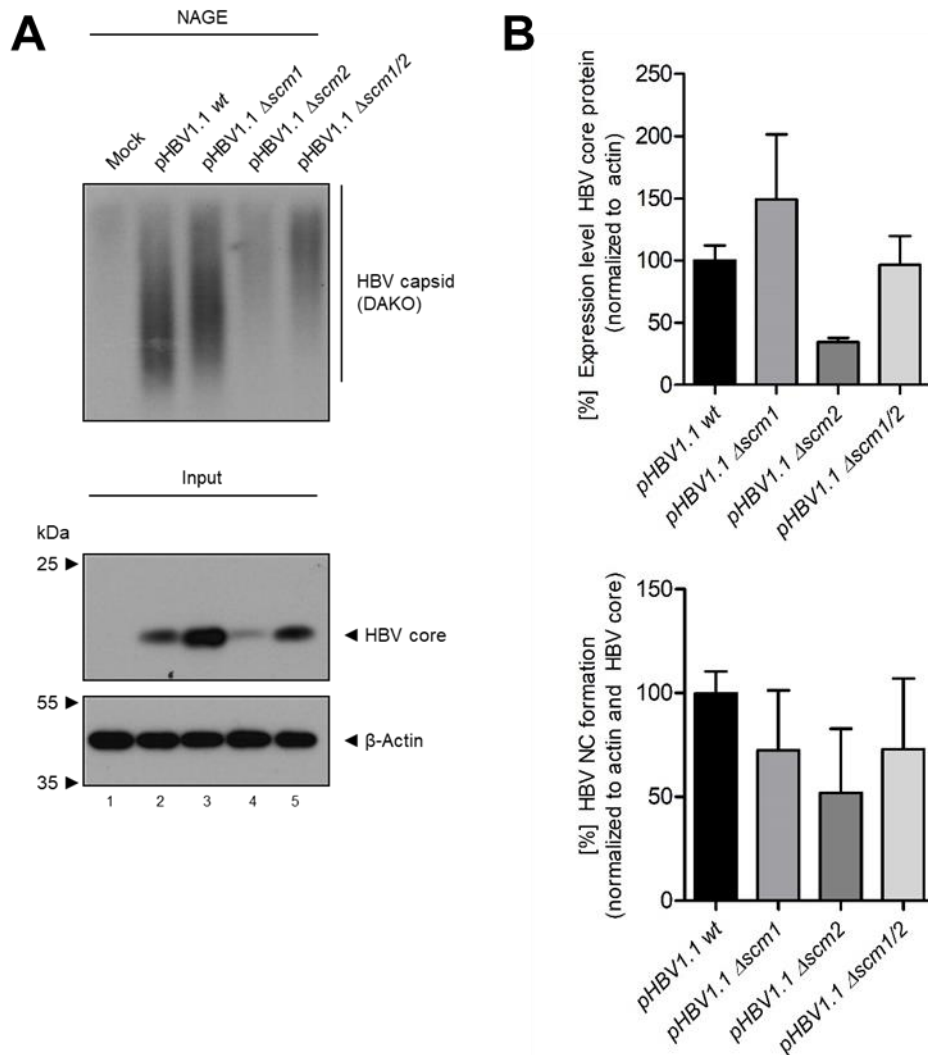
Figure 17: SCM mutations only mildly impact HBV nucleocapsid formation. A, B HepaRG cells were transfected with 5 µg of pHBV1.1 *wt* (**A**, lane 2), *Δscm1* (**A** lane 3), *Δscm2* (**A** lane 4), *Δscm1/2* (**A** lane 5), or pcDNA-HA empty vector control (**A** lane 1). Cells were harvested 48h post transfection and lysed using low-stringent NP40 lysis buffer, retaining the native structure of HBV nucleocapsids. Native lysates were analyzed by NAGE and immunoblotting using anti-HBV capsid antibody (DAKO, B0586). Steady state HBV core protein expression levels were determined using denaturing SDS-PAGE and western blot using anti-HBV core (8C9) and anti-β-Actin (AC-15) antibodies. Molecular weights are depicted on the left, respective proteins are indicated on the right of each blot. **B** Western blot and NAGE signals were analyzed by densitrometry using *FiJi* (version 1.45s). Signals for HBV core protein expression levels were normalized to β-Actin input and nucleocapsid formation was normalized to β-Actin and HBV core protein input levels. Graphs were visualized using GraphPad *PRISM5*. Data are representative for two independent biological replicates. NC = nucleocapsid.

Transfection of this plasmid results in expression of a pgRNA, serving as template for HBV core and polymerase translation. HBV core packages the pgRNA bound to the polymerase,

rcDNA synthesis takes place and the mature nucleocapsid can re-shuttle back to the nucleus. There, cccDNA can be established (*75, 132, 133, 182*). To analyse the impact of HBV core SUMO PTM on the viral life cycle, arginine mutations were introduced for either individual SCMs (pHBV1.1 *Δscm1* and pHBV1.1 *Δscm2*) or both SCMs together (pHBV1.1 *Δscm1/2*).

First, disturbances of lysine to arginine mutations in HBV nucleocapsid formation, as well as core protein expression were determined by transfection of pHBV1.1 *wt*, *Δscm1*, *Δscm2*, or *Δscm1/2* into HepaRG cells followed by analysis using NAGE and western blot (see figure 17 A). Mutation of SCM2 to arginine induced a decrease in both, HBV core protein expression level as well as formation of nucleocapsids compared to pHBV1.1 *wt*. This phenotype was probably caused by loss of HBV core protein (see figure 17 A, lanes 2, 4, figure 17 B). SCM1 mutation, in contrast, induced higher expression levels of HBV core accompanied by higher formation of HBV nucleocapsids than pHBV1.1 *wt* (see figure 17 A, lanes 2, 3, figure 17 B). In line with this observation, mutation of SCM1 and SCM2 together in pHBV1.1 *Δscm1/2* showed similar core protein expression and nucleocapsid formation compared to *wt* pHBV1.1 (see figure 17 A, lanes 2, 5, figure 17 B).

Using the *wt* and SCM mutant plasmid-based replicon systems, impact of HBV core SUMOylation on formation of complete HBV DNA, including rcDNA as well as replication intermediates, and cccDNA was analyzed. HepaRG cells were transfected with either *wt*, *Δscm1*, *Δscm2*, or *Δscm1/2* pHBV1.1 and complete HBV DNA as well as cccDNA were analyzed using qPCR. On the level of complete HBV DNA, only minor differences between the *wt* and the SCM mutant HBV replicon systems could be observed (see figure 18 A). Monitoring cccDNA levels, however, a severe and significant deficiency in cccDNA formation could be detected for the *Δscm2* and *Δscm1/2* HBV replicon system, while *Δscm1* showed slightly elevated cccDNA levels (see figure 18 B).

The importance of HBV core protein SUMOylation and subsequent PML association in HBV replication was further determined by transfection of pHBV1.1 *wt* and *Δscm1/2* in HepaRG *shPML* cells, with a stable shRNA mediated knockdown of PML proteins (see figure 18 E, left panel, lane 2), and in HepaRG *SUMO2* cells, overexpressing His$_6$-SUMO2 (see figure 18 E, right panel, lane 2). HepaRG *shCTL*, which were transduced with a scrambled control shRNA (see figure 18 E, left panel, lane 1), and HepaRG *His/HA*, expressing His$_6$-HA (see Figure 18 E, right panel, lane 1), were used as respective control cells.
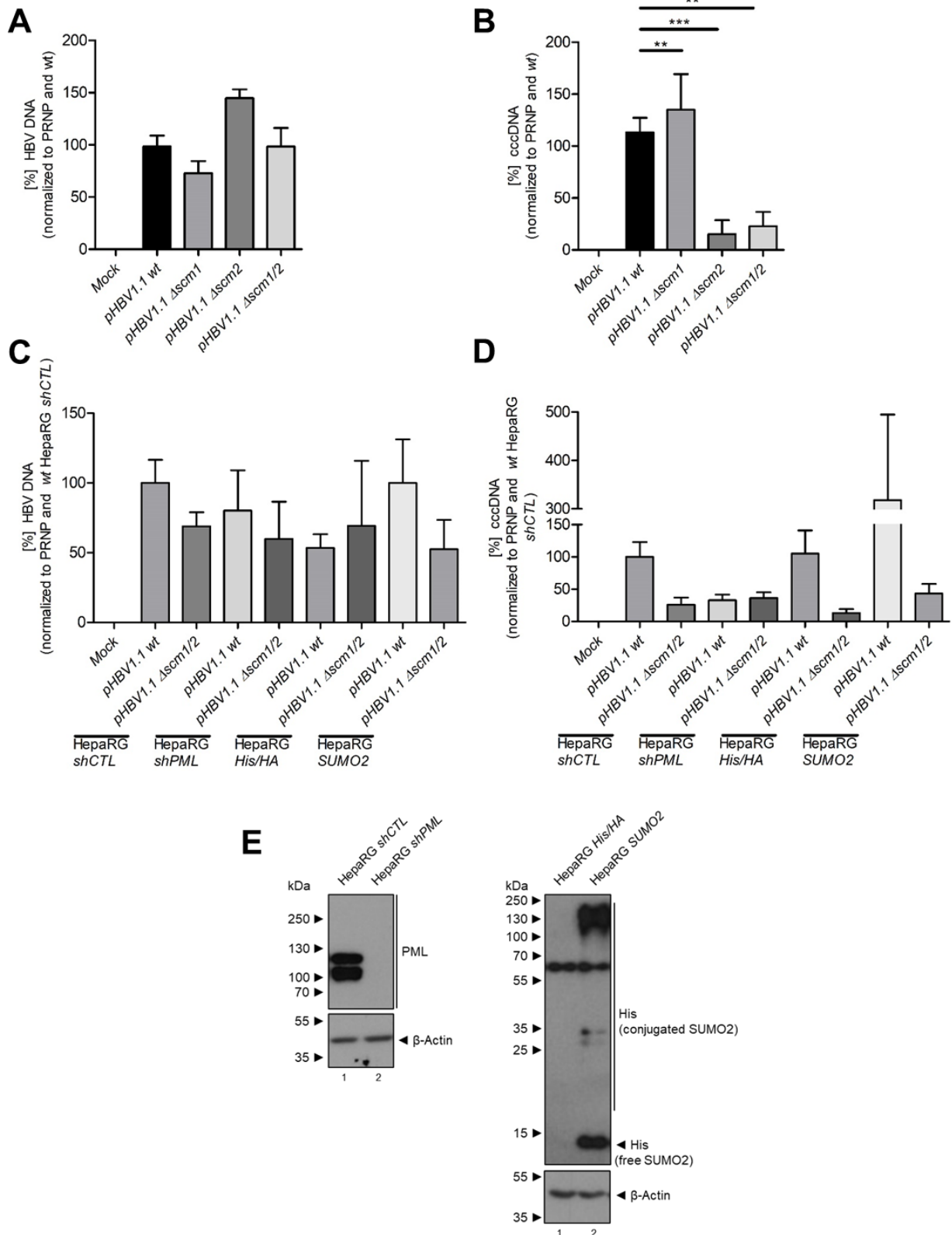
Figure 18: HBV core protein SUMOylation and PML association mediates cccDNA formation A,B HepaRG parental cells were transfected with 3µg of pHBV1.1 *wt*, *Δscm1*, *Δscm2*, or *Δscm1/2* and total DNA was extracted using the MachereyNagel NucleoSpin Tissue Kit 8d post transfection. **A** Complete HBV DNA and **B** cccDNA were determined using qPCR and normalized to PRNP. Bar charts were visualized using GraphPad *PRISM5* and correspond to three biological replicates measured in duplicates. **C, D** HepaRG *shPML*, HepaRG *shCTL*, HepaRG *SUMO2*, and HepaRG *His/HA* were transfected with 3µg of pHBV1.1. *wt* or *Δscm1/2* and total DNA was extracted using the MachereyNagel NucleoSpin Tissue Kit 8d post transfection. **C** Complete HBV DNA and **D** cccDNA were

77

determined by qPCR and normalized to PRNP. Bar charts were visualized using GraphPad *PRISM5* and correspond to six biological replicates measured in triplicates. **E** Whole-cell protein lysates of HepaRG *shPML*, HepaRG *shCTL*, HepaRG *SUMO2*, and HepaRG *His/HA* were analyzed by SDS-PAGE and western blot using anti-PML (NB100-59787), anti-His$_6$ (6-His) and anti-β-Actin (AC-15) antibodies. Molecular weights are depicted on the left, respective proteins are indicated on the right of each blot. Statistical significance was calculated using Oneway ANOVA and Dunn's post test. n.s.: not significant, *: $p<0.05$, **: $p<0.01$, ***: $p<0.001$

For complete HBV DNA levels as already observed for parental HepaRG cells (see figure 18 A), only minor differences could be determined by qPCR (see figure 18 C). On cccDNA levels, however, a severe defect was observed for the double SCM mutant *Δscm1/2* compared to the *wt* in both control cell lines HepaRG *shCTL* and *His/HA* (see figure 18 D). Strikingly, in HepaRG cells depleted for PML, not only the *Δscm1/2* mutant pHBV1.1 was deficient in cccDNA formation, but also the *wt* cccDNA levels were similarly reduced (see figure 18 D). These results indicate that lack of PML expression mimicked the phenotype of absent HBV core protein SUMOylation. In line with the severe impact of HBV core protein SUMO PTM on cccDNA formation, overexpression of His$_6$-SUMO2 induced a profound increase in cccDNA formation (see figure 18 D).

The severe defect of pHBV1.1 *Δscm1/2* mutant in cccDNA formation raised the question if reintroduction of *wt* HBV core protein *in trans* could restore cccDNA generation. Therefore, HepaRG cells were co-transfected with pHBV1.1 *wt* or *Δscm1/2* and pcore-HA *wt* or *Δscm1/2*. As already observed before, no striking differences on the level of complete HBV DNA could be observed (see figure 19 A). On cccDNA level, co-expression of either *wt* or *Δscm1/2* HA-tagged HBV core protein induced cccDNA formation by at least twofold, compared to transfection of pHBV1.1 *wt* and pcDNA-HA empty vector (see figure 19 B, figure 19 C). In contrast, for pHBV1.1 *Δscm1/2*, indeed a significant reconstitution of cccDNA formation was observed in cells co-transfected with pcore-HA *wt*. This was not the case for *in trans* expression of HA-tagged *Δscm1/2* HBV core protein (see figure 19 B, figure 19 D). Taken together these data indicated a strong dependence of cccDNA formation on HBV core protein SUMOylation as well as PML association.
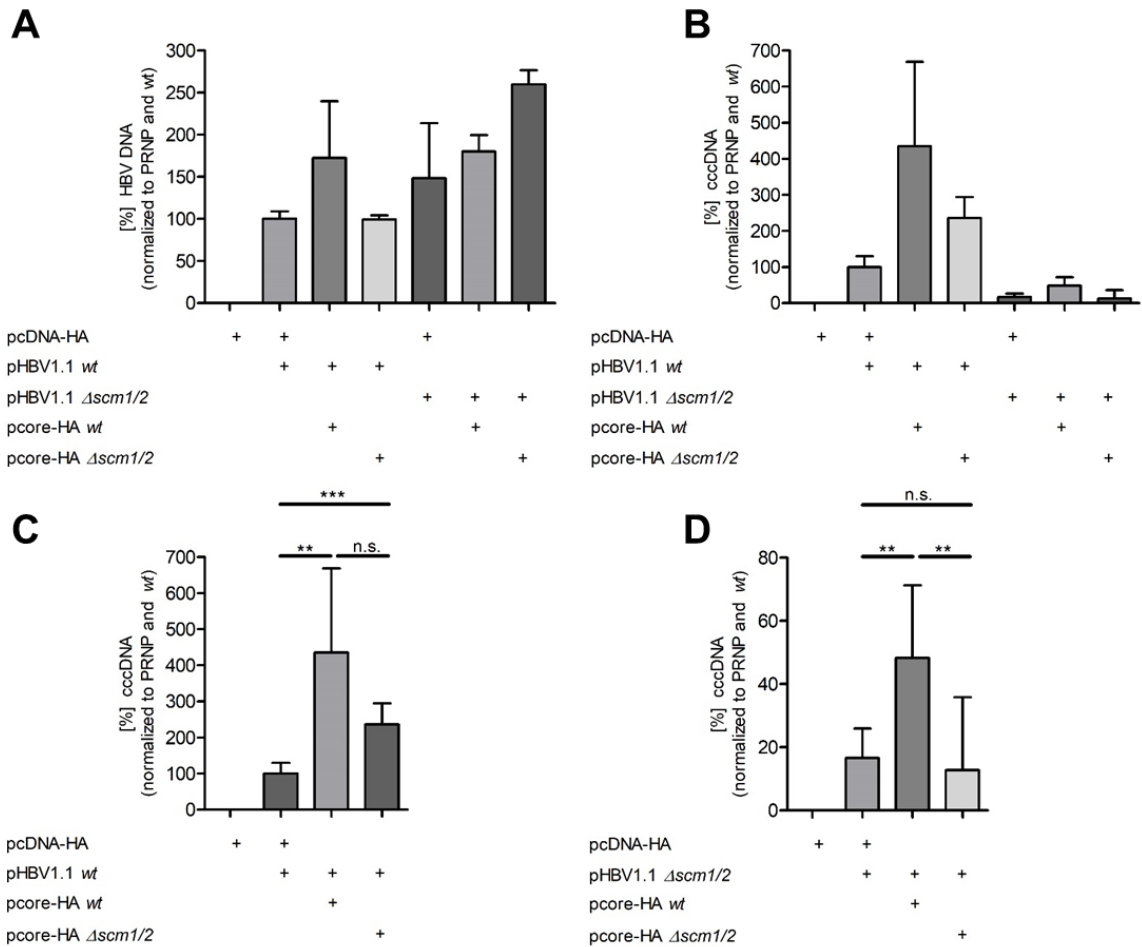
Figure 19: Transcomplementation of *wt* HBV core protein can rescue cccDNA formation from pHBV1.1 *Δscm1/2*. **A-D** HepaRG cells were transfected with 3µg of pHBV1.1 *wt* or *Δscm1/2*, co-transfected with 1µg of pcDNA-HA empty control, pcore-HA *wt*, or *Δscm1/2* and 8d post transfection complete DNA was isolated using the MachereyNagel NucleoSpin Tissue Kit. **A** Complete HBV DNA and **B** cccDNA was determined by qPCR relative to PRNP. For better visualization, **C** shows values of for pHBV1.1. *wt* co-transfected with pcDNA-HA empty, pcore-HA*wt*, or *Δscm1/2* and **D** shows values for pHBV1.1 *Δscm1/2* co-transfected with pcDNA-HA empty, pcore-HA*wt*, or *Δscm1/2*. Bar charts were visualized using GraphPad *PRISM5* and correspond to three biological replicates measured in duplicates. Statistical significance was calculated using Oneway ANOVA and Dunn's post test. n.s.: not significant, *: $p<0.05$, **: $p<0.01$, ***: $p<0.001$

4.4 HBV replication depends on expression of specific PML isoforms

4.4.1 Generation of HepG2-NTCP-K7 based cell lines expressing single PML isoforms

HBV core protein was found to associate with specific and not all PML-NBs in transfected, as well as infected cells (see figure 9, figure 10, figure 11, figure 12, figure 15) and PML-NB composition is known to be dynamically regulated by different cellular stimuli (*315, 316*). We therefore aimed to further dissect the composition of the PML-NBs which interact with HBV core protein and support cccDNA formation. To get first insights into which factors drive cccDNA formation, HepG2-NTCP-K7 based cell lines expressing single PML isoforms in the background of shRNA mediated PML depletion were generated by lentiviral transduction.
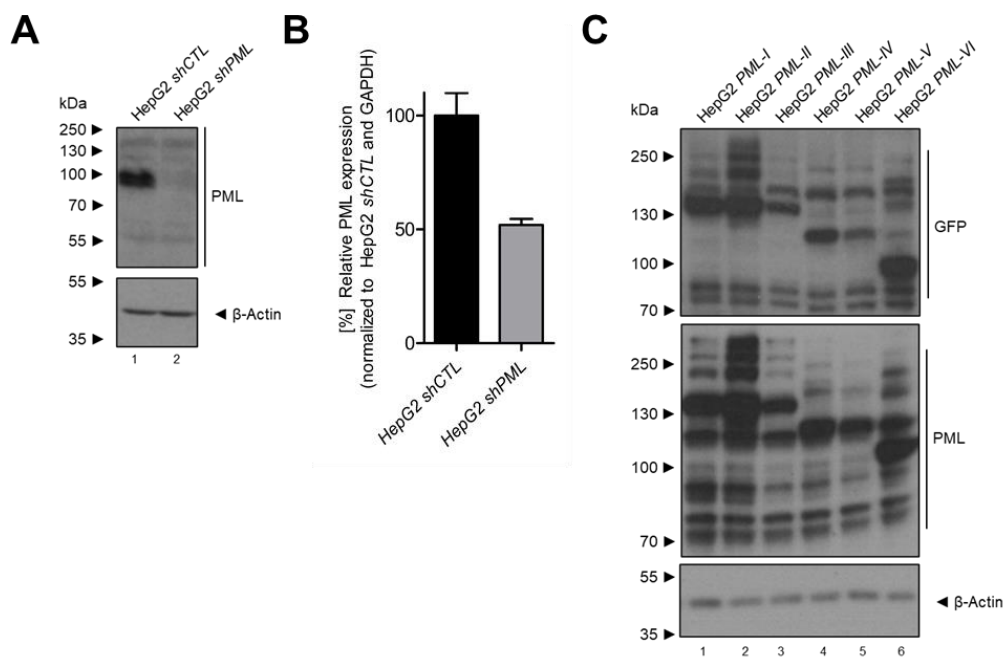
Figure 20: Generation of HepG2-NTCP-K7 based cell lines expressing single GFP-tagged PML isoforms I to VI. A, B HepG2-NTCP-K7 cells were either transduced with lentiviral vectors encoding a control shRNA (HepG2 *shCTL*, **A** lane 1) or a shRNA directed against PML (HepG2 *shPML*, **A** lane 2) and selection was achieved using puromycin. **A** Whole-cell protein lysates of generated cell lines were prepared and analyzed using SDS-PAGE and western blot with anti-PML (ab72137) and anti-β-Actin (AC-15) antibodies. Molecular weights are depicted on the left, respective proteins are indicated on the right of each blot. Data are representative for two independent biological replicates. **B** mRNA of HepG2 *shPML* and HepG2 *shCTL* cells was isolated using TRIzol and transcribed into cDNA. PML expression levels were determined by qPCR relative to GAPDH as housekeeping gene. Bar charts were visualized using GraphPad *PRISM5* and represent three biological replicates. **C** HepG2 *shPML* cells were further transduced with lentiviral vectors encoding shRNA resistant GFP-tagged single PML isoforms I to VI and selection was achieved using G418. Whole-cell protein lysates of generated cell lines were prepared and analyzed using SDS-PAGE and western blot with anti-GFP (ab290), anti-PML (ab72137) and anti-β-Actin (AC-15) antibodies. Molecular weights are depicted on the left, respective proteins are indicated on the right of each blot. Data are representative for two independent biological replicates.

In a first step, HepG2-NTCP-K7 cells were stably transduced with lentiviral vectors encoding either a control shRNA (HepG2 *shCTL*) or a validated PML shRNA (HepG2 *shPML*) (*429*). After selection via puromycin, depletion of PML was verified by western blot and qPCR. Compared to HepG2 *shCTL* (see figure 20 A, lane 1), the HepG2 *shPML* cell line showed severely

decreased PML steady state levels (see figure 20 A, lane 2). This finding was confirmed using qPCR determination of PML mRNA levels. Here, a decrease to 50% PML expression could be found in the HepG2 *shPML* cell line compared to HepG2 *shCTL* (see figure 20 B). HepG2 *shPML* cells were therefore used as basis for the generation of HepG2-NTCP-K7 based cell lines expressing single shRNA resistant and GFP-tagged nuclear PML isoforms I to VI (*338*). Cells were selected using G418 and expression of GFP-tagged PML isoforms was verified by western blot, showing sufficient expression of all nuclear GFP-tagged PML isoforms I to VI. PML-I, -II and -VI (see figure 20 C, lanes 1, 2, 6) showed higher steady state levels compared to PML-III, -IV and -V (see figure 20 C, lanes 3, 4, 5). PML depletion in HepG2 *shPML*, as well as expression of GFP-tagged PML isoforms in HepG2 *PML-I* to *PML-VI* was further analyzed by immunofluorescence staining using PML (see figure 21), as well as GFP antibodies (see figure 22). Immunofluorescence analysis of PML expression revealed that despite a strong reduction of steady state protein levels observed in the western blot (see figure 20 A, lane 2), still 54.1% of cells in the HepG2 *shPML* cell line showed detectable nuclear PML staining (see figure 21 A, panels e, f, figure 21 B) compared to 100 % of cells for the control cell line HepG2 *shCTL* (see figure 21 A, panels b, c, figure 21 B). These findings corresponded well with the reduction of PML mRNA levels to 50% in HepG2 *shPML* compared to HepG2 *shCTL* (see figure 20 B). For the HepG2 cell lines expressing single PML isoforms, 97.3% of cells were PML positive for HepG2 *PML-I* (see figure 21 A, panels h, i, figure 21 B), 98.1 % for HepG2 *PML-II* (see figure 21 A, panels k, l, figure 21 B), 93.2% for HepG2 *PML-III* (see figure 21 A, panels n, o, figure 21 B), 92.5% for HepG2 *PML-IV* (see figure 21 A, panels q, r, figure 21 B), 95.3% for HepG2 *PML-V* (see figure 21 A, panels t, u, figure 21 B), and 92.5% for HepG2 *PML-VI* (see figure 21 A, panels w, x, figure 21 B), indicating an efficient reconstitution of the expression of single nuclear PML isoforms.
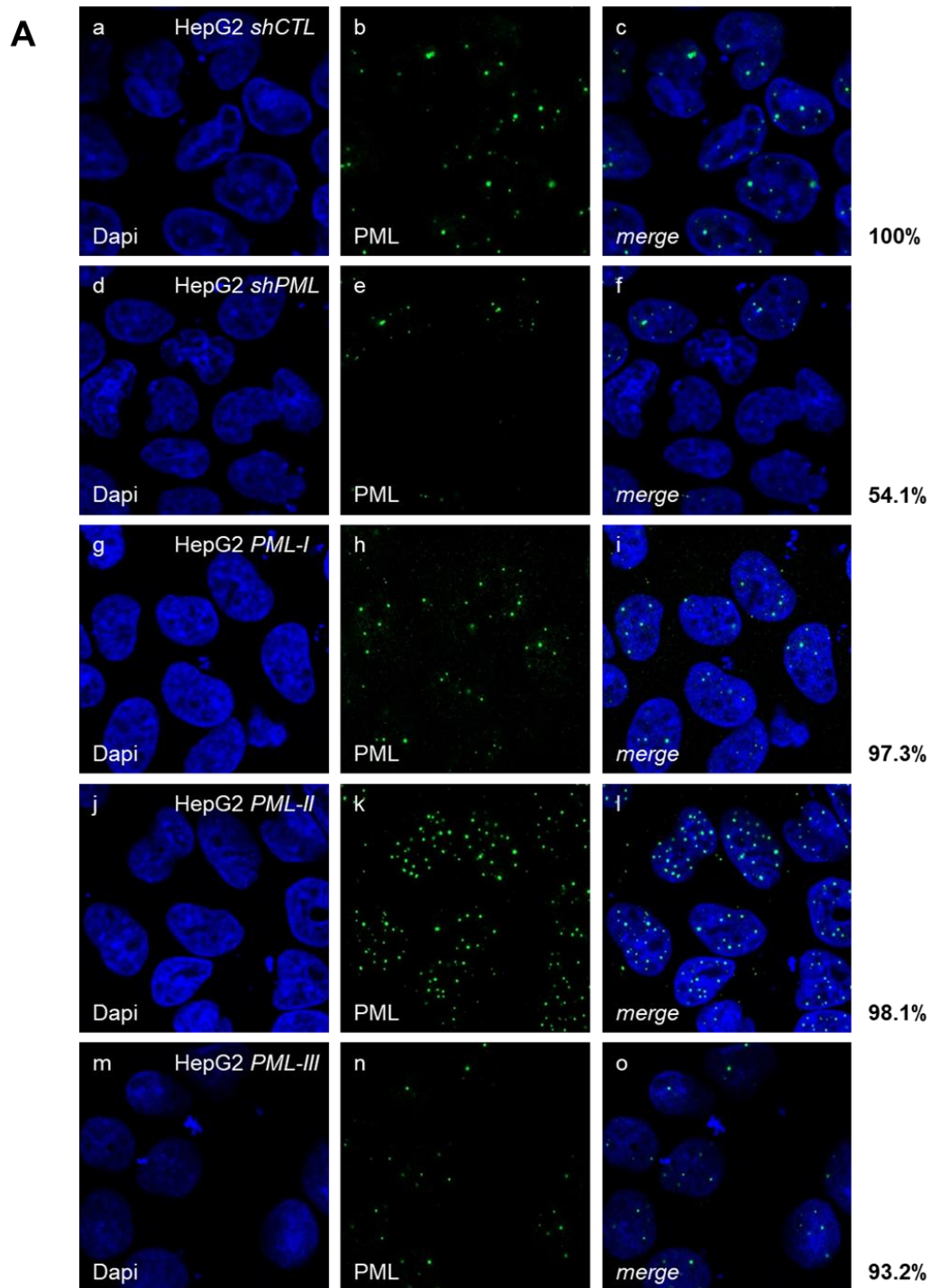
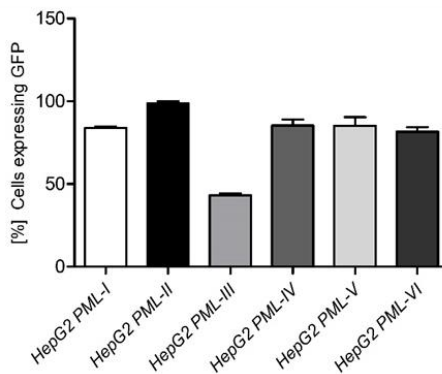**Figure 21: Verification of HepG2-NTCP-K7 based cell lines expressing single GFP-tagged nuclear PML isoforms I to VI by PML staining. A, B** HepG2-NTCP-K7 cells were either transduced with lentiviral vectors encoding a control shRNA (HepG2 *shCTL*, **A** panels a-c) or a shRNA directed against PML (HepG2 *shPML*, **A** panels d-f) and selection was achieved using puromycin. HepG2 *shPML* cells were further transduced with lentiviral vectors encoding shRNA resistant GFP-tagged single PML isoforms I to VI and selection was achieved using G418 resulting in HepG2 *PML-I* (**A** panels g-i), HepG2 *PML-II* (**A** panels j-l), HepG2 *PML-III* (**A** panels m-o), HepG2 *PML-IV* (**A** panels q-r), HepG2 *PML-V* (**A** panels s-u), and HepG2 *PML-VI* (**A** panels v-x). Cells were stained using anti-PML (ab72137) antibody, which was detected using Alexa 488 (green, PML) conjugated secondary antibodies, and the nuclei were co-stained using Dapi. Pictures were taken using a Zeiss LSM 980 laser scanning microscope. Images are representative for at least 60 cells. **B** PML expressing cells from two viewfields were counted and visualized as [%] PML expressing cells using GraphPad *PRISM5*.
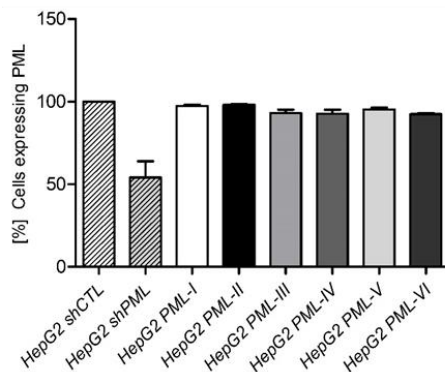
A (cont.)

B

Figure 21: Verification of HepG2-NTCP-K7 based cell lines expressing single GFP-tagged nuclear PML isoforms I to VI by PML staining (continued).

Further analysis by immunofluorescence using a GFP antibody to detect only the reintroduced single PML isoforms revealed efficient expression of GFP-tagged PML isoforms in HepG2 *PML-I* with 84.0% GFP positive cells (see figure 22 A, panels h, i, figure 22 B), 98.5% for HepG2 *PML-II* (see figure 22 A, panels k, l, figure 22 B), 85.3% for HepG2 *PML-IV* (see figure 22 A, panels q, r, figure 22 B), 85.2% for HepG2 *PML-V* (see figure 22 A, panels t, u, figure 22 B) and 81.5% for HepG2 *PML-VI* (see figure 22 A, panels w, x, figure 22 B).
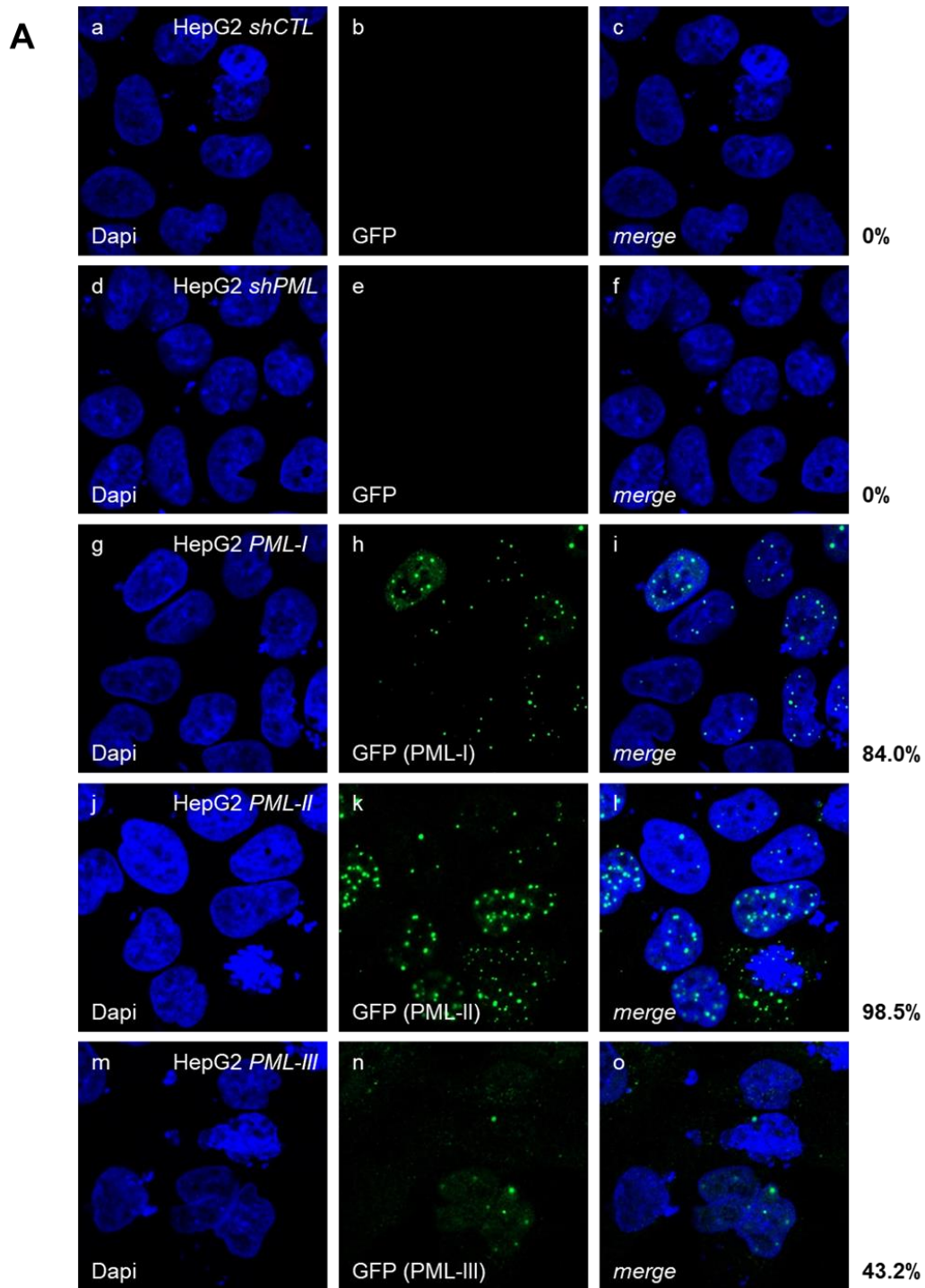
Figure 22: Verification of HepG2-NTCP-K7 based cell lines expressing single GFP-tagged nuclear PML isoforms I to VI by GFP staining. A, B HepG2-NTCP-K7 cells were either transduced with lentiviral vectors encoding a control shRNA (HepG2 *shCTL*, **A** panels a-c) or a shRNA directed against PML (HepG2 *shPML*, **A** panels d-f) and selection was achieved using puromycin. HepG2 *shPML* cells were further transduced with lentiviral vectors encoding shRNA resistant GFP-tagged single PML isoforms I to VI and selection was achieved using G418 resulting in HepG2 *PML-I* (**A** panels g-i), HepG2 *PML-II* (**A** panels j-l), HepG2 *PML-III* (**A** panels m-o), HepG2 *PML-IV* (**A** panels q-r), HepG2 *PML-V* (**A** panels s-u), and HepG2 *PML-VI* (**A** panels v-x). Cells were stained using anti-GFP (ab290) antibody, which was detected using Alexa 488 (green, GFP) conjugated secondary antibodies, and the nuclei were co-stained using Dapi. Pictures were taken using a Zeiss LSM 980 laser scanning microscope. Images are representative for at least 60 cells. **B** GFP expressing cells from two viewfields were counted and visualized as [%] GFP expressing cells using GraphPad *PRISM5*.
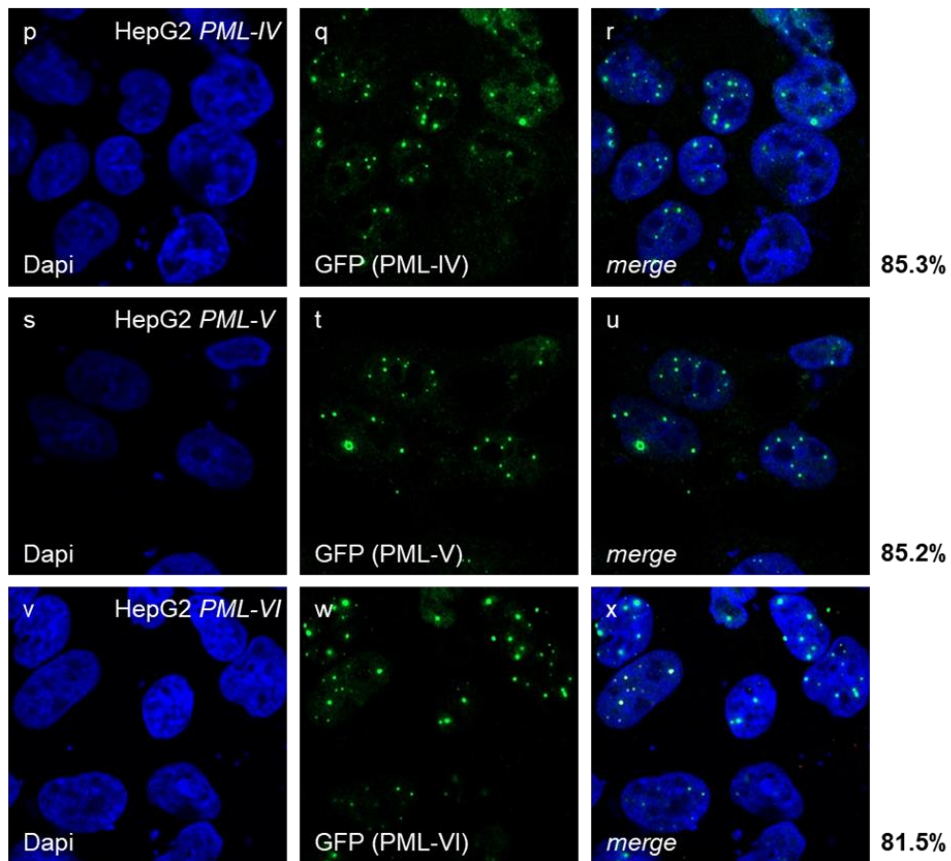
A (cont.)

B

Figure 22: Verification of HepG2-NTCP-K7 based cell lines expressing single GFP-tagged nuclear PML isoforms I to VI by GFP staining (continued).

For HepG2 *PML-III*, however, only a minor degree of GFP-tagged PML-III expression could be observed, with only 43.2% of GFP positive cells (see figure 22 A, panels n, o, figure 22 B). HepG2 *shCTL* (see figure 22 A, panels b, c) and HepG2 *shPML* (see figure 22 A, panels e, f) which were not transduced using GFP expressing lentiviral vectors did, as expected, not show GFP staining. Summarized, HepG2-NTCP-K7 cell lines robustly expressing single nuclear PML isoforms I to VI could be established.

4.4.2 HBV core protein associates with specific PML isoforms

To get a first insight into the interaction of HBV core protein with specific PML isoforms, pcore-HA *wt* was transfected into HepG2 cells expressing single GFP-tagged PML isoforms I to VI, as well as HepG2 *shCTL* and HepG2 *shPML* as corresponding control. A slight increase in steady state levels of HA-tagged HBV core protein in cells depleted for PML (HepG2 *shPML*, see figure 23, input, lane 3, figure 23 B) and HepG2 cells expressing single PML isoforms I to VI (see figure 23, input, lanes 4-9, figure 23 B) compared to HepG2 *shCTL* cells (see figure 23, input, lane 2, figure 23 B) was found. Analysis of steady state protein levels of PML and GFP revealed stable expression of GFP-tagged single PML isoforms I to VI (see figure 23 A, input, lanes 4-9) and sufficient depletion of PML in the HepG2 *shPML* cell line (see figure 23 A, input, lane 3) compared to HepG2 *shCTL* (see figure 23 A, input, lanes 1, 2). These results confirmed the successful generation of HepG2-NTCP-K7 based cell lines depleted for PML and expressing single GFP-tagged PML isoforms. Using immunoprecipitation of the HA-tag of HBV core protein, a weak interaction of HA-tagged HBV core protein with PML isoform I could be observed (see figure 23 A, IP-HA, lane 4). Contrary, immunoprecipitation of single GFP-tagged PML isoforms I to VI using a GFP antibody co-precipitated HA-tagged HBV core protein only in the presence of GFP-PML-II (see figure 23 A, IP-GFP, lane 5). In summary, these data from immunoprecipitation studies suggested a site-specific interaction of HBV core protein with the two PML isoforms I and II.
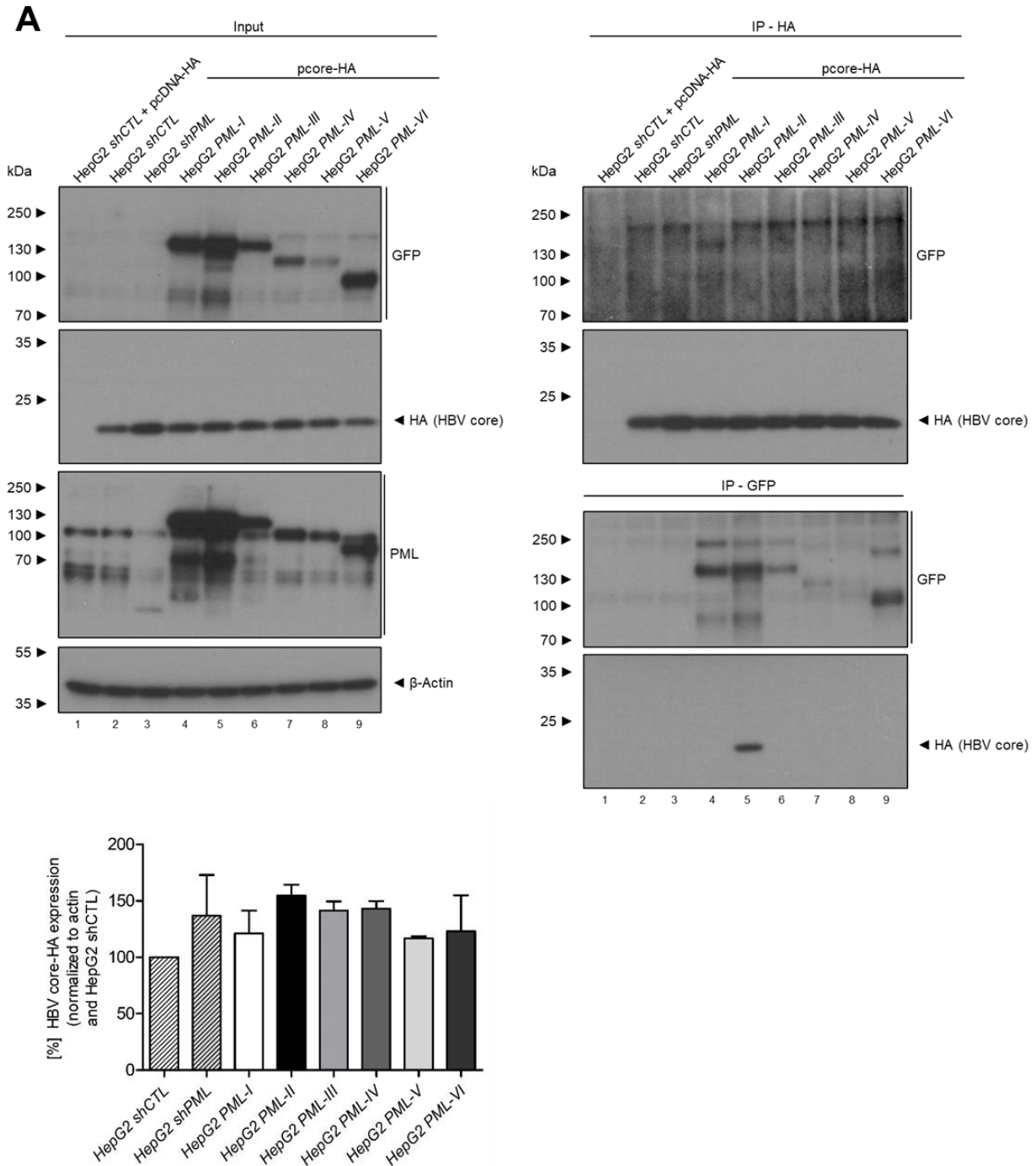
Figure 23: HBV core protein interacts with PML isoforms I and II. A, B HepG2 *shCTL* (**A** lane 2), HepG2 *shPML* (**A** lane 3), HepG2 *PML-I* (**A** lane 4), HepG2 *PML-II* (**A** lane 5), HepG2 *PML-III* (**A** lane 6), HepG2 *PML-IV* (**A** lane 7), HepG2 *PML-V* (**A** lane 8), and HepG2 *PML-VI* (**A** lane 9) were transfected with 10µg of pcore-HA. As control, HepG2 *shCTL* were transfected with 10µg of pcDNA-HA empty (**A** lane 1). **A** Whole-cell protein lysates were prepared 48h post transfection and immunoprecipitation using an anti-HA (3F10) and anti-GFP (ab290) antibody was performed. Protein lysates and immunoprecipitation were analyzed by SDS-PAGE and western blot using anti-PML (ab72137), anti-HA (3F10), anti-GFP (ab290) and anti-β-Actin (AC-15) antibodies. Molecular weights are depicted on the left, respective proteins are indicated on the right of each blot. Data are representative for two independent biological replicates. **B** Western blot signals of HA-tagged HBV core protein steady state levels were analyzed by densitometry using *FiJi* (version 1.45s). Signals for HA-tagged HBV core protein were normalized to β-Actin. The graph was visualized using GraphPad *PRISM5*. Data are representative for two independent biological replicates.

For further validation of the interaction of HBV core protein with PML isoforms I and II, immunofluorescence stainings of HepG2 cells expressing single PML isoforms I to VI (see figure 24, panels u-ab for HepG2 *PML-I*, ac-aj for HepG2 *PML-II*, ak-ar for HepG2 *PML-III*, as-az for HepG2 *PML-IV*, ba-bh for HepG2 *PML-V* and bi-bp for HepG2 *PML-VI*) transfected with HA-tagged HBV core protein were performed using anti-PML and anti-HA antibodies. HepG2 *shCTL* (see figure 24, panels a-l) and HepG2 *shPML* (see figure 24, panels m-t) were used as corresponding controls. Analysis of localization of HA-tagged HBV core protein in HepG2 *shCTL* cells, expressing all PML isoforms, revealed an efficient and distinct co-localization of HBV core protein with PML in 90.1% of observed cells (see figure 24, panels f-h, j-l, figure 25 B). This further confirmed the association of HBV core protein with PML found in HepaRG cells in chapter 4.1. For HepG2 *shPML* cells depleted for PML proteins via shRNA, two different localizations of HA-tagged HBV core protein were detected in a ratio of almost 50:50. HBV core protein either localized in distinct nuclear foci, even in absence of nuclear PML (see figure 24, panels n-p) which occured in 46.4% of cells, or it showed a diffuse and preferentially cytoplasmic localization (see figure 24, panels r-t) for 53.6% of cells.

Despite specific interaction of HBV core protein with PML isoforms I and II, as observed by immunoprecipitation (see figure 23), HA-tagged HBV core protein localization to PML was found to be very similar among HepG2 *PML-I* (see figure 24, panels v-x, z-ab, figure 25 B) with 75.7% of cells showing co-localization of HBV core protein and PML, HepG2 *PML-II* (see figure 24, panels ad-af, ah-aj, figure 25 B) with 75.9%, HepG2 *PML-IV* (see figure 24, panels at-av, ax-az, figure 25 B) with 76.5%, HepG2 *PML-V* (see figure 24, panels bb-bd, bf-bh, figure 25 B) with 78.8%, and HepG2 *PML-VI* (see figure 24, panels bj-bl, bn-bp, figure 25 B) with 72.2% of cells showing co-localization. For HepG2 *PML-III*, a different picture was observed. Here, co-localization of HBV core with PML could only be detected for 55.9% of cells (see figure 24, panels al-an, ap-ar, figure 25 B). The co-localization of HBV core protein with PML in the different HepG2 cell lines was further assessed using the Pearson correlation coefficient, however here, no distinct differences in the calculated co-localization were identified (see figure 25 A), which might be due to a diffuse background of the HBV core protein staining not observed in HepaRG cells (see figure 9, figure 15 compared to figure 24).
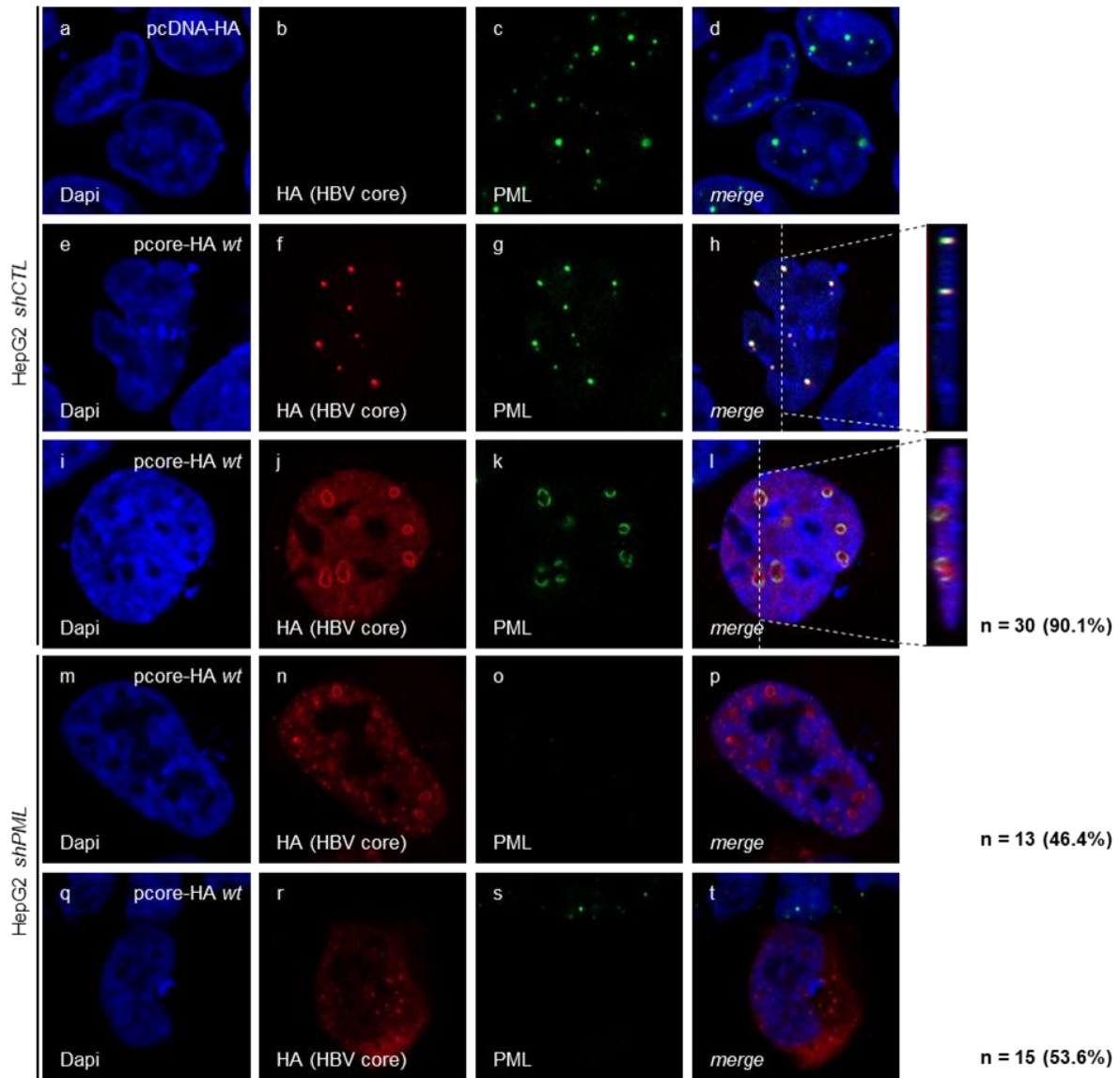
**Figure 24: Co-staining of HBV core protein and PML in HepG2 cells expressing single PML isoforms shows no isoform specific co-localization.** HepG2 *shCTL* (panels e-l), HepG2 *shPML* (panels m-t), HepG2 *PML-I* (panels u-ab), HepG2 *PML-II* (panels ac-aj), HepG2 *PML-III* (panels ak-ar), HepG2 *PML-IV* (panels as-az), HepG2 *PML-V* (panels ba-bh), and HepG2 *PML-VI* (panels bi-bp) were transfected with 10µg of pcore-HA. As control, HepG2 *shCTL* were transfected with 10µg of pcDNA-HA empty (panels a-d). Cells were fixed with 4% PFA at 48h post transfection and and double stained with anti-PML (ab72137) and anti-HA (3F10) antibodies. Primary antibodies were detected using Alexa 488 (green, PML) and Alexa 647 (red, HA) conjugated secondary antibodies and the nuclei were co-stained using Dapi. Pictures and Z-stacks were taken using a Zeiss LSM 980 laser scanning microscope. Representative images for at least 28 cells are shown.
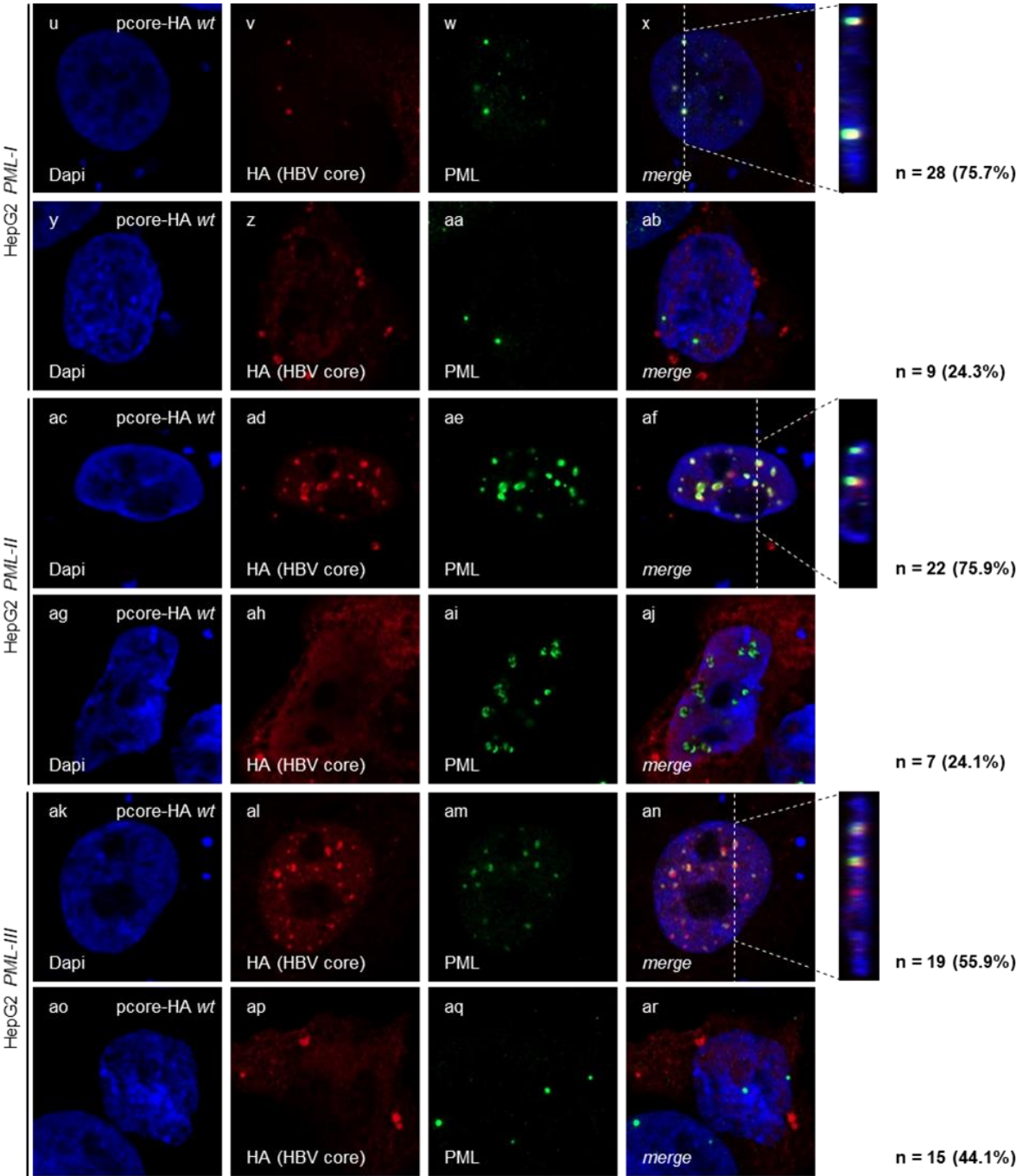
Figure 24: Co-staining of HBV core protein and PML in HepG2 cells expressing single PML isoforms shows no isoform specific co-localization (continued).
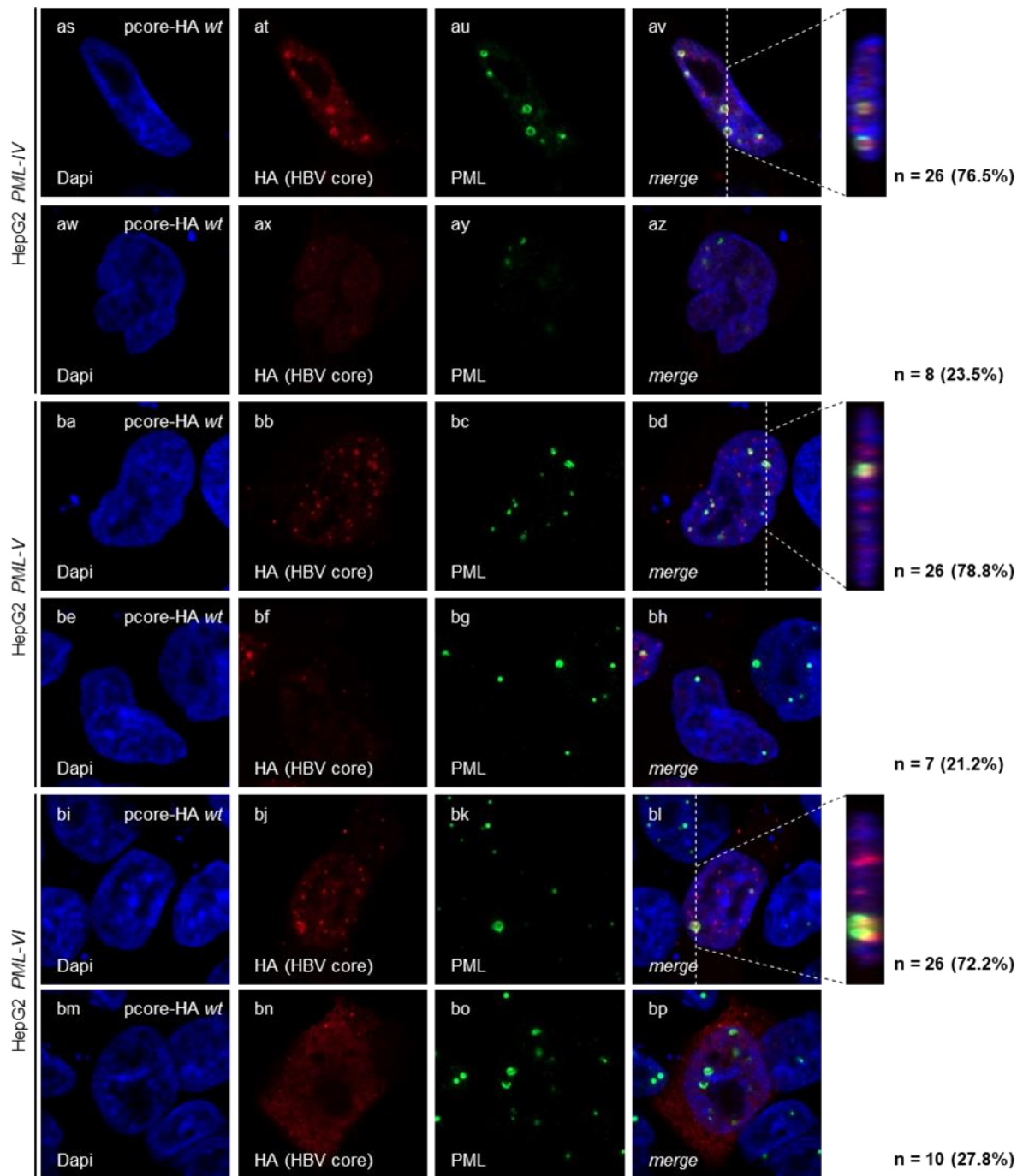
Figure 24: Co-staining of HBV core protein and PML in HepG2 cells expressing single PML isoforms shows no isoform specific co-localization (continued).
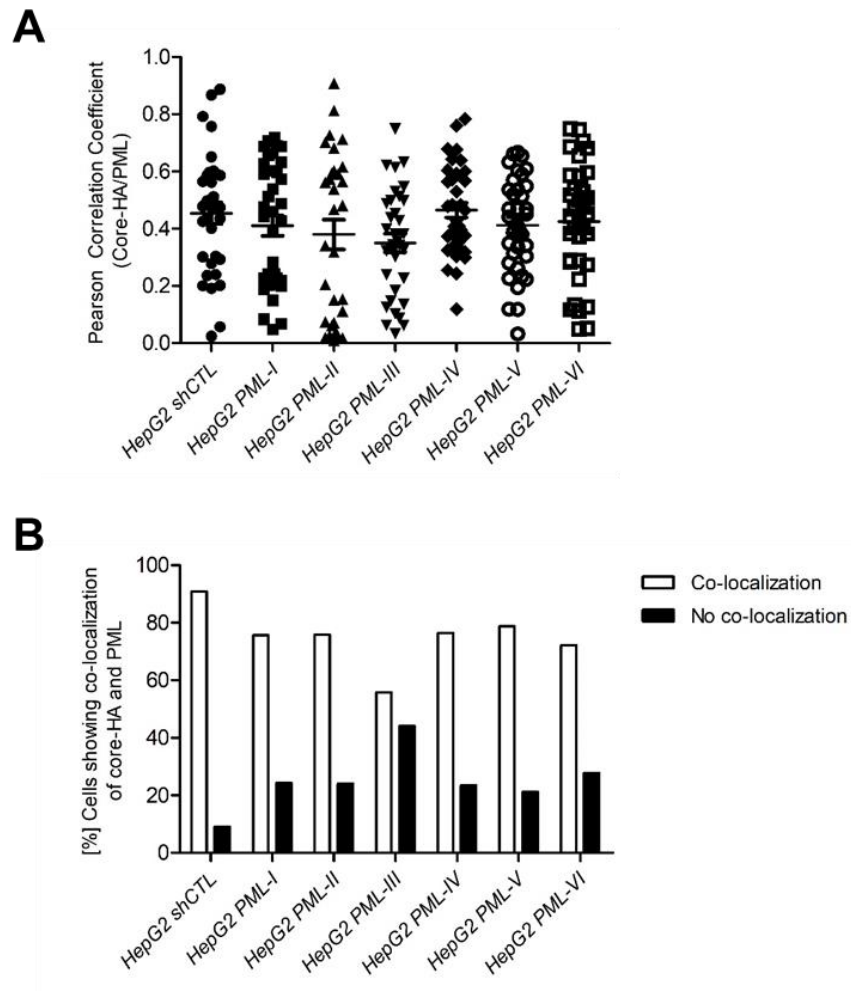
Figure 25: HBV core protein co-localizes with PML isoforms I, II, IV, V and VI when co-stained with PML. A Cells from figure 24 were analyzed for co-localization of HA-tagged HBV core protein with PML using Pearson correlation coefficient and the software *FiJi* (version 1.45s). Data were visualized using GraphPad *PRISM5* and represent at least 28 cells. **B** Cells from figure 24 were distributed in categories of cells showing co-localization of HA-tagged HBV core protein with PML and cells without co-localization. Data were visualized using GraphPad *PRISM5* and represent at least 28 cells.

The HepG2 *shPML* cells, which served as basis for the generation of HepG2 cells expessing single nuclear PML isoforms I to VI, still showed a background PML expression in around 50% of cells (see figure 20 B, figure 21). As no specific co-localization of HBV core protein with single PML isoforms could be observed using a PML staining (see figure 24, figure 25), HBV core-PML associations were further analyzed by co-staining of the GFP-tag of the single PML isoforms and HA-tagged HBV core protein.
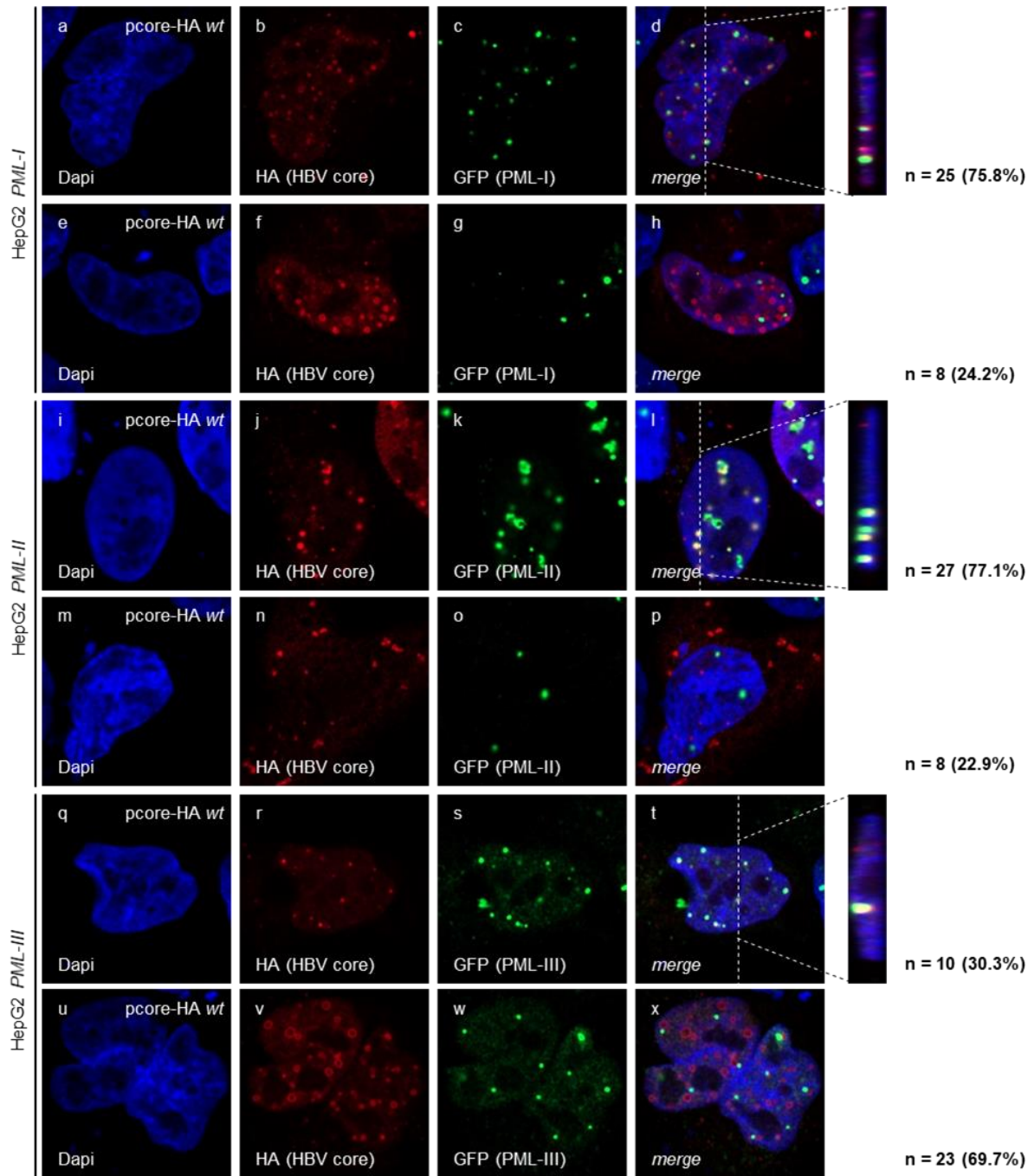
Figure 26: HBV core protein preferentially associates with PML isoforms I and II. HepG2 *PML-I* (panels a-h), HepG2 *PML-II* (panels i-p), HepG2 *PML-III* (panels q-x), HepG2 *PML-IV* (panels y-af), HepG2 *PML-V* (panels ag-an), and HepG2 *PML-VI* (panels ao-av) were transfected with 10µg of pcore-HA. Cells were fixed with 4% PFA at 48h post transfection and and double stained with anti-GFP (ab290) and anti-HA (3F10) antibodies. Primary antibodies were detected using Alexa 488 (green, GFP) and Alexa 647 (red, HA) conjugated secondary antibodies and the nuclei were co-stained using Dapi. Pictures and Z-stacks were taken using a Zeiss LSM 980 laser scanning microscope. Representative images for at least 30 cells are shown.
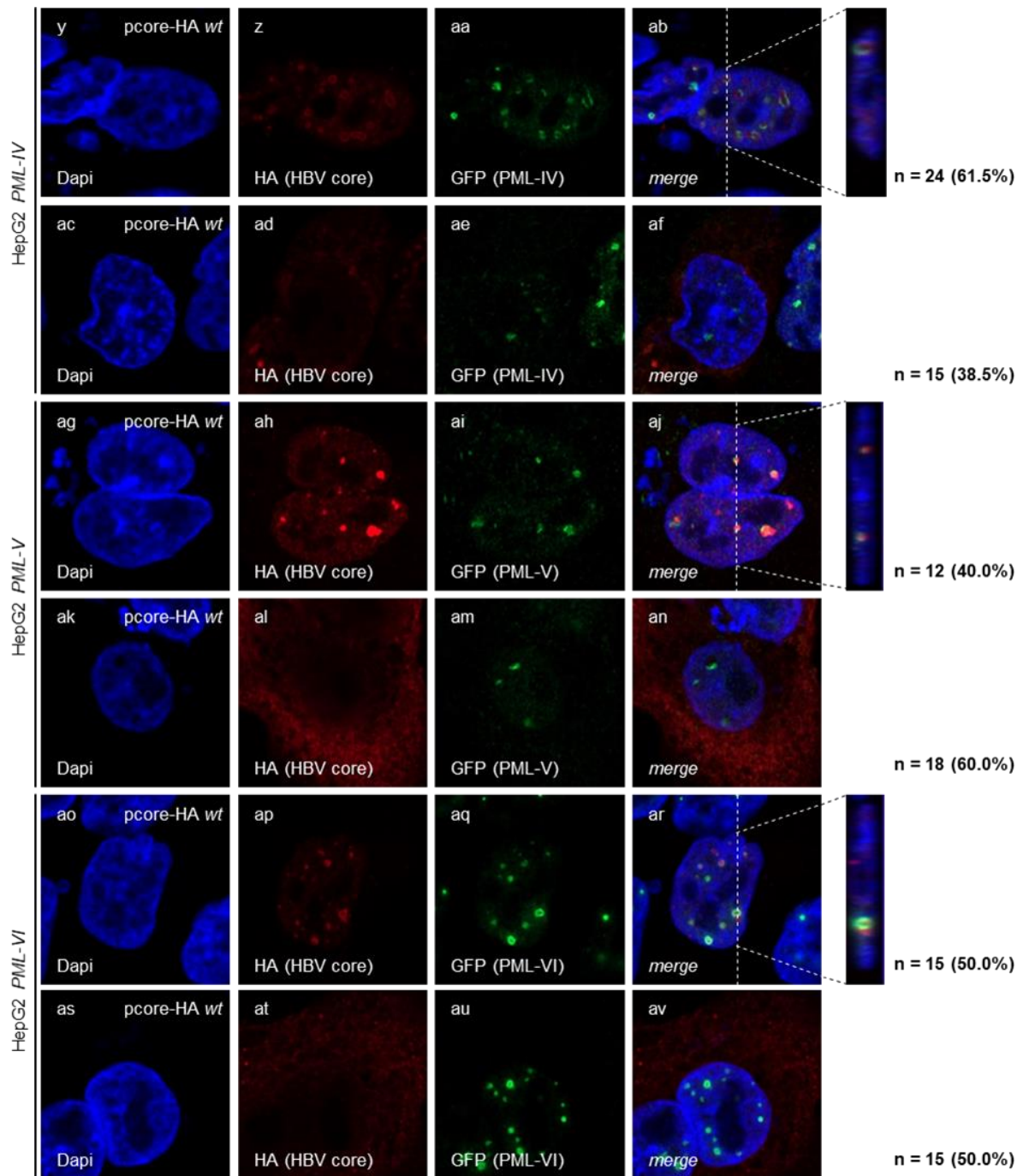
Figure 26: HBV core protein preferentially associates with PML isoforms I and II (continued).

Here, co-localization of HBV core protein with GFP-tagged PML isoforms could be most prominently observed in HepG2 *PML-I* (see figure 26, panels b-d, f-h, figure 27 B) with 75.8% of cells showing co-localization of GFP-PML-I and HBV core protein and HepG2 *PML-II* (see figure 26, panels j-l, n-p, figure 27 B) with 77.1% co-localization. These data were consistent with interaction of HBV core protein with GFP-tagged PML isoforms I and II observed using immunoprecipitation (see figure 23). In HepG2 *PML-IV* cells, still a substantial amount of 61.5% cells had co-localization of HBV core protein with the GFP-tagged single PML isoform (see figure 26, panels z-ab, ad-af, figure 27 B), while this was reduced to 50% of cells in the HepG2 *PML-VI* cell line (see figure 26, panels ap-ar, at-av, figure 27 B). The lowest association between HA-tagged HBV core protein and GFP-tagged single PML isoforms was found for HepG2 *PML-V* cells where 40% of cells showed co-localization (see figure 26, panels ah-aj, al-an, figure 27 B) and HepG2 *PML-III* with co-localization observed in 30.3% of cells (see figure 26, panels r-t, v-x, figure 27 B). This association was further analyzed using determination of the Pearson correlation coefficient between HA-tagged HBV core protein and GFP-tagged single PML isoforms. As already described for the Pearson correlation coefficient analysis for PML and HBV core (see figure 25 A), however, no clear difference between the single PML isoforms could be observed. This was probably due to the more diffuse localization of HA-tagged HBV core protein in HepG2 cells compared to HepaRG (see figure 9, figure 15 compared to figure 24, figure 26). Taken together, these results indicated a preferential association of HBV core protein with specific PML isoforms I and II during transfection of HBV core in absence of other viral factors.

A

B
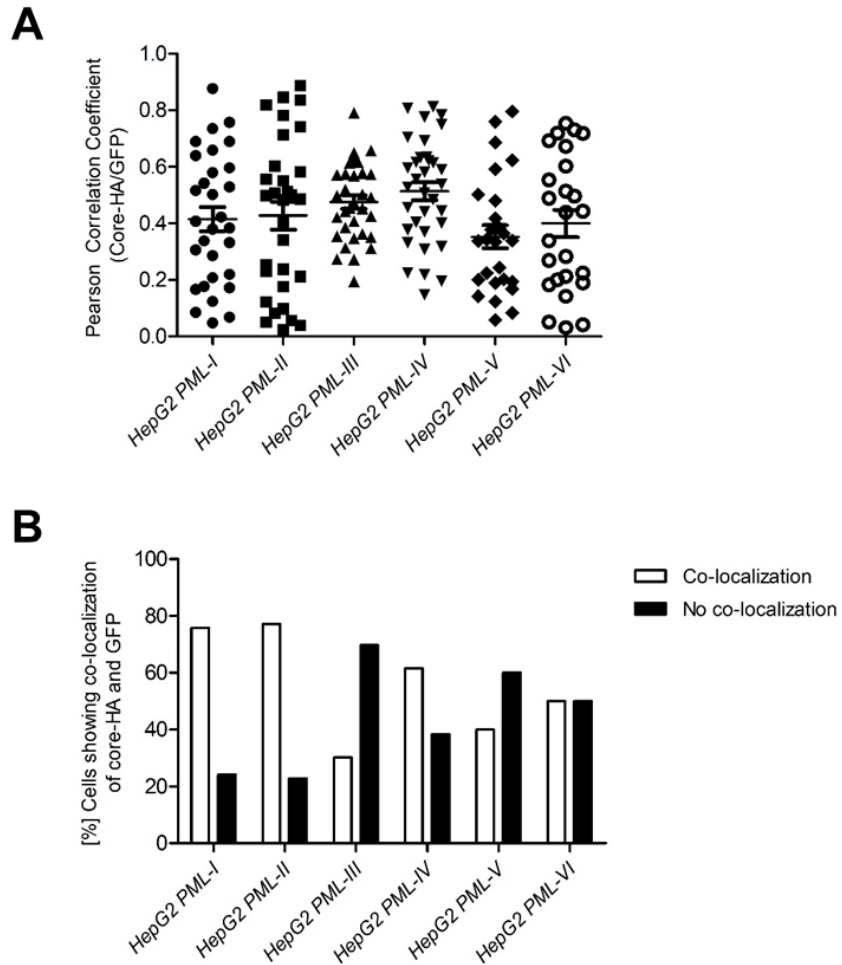
Figure 27: HBV core protein shows association to PML isoforms I and II. A Cells from figure 26 were analyzed for co-localization of HA-tagged HBV core protein with GFP-tagged single PML isoforms using Pearson correlation coefficient and the software *FiJi* (version 1.45s). Data were visualized using GraphPad *PRISM5* and represent at least 30 cells. **B** Cells from figure 26 were distributed in categories of cells showing co-localization of HA-tagged HBV core protein with GFP-tagged single PML isoforms and cells without co-localization. Data were visualized using GraphPad *PRISM5* and represent at least 30 cells.

4.4.3 PML-II and PML-VI support cccDNA formation

To further dissect the role of single PML isoforms in cccDNA generation, HepG2 *shCTL,* HepG2 *shPML* as well as HepG2 *PML-I* to *PML-VI* were infected with HBV and the levels of complete HBV DNA, including replication intermediates as well as rcDNA, and cccDNA specifically were determined by qPCR. For complete HBV DNA, a decrease in DNA levels for PML depleted HepG2 *shPML*, as well as single PML isoform expressing HepG2 *PML-I*, HepG2 *PML-II*, HepG2 *PML-III*, and, most prominently HepG2 *PML*-IV as well as HepG2 *PML-V* was observed (see figure 28 A). In contrast, HBV infection in HepG2 *PML-VI* cells resulted in HBV DNA levels similar to those observed in HepG2 *shCTL* cells, expressing all PML isoforms (see figure 28 A).
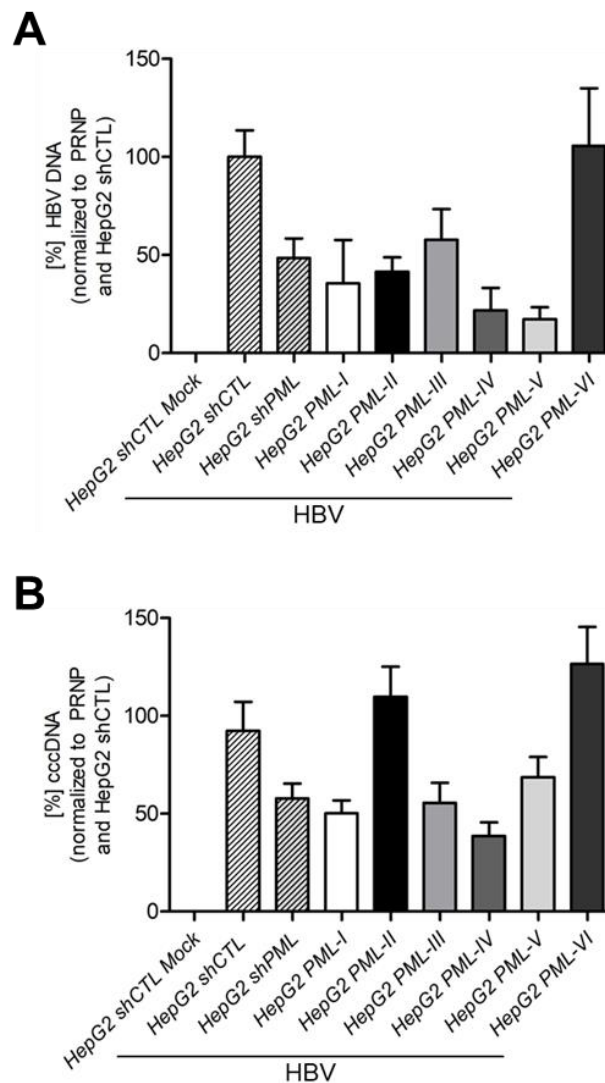
Figure 28 PML isoforms II and VI support cccDNA formation, while only isoform VI grants transcriptional activity.
HepG2 *shCTL*, HepG2 *shPML* and HepG2 *PML-I* to *PML-VI* were differentiated by addition of 2.5% DMSO for 2d. Cells were infected with HBV at a MOI of 200 GE/cell and total DNA was extracted using the MachereyNagel NucleoSpin Tissue Kit 7d.p.i.. As control, non-infected HepG2 *shCTL* cells were used. **A** Complete HBV DNA and **B** cccDNA were determined using qPCR and normalized to PRNP. Bar charts were visualized using GraphPad *PRISM5* and correspond to six biological replicates measured in triplicates.

On the level of cccDNA, a decrease in cccDNA levels to around 50% compared to HepG2 *shCTL* cells, expressing all endogenous PML isoforms, was observed in the PML depleted HepG2 *shPML* cells (see figure 36 B). These data were consistent with the reduction of PML expressing cells to around 50% in HepG2 *shPML* (see figure 20 B, figure 21). A similar repression in cccDNA formation was found in single PML isoform expressing cell lines HepG2 *PML-I*, HepG2 *PML-III*, HepG2 *PML-IV* and HepG2 *PML-V*, partially contrary to the interaction of HBV core protein with PML-I as determined by immunoprecipitation (see figure 23) and immunofluorescence (see figure 26, figure 27). The two PML isoforms PML-II and PML-VI were found to support efficient cccDNA formation, similar to presence of all endogenous PML isoforms in HepG2 *shCTL* (see figure 28 B). These findings were partially consistent with the interaction and association of HBV core protein with PML isoform II determined by immunoprecipitation (see figure 23) and immunofluorescence (see figure 26, figure 27). In sum, these results stress the importance of PML in cccDNA formation and pointed out a specific role of PML isoforms II and VI in supporting cccDNA generation during HBV infection. Furthermore, PML isoforms might differentially regulate cccDNA transcription, as HepG2 *PML-II* cells supported cccDNA formation, but have reduced complete HBV DNA levels as compared to HepG2 *shCTL* cells, while HepG2 *PML-VI* cells supported efficient complete HBV DNA formation (see figure 28 A, figure 28 B).

4.5 SUMO PTM of HBV core induces HBV capsid disassembly

HBV nucleocapsid assembly and disassembly is strictly and dynamically regulated by HBV core protein PTMs (see chapter 3.1.5.3). Therefore, the question arose if HBV core protein SUMOylation might impact HBV nucleocapsid stability and integrity. To address this, the structures of HBV core protein with arginine mutations in SCM1 and/or SCM2 were modeled using the *Swiss Model* online tool (*422*) based on the tetrameric structure of HBV core protein (PDB: 3J2V) (*197*). No severe impact of the lysine to arginine mutations at SCM1 and/or SCM2 could be observed, neither on the overall secondary, tertiary, and quartary structure (see figure 29 A, panels a-d), nor on the molecular level (see figure 29 A, panels e-f).

Subsequently, the docking of SUMO2 (PDB: 2CHK_2) to HBV core protein in a tetrameric structure (PDB: 3J2V), which represents the asymmetric unit of T=4 HBV nucleocapsids, was predicted by *in silico* modeling using *ZDOCK Server* (*424*). Here, a sterical overlap between the SUMO2 protein (red) conjugated to either SCM1 (see figure 29, panels a, b) or SCM2 (see figure 29, panels c, d) of one HBV core monomer (dark blue) with the adjacent HBV core protein monomer (light blue) within the tetrameric structure was observed. This overlap might cause disruption of HBV nucleocapsids due to sterical constraints.
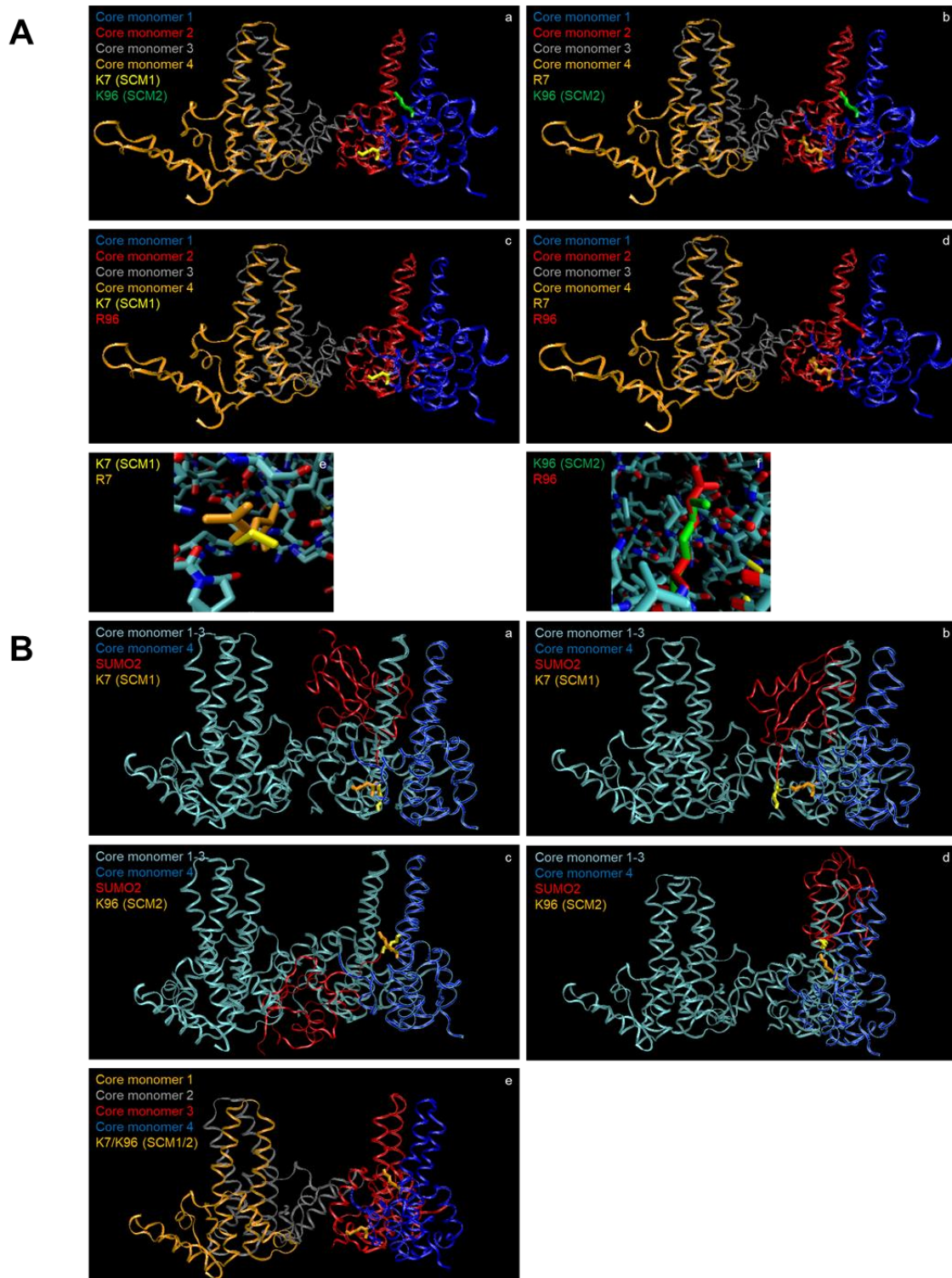
Figure 29 *In silico* modeling suggests effects of HBV core SUMOylation on HBV capsid integrity. **A** Effects of lysine to arginine mutations at SCM1 (panels b, e), SCM2 (panels c, f) or both SCMs (panel d) in HBV core protein on HBV core structure was determined by molecular modeling using *Swiss Model* (*422*). Structure predictions were calculated based on PDB 3J2V (*197*) and superimposed with the original tetrameric HBV core protein structure 3J2V using *VMD* (*423*). **B** *In silico* docking of SUMO2 (PDB: 2CHK_2) (*433*) to SCM1 (panels a, b) or SCM2 (panels c, d) of HBV core protein in the tetrameric asymmetric unit of T=4 HBV capsids (PDB: 3J2V) (*197*) was simulated using *ZDOCK Server* (*424*). Predicted docking structures were visualized using *VMD* (*423*).

To assess this hypothesis, *in vitro* SUMOylation assays were performed with purified recombinantly expressed HBV capsids. When *wt* HBV capsids were subjected to the purified SUMOylation machinery, a loss of signal in the NAGE could be observed, which indicated disruption of HBV nucleocapsid integrity (see figure 30, left panel, lanes 1, 2). Simultaneously, treatment of HBV nucleocapsids with the *in vitro* SUMOylation kit induced higher migrating bands in the western blot input (see figure 30, right panel, lanes 1, 2), indicative of SUMO PTM occurring on HBV core protein derived from HBV nucleocapsids. Interestingly, also effects of *in vitro* SUMOylation on HBV nucleocapsid integrity and HBV core protein SUMO modification could be observed in samples, where Mg-ATP was omitted (see figure 30, both panels, lane 2). Omission of Mg-ATP should serve as internal control, as the activation of the SUMO machinery requires ATP (*283*). To further test the hypothesis that SUMO PTM of HBV core induces HBV capsid disassembly, *wt* as well as SUMOylation deficient *Δscm1/2* HBV capsids were subjected to the *in vitro* SUMOylation machinery. Here, SUMO proteins were omitted as negative control. For *wt* capsids again loss of nucleocapsids was observed during treatment with the *in vitro* SUMOylation kit and SUMO proteins (see figure 30 B, left panel, lanes 1, 2, figure 30 C), accompanied with higher migrating bands in the western blot (see figure 30 B, right panel, lanes 1, 2). For the *Δscm1/2* mutant HBV capsid, no effect in the NAGE (see figure 30 B, left panel, lanes 3, 4, figure 30 C), nor in the western blot (see figure 30 B, right panel, lanes 1, 2) could be observed, indicating a deficiency in SUMOylation and SUMO induced capsid disassembly. Taken together, these results indicated that HBV core protein SUMOylation occured in HBV capsids and triggered disruption of HBV capsids.

A

B

C
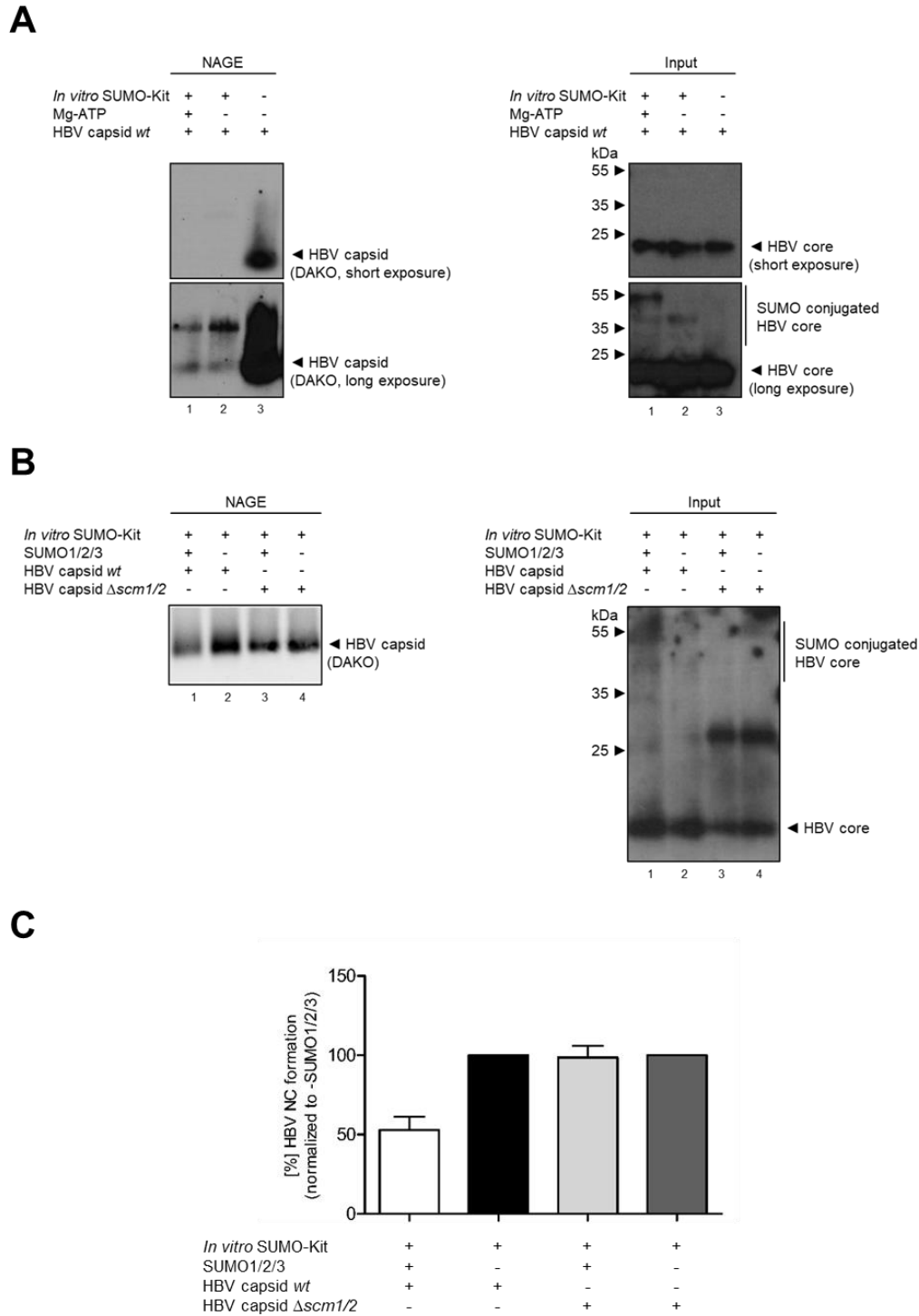
Figure 30 HBV core protein SUMOylation induces nucleocapsid disruption. A Recombinantly expressed *wt* HBV capsids were treated with an *in vitro* SUMOylation assay kit (lane 1) using omission of Mg-ATP (lane 2) or of the complete SUMO machinery (lane 3) as control. Samples were analyzed by NAGE and immunoblotting using anti-HBV capsid antibody (DAKO, B0586) and denaturing SDS-PAGE and western blot using anti-HBV core (8C9) antibody. Molecular weights are depicted on the left, respective proteins are indicated on the right of each blot. **B** Recombinantly expressed *wt* (lanes 1, 2) and *Δscm1/2* (lanes 3, 4) HBV capsids were treated with an *in vitro* SUMOylation assay kit using omission of SUMO proteins as control (lanes 2, 4). Samples were analyzed by NAGE and immunoblotting using anti-HBV capsid antibody (DAKO, B0586) and denaturing SDS-PAGE and western blot using anti-HBV core (8C9) antibody. Molecular weights are depicted on the left, respective proteins are indicated on the right of each blot. **C** NAGE signals of **B** were analyzed by densitrometry using *FiJi* (version 1.45s). Graphs were visualized using GraphPad *PRISM5*. Data are representative for two independent biological replicates.

102

4.6 SUMOylation of HBV core is essential to nuclear entry

SUMOylation of HBV core protein was observed to play a role in HBV capsid disassembly (see chapter 4.5). Therefore, localization of *wt* and *Δscm1/2* HBV core protein and capsids in presence of other viral proteins and viral replication were analyzed using transfection of pHBV1.1 *wt* and *Δscm1/2* into HepaRG cells. For pHBV1.1 *wt*, a diffuse localization of HBV core was observed using antibodies directed against assembled capsids and capsid intermediates (see figure 31, panels f-h, j-l) or a linear epitope in the HBV core protein (see figure 32, panels f-h, j-l) as previously published for HBV infection (*103, 110, 195, 220-226*).
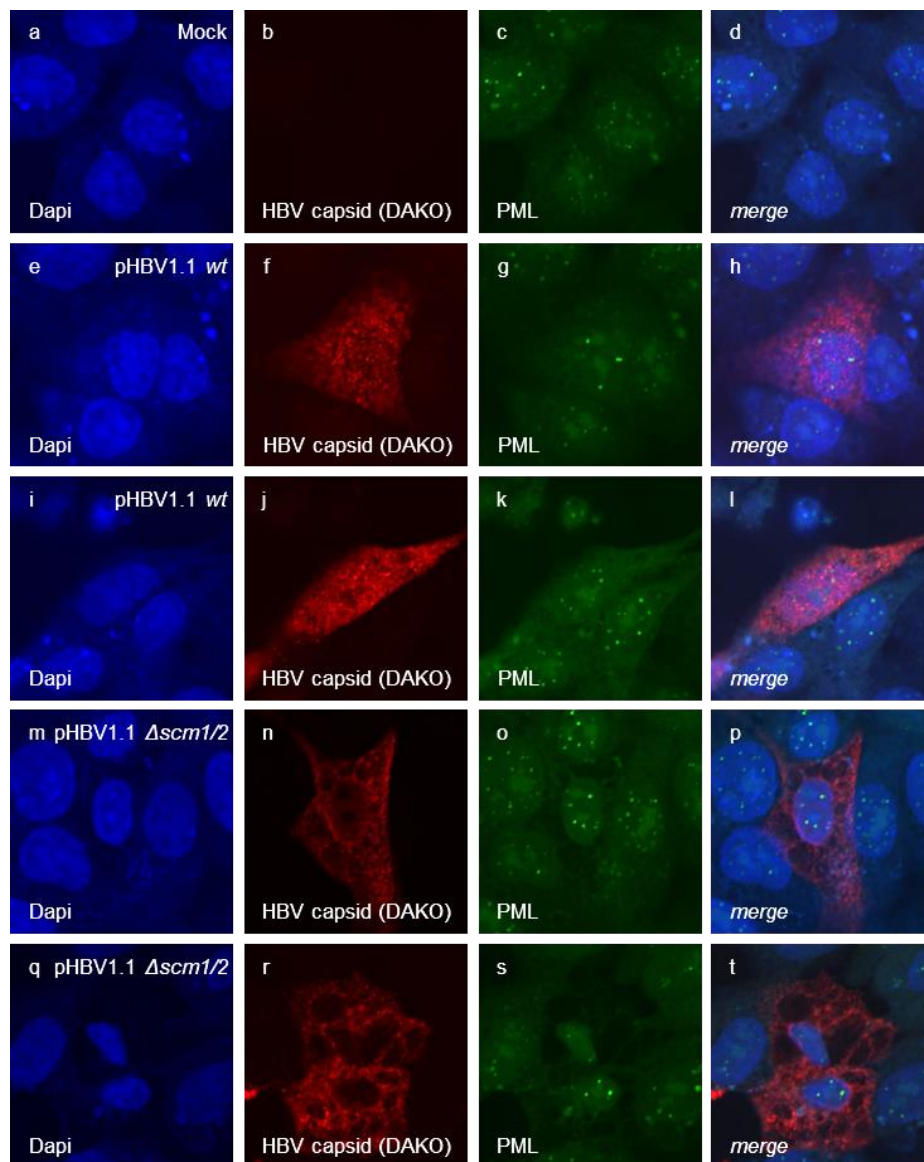
Figure 31: HBV core protein SUMOylation mediates nuclear recycling. HepaRG cells were transfected with 3μg of pHBV1.1 *wt* (panels e-l) or *Δscm1/2* (panels m-t). Cells were fixed 48h post transfection with 4 % PFA and stained using anti-PML (sc-966) and anti-HBV capsid (DAKO B0586) antibodies. Primary antibodies were detected using Alexa 488 (green, PML) and Alexa 647 (red, HBV capsid) conjugated secondary antibodies and the nuclei were co-stained using Dapi. Pictures were taken using a Nikon TiE laser scanning microscope. Images are representative for at least 30 mock and transfected cells.

This localization of HBV core proteins drastically changed during transfection of pHBV1.1 *Δscm1/2*. Here, an almost exclusive cytoplasmic localization of HBV core protein was found using the antibody detecting HBV nucleocapsids and capsid intermediates (see figure 31, panels n-p, r-t) or the antibody directed against a linear epitope in HBV core (see figure 32, panels n-p, r-t), with almost no signal of HBV core protein in the nucleus.
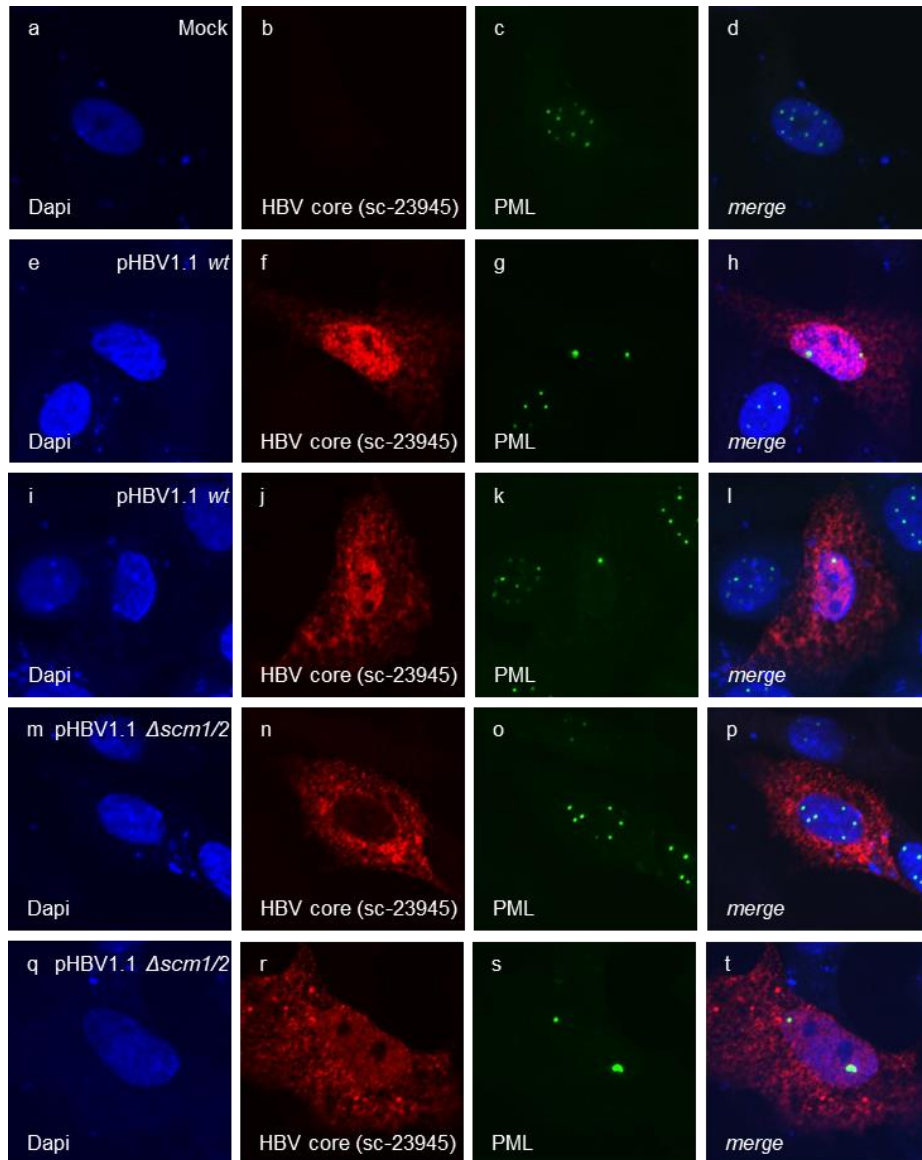
Figure 32 HBV core protein SUMOylation mediates nuclear recycling. HepaRG cells were transfected with 3µg of pHBV1.1 *wt* (panels e-l) or *Δscm1/2* (panels m-t). Cells were fixed 48h post transfection with 4 % PFA and stained using anti-PML (NB100-59787) and anti-HBV core (sc-23945) antibodies. Primary antibodies were detected using Alexa 488 (green, PML) and Alexa 647 (red, HBV core) conjugated secondary antibodies and the nuclei were co-stained using Dapi. Pictures were taken using a Nikon TiE laser scanning microscope. Images are representative for at least 30 mock and transfected cells.

These results were further confirmed by determination of the co-localization between Dapi staining of the nucleus and HBV core protein using the Pearson correlation coefficient method, where a significant and severe decrease in co-localization between Dapi and the HBV core protein could be observed for pHBV1.1 *Δscm1/2* (see figure 33).
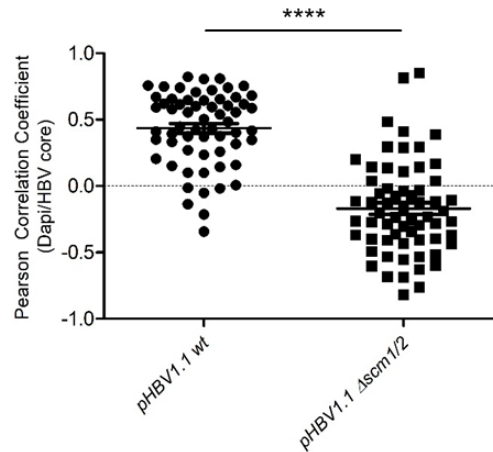
Figure 33: HBV core protein SUMOylation mediates nuclear localization. Pearson correlation coefficient for co-localization of HBV core and Dapi for at least 60 cells from two independent biological replicates were calculated using *FiJi* (version 1.45s) and visualized using GraphPad *PRISM5*. Statistical significance was calculated using Oneway ANOVA and Dunn's post test. n.s.: not significant, *: $p<0.05$, **: $p<0.01$, ***: $p<0.001$, ****: $p<0.0001$.

To additionally analyse the impact of HBV core protein SUMO PTM on nuclear entry of HBV virions during HBV infection, *wt*, *Δscm1*, *Δscm2*, and *Δscm1/2* HBV particles were isolated from supernatants of HepaRG cells transfected with pHBV1.1 *wt*, *Δscm1*, *Δscm2*, and *Δscm1/2*. The relative secretion of viral particles compared to the supernatant of pHBV1.1 *wt* transfected cells was determined using NAGE. Here, it could be shown that transfection of HepaRG cells with pHBV1.1 *wt*, *Δscm1* and *Δscm2* lead to secretion of similar amounts of viral particles, while the *Δscm1/2* double SCM mutant showed reduced secretion of viral particles (see figure 34).
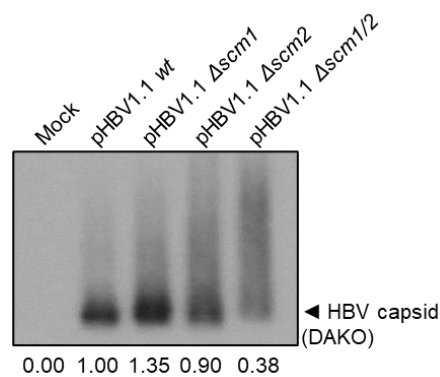
Figure 34: HBV core protein SUMOylation affects secretion of viral particles. HepaRG cells were transfected with 10µg pHBV1.1 *wt*, *Δscm1*, *Δscm2*, and *Δscm1/2*. Medium was collected 3, 6 and 9d post transfection and HBV virions were isolated by PEG precipitation. Relative amounts of isolated HBV particles compared to *wt* were determined using NAGE and densitometric analysis using *FiJi* (version 1.45s).

Differentiated HepG2-NTCP-K7 cells were infected with comparable amounts of *wt*, *Δscm1*, *Δscm2*, and *Δscm1/2* HBV particles and fixed 24h.p.i., to further clarify the role of HBV core protein SUMOylation during viral entry steps.
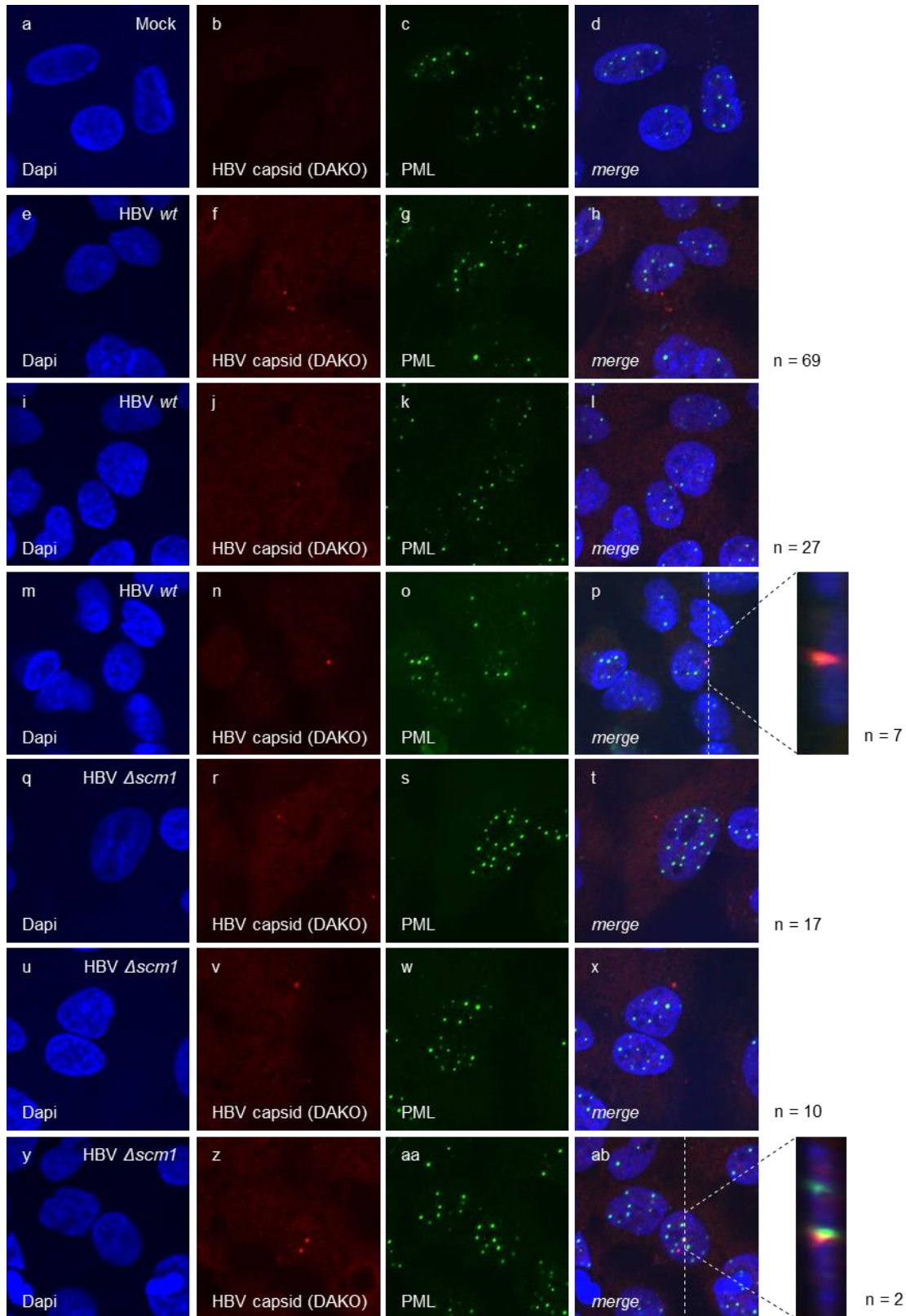
Figure 35: HBV core protein SUMOylation is essential to nuclear entry during HBV infection. HepG2-NTCP-K7 cells were differentiated by addition of 2.5% DMSO for 2d. Cells were infected with comparable amounts *wt* (panels e-p), *Δscm1* (panels q-ab), *Δscm2* (panels ac-an), and *Δscm1/2* (panels ao-az) HBV particles as assessed by NAGE (see figure 34) and fixed with 4% PFA at 24h.p.i.. Cells were stained using anti-PML (sc-966) and anti-HBV capsid (DAKO B0586) antibodies. Primary antibodies were detected using Alexa 488 (green, PML) and Alexa 647 (red, HBV capsid) conjugated secondary antibodies and the nuclei were co-stained using Dapi. Pictures and Z-stacks were taken using a Nikon TiE laser scanning microscope. Images are representative for at least 21 mock and infected cells.
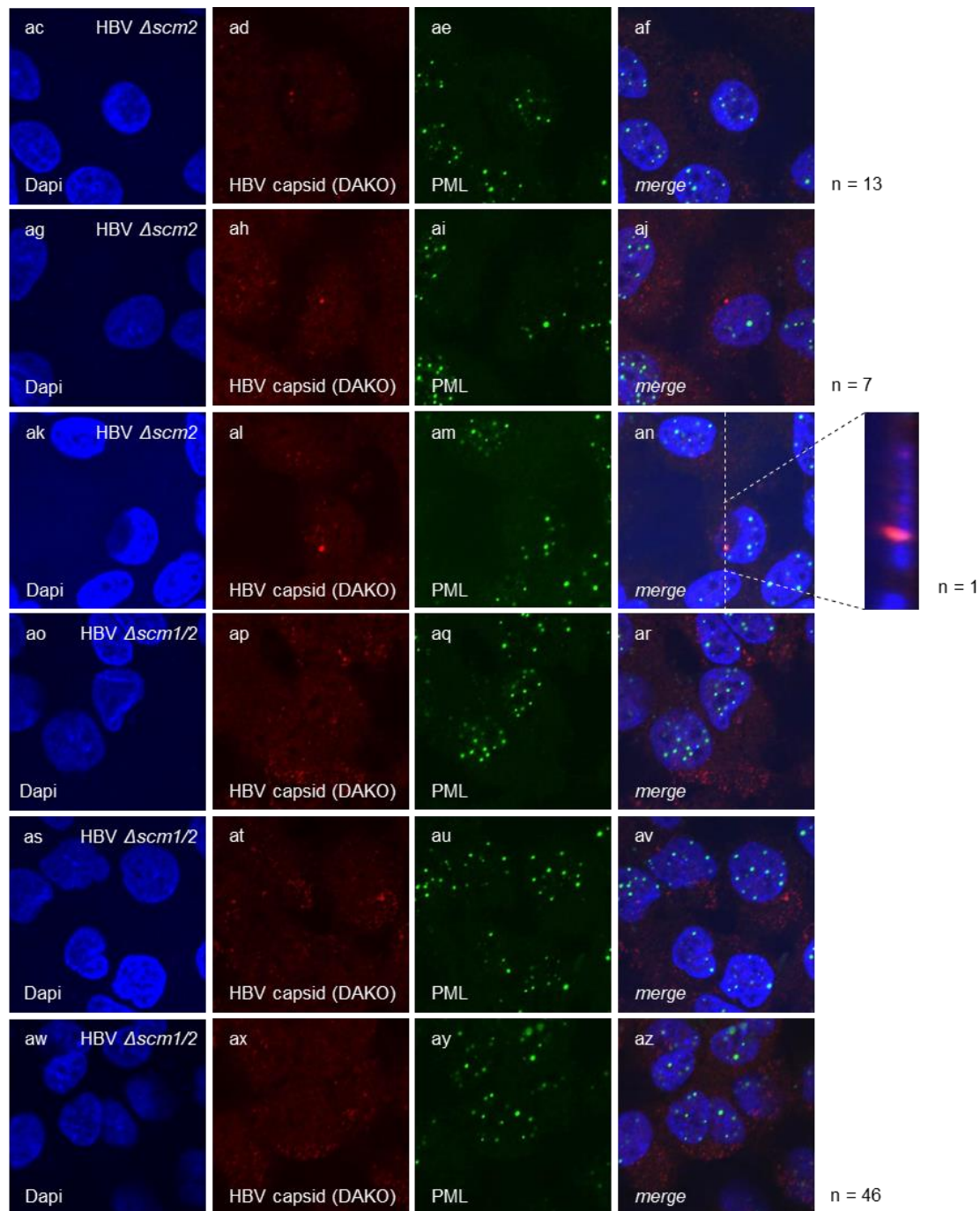
Figure 35: HBV core protein SUMOylation is essential to nuclear entry during HBV infection (continued).

For *wt* HBV virions, the complete course of viral entry could be visualized, starting with cytoplasmic localization (see figure 35, panels f-h), followed by transport to the nucleus (see figure 35, panels j-l), and eventually nuclear localization as well as recruitment to specific PML-NBs (see figure 35, panels n-p). A similar distribution was observed for the single SCM mutants *Δscm1* and *Δscm2*. Also here, most of the HBV capsids were observed to localize to the cytoplasm (see figure 35, panels r-t and panels ad-af, respectively), less to the nucleus (see figure 35, panels v-x and panels ag-aj, respectively) and only a small proportion to PML-NBs (see figure 35, panels z-ab and panels ax-az, respectively). For HBV *Δscm1/2* particles,

107

in which both SCMs were mutated to arginine residues, exclusive localization to the cytoplasm (see figure 35, panels ap-ar and at-av) and the nuclear envelope (see figure 35, panels ax-az) was observed. This phenotype was in line with the deficiency in SUMO mediated capsid disruption (see figure 30 B, lanes 3, 4, figure 30 C). Summarized, these data indicated a distinct role of HBV core protein SUMOylation in the process of nuclear entry of rcDNA containing nucleocapsids during HBV infection.

4.7 HBV DNA is recruited to PML-NBs

The association and interplay of HBV DNA and PML-NBs was further assessed by CUT&RUN assay, to determine binding of PML to viral DNA. Therefore, antibodies for the protein of interest direct a MNase nuclease to DNA interacting with the respective protein. Cleaved DNA can be released from digitonin permeabilized cells by diffusion and analyzed by qPCR (*436, 437*). Using this assay system, binding of PML to several regions of nuclear HBV DNA, which is mostly cccDNA (*215*), was observed (see figure 36). Our results showed that PML preferentially interacted with cccDNA regions around CpG island 3 (see figure 36), which was also shown to be bound by HBV core protein (*215*). PML binding to HBV DNA was furthermore observed in HBV core protein occupied CpG island 2 (*215*), albeit to a lesser extent than in CpG island 3 (see figure 36). PML additionally interacted with HBV DNA at CpG island 1 and in the PreS1 region (see figure 36), which are both not in contact with HBV core proteins (*215*). These findings further stress the importance of PML-NBs in the regulation of HBV cccDNA and substantiated the role of HBV core protein in bridging the interaction between HBV DNA and PML-NBs.
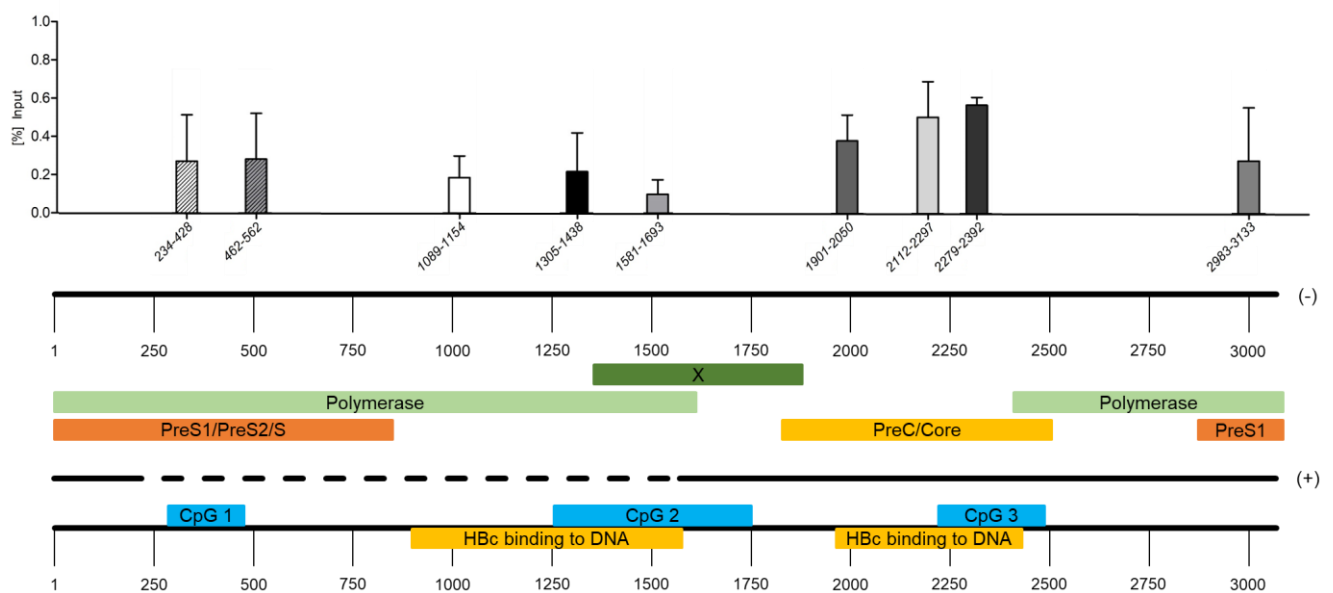
Figure 36 PML binds cccDNA preferentially in HBV core protein occupied regions. HepG2-NTCP-K7 cells were differentiated by addition of 2.5% DMSO for 2d. Cells were infected with HBV at a MOI of 1000 GE/cell. After 7d.p.i., the cells were harvested and subjected to CUT&RUN assay kit to determine interaction of PML with HBV DNA using an anti-PML antibody (ab72137). DNA levels of enriched chromatin and input were determined using qPCR and calculated as [%] input. Bar charts were visualized using GraphPad *PRISM5* and represent data from two independent biological replicates measured in duplicates. A schematic representation of the HBV genome and the corresponding ORFs is depicted below the graph. Additionally, the localization of CpG islands 1-3 and regions of HBV core protein occupied HBV DNA are shown based on (*215*). HBc = HBV core protein

4.8 Inhibition of SUMOylation impedes efficient HBV infection

4.8.1 Inhibition of SUMOylation interferes with nuclear entry of HBV capsids

Taken together, the results presented above pinpointed the role of HBV core protein SUMO PTM towards the nuclear entry and early events in cccDNA biogenesis directly after nuclear entry. To further confirm the importance of HBV core protein SUMOylation in nuclear entry as well as cccDNA formation, and as proof-of-concept, the cellular SUMOylation machinery was inhibited using ginkgolic acid (GA). Ginkgolic acid globally interferes with SUMOylation by binding to the SUMO E1 activating enzyme and inhibition of E1-SUMO intermediate formation (*438*). Differentiated HepG2 cells were treated for a total of 24h at concentrations, which were shown to interfere with efficient SUMO modification, but had no effect on proliferation of HepG2 cells (*439, 440*). Inhibition of SUMOylation was primed 8h before infection by addition of 10 or 15µM GA, and GA was left on the cells during HBV infection. After removal of the inoculum 16h post infection (24h post treatment), cells were harvested to assess the impact of GA on cellular SUMOylation and HBV nuclear entry. Western blot analysis of whole-cell protein lysates at 24h post treatment and 16h post infection confirmed an efficient reduction of poly-SUMOylated proteins using 10 and 15µM GA (see figure 37, left panel, lanes 1-4). Free SUMO steady state levels (see figure 37, left panel, lanes 1-4) or levels of incoming or cell associated HBV core protein (see figure 37, right panel, lanes 2-4) were unaffected by GA.
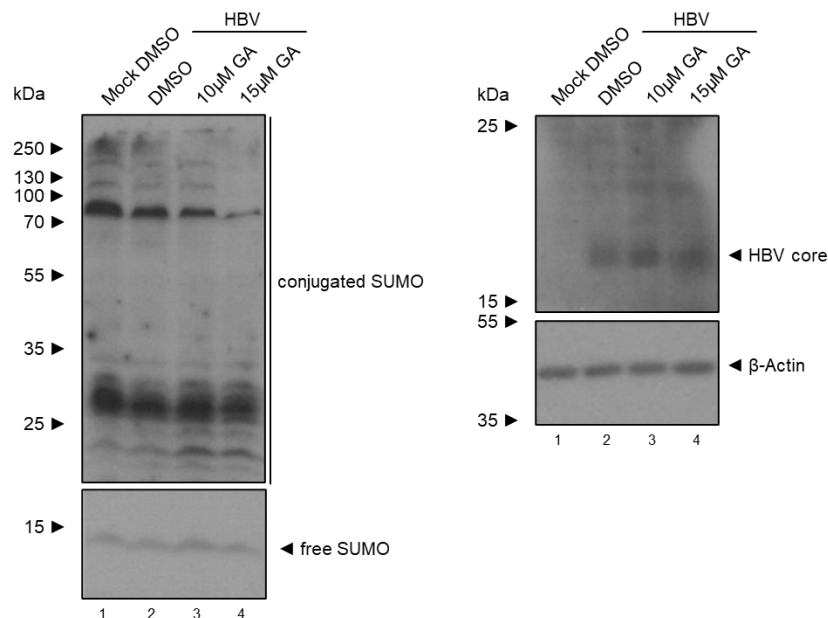
Figure 37: GA treatment interferes with efficient poly-SUMOylation. HepG2-NTCP-K7 cells were differentiated by addition of 2.5% DMSO for 2d. 8h prior to infection, cells were treated with 10 or 15µM GA. As negative control, DMSO was used. Cells were infected with HBV at a MOI of 200 GE/cell in presence of 10 or 15µM GA, or DMSO as control and harvested 16h.p.i. (24h post treatment). Whole-cell protein lysates were prepared and analyzed by SDS-PAGE and western blot using anti-SUMO (ab81371), anti-core (8C9) and anti-β-Actin (AC-15) antibodies. Molecular weights are depicted on the left, respective proteins are indicated on the right of each blot.

HBV infected cells with and without GA treatment were further analyzed using immunofluorescence stainings for incoming HBV capsids or capsid intermediates and PML at 16h.p.i (24h post treatment). In the DMSO control, the results shown above could be further confirmed. The majority of incoming HBV capsids was observed to still reside in the cytoplasm (see figure 38, panels f-h, figure 39 A, E), while 27.2% were found at the nuclear membrane (see figure 38, panels j-l, figure 39 A, D) and 21.5% of incoming HBV particles already processed to the nucleus (see figure 38, panels n-p, figure 39 A, C). A small fraction of 1.3% of incoming HBV particles and HBV core protein was observed to localize to PML-NBs in untreated cells (see figure 38, panels r-t, figure 39 A, B).
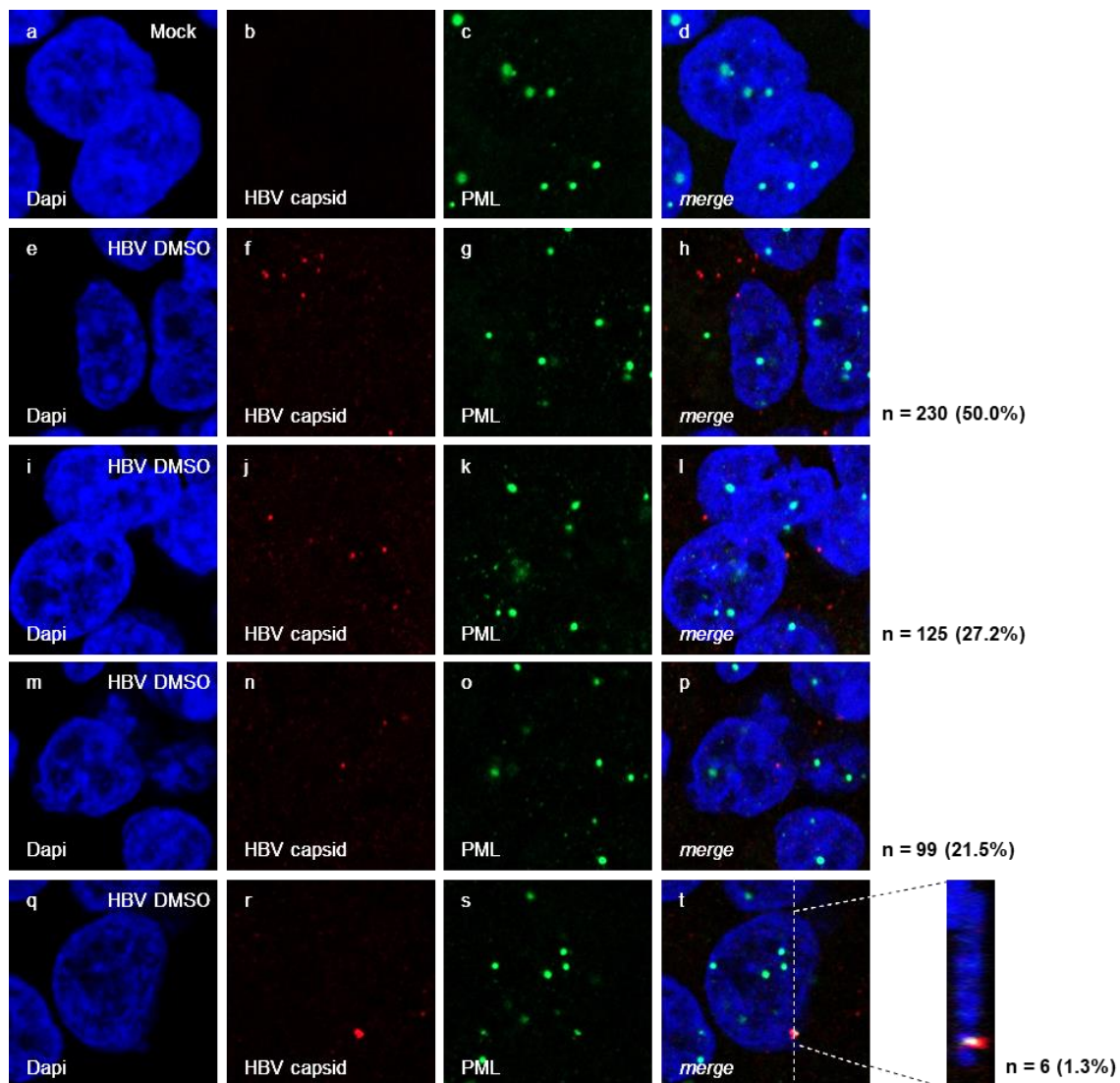
Figure 38: GA disrupts nuclear entry of incoming HBV capsids. HepG2-NTCP-K7 cells were were differentiated by addition of 2.5% DMSO for 2d. 8h prior to infection, cells were treated with 10 or 15μM GA. As negative control, DMSO was used. Cells were infected with HBV at a MOI of 400 GE/cell in presence of 10 or 15μM GA and DMSO as control and fixed with 4% PFA at16h.p.i. (24h post treatment). Cells were stained using anti-PML (sc-966) and anti-HBV capsid (DAKO B0586) antibodies. Primary antibodies were detected using Alexa 488 (green, PML) and Alexa 647 (red, HBV capsid) conjugated secondary antibodies and the nuclei were co-stained using Dapi. Pictures and Z-stacks were taken using a Zeiss LSM 980 laser scanning microscope. Representative images for at least 383 cells are shown.
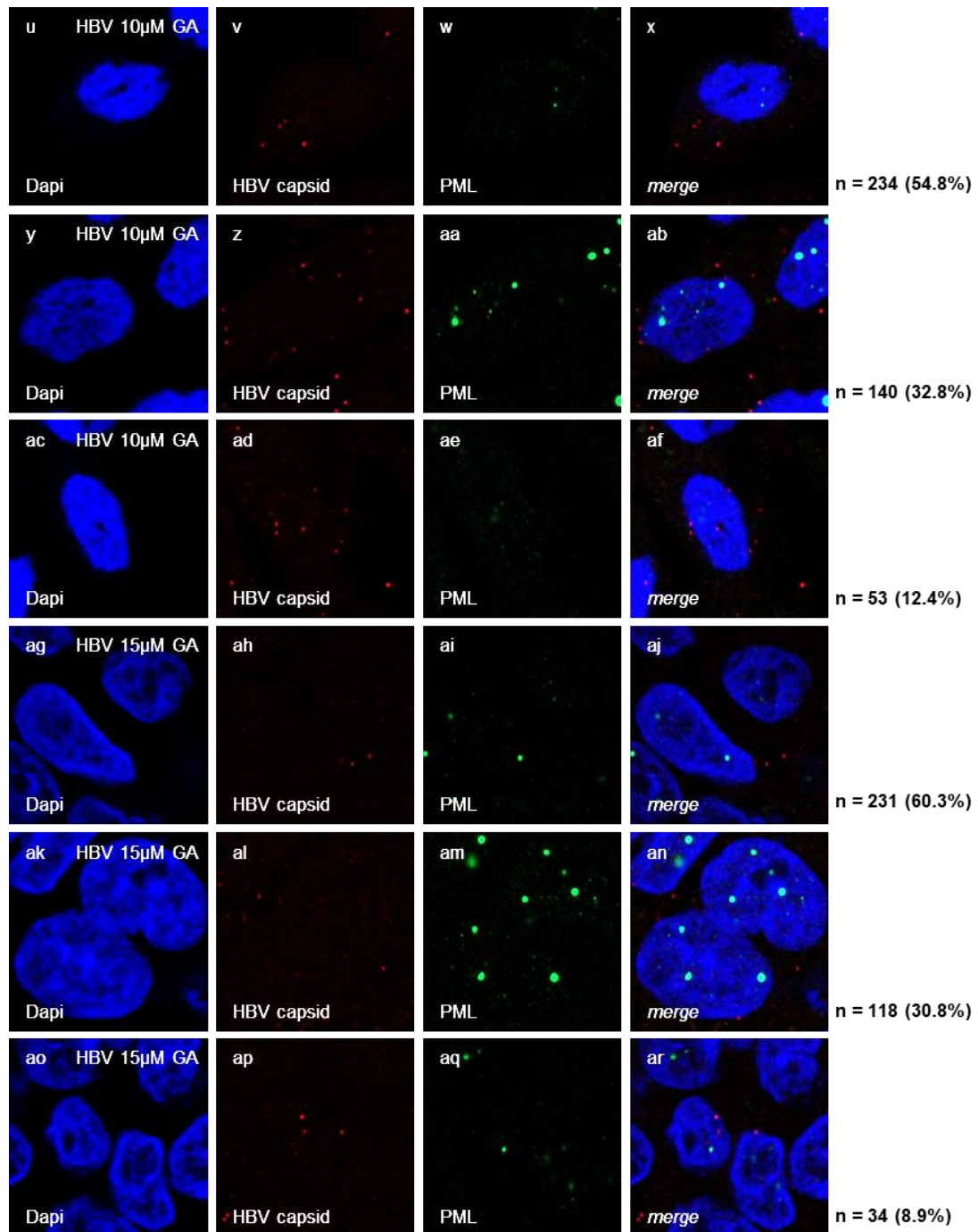
Figure 38: GA disrupts nuclear entry of incoming HBV capsids (continued).

Treatment with 10µM of GA gradually decreased the proportion of nuclear HBV capsid staining to 12.4% (see figure 38, panels ad-af, figure 39 A, C) whilst enhancing the degree of HBV capsids observed at the nuclear membrane with 32.8% (see figure 38, panels z-ab, figure 39 A, D) and in the cytoplasm with 54.8% (see figure 38, panels v-x, figure 39 A, E). Increasing the GA concentration to 15µM resulted in a further loss of nuclear HBV capsids to 8.9% (see figure 38, panels ap-ar, figure 39 A, C) and a strong increase in HBV capsid localization at the nuclear membrane with 30.8% (see figure 38, panels al-an, figure 39 A, D) and especially in the cytoplasm with 60.3% (see figure 38, panels ah-aj, figure 39 A, E).
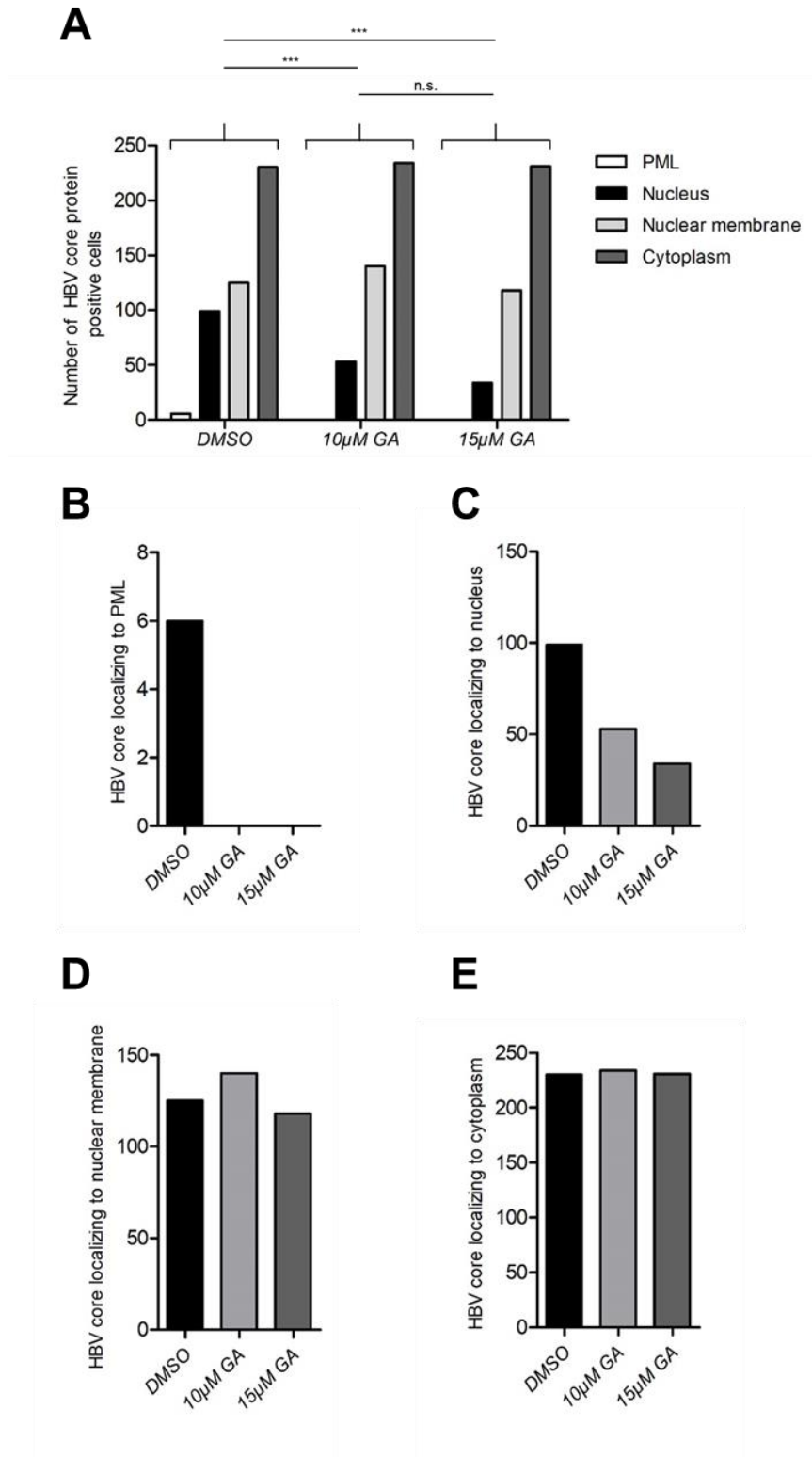
Figure 39: GA significantly inhibits HBV capsid nuclear entry and PML association. Cells from figure 38 were further analyzed for HBV capsid localization to the cytoplasm **(A, E)**, the nuclear membrane **(A, D)**, the nucleus **(A, C)**, or PML-NBs **(A, B)**. Data were visualized using GraphPad *PRISM5* and are representative for at least 383 cells. Statistical significance was calculated using Chi-square test. n.s.: not significant, *: $p<0.05$, **: $p<0.01$, ***: $p<0.001$ **(A)**.

Noteworthy, no localization of HBV capsids to nuclear PML-NBs could be observed during treatment with 10 or 15µM of GA (see figure 39 A, B), all in all resulting in a significant decrease of HBV capsid nuclear entry in cells treated with GA (see figure 39 A, C).

4.8.2 The cellular SUMOylation machinery is crucial to cccDNA formation

As interference with SUMOylation by treatment with GA efficiently counteracted HBV capsid nuclear entry and PML association (see figure 38, figure 39), the effect of GA on HBV replication at later timepoints was further investigated.
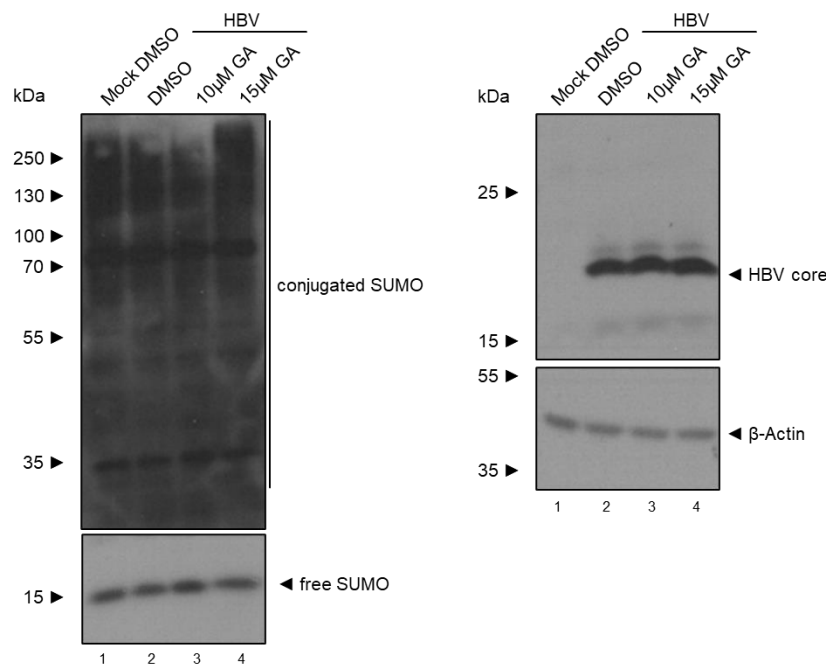
Figure 40: Levels of cellular poly-SUMOylation recover after 6d without GA treatment. HepG2-NTCP-K7 cells were differentiated by addition of 2.5% DMSO for 2d. 8h prior to infection, cells were treated with 10 or 15µM GA. As negative control, DMSO was used. Cells were infected with HBV at a MOI of 200 GE/cell in presence of 10 or 15µM GA and DMSO as control and GA was removed together with the inoculum. Cells were harvested 7d.p.i. and whole-cell protein lysates were prepared and analyzed by SDS-PAGE and western blot using anti-SUMO (ab81371), anti-core (8C9) and anti-β-Actin (AC-15) antibodies. Molecular weights are depicted on the left, respective proteins are indicated on the right of each blot.

Differentiated HepG2-NTCP-K7 cells were pre-treated with 10 or 15µM GA 8h prior to infection and GA was left on the cells during HBV infection. After 16h, the inoculum as well as the GA were removed and the cells were incubated in medium without compound for further 6d. Western blot analysis of whole-cell protein lysates confirmed that the levels of cellular poly-SUMOylation had widely recovered after 6d without presence of GA (see figure 40, left panel, lanes 1-4). Additionally, the steady state levels of HBV core protein were unaffected by 24h of treatment with GA (see figure 40, right panel, lanes 2-4). This finding correlated with the results of the determination of complete HBV DNA levels via qPCR, where only a minor effect of GA treatment with a reduction to around 90% of DMSO treated cells could be observed (see figure 41 A). In contrast, cccDNA levels were strongly and specifically reduced

114

during GA treatment with a reduction to 74.5% for 10µM and 62.8% for 15µM GA compared to DMSO treatment (see figure 41 B). This finding indicated that an efficient HBV infection and cccDNA generation did not appear, even after omission of GA for 6d. Taken together, these results underlined the importance of SUMOylation in the entry process of HBV capsids and in early events during cccDNA formation.
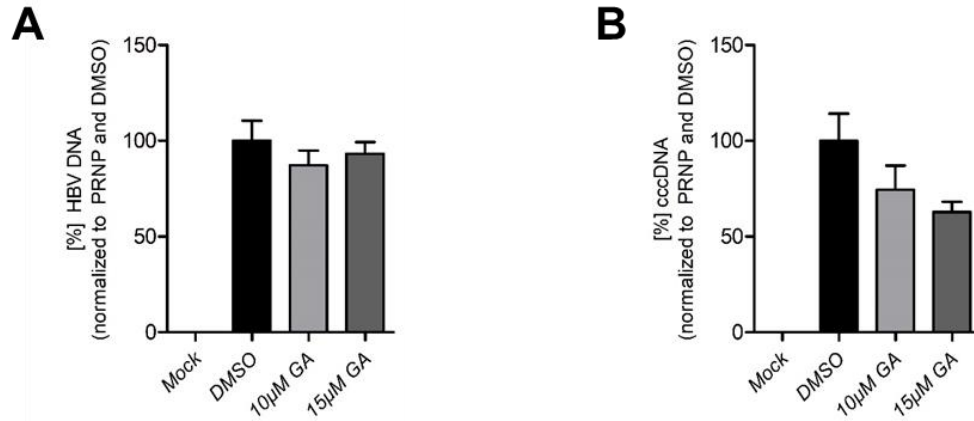
Figure 41: SUMOylation is a crucial factor for cccDNA generation. A, B HepG2-NTCP-K7 cells were differentiated by addition of 2.5% DMSO for 2d. 8h prior to infection, cells were treated with 10 or 15µM GA. As negative control, DMSO was used. Cells were infected with HBV at a MOI of 200 GE/cell in presence of 10 or 15µM GA and DMSO as control and GA was removed together with the inoculum. Total DNA was extracted using the MachereyNagel NucleoSpin Tissue Kit 7d.p.i.. **A** Complete HBV DNA and **B** cccDNA were determined using qPCR and normalized to PRNP. Bar charts were visualized using GraphPad *PRISM5* and correspond to three biological replicates measured in triplicates.

5. Discussion

Although an effective and broadly available vaccination strategy against HBV infections exists since almost 40 years, CHB is still a major global health threat, affecting a noteworthy proportion of humanity (*19-22*). This is mainly due to the stable nature of the epsiomal cccDNA. The cccDNA represents the persistence reservoir of the virus and key to a functional cure, which is not directly targeted by the currently used treatment options (*23-27, 48*). Despite extensive studies on viral entry (see chapter 1.1.5.1) and the generation of cccDNA from incoming rcDNA (see chapter 1.1.4), little is known about the exact events that induce and organize capsid disassembly, nuclear entry, as well as subsequent DDR mediated repair of the rcDNA.

PML-NBs are known as dynamically regulated molecular hubs for several key cellular processes, including the DDR. Their composition is mainly governed by SUMO-SIM interactions with hundreds of host proteins (see chapter 1.2.2). Recent studies implicated an interaction of HBV core with PML (*250*) and SUMO2/3 and 4 (*246*). Due to its strong association with nuclear entry of rcDNA as well as subsequent cccDNA formation (see chapter 1.1.5.1) and the dynamic regulation of HBV core protein functions by PTM throughout the viral life cycle (see chapter 1.1.5.3), the functional consequences of HBV core protein SUMOylation and the role of PML and SUMO in the HBV replication cycle were investigated.

5.1 SUMOylation – A novel HBV core protein PTM regulating PML-NB association

The variety of functions which the HBV core protein takes over during infection are dynamically and strictly regulated by a plethora of PTMs within its CTD and NTD, including phosphorylation, arginine methylation and ubiquitinylation (*155, 183-185, 190, 193, 251-254, 269, 270*).

Using *in silico* prediction, we could expand the panel of regulative HBV core protein PTM by identification of two SCMs at K7 (SCM1) and K96 (SCM2) within the HBV core protein NTD, which were highly conserved among all analyzed HBV genotypes (see figure 13 A, figure 13 C). SCM1 was observed to be in the globular domain, while SCM2 was found within the spike of HBV core (see figure 13 B). SUMOylation of HBV core was confirmed in transfection experiments using *wt* HA-tagged HBV core protein, where stable SUMO2 PTM could be observed (see figure 14 A, lane 2, figure 14 B). Arginine mutations of SCM1 and SCM2 alone could show that both lysine resides were indeed targeted by SUMOylation (see figure 14 A, lanes 2-5, figure 14 B). The strong decrease in HBV core protein SUMOylation to 30% of *wt* SUMO PTM found for the single SCM mutants pcore-HA *Δscm1* and *Δscm2* indicated a

possible cooperativity between those two SCM sites (see figure 14 A, lanes 2-4, figure 14 B). The complete loss of HBV core protein SUMOylation in the double SCM mutant pcore-HA _Δscm1/2_ further confirmed the identity of SCM1 and SCM2 as the sole sites for SUMO conjugation within the HBV core protein (see figure 14 A, lanes 2-5, figure 14 B).

Previous work on ubiquitin PTM of HBV core indicated that arginine mutation of K7 and K96 did not alter release of newly produced viral particles and suggested K7 as the major site for ubiquitinylation in HBV core (_269, 270_). In contrast to this work, where mutation of both lysine residues resulted in complete abrogation of SUMO2 modification (see figure 14 A, lanes 2-5, figure 14 B), Langerovà et al. still found HBV core protein ubiquitinylation even in the absence of K7 and K96. These findings indicated the presence of additional sites for ubiquitin PTM, including S44, S49, T67, or S157 (_270_), which are no target for SUMOylation. Additionally, K7 was identified as the preferred site for ubiquitinylation compared to the minor site K96 (_270_). Here, however, no preferential site for SUMOylation was found, as mutation of SCM1 and SCM2 yielded a comparable decrease in HBV core protein SUMO PTM (see figure 14 A, lanes 2-4, figure 14 B). In line with our results showing an efficient SUMO2 PTM of the HBV core protein in HepaRG cells overexpressing His$_6$-SUMO2, a recent proteomics study using HBV core protein expressing HepaRG cell lines suggested interaction of HBV core protein with SUMO2/3 and 4 (_246_)

Studies by Chung et al., which aimed at identifying reasons for HBV reactivation and exacerbation during radio- and chemotherapy, indicated an association of HBV core protein with PML-NBs in HBV producing hepatocyte cell lines during DNA damage stress (_250_). Our work expanded the knowledge on HBV core-PML interactions by providing evidence for SUMO PTM mediated regulation of the HBV core protein-PML association. Previously published data indicated protein SUMOylation as a prerequisite for association with and recruitment to PML-NBs (_284, 312-318, 441_). Consistently with these studies, transfected _wt_ HBV core protein was observed to interact with and localize to PML (see figure 9 A, lane 2, figure 9 B panels f-h, j-l). Consequently, mutation of both SCMs in HBV core protein, either alone or in combination, by conservative arginine exchange, resulted in a more diffuse distribution of HBV core protein within the transfected hepatocytes and a significantly reduced PML association (see figure 15 A, panels n-p, r-t, v-x, z-ab, ad-af, ai-ak, figure 15 B). The role of SUMOylation as mediator for the HBV core-PML association was further confirmed by co-IP experiments which showed interaction of the SUMOylated _wt_ HBV core protein with PML and a loss of this interaction for the SUMOylation deficient _Δscm1/2_ mutant protein (see figure 16 A, lanes 2,3, figure 16 B).

Importantly, our work not only showed the association of HBV core protein with PML during transfection and CMV promoter mediated overexpression of HBV core, but also during infection. Here, two differentially organized fractions of the HBV core protein could be identified. The first fraction showed a diffuse distribution within the nucleus and cytoplasm as previously published (*103, 110, 195, 220-226*) (see figure 10, panels f-h, j-l, figure 11 panels f-h, j-l) and was presumably involved in pgRNA packaging and subsequent generation of infectious progeny virions (*107, 117, 124, 215, 216, 236-238, 243, 247, 248, 442-445*). The second fraction, in contrast, was associated with specific, but not all PML-NBs within the nuclear matrix and presumably consisted of SUMOylated HBV core protein (see figure 10 panels r-t, v-x, figure 11 panels r-t, v-x, figure 12). PML-NBs are models for phase separation in liquid-liquid interfaces (*371-373*). Therefore, it is tempting to speculate that those specific PML-NBs, which recruit HBV core protein, harbor unique interactor or scaffold PML proteins, generating binding sites for SUMO modified HBV core protein. Presence of SUMO modified HBV core might subsequently induce a further change in PML-NB composition, leading to the recruitment of factors necessary for cccDNA biogenesis. Taken together, our work could expand the knowledge on the dynamic PTM mediated regulation of HBV core by adding the novel ubiquitin-like SUMOylation. SUMO modification of HBV core in turn regulated the association of HBV core proteins with PML during transfection and infection.

5.2 HBV core protein SUMOylation represents the missing link in HBV nuclear entry

The process of HBV nucleocapsid assembly and disassembly is dynamically regulated by PTMs within the HBV core protein and is especially governed by phosphorylation. The CTD was observed to be phosphorylated during early assembly events to prevent unspecific binding of host cellular mRNAs (*90, 212, 213, 255*). Binding of the pgRNA induces first dephosphorylation events and the HBV core protein is further dephosphorylated during rcDNA reverse transcription and capsid maturation (*183, 184, 213, 251, 258, 260, 261*). In the entry process of HBV virions in infection, re-phosphorylation of the CTD (*189*) and the NTD (*155*) occurs, which is probably mediated by a co-packaged CDK2 or CDK2-like kinase (*155, 263*). Only re-phosphorylated, mature HBV virions are then transported to the NPC. There, they are stalled in the nuclear basket by a strong interaction between phosphorylated HBV core and Nup153 (*111, 113*). Disassembly of mature capsids occurs within the nuclear basket and depends on NTD phosphorylation, which presumably destabilizes the HBV capsid structure. However, NTD phosphorylation *per se* is not sufficient to induce capsid disassembly. The final trigger for HBV capsid disruption in the nuclear basket is therefore currently unknown (*109, 155*). Interestingly, several groups observed a strong association

between phosphorylation and SUMOylation, with phosphorylation being a prerequisite for efficient SUMO modification (*294-298*). Attachment of the 11kDa SUMO protein to a lysine residue in a target protein is proposed to induce structural rearrangements and is known to be a mediator for nuclear localization (*305, 306*).

In line with these studies, *in silico* modeling of HBV core protein SUMOylation within the tetrameric asymmetric unit of the HBV capsid resulted in a sterical overlap between the SUMO moiety at SCM1 (see figure 29 B, panels a, b) and SCM2 (see figure 29 B, panels c, d) with the adjacent HBV core protein monomer. This overlap might induce sterical constraints, which favor capsid disruption. These *in silico* findings first indicated that HBV core protein SUMOylation within the HBV capsid represented the missing factor in disassembly of mature capsids at the NPC.

Further *in vitro* SUMOylation experiments using recombinantly expressed HBV capsids could confirm this hypothesis by showing disassembly and concomitant SUMOylation of *wt* HBV capsids (see figure 30 A, lanes 1-3, figure 30 B, lanes 1, 2, figure 30 C). *Vice versa*, disassembly and SUMO PTM did not occur in SUMOylation deficient *Δscm1/2* capsids, as these were left unaltered after treatment with the *in vitro* SUMOylation assay kit (see figure 30 B, lanes 3, 4, figure 30 C). The disassembly and SUMOylation of *wt* HBV capsids in samples containing the *in vitro* SUMOylation machinery omitted for Mg-ATP (see figure 30 A, lane 2) might be explained by the presence of co-packaged ATP inside the HBV capsids which diffused into the surrounding reaction mixture through the pores present in the capsid structure (*2, 6, 7, 70, 143, 155*).

Several previous studies suggested that SUMOylation induces nuclear localization (*305, 306*). Consistently with the SUMO mediated disassembly of HBV capsids, experiments using the plasmid-based HBV replicon system pHBV1.1 showed a severe defect in HBV core protein nuclear localization for the SUMO PTM deficient pHBV1.1 *Δscm1/2* (see figure 31, panels n-p, r-t, figure 32, panels n-p, r-t, figure 33). These findings further confirmed the substantial role of HBV core protein SUMOylation in efficient nuclear entry of HBV capsids. Infection of differentiated HepG2-NTCP-K7 cells with either *wt* HBV virions or virions with arginine mutations at SCM1, SCM2, or both SCMs proved that SUMO modification of HBV core at either SCM1 or SCM2 was necessary and sufficient for nuclear entry and association of incoming HBV core proteins to PML-NBs. The single SCM mutants HBV *Δscm1* (see figure 35, panels q-ab) and *Δscm2* (see figure 35, panels ac-an) showed similar distributions to *wt* HBV (see figure 35, panels e-p). This indicated that the reduced residual degree of SUMO PTM observed for *Δscm1* and *Δscm2* HBV core protein (see figure 14 A, lanes 2-5, figure 14

B) was still enough to trigger HBV capsid disassembly at the nuclear basket and subsequent recruitment to PML-NBs. The double SCM mutant HBV *Δscm1/2* was observed to be completely incompetent for nuclear entry and accumulated in the cytoplasm and at the nuclear membrane (see figure 35, panels ao-az).

Packaging of pgRNA and subsequent rcDNA formation within HBV capsids induces HBV core protein dephosphorylation(*183, 184, 213, 251, 258, 260, 261*). As phosphorylation is often a prerequisite for SUMO modification (*294-298*), HBV core protein dephosphorylation during capsid formation might prevent subsequent SUMO PTM, allowing efficient assembly of mature rcDNA containing capsids. This could further explain the presence of the two fractions of HBV core protein observed during HBV infection: A major dephosphorylated and deSUMOylated HBV core protein fraction (see figure 10, panels f-h, j-l, figure 11 panels f-h, j-l) necessary for the generation and secretion of novel infectious viral particles (*107, 117, 124, 215, 216, 236-238, 243, 247, 248, 442-445*), and a second, minor re-phosphorylated and SUMOylated HBV core protein fraction from incoming virions, which is associated with PML-NBs (see figure 10 r-t, v-x, figure 11 r-t, v-x, figure 12). SUMOylation might therefore represent a novel functional switch in the dynamic PTM based regulation of HBV core.

Based on these results, the following model for HBV entry into the nucleus is proposed: Mature HBV capsids, harboring phosphorylated HBV core proteins, are transported into the nucleus and halted at the nuclear basket of the NPC (*111, 113*). Phosphorylated HBV core proteins are subsequently SUMO modified by the host cell SUMOylation machinery, which has access to the nuclear basket (*446*). SUMO PTM of HBV core within the HBV capsid subsequently induces capsid disruption, entry of HBV core protein into the nucleoplasm and recruitment into PML-NBs.

5.3 PML-NBs and SUMOylation serve as molecular hubs in cccDNA biogenesis

PML-NBs are known to serve as molecular hub for the host cell DDR (*318, 367-369, 378, 379*) and their function is orchestrated by regulative SUMOylation (*284, 305, 307-311*). Based on the observation that HBV core protein SUMOylation mediated nuclear entry and its association with PML-NBs, the effect of SUMO PTM and PML-NBs on rc- to cccDNA conversion were further investigated.

Introduction of arginine mutations in HBV core at either SCM1, SCM2 or at both SCMs in the plasmid-based replicon system pHBV1.1 allowed analysis of the interplay between HBV core protein SUMOylation and the HBV replication cycle. Molecular modeling of the influence of lysine to arginine mutations at SCM1 and SCM2 on HBV core protein structure could confirm

the conservative nature of this amino acid substitution. Neither a change in the overall secondary, tertiary, or quartary structure (see figure 29 A, panels a-d), nor an effect on the molecular environment of SCM1 or SCM2 was predicted (see figure 29, panels e, f). In contrast to these findings, arginine mutation of SCM2 in the HBV replicon system induced a decrease in the expression of HBV core proteins as well as the generation of HBV nucleocapsids (see figure 17 A, figure 17 B). Conversely, it did not severely alter the secretion of virions into the supernatant of transfected cells (see figure 34). Co-expression of ubiquitin harboring only K63 together with HBV core proteins was recently shown to induce a similar behavior of HBV core protein expression levels, with a reduction observed for K96R, but not *wt*, K7R or K7/96R. These obseravtions indicated a switch in ubiquitinylation as well as an enhanced degradation of the K96R mutant under certain conditions (*270*) and might therefore explain the lower steady state levels of the *Δscm2* mutant. K96 was further identified as one of the residues which is critical for capsid envelopment. Alanine mutations of K96 abrogated interaction of HBV core with L HBsAg and therefore interfered with the secretion of enveloped viral particles (*188, 227-230*). In contrast to these studies, here only a minor effect of the arginine mutation in SCM2 on secretion of viral particles could be observed (see figure 34). This was probably due to the use of a more conservative arginine mutation, which partially retained the physicochemical properties, compared to mutation to alanine. Further previous studies on HBV capsid formation and secretion did not observe reduced steady state levels or capsid formation for HBV core protein K96A. However, those studies preferentially used HBV replicon systems deficient for HBV core expression and trans-complemented HBV core from single expressing vectors (*188, 229*), where we also could observe *wt*-like HBV core protein expression for the K96R mutant (see figure 14 A, lanes 2, 4, 7, 9).

Concomitantly with the reduced expression of HBV core protein and formation of intracellular HBV nucleocapsids (see figure 17 A, lane 4, figure 17 B), transfection of pHBV1.1 *Δscm2* resulted in an almost negligible degree of cccDNA formation (see figure 18 B). This finding was not surprising, as cccDNA formation from pHBV1.1 depends on formation of rcDNA containing mature HBV capsids which shuttle back to the nucleus (*75, 132, 133, 182*). The loss of cccDNA formation for pHBV1.1 *Δscm2* was therefore most probably caused by the combination of decreased HBV core protein expression and capsid formation (see figure 17 A, lane 4, figure 17 B) and the *wt*-like secretion of viral particles (see figure 34). Both events depleted the pool of available mature capsids for nuclear re-shuttling. Intriguingly, Cui et al. observed an enhanced formation of cccDNA from a HBV plasmid-based replicon carrying a K96A mutation within HBV core (*154*). The authors suggest that this phenotype was caused by an enhanced degree of nuclear re-shuttling of the envelopment deficient HBV core protein

mutant (*154, 188, 447*). This discrepancy between our work and previously published data was probably due to the different amino acid substitution used. In our case, arginine mutation at SCM2 resulted in a phenotype with reduced HBV core protein expression as well as capsid formation (see figure 17 A, lane 4, figure 17 B) and the ability to efficiently secrete viral particles (see figure 34). Both decreased the availability of HBV capsids for nuclear re-shuttling. Additionally, the change in size and charge of the lysine to alanine mutation used by Cui et al. might have further destabilized the resulting nucleocapsids and therefore favoured disassembly at the NPC (*154*).

Consistently with the abrogation of nuclear entry and PML-NB association observed for pHBV1.1 *Δscm1/2* (see figure 31, figure 32, figure 33) and HBV virions derived from it (see figure 35), transfection of pHBV1.1 *Δscm1/2* showed a severe and significant deficiency in cccDNA formation in several HepaRG based cell lines (see figure 18 B, figure 18 D). These findings further stressed the importance of SUMOylation and PML-NB association in the HBV life cycle and on formation of the HBV persistence reservoir. The role of SUMO PTM in cccDNA generation was additionally underlined by the strong induction of cccDNA levels observed during transfection of pHBV1.1 *wt* into HepaRG cells overexpressing His$_6$-tagged SUMO2 (see figure 18 D). This phenotype was most presumably evoked by i) an increased degree of nuclear entry of mature HBV capsids and more efficient release of rcDNA from nucleocapsids at the NPC and ii) by enhanced rc- to cccDNA formation by the host cell DDR in SUMO overexpressing cells. *Vice versa*, shRNA mediated depletion of PML proteins induced a cccDNA deficient phenotype for pHBV1.1 *wt*, which was highly similar to that observed for the double SCM mutant pHBV1.1 *Δscm1/2*. In both cases, almost no cccDNA formation could be observed (see figure 18 D). Similar results were obtained in experiments using HBV infection in HepG2-NTCP-K7 cells depleted for PML. Also here, a reduction of cccDNA formation to 50% compared to HepG2 *shCTL* could be observed (see figure 28 B), consistently with the decrease in PML expressing cells to around 50% in the HepG2 *shPML* cell line (see figure 20 B, figure 21). These findings further confirmed the importance of PML in the organization of the host cell DDR to allow efficient rc- to cccDNA conversion. Additional evidence for HBV core protein SUMO PTM and PML association being crucial regulators in cccDNA formation could be obtained by co-expression of *wt* HBV core protein in pHBV1.1 *Δscm1/2* transfected cells, which could at least partially reconstitute cccDNA formation (see figure 19 B, figure 19 D). Co-expression of *Δscm1/2* HBV core protein, in contrast, did not transcomplement the cccDNA defective phenotype of pHBV1.1 *Δscm1/2*. Taken together, these observations indicated that a small degree of SUMOylated HBV core protein within HBV capsids was sufficient to induce capsid disruption and rcDNA recruitment to PML-NBs (see

figure 19 B, figure 19 D). The increase in cccDNA formation observed in cells co-transfected with pHBV1.1 *wt* and *wt* or *Δscm1/2* HBV core protein (see figure 19 B, figure 19 C) was presumably due to the presence of a higher amount of HBV core protein that could package pgRNA and yield mature HBV capsids. This might have enhanced the cccDNA pool by re-shuttling into the nucleus (*75, 132, 133, 182*).

Previous studies on DDR factors involved in cccDNA formation (*162-166, 171*) could provide evidence for regulative SUMOylation and PML association for several proteins. These include FEN1 (*318, 383-385*), polymerases α and λ (*385, 387*), DNA ligase 1 (*166, 171, 385*), Top1 and 2 (*388-391*), as well as PCNA (*391, 395-401*). Our data could additionally prove the influence of HBV core protein SUMO modification and the subsequent association with PML-NBs on formation of HBV cccDNA. We therefore propose that incoming SUMOylated HBV core protein, which is still bound to the rcDNA, is directed into specific PML-NBs that further harbor and/or recruit the SUMO modified DDR proteins necessary for cccDNA formation. Due to the high degree of SUMO PTM found for proteins involved in cccDNA generation and the regulation of PML-NB composition by phase separation in liquid-liquid interfaces, it is tempting to speculate that the PML-NBs, which can recruit those SUMO-high protein interactors, are themselves SUMO-low (*371-373*). A further level of regulation might even be added by PML phosphorylation which could enhance their affinity for SUMOylated proteins (*372, 374-377*). In line with this hypothesis, PML proteins were shown to be phosphorylated during DNA damage by the DNA damage activated kinases ATM, ATR, HIPK2 or CHK2 (*318, 369, 378, 379*) and ATR was recently implicated in cccDNA formation (*172*). The enhanced cccDNA formation observed in HepaRG cells overexpressing His$_6$-SUMO2 transfected with pHBV1.1 *wt* might therefore be additionally explained by an enhanced SUMO PTM of DDR factors involved in cccDNA formation. Those factors were then preferentially recruited into SUMO-low PML-NBs containing SUMOylated HBV core protein and rcDNA.

HBV core protein was reported to interact with cccDNA to promote a transcriptionally active state. Preferential association of HBV core with CpG island 2 and 3 was observed, and HBV core binding to cccDNA was accompanied by recruitment of CBP and a loss of HDAC1 (*215*). In line with our hypothesis that SUMO modified HBV core protein bridges the interaction between HBV DNA and PML, we observed binding of PML proteins to cccDNA. This interplay preferentially occurred in the HBV core protein occupied region around CpG island 3 (see figure 36). Additionally, PML interaction with cccDNA was localized to the HBV core protein bound CpG island 2, albeit to a lesser extent, and to cccDNA regions which were not shown to be associated with HBV core protein. These findings indicated that HBV core protein in a first step acted as a mediator of PML association to HBV DNA and lateron PML binding to

cccDNA occured independently of HBV core protein and might be mediated by further PML-NB associated proteins.

Noteworthy, in depth analysis of incoming *wt* HBV virions into differentiated hepatocytes by immunofluorescence could provide evidence that 21.5% of HBV core protein reached the nucleoplasm, but only a small fraction of 1.3% of entering HBV core protein localized to PML-NBs (see figure 38, panels m-t). This minor fraction of PML associated incoming HBV core protein correlated well with recent studies on HBV entry into hepatocytes, showing that only around 20% of HBV particles enter the nucleus and less than 1% are able to produce cccDNA (*448*). These findings indicated that association of incoming SUMO modified, rcDNA carrying HBV core proteins to PML-NBs was the rate limiting factor in generation of cccDNA during HBV infection. As 1.3% of incoming HBV particles were observed to localize to PML-NBs but only less than 1% of incoming HBV particles form cccDNA (*448*), probably additional factors, including the composition of the PML-NBs, to which HBV core is recruited, or loss of rcDNA during transport of SUMOylated HBV core protein to PML-NBs might play a role.

Despite the striking differences in cccDNA generation observed using the plasmid-based replicon system pHBV1.1 *wt* compared to *Δscm1/2*, only minor effects on complete HBV DNA, including rcDNA and replication intermediates could be found (see figure 18, figure 19). This discrepancy could probably be attributed to the characteristics of the used plasmid-based replicon system. The pgRNA was transcribed from a constitutively active CMV promoter (*182*), which probably resulted in similar amounts of pgRNA. Therefore, similar levels of translated HBV core protein and polymerase could subsequently package and reverse transcribe pgRNA to rcDNA. The cccDNA is greatly outnumbered by levels of rcDNA and replication intermediates (*7, 60*). Consequently, it comes as no surprise that the severe effects of SUMOylation and PML association observed for cccDNA in the plasmid-based replicon system were not found in the levels of complete HBV DNA. In contrast, reduction of cccDNA in *wt* HBV infected HepG2 *shPML* cells was found to be accompanied by a similar decrease in complete HBV DNA levels (see figure 28 A, figure 28 B) which further confirmed this hypothesis.

Administration of IFNα or its PEGylated derivatives still serves as standard treatment for CHB patients, but often fails to induce a complete remission (*47, 48*). PML-NBs are known as interferon inducible structures and PML expression as well as size of PML-NBs is increased during treatment with IFNs (*345, 402-405*). Our studies showed a novel role for PML within the HBV replication cycle, providing the scaffold for the organization of rc- to cccDNA conversion. The anti-HBV effect of IFN treatment, which in turn induces PML expression,

seemed therefore, at a first glance, paradox. However, recent studies on the impact of IFN treatment on the cellular SUMO proteome could show that IFN treatment leads to an enhanced SUMO modification of cellular substrates including PML. Additionally, IFN induces recruitment of the only known SUMO E2 conjugating enzyme Ubc9 into the nuclear matrix and to PML-NBs (*449*). According to our data, this could impede efficient HBV replication on several levels: i) The increased SUMOylation of cellular substrates might deplete the pool of freely available SUMO mojeties for SUMO PTM of viral proteins, interfering with their function. ii) As outlined above, it is likely that the PML-NBs, which harbor the capacity to recruit SUMOylated HBV core protein together with the incoming rcDNA and the DDR factors necessary for cccDNA formation, are themselves SUMO-low. IFN induced enhancement of PML SUMOylation might therefore interfere with an efficient recruitment of SUMO modified HBV core protein and SUMOylated DDR factors. iii) To enable disruption of incoming HBV nucleocapsids in the nuclear basket of the NPC by SUMO PTM, access of Ubc9 and the cellular SUMOylation machinery is necessary. As IFN treatment induces relocalization of Ubc9 into the nuclear matrix and to PML-NBs, no efficient nuclear entry of HBV particles might be possible anymore which further interferes with HBV infection.

Taken together our research provided evidence for a far-reaching role of HBV core protein SUMOylation and PML-NBs in the regulation and organization of rc- to cccDNA conversion.

5.4 PML-II and -VI build the backbone of cccDNA biogenesis supporting PML-NBs

PML comprises six nuclear isoforms PML-I to -VI which differ in their C-terminal domains due to alternative splicing. The C-terminal domains are believed to confer specificity to the functions which the isoforms take over within a PML-NB and are associated with interactions with specific proteins (*313, 326-328*). Identification of those PML isoforms which interact with HBV core protein and allow cccDNA formation might therefore provide first insights into the composition of the specific PML-NBs harboring the capacity for rc- to cccDNA conversion.

Co-immunoprecipitation (see figure 23) and immunofluorescence (see figure 24, figure 25, figure 26, figure 27) experiments using HA-tagged *wt* HBV core protein could identify PML isoforms I and II as interaction partners for HBV core protein. Clear differences in co-localization of HBV core protein with different PML isoforms could only be determined using immunofluorescene staining of the GFP-tag fused to the single PML isoforms (see figure 26, figure 27) and not for stainings using an antibody recognizing all PML isoforms (see figure 24, figure 25). This was probably due to the 50% of residual PML expression in the HepG2 *shPML* cell line used to generate the HepG2 cell lines expressing single PML isoforms (see figure 20

B, figure 21). PML-I and PML-II strongly differ in the composition of their specific C-terminal domains, which consists of exons 8a and 9 for PML-I and exon 7b for PML-II (see figure 7) (*310, 329*). These differences might further explain the different interaction behavior between HBV core and PML-I and -II which could only be detected by pulldown of the HA-tag of HBV core for PML-I and by precipitation of the GFP epitope for PML-II (see figure 23, right panel, lanes 4, 5).

In contrast to the results showing interaction of HBV core protein with PML isoforms I and II (see figure 23, figure 26, figure 27), only PML-II and -VI were able to efficiently support cccDNA generation during infection (see figure 28 B). The other isoforms PML-I, -III, -IV and -V showed a similar deficiency in cccDNA generation as HepG2 *shPML* cells (see figure 28 B). Interaction of HBV core protein with PML-I might therefore represent a dead end pathway in the HBV replication cycle. This would further explain the discrepancy between the 1.3% of incoming HBV core particles, which were observed to localize to PML-NBs during the entry process (see figure 38, panels q-t), compared to only less than 1% of HBV particles forming cccDNA (*448*). In line with a strong and direct interaction of HBV core with PML-II (see figure 23, right panel, lane 5, figure 26, figure 27), infection of HepG2 *PML-II* cells resulted in an efficient formation of cccDNA. Noteworthy, PML-II was observed to localize to the inner nuclear membrane in several hepatocyte cells, including HepG2, Huh7 and human hepatocarcinomas. This distribution along the inner nuclear envelope is mediated by its unique C-terminal domain (*450, 451*). It is therefore tempting to speculate, that those nuclear membrane associated PML-NBs built up by PML-II might be involved in regulation of the disruption of incoming HBV capsids in the nuclear basket of the NPC and subsequently directly recruit the SUMO modified HBV core protein carrying the rcDNA. Surprisingly, single expression of PML-II isoform only supported cccDNA formation but in turn did not allow for efficient transcription of the cccDNA, as the levels of complete HBV DNA including rcDNA and replication intermediates was observed to be in a similar range as in cells without efficient cccDNA synthesis (see figure 28). These findings might indicate that PML-NBs based on PML-II alone harbored the factors necessary for efficient rc- to cccDNA conversion at early steps of infection, but might then interfere with efficient transcription, probably by epigenetic repression of the cccDNA. This might be due to the association of PML isoform II with expression of interferon stimulated genes. These include ISG20, which was shown to repress HBV infection by binding to pgRNA (*452, 453*). Intriguingly, the second PML isoforms which supported efficient cccDNA formation, PML-VI, also allowed efficient transcription of the cccDNA (see figure 28). PML-VI, being the shortest of all nuclear PML isoforms, lacks the SIM motif (*358*). When expressed in absence of other PML isoforms, PML-VI, as also observed for

PML-II, forms dot like assemblies, in contrast to ring-like distributions for PML isoforms I, III, IV and V (*329*). These similar ultrastructures of the PML-NBs built by PML-II and -VI might indicate recruitment of similar factors to the PML-NBs, which in both cases could support cccDNA formation. As PML-VI lacks the ability to specifically induce ISG expression (*452*), this might further explain why PML-VI supported subsequent efficient transcription, while PML-II did not (see figure 28). However, further research on the exact composition of the PML-II and PML-VI containing PML-NBs, which support cccDNA formation and transcription is urgently necessary, to identify further factors important in rc- to cccDNA conversion.

Most strikingly, mouse cells, in contrast to human cells, only express two PML isoforms, which are highly similar to the human isoforms PML-I and -V. Therefore, PML isoforms II, III, IV and VI have no direct counterparts in mice (*335, 454, 455*). Additionally, mice were not found to be suitable model systems for HBV infection. HBV nucleocapsid particles cannot cross the hepatocyte nuclear membrane in mice (*456*) and mouse hepatocytes do not support cccDNA formation, even when they express human NTCP (*457*). These findings might be explained by our data, which stressed the importance of PML isoforms II and VI in cccDNA formation. As those two PML isoforms are not present in mice (*335, 454, 455*), re-introduction *in trans* might reconstitute cccDNA formation in mouse hepatocytes and help in the generation of novel and more suitable animal model systems for HBV infection.

Summarized, our data indicated PML isoforms II and VI as the important factors building the backbone for efficient cccDNA formation.

5.5 Direct interference with HBV core protein SUMOylation and PML association as potential novel therapeutic target

The currently approved clinical treatment strategies against HBV infections are based on the reconstitution of the terminally exhausted immune response of the infected host, mainly by treatment with IFNα and its PEGylated derivatives (*47, 48*), or block HBV reverse transcription and virus reactivation using nucleos(t)ide analogues (*46, 47*). Both strategies, however, rarely cure the patient and mostly suppress symptomatic infection. Further direct acting antivirals are in clinical development and early clinical trials. Those either aim at inhibition of HBV entry into the host hepatocyte by blockage of the NTCP receptor (*50-54*) or directly target the HBV core protein using core protein allosteric modulators (CpAMs) (*48, 49*). CpAMs either interfere with correct assembly of pgRNA containing HBV capsids or accelerate the kinetics of HBV capsid assembly. Both compound classes induce the formation of empty capsids or abberant capsid structures deficient in replication (*48, 49*). CpAMs can therefore interfere with cccDNA replenishment by nuclear re-shuttling of mature HBV capsids or are even thought to stop *de*

novo infection by targeting incoming HBV capsids (*48, 49*). None of the treatment regimens outlined above, however, is able to efficiently interfere with the established nuclear pool of cccDNA, representing the viral persistence reservoir and the key to a functional cure (*46-54*).

Our work could prove a substantial interplay between PML-NBs, HBV core protein SUMOylation and rc- to cccDNA conversion by the host cell DDR. HBV core protein SUMO PTM was not only shown to be critical to nuclear entry of HBV capsids and the rcDNA, but also for the subsequent association of HBV core and, most presumably, also of HBV DNA towards PML-NBs, regulating formation of cccDNA but also efficient cccDNA transcription. Whole scale inhibition of the cellular SUMOylation machinery using GA during early events of HBV infection was therefore assumed to greatly interfere with efficient HBV replication. In line with a dose dependent decrease in global cellular poly-SUMOylation after 24h of GA treatment (see figure 37), nuclear entry of HBV core protein and subsequent association to PML-NBs was significantly reduced in cells primed by treatment with GA (see figure 38, figure 39). *Vice versa*, the degree of HBV core protein stalled at the nuclear membrane or stuck in the cytoplasm increased during GA application (see figure 38, figure 39). These findings provided further evidence for the role of HBV core protein SUMO PTM as the trigger for capsid disruption in the nuclear basket of the NPC and the subsequent nuclear entry and recruitment to PML-NBs. Analysis of cellular SUMO levels 6d post treatment and 7d post infection confirmed that the global cellular poly-SUMOylation was re-established after omission of GA (see figure 40). In contrast, a dose dependent decrease in cccDNA levels was observed (see figure 41). This indicated that HBV infection did not recover from the initial inhibition of nuclear entry and recruitment of HBV core together with the rcDNA to PML-NBs as site of cccDNA formation. Several of the proteins known to be involved in cccDNA generation are SUMO modified and regulated by SUMOylation (*162-166, 171, 318, 383-385, 387-391, 395-401*). Therefore, inhibition of SUMOylation during early stages of HBV infection might have additionally interfered with efficient recruitment of DDR factors necessary for rc- to cccDNA conversion. Altogether, these findings served as proof-of-concept for our hypothesis showing that nuclear entry of HBV core protein and the rcDNA depends on HBV core SUMO PTM and that rc- to cccDNA conversion is governed by SUMOylation and PML-NBs.

Complete and long lasting inhibition of global cellular SUMOylation was reported to be toxic for cells (*458-461*) which is why GA treatment was only used for a limited time of 24h to serve as proof-of-concept. The results, however, indicated that specific interference with HBV core protein SUMO modification might indeed represent a promising novel target for the development of antiviral agents against HBV infection. Similar to the mode of action observed for CpAM treatment (*48, 49*), interference with HBV core protein SUMOylation most

presumably mainly inhibited the intracellular cccDNA amplification pathway by blocking nuclear entry of mature HBV capsids (*75, 132, 133*). A further function of HBV core is the maintenance and transcriptional activity of cccDNA, which is achieved by direct binding to specific CpG islands in the nuclear cccDNA (*114, 215*). Our data showed an association of PML-NBs with cccDNA (see figure 36) and the transcription of cccDNA, which is enhanced by PML-VI (see figure 28). These findings indicated that loss of HBV core SUMO PTM might further interfere with the presence and transcriptional activity of cccDNA at PML-NBs, thereby additionally inhibiting efficient HBV replication.

Taken together, specific inhibition of HBV core protein SUMO modification might serve as a potential novel target for the development of antivirals against HBV infection.

5.6 Conclusion and hypothesis

Despite its strong clinical relevance, knowledge on the molecular mechanisms governing HBV nuclear entry and rc- to cccDNA is scarce (*109, 155, 171*). Our results provided novel insights into those black boxes in the molecular life cycle of HBV. Based on the data presented in this work, we build the following hypothesis: HBV core proteins within mature rcDNA containing HBV nucleocapsids, which are stalled in the nuclear basket of the NPC (*111, 113*), become SUMO modified by the host cell SUMO machinery that has access to the NPC (*446*). SUMOylation of several HBV core protein monomers within the capsid structure triggers capsid disruption and release of HBV core protein monomers together with the rcDNA into the nucleoplasm (see figure 42 A, [1]). Rc-DNA bound to SUMO modified HBV core proteins is recruited into SUMO-low PML-NBs, preferentially by interaction with PML isoforms I and II (see figure 42 A, [2]) where rc- to cccDNA conversion by SUMO modified proteins of the host cell DDR takes place (see figure 42 A, [3]). The specific PML-NBs which harbor the capacity for cccDNA generation are based on the presence of PML isoforms II and VI. Later in infection, chromatinized cccDNA stays associated with PML-NBs (see figure 42 A, [4]) and transcriptional activity is, among others, mediated by HBV core protein and PML-VI (see figure 42 A, [5]) (*215*).

In proof-of-concept experiments using the global SUMO inhibitor GA, we could confirm that only a brief inhibition of cellular SUMOylation during early steps of infection lead to long-lasting interference with efficient HBV replication and drastically decreased cccDNA formation. We hypothesize that GA mediated blockage of HBV core protein SUMOylation impedes disassembly of incoming HBV capsids at the NPC. GA therefore stops nuclear entry (see figure 42 B, [1]) and subsequent recruitment of SUMO modified HBV core together with the rcDNA to PML-NBs (see figure 42 B, [2]). This, in combination with the decrease in

5. Discussion

SUMOylation of cellular DDR proteins involved in cccDNA formation, induces a loss of efficient rc- to cccDNA conversion at PML-NBs (see figure 42 B, [3]).
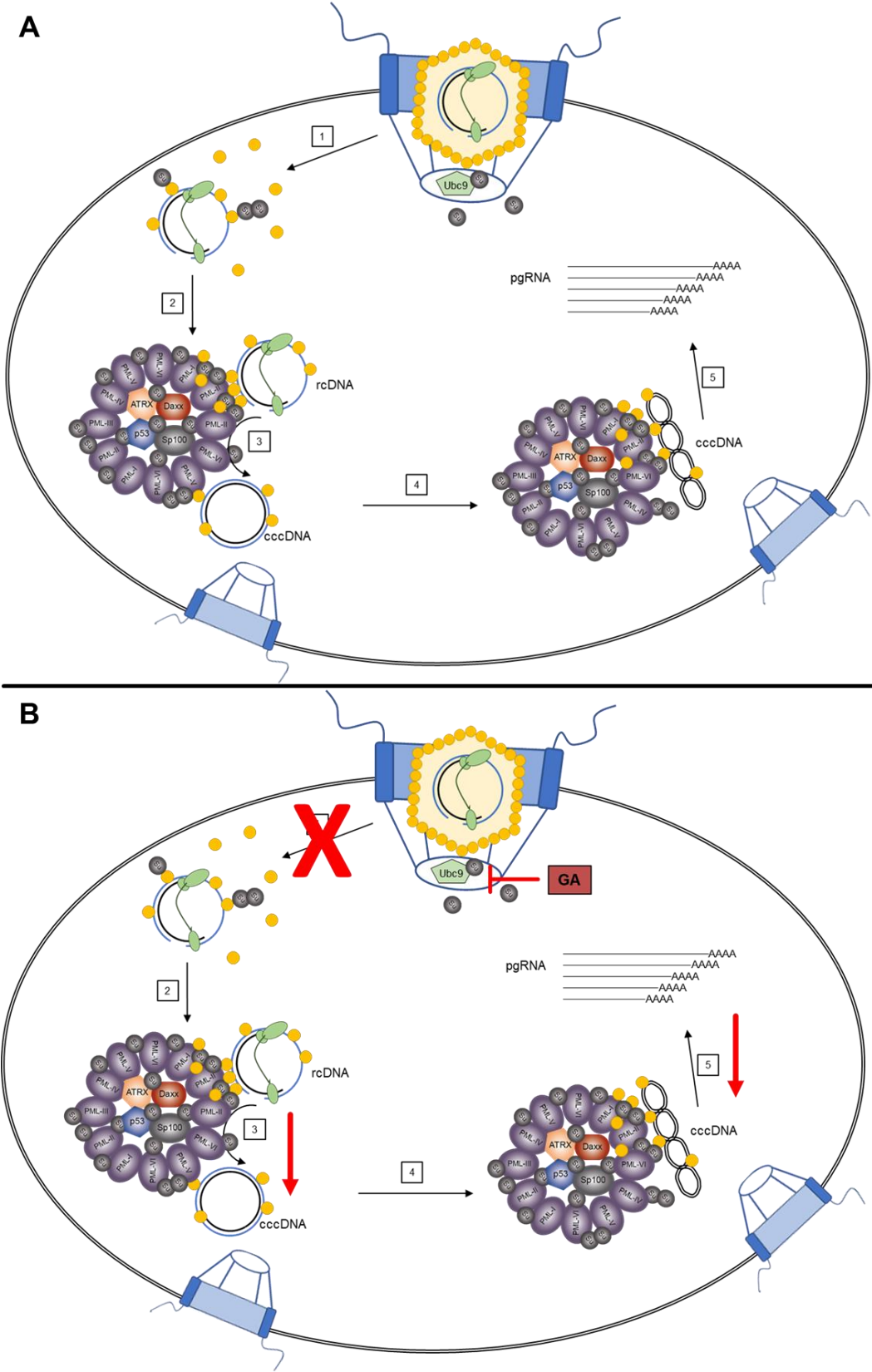
Figure 42: A Schematic representation of the findings presented in this work and B Mode of action proposed for the anti-HBV activity of GA treatment. Further information is given in the text.

Additionally, our data indicated that HBV core protein acts as a bridge between PML and cccDNA at later stages of infection and HBV core protein association with cccDNA mediates transcriptional activity of cccDNA (*215*). Therefore, inhibition of HBV core SUMO PTM might additionally interfere with efficient transcription of HBV cccDNA (see figure 42 B, [5]).

Taken together, our data highlighted a siginificant role of HBV core protein SUMOylation and PML association on rc- to cccDNA conversion. We therefore propose interference with HBV core SUMO PTM and PML interaction as an innovative therapeutic target in the eradication of acute and chronic HBV infection.

6. Addendum

6.1 List of Figures

6.2 List of Tables

7. References

1.   C. Seeger, W. S. Mason, Hepatitis B virus biology. *Microbiol Mol Biol Rev* **64**, 51-68 (2000).
2.   C. Seeger, W. S. Mason, Molecular biology of hepatitis B virus infection. *Virology* **479-480**, 672-686 (2015).
3.   B. S. Blumberg, B. J. Gerstley, D. A. Hungerford, W. T. London, A. I. Sutnick, A serum antigen (Australia antigen) in Down's syndrome, leukemia, and hepatitis. *Ann Intern Med* **66**, 924-931 (1967).
4.   D. S. Dane, C. H. Cameron, M. Briggs, Virus-like particles in serum of patients with Australia-antigen-associated hepatitis. *Lancet* **1**, 695-698 (1970).
5.   K. Kidd-Ljunggren, Y. Miyakawa, A. H. Kidd, Genetic variability in hepatitis B viruses. *J Gen Virol* **83**, 1267-1280 (2002).
6.   J. Hu, C. Seeger, Hepadnavirus Genome Replication and Persistence. *Cold Spring Harb Perspect Med* **5**, a021386 (2015).
7.   M. Nassal, HBV cccDNA: viral persistence reservoir and key obstacle for a cure of chronic hepatitis B. *Gut* **64**, 1972-1984 (2015).
8.   C. R. Bonvicino, M. A. Moreira, M. A. Soares, Hepatitis B virus lineages in mammalian hosts: Potential for bidirectional cross-species transmission. *World J Gastroenterol* **20**, 7665-7674 (2014).
9.   S. Schaefer, Hepatitis B virus taxonomy and hepatitis B virus genotypes. *World J Gastroenterol* **13**, 14-21 (2007).
10.   R. E. Lanford, D. Chavez, K. M. Brasky, R. B. Burns, 3rd, R. Rico-Hesse, Isolation of a hepadnavirus from the woolly monkey, a New World primate. *Proc Natl Acad Sci U S A* **95**, 5757-5761 (1998).
11.   J. Summers, J. M. Smolec, R. Snyder, A virus similar to human hepatitis B virus associated with hepatitis and hepatoma in woodchucks. *Proc Natl Acad Sci U S A* **75**, 4533-4537 (1978).
12.   W. S. Mason, G. Seal, J. Summers, Virus of Pekin ducks with structural and biological relatedness to human hepatitis B virus. *J Virol* **36**, 829-836 (1980).
13.   J. Hu, K. Liu, Complete and Incomplete Hepatitis B Virus Particles: Formation, Function, and Application. *Viruses* **9**, (2017).
14.   N. Rajoriya, C. Combet, F. Zoulim, H. L. A. Janssen, How viral genetic variants and genotypes influence disease and treatment outcome of chronic hepatitis B. Time for an individualised approach? *J Hepatol* **67**, 1281-1297 (2017).
15.   M. Guvenir, A. Arikan, Hepatitis B Virus: From Diagnosis to Treatment. *Pol J Microbiol* **69**, 391-399 (2020).
16.   A. Arikan *et al.*, [Molecular epidemiology of hepatitis B virus in Northern Cyprus]. *Mikrobiyol Bul* **50**, 86-93 (2016).
17.   M. Mahmood, M. A. Anwar, A. Khanum, N. Zaman, A. Raza, Distribution and clinical significance of hepatitis B virus genotypes in Pakistan. *BMC Gastroenterol* **16**, 104 (2016).
18.   K. Tatematsu *et al.*, A genetic variant of hepatitis B virus divergent from known human and ape genotypes isolated from a Japanese patient and provisionally assigned to new genotype J. *J Virol* **83**, 10538-10547 (2009).
19.   E. E. Mast *et al.*, A comprehensive immunization strategy to eliminate transmission of hepatitis B virus infection in the United States: recommendations of the Advisory Committee on Immunization Practices (ACIP) part 1: immunization of infants, children, and adolescents. *MMWR Recomm Rep* **54**, 1-31 (2005).
20.   C. W. Shepard, E. P. Simard, L. Finelli, A. E. Fiore, B. P. Bell, Hepatitis B virus infection: epidemiology and vaccination. *Epidemiol Rev* **28**, 112-125 (2006).
21.   WHO. (2019).

22.   P. Van Damme, Long-term Protection After Hepatitis B Vaccine. *J Infect Dis* **214**, 1-3 (2016).
23.   M. H. Chang *et al.*, Decreased incidence of hepatocellular carcinoma in hepatitis B vaccinees: a 20-year follow-up study. *J Natl Cancer Inst* **101**, 1348-1355 (2009).
24.   C. Trepo, H. L. Chan, A. Lok, Hepatitis B virus infection. *Lancet* **384**, 2053-2063 (2014).
25.   F. Zoulim, S. Locarnini, Hepatitis B virus resistance to nucleos(t)ide analogues. *Gastroenterology* **137**, 1593-1608 e1591-1592 (2009).
26.   S. Chevaliez, C. Hezode, S. Bahrami, M. Grare, J. M. Pawlotsky, Long-term hepatitis B surface antigen (HBsAg) kinetics during nucleoside/nucleotide analogue therapy: finite treatment duration unlikely. *J Hepatol* **58**, 676-683 (2013).
27.   B. Rehermann, C. Ferrari, C. Pasquinelli, F. V. Chisari, The hepatitis B virus persists for decades after patients' recovery from acute viral hepatitis despite active maintenance of a cytotoxic T-lymphocyte response. *Nat Med* **2**, 1104-1108 (1996).
28.   P. Revill, Z. Yuan, New insights into how HBV manipulates the innate immune response to establish acute and persistent infection. *Antivir Ther* **18**, 1-15 (2013).
29.   M. Wang, D. Xi, Q. Ning, Virus-induced hepatocellular carcinoma with special emphasis on HBV. *Hepatol Int* **11**, 171-180 (2017).
30.   H. W. Lee, S. H. Ahn, Prediction models of hepatocellular carcinoma development in chronic hepatitis B patients. *World J Gastroenterol* **22**, 8314-8321 (2016).
31.   D. Y. Lee, E. H. Kim, Therapeutic Effects of Amino Acids in Liver Diseases: Current Studies and Future Perspectives. *J Cancer Prev* **24**, 72-78 (2019).
32.   R. J. Lamontagne, S. Bagga, M. J. Bouchard, Hepatitis B virus molecular biology and pathogenesis. *Hepatoma Res* **2**, 163-186 (2016).
33.   L. G. Guidotti, F. V. Chisari, Immunobiology and pathogenesis of viral hepatitis. *Annu Rev Pathol* **1**, 23-61 (2006).
34.   F. V. Chisari, C. Ferrari, M. U. Mondelli, Hepatitis B virus structure and biology. *Microb Pathog* **6**, 311-325 (1989).
35.   F. V. Chisari, Hepatitis B virus biology and pathogenesis. *Mol Genet Med* **2**, 67-104 (1992).
36.   F. V. Chisari, Rous-Whipple Award Lecture. Viruses, immunity, and cancer: lessons from hepatitis B. *Am J Pathol* **156**, 1117-1132 (2000).
37.   M. U. Mondelli *et al.*, Significance of the immune response to a major, conformational B-cell epitope on the hepatitis C virus NS3 region defined by a human monoclonal antibody. *J Virol* **68**, 4829-4836 (1994).
38.   N. A. Terrault *et al.*, Update on prevention, diagnosis, and treatment of chronic hepatitis B: AASLD 2018 hepatitis B guidance. *Hepatology* **67**, 1560-1599 (2018).
39.   T. T. Than *et al.*, High Environmental Stability of Hepatitis B Virus and Inactivation Requirements for Chemical Biocides. *J Infect Dis* **219**, 1044-1048 (2019).
40.   R. W. Almeida *et al.*, Hepatitis B virus DNA stability in plasma samples under short-term storage at 42 degrees C. *Braz J Med Biol Res* **48**, 553-556 (2015).
41.   V. J. Desmet, M. Gerber, J. H. Hoofnagle, M. Manns, P. J. Scheuer, Classification of chronic hepatitis: diagnosis, grading and staging. *Hepatology* **19**, 1513-1520 (1994).
42.   T. J. Liang, Hepatitis B: the virus and disease. *Hepatology* **49**, S13-21 (2009).
43.   B. Hyun Kim, W. Ray Kim, Epidemiology of Hepatitis B Virus Infection in the United States. *Clin Liver Dis (Hoboken)* **12**, 1-4 (2018).
44.   M. Jefferies, B. Rauff, H. Rashid, T. Lam, S. Rafiq, Update on global epidemiology of viral hepatitis and preventive strategies. *World J Clin Cases* **6**, 589-599 (2018).
45.   T. Tu, J. M. Block, S. Wang, C. Cohen, M. W. Douglas, The Lived Experience of Chronic Hepatitis B: A Broader View of Its Impacts and Why We Need a Cure. *Viruses* **12**, (2020).
46.   R. N. Chien, Y. F. Liaw, Nucleos(t)ide analogues for hepatitis B virus: strategies for long-term success. *Best Pract Res Clin Gastroenterol* **22**, 1081-1092 (2008).

47. M. F. Yuen, C. L. Lai, Treatment of chronic hepatitis B: Evolution over two decades. *J Gastroenterol Hepatol* **26 Suppl 1**, 138-143 (2011).

48. G. C. Fanning, F. Zoulim, J. Hou, A. Bertoletti, Therapeutic strategies for hepatitis B virus infection: towards a cure. *Nature Reviews Drug Discovery*, (2019).

49. B. Nijampatnam, D. C. Liotta, Recent advances in the development of HBV capsid assembly modulators. *Curr Opin Chem Biol* **50**, 73-79 (2019).

50. W. Li, S. Urban, Entry of hepatitis B and hepatitis D virus into hepatocytes: Basic insights and clinical implications. *J Hepatol* **64**, S32-S40 (2016).

51. A. Schulze, A. Schieck, Y. Ni, W. Mier, S. Urban, Fine mapping of pre-S sequence requirements for hepatitis B virus large envelope protein-mediated receptor interaction. *J Virol* **84**, 1989-2000 (2010).

52. A. Blank *et al.*, First-in-human application of the novel hepatitis B and hepatitis D virus entry inhibitor myrcludex B. *J Hepatol* **65**, 483-489 (2016).

53. A. Schieck *et al.*, Hepatitis B virus hepatotropism is mediated by specific receptor recognition in the liver and not restricted to susceptible hosts. *Hepatology* **58**, 43-53 (2013).

54. P. Bogomolov *et al.*, Treatment of chronic hepatitis D with the entry inhibitor myrcludex B: First results of a phase Ib/IIa study. *J Hepatol* **65**, 490-498 (2016).

55. F. Bohne *et al.*, T cells redirected against hepatitis B virus surface proteins eliminate infected hepatocytes. *Gastroenterology* **134**, 239-247 (2008).

56. K. Ueda, T. Tsurimoto, K. Matsubara, Three Envelope Proteins of Hepatitis B Virus: Large S, Middle S, and Major S Proteins Needed for the Formation of Dane Particles. *J Virol* **65**, 3521-3529 (1991).

57. P. Tiollais, C. Pourcel, A. Dejean, The hepatitis B virus. *Nature* **317**, 489-495 (1985).

58. R. A. Crowther *et al.*, Three-dimensional structure of hepatitis B virus core particles determined by electron cryomicroscopy. *Cell* **77**, 943-950 (1994).

59. J. M. Kenney, C. H. von Bonsdorff, M. Nassal, S. D. Fuller, Evolutionary conservation in the hepatitis B virus core structure: comparison of human and duck cores. *Structure* **3**, 1009-1019 (1995).

60. S. Schreiner, M. Nassal, A Role for the Host DNA Damage Response in Hepatitis B Virus cccDNA Formation-and Beyond? *Viruses* **9**, (2017).

61. W. H. Gerlich, Medical virology of hepatitis B: how it began and where we are now. *Virol J* **10**, 239 (2013).

62. J. T. Guo, H. Guo, Metabolism and function of hepatitis B virus cccDNA: Implications for the development of cccDNA-targeting antiviral therapeutics. *Antiviral Res* **122**, 91-100 (2015).

63. A. L. Marchetti, H. Guo, New Insights on Molecular Mechanism of Hepatitis B Virus Covalently Closed Circular DNA Formation. *Cells* **9**, (2020).

64. W. H. Gerlich, W. S. Robinson, Hepatitis Virus Contains Protein Attached to the 5' Terminus of Its Complete DNA Strand. *Cell* **21**, 801-809 (1980).

65. S. Datta, S. Chatterjee, V. Veer, R. Chakravarty, Molecular biology of the hepatitis B virus for clinicians. *J Clin Exp Hepatol* **2**, 353-365 (2012).

66. J. Quarleri, Core promoter: a critical region where the hepatitis B virus makes decisions. *World J Gastroenterol* **20**, 425-435 (2014).

67. A. Kay, F. Zoulim, Hepatitis B virus genetic variability and evolution. *Virus Res* **127**, 164-176 (2007).

68. N. Moolla, M. Kew, P. Arbuthnot, Regulatory elements of hepatitis B virus transcription. *J Viral Hepat* **9**, 323-331 (2002).

69. C. Seeger, D. Ganem, H. E. Varmus, Biochemical and genetic evidence for the hepatitis B virus replication strategy. *Science* **232**, 477-484 (1986).

70. J. W. Habig, D. D. Loeb, Sequence identity of the direct repeats, DR1 and DR2, contributes to the discrimination between primer translocation and in situ priming during replication of the duck hepatitis B virus. *J Mol Biol* **364**, 32-43 (2006).

71. M. Levrero *et al.*, Control of cccDNA function in hepatitis B virus infection. *J Hepatol* **51**, 581-592 (2009).
72. J. K. Yee, A liver-specific enhancer in the core promoter region of human hepatitis B virus. *Science* **246**, 658-661 (1989).
73. J. Li, J. H. Ou, Differential regulation of hepatitis B virus gene expression by the Sp1 transcription factor. *J Virol* **75**, 8400-8406 (2001).
74. H. Guo *et al.*, Characterization of the intracellular deproteinized relaxed circular DNA of hepatitis B virus: an intermediate of covalently closed circular DNA formation. *J Virol* **81**, 12472-12484 (2007).
75. J. S. Tuttleman, C. Pourcel, J. Summers, Formation of the pool of covalently closed circular viral DNA in hepadnavirus-infected cells. *Cell* **47**, 451-460 (1986).
76. J. Summers, W. S. Mason, Replication of the genome of a hepatitis B--like virus by reverse transcription of an RNA intermediate. *Cell* **29**, 403-415 (1982).
77. M. Nassal, Hepatitis B viruses: reverse transcription a different way. *Virus Res* **134**, 235-249 (2008).
78. M. T. Chen *et al.*, A function of the hepatitis B virus precore protein is to regulate the immune response to the core antigen. *Proc Natl Acad Sci U S A* **101**, 14913-14918 (2004).
79. L. M. Cabuang *et al.*, In vitro replication phenotype of a novel (-1G) hepatitis B virus variant associated with HIV co-infection. *J Med Virol* **84**, 1166-1176 (2012).
80. D. R. Milich, M. K. Chen, J. L. Hughes, J. E. Jones, The secreted hepatitis B precore antigen can modulate the immune response to the nucleocapsid: a mechanism for persistence. *J Immunol* **160**, 2013-2021 (1998).
81. D. R. Milich *et al.*, Role of B cells in antigen presentation of the hepatitis B core. *Proc Natl Acad Sci U S A* **94**, 14648-14653 (1997).
82. R. Walsh, S. Locarnini, Hepatitis B precore protein: pathogenic potential and therapeutic promise. *Yonsei Med J* **53**, 875-885 (2012).
83. C. Chang *et al.*, Expression of the precore region of an avian hepatitis B virus is not required for viral replication. *J Virol* **61**, 3322-3325 (1987).
84. B. Rehermann, M. Nascimbeni, Immunology of hepatitis B virus and hepatitis C virus infection. *Nat Rev Immunol* **5**, 215-229 (2005).
85. D. Ganem, A. M. Prince, Hepatitis B virus infection--natural history and clinical consequences. *N Engl J Med* **350**, 1118-1129 (2004).
86. D. Ganem, Assembly of hepadnaviral virions and subviral particles. *Curr Top Microbiol Immunol* **168**, 61-83 (1991).
87. K. H. Heermann *et al.*, Large surface proteins of hepatitis B virus containing the pre-s sequence. *J Virol* **52**, 396-402 (1984).
88. N. Chai *et al.*, Properties of subviral particles of hepatitis B virus. *J Virol* **82**, 7812-7817 (2008).
89. L. Luckenbaugh, K. M. Kitrinos, W. E. t. Delaney, J. Hu, Genome-free hepatitis B virion levels in patient sera as a potential marker to monitor response to antiviral therapy. *J Viral Hepat* **22**, 561-570 (2015).
90. X. Ning *et al.*, Secretion of genome-free hepatitis B virus--single strand blocking model for virion morphogenesis of para-retrovirus. *PLoS Pathog* **7**, e1002255 (2011).
91. G. Radziwill, W. Tucker, H. Schaller, Mutational Analysis of the Hepatitis B Virus P Gene Product: Domain Structure and RNase H Activity. *J Virol* **64**, 613-620 (1990).
92. S. A. Jones, D. N. Clark, F. Cao, J. E. Tavis, J. Hu, Comparative analysis of hepatitis B virus polymerase sequences required for viral RNA binding, RNA packaging, and protein priming. *J Virol* **88**, 1564-1572 (2014).
93. M. Melegari, S. K. Wolf, R. J. Schneider, Hepatitis B virus DNA replication is coordinated by core protein serine phosphorylation and HBx expression. *J Virol* **79**, 9810-9820 (2005).

94. A. Decorsiere *et al.*, Hepatitis B virus X protein identifies the Smc5/6 complex as a host restriction factor. *Nature* **531**, 386-389 (2016).

95. L. Belloni *et al.*, Nuclear HBx binds the HBV minichromosome and modifies the epigenetic regulation of cccDNA function. *Proc Natl Acad Sci U S A* **106**, 19975-19979 (2009).

96. J. A. Kwon, H. M. Rho, Transcriptional repression of the human p53 gene by hepatitis B viral core protein (HBc) in human liver cells. *Biol Chem* **384**, 203-212 (2003).

97. A. Schulze, P. Gripon, S. Urban, Hepatitis B virus infection initiates with a large surface protein-dependent binding to heparan sulfate proteoglycans. *Hepatology* **46**, 1759-1768 (2007).

98. M. Iwamoto *et al.*, Epidermal growth factor receptor is a host-entry cofactor triggering hepatitis B virus internalization. *Proc Natl Acad Sci U S A* **116**, 8487-8492 (2019).

99. M. Iwamoto *et al.*, The machinery for endocytosis of epidermal growth factor receptor coordinates the transport of incoming hepatitis B virus to the endosomal network. *J Biol Chem* **295**, 800-807 (2020).

100. H. C. Huang, C. C. Chen, W. C. Chang, M. H. Tao, C. Huang, Entry of hepatitis B virus into immortalized human primary hepatocytes by clathrin-dependent endocytosis. *J Virol* **86**, 9443-9453 (2012).

101. H. Yan *et al.*, Sodium taurocholate cotransporting polypeptide is a functional receptor for human hepatitis B and D virus. *Elife* **1**, e00049 (2012).

102. C. Herrscher *et al.*, Hepatitis B virus entry into HepG2-NTCP cells requires clathrin-mediated endocytosis. *Cell Microbiol* **22**, e13205 (2020).

103. W. Liao, J. H. Ou, Phosphorylation and nuclear localization of the hepatitis B virus core protein: significance of serine in the three repeated SPRRR motifs. *J Virol* **69**, 1025-1029 (1995).

104. S. G. Eckhardt, D. R. Milich, A. McLachlan, Hepatitis B virus core antigen has two nuclear localization sequences in the arginine-rich carboxyl terminus. *J Virol* **65**, 575-582 (1991).

105. H. Guo, R. Mao, T. M. Block, J. T. Guo, Production and function of the cytoplasmic deproteinized relaxed circular DNA of hepadnaviruses. *J Virol* **84**, 387-396 (2010).

106. M. L. Blondot, V. Bruss, M. Kann, Intracellular transport and egress of hepatitis B virus. *J Hepatol* **64**, S49-S59 (2016).

107. M. Kann, A. Schmitz, B. Rabe, Intracellular transport of hepatitis B virus. *World J Gastroenterol* **13**, 39-47 (2007).

108. B. Rabe *et al.*, Nuclear entry of hepatitis B virus capsids involves disintegration to protein dimers followed by nuclear reassociation to capsids. *PLoS Pathog* **5**, e1000563 (2009).

109. L. Gallucci, M. Kann, Nuclear Import of Hepatitis B Virus Capsids and Genome. *Viruses* **9**, (2017).

110. B. Rabe, A. Vlachou, N. Pante, A. Helenius, M. Kann, Nuclear import of hepatitis B virus capsids and release of the viral genome. *Proc Natl Acad Sci U S A* **100**, 9849-9854 (2003).

111. A. Schmitz *et al.*, Nucleoporin 153 arrests the nuclear import of hepatitis B virus capsids in the nuclear basket. *PLoS Pathog* **6**, e1000741 (2010).

112. J. Kock, M. Kann, G. Putz, H. E. Blum, F. Von Weizsacker, Central role of a serine phosphorylation site within duck hepatitis B virus core protein for capsid trafficking and genome release. *J Biol Chem* **278**, 28123-28129 (2003).

113. M. Kann, B. Sodeik, A. Vlachou, W. H. Gerlich, A. Helenius, Phosphorylation-dependent binding of hepatitis B virus core particles to the nuclear pore complex. *J Cell Biol* **145**, 45-55 (1999).

114.   Y. Xia, H. Guo, Hepatitis B virus cccDNA: Formation, regulation and therapeutic potential. *Antiviral Res* **180**, 104824 (2020).

115.   T. Pollicino *et al.*, Hepatitis B virus replication is regulated by the acetylation status of hepatitis B virus cccDNA-bound H3 and H4 histones. *Gastroenterology* **130**, 823-837 (2006).

116.   P. Tropberger *et al.*, Mapping of histone modifications in episomal HBV cccDNA uncovers an unusual chromatin organization amenable to epigenetic manipulation. *Proc Natl Acad Sci U S A* **112**, E5715-5724 (2015).

117.   C. T. Bock *et al.*, Structural organization of the hepatitis B virus minichromosome. *J Mol Biol* **307**, 183-196 (2001).

118.   M. Qiao, C. A. Scougall, A. Duszynski, C. J. Burrell, Kinetics of early molecular events in duck hepatitis B virus replication in primary duck hepatocytes. *J Gen Virol* **80 (Pt 8)**, 2127-2135 (1999).

119.   J. E. Newbold *et al.*, The covalently closed duplex form of the hepadnavirus genome exists in situ as a heterogeneous population of viral minichromosomes. *J Virol* **69**, 3350-3357 (1995).

120.   C. T. Bock, P. Schranz, C. H. Schroder, H. Zentgraf, Hepatitis B virus genome is organized into nucleosomes in the nucleus of the infected cell. *Virus Genes* **8**, 215-229 (1994).

121.   D. H. Nguyen, L. Ludgate, J. Hu, Hepatitis B virus-cell interactions and pathogenesis. *J Cell Physiol* **216**, 289-294 (2008).

122.   R. C. Hirsch, J. E. Lavine, L. J. Chang, H. E. Varmus, D. Ganem, Polymerase gene products of hepatitis B viruses are required for genomic RNA packaging as wel as for reverse transcription. *Nature* **344**, 552-555 (1990).

123.   R. Bartenschlager, H. Schaller, Hepadnaviral assembly is initiated by polymerase binding to the encapsidation signal in the viral RNA genome. *EMBO J* **11**, 3413-3420 (1992).

124.   R. Bartenschlager, M. Junker-Niepmann, H. Schaller, The P gene product of hepatitis B virus is required as a structural component for genomic RNA encapsidation. *J Virol* **64**, 5324-5332 (1990).

125.   A. Zajakina *et al.*, Translation of hepatitis B virus (HBV) surface proteins from the HBV pregenome and precore RNAs in Semliki Forest virus-driven expression. *J Gen Virol* **85**, 3343-3351 (2004).

126.   N. Fouillot, S. Tlouzeau, J. M. Rossignol, O. Jean-Jean, Translation of the hepatitis B virus P gene by ribosomal scanning as an alternative to internal initiation. *J Virol* **67**, 4886-4895 (1993).

127.   R. Cattaneo, H. Will, H. Schaller, Hepatitis B virus transcription in the infected liver. *EMBO J* **3**, 2191-2196 (1984).

128.   G. H. Enders, D. Ganem, H. Varmus, Mapping the major transcripts of ground squirrel hepatitis virus: the presumptive template for reverse transcriptase is terminally redundant. *Cell* **42**, 297-308 (1985).

129.   J. C. Wang, D. G. Nickens, T. B. Lentz, D. D. Loeb, A. Zlotnick, Encapsidated hepatitis B virus reverse transcriptase is poised on an ordered RNA lattice. *Proc Natl Acad Sci U S A* **111**, 11329-11334 (2014).

130.   Z. Tan *et al.*, The interface between hepatitis B virus capsid proteins affects self-assembly, pregenomic RNA packaging, and reverse transcription. *J Virol* **89**, 3275-3284 (2015).

131.   K. Liu, L. Luckenbaugh, X. Ning, J. Xi, J. Hu, Multiple roles of core protein linker in hepatitis B virus replication. *PLoS Pathog* **14**, e1007085 (2018).

132.   J. Kock *et al.*, Generation of covalently closed circular DNA of hepatitis B viruses via intracellular recycling is regulated in a virus specific manner. *PLoS Pathog* **6**, e1001082 (2010).

133. C. Ko *et al.*, Hepatitis B virus genome recycling and de novo secondary infection events maintain stable cccDNA levels. *J Hepatol* **69**, 1231-1241 (2018).

134. T. Tu, B. Zehnder, B. Qu, S. Urban, D e novo synthesis of hepatitis B virus nucleocapsids is dispensable for the maintenance and transcriptional regulation of cccDNA. *JHEP Rep* **3**, 100195 (2021).

135. W. H. Gerlich, W. S. Robinson, Hepatitis B virus contains protein attached to the 5' terminus of its complete DNA strand. *Cell* **21**, 801-809 (1980).

136. R. E. Lanford, L. Notvall, B. Beames, Nucleotide priming and reverse transcriptase activity of hepatitis B virus polymerase expressed in insect cells. *J Virol* **69**, 4431-4439 (1995).

137. R. Bartenschlager, H. Schaller, The amino-terminal domain of the hepadnaviral P-gene encodes the terminal protein (genome-linked protein) believed to prime reverse transcription. *EMBO J* **7**, 4185-4192 (1988).

138. K. L. Molnar-Kimber, J. Summers, J. M. Taylor, W. S. Mason, Protein covalently bound to minus-strand DNA intermediates of duck hepatitis B virus. *J Virol* **45**, 165-172 (1983).

139. M. Junker-Niepmann, R. Bartenschlager, H. Schaller, A short cis-acting sequence is required for hepatitis B virus pregenome encapsidation and sufficient for packaging of foreign RNA. *EMBO J* **9**, 3389-3396 (1990).

140. D. D. Loeb, R. C. Hirsch, D. Ganem, Sequence-independent RNA cleavages generate the primers for plus strand DNA synthesis in hepatitis B viruses: implications for other reverse transcribing elements. *EMBO J* **10**, 3533-3540 (1991).

141. J. E. Tavis, E. Lomonosova, The hepatitis B virus ribonuclease H as a drug target. *Antiviral Res* **118**, 132-138 (2015).

142. M. B. Havert, D. D. Loeb, cis-Acting sequences in addition to donor and acceptor sites are required for template switching during synthesis of plus-strand DNA for duck hepatitis B virus. *J Virol* **71**, 5336-5344 (1997).

143. J. M. Lien, C. E. Aldrich, W. S. Mason, Evidence that a capped oligoribonucleotide is the primer for duck hepatitis B virus plus-strand DNA synthesis. *J Virol* **57**, 229-236 (1986).

144. S. Staprans, D. D. Loeb, D. Ganem, Mutations affecting hepadnavirus plus-strand DNA synthesis dissociate primer cleavage from translocation and reveal the origin of linear viral DNA. *J Virol* **65**, 1255-1262 (1991).

145. K. M. Haines, D. D. Loeb, The sequence of the RNA primer and the DNA template influence the initiation of plus-strand DNA synthesis in hepatitis B virus. *J Mol Biol* **370**, 471-480 (2007).

146. N. Liu, L. Ji, M. L. Maguire, D. D. Loeb, cis-Acting sequences that contribute to the synthesis of relaxed-circular DNA of human hepatitis B virus. *J Virol* **78**, 642-649 (2004).

147. C. Ko, T. Michler, U. Protzer, Novel viral and host targets to cure hepatitis B. *Curr Opin Virol* **24**, 38-45 (2017).

148. C. I. Wooddell *et al.*, RNAi-based treatment of chronically infected patients and chimpanzees reveals that integrated hepatitis B virus DNA is a source of HBsAg. *Sci Transl Med* **9**, (2017).

149. T. Tu, M. A. Budzinska, N. A. Shackel, S. Urban, HBV DNA Integration: Molecular Mechanisms and Clinical Implications. *Viruses* **9**, (2017).

150. W. Yang, J. Summers, Integration of hepadnavirus DNA in infected liver: evidence for a linear precursor. *J Virol* **73**, 9710-9717 (1999).

151. Y. Ogawa, Y. Miyamoto, M. Oka, Y. Yoneda, The interaction between importin-alpha and Nup153 promotes importin-alpha/beta-mediated nuclear import. *Traffic* **13**, 934-946 (2012).

152.   C. Chen *et al.*, Importin beta Can Bind Hepatitis B Virus Core Protein and Empty Core-Like Particles and Induce Structural Changes. *PLoS Pathog* **12**, e1005802 (2016).

153.   X. Cui, L. Ludgate, X. Ning, J. Hu, Maturation-associated destabilization of hepatitis B virus nucleocapsid. *J Virol* **87**, 11494-11503 (2013).

154.   X. Cui, L. Luckenbaugh, V. Bruss, J. Hu, Alteration of Mature Nucleocapsid and Enhancement of Covalently Closed Circular DNA Formation by Hepatitis B Virus Core Mutants Defective in Complete-Virion Formation. *J Virol* **89**, 10064-10072 (2015).

155.   J. Luo, J. Xi, L. Gao, J. Hu, Role of Hepatitis B virus capsid phosphorylation in nucleocapsid disassembly and covalently closed circular DNA formation. *PLoS Pathog* **16**, e1008459 (2020).

156.   J. Kock, H. J. Schlicht, Analysis of the earliest steps of hepadnavirus replication: genome repair after infectious entry into hepatocytes does not depend on viral polymerase activity. *J Virol* **67**, 4867-4874 (1993).

157.   W. Gao, J. Hu, Formation of hepatitis B virus covalently closed circular DNA: removal of genome-linked protein. *J Virol* **81**, 6164-6174 (2007).

158.   J. Lucifora, U. Protzer, Attacking hepatitis B virus cccDNA--The holy grail to hepatitis B cure. *J Hepatol* **64**, S41-48 (2016).

159.   J. A. Sohn, S. Litwin, C. Seeger, Mechanism for CCC DNA synthesis in hepadnaviruses. *PLoS One* **4**, e8093 (2009).

160.   C. Koniger *et al.*, Involvement of the host DNA-repair enzyme TDP2 in formation of the covalently closed circular DNA persistence reservoir of hepatitis B viruses. *Proc Natl Acad Sci U S A* **111**, E4244-4253 (2014).

161.   X. Cui *et al.*, Does Tyrosyl DNA Phosphodiesterase-2 Play a Role in Hepatitis B Virus Genome Repair? *PLoS One* **10**, e0128401 (2015).

162.   K. Kitamura *et al.*, Flap endonuclease 1 is involved in cccDNA formation in the hepatitis B virus. *PLoS Pathog* **14**, e1007124 (2018).

163.   Y. Qi *et al.*, DNA Polymerase kappa Is a Key Cellular Factor for the Formation of Covalently Closed Circular DNA of Hepatitis B Virus. *PLoS Pathog* **12**, e1005893 (2016).

164.   L. Tang, M. Sheraz, M. McGrane, J. Chang, J. T. Guo, DNA Polymerase alpha is essential for intracellular amplification of hepatitis B virus covalently closed circular DNA. *PLoS Pathog* **15**, e1007742 (2019).

165.   M. Sheraz, J. Cheng, L. Tang, J. Chang, J. T. Guo, Cellular DNA Topoisomerases Are Required for the Synthesis of Hepatitis B Virus Covalently Closed Circular DNA. *J Virol* **93**, (2019).

166.   Q. Long *et al.*, The role of host DNA ligases in hepadnavirus covalently closed circular DNA formation. *PLoS Pathog* **13**, e1006784 (2017).

167.   F. Cortes Ledesma, S. F. El Khamisy, M. C. Zuma, K. Osborn, K. W. Caldecott, A human 5'-tyrosyl DNA phosphodiesterase that repairs topoisomerase-mediated DNA damage. *Nature* **461**, 674-678 (2009).

168.   S. A. Jones, R. Boregowda, T. E. Spratt, J. Hu, In vitro epsilon RNA-dependent protein priming activity of human hepatitis B virus polymerase. *J Virol* **86**, 5134-5150 (2012).

169.   L. Balakrishnan, R. A. Bambara, Flap endonuclease 1. *Annu Rev Biochem* **82**, 119-138 (2013).

170.   P. A. Wing *et al.*, A dual role for SAMHD1 in regulating HBV cccDNA and RT-dependent particle genesis. *Life Sci Alliance* **2**, (2019).

171.   L. Wei, A. Ploss, Core components of DNA lagging strand synthesis machinery are essential for hepatitis B virus cccDNA formation. *Nat Microbiol* **5**, 715-726 (2020).

172.   J. Luo *et al.*, Involvement of Host ATR-CHK1 Pathway in Hepatitis B Virus Covalently Closed Circular DNA Formation. *mBio* **11**, (2020).

173. F. Birnbaum, M. Nassal, Hepatitis B virus nucleocapsid assembly: primary structure requirements in the core protein. *J Virol* **64**, 3319-3330 (1990).
174. A. Gallina *et al.*, A recombinant hepatitis B core antigen polypeptide with the protamine-like domain deleted self-assembles into capsid particles but fails to bind nucleic acids. *J Virol* **63**, 4645-4652 (1989).
175. T. Hatton, S. Zhou, D. N. Standring, RNA- and DNA-binding activities in hepatitis B virus capsid protein: a model for their roles in viral replication. *J Virol* **66**, 5232-5241 (1992).
176. M. Newman, F. M. Suk, M. Cajimat, P. K. Chua, C. Shih, Stability and morphology comparisons of self-assembled virus-like particles from wild-type and mutant human hepatitis B virus capsid proteins. *J Virol* **77**, 12950-12960 (2003).
177. P. T. Wingfield, S. J. Stahl, R. W. Williams, A. C. Steven, Hepatitis core antigen produced in Escherichia coli: subunit composition, conformational analysis, and in vitro capsid assembly. *Biochemistry* **34**, 4919-4932 (1995).
178. A. C. Steven *et al.*, Structure, assembly, and antigenicity of hepatitis B virus capsid proteins. *Adv Virus Res* **64**, 125-164 (2005).
179. P. P. Scaglioni, M. Melegari, J. R. Wands, Posttranscriptional regulation of hepatitis B virus replication by the precore protein. *J Virol* **71**, 345-353 (1997).
180. A. Zlotnick *et al.*, Core protein: A pleiotropic keystone in the HBV lifecycle. *Antiviral Res* **121**, 82-93 (2015).
181. B. Venkatakrishnan, A. Zlotnick, The Structural Biology of Hepatitis B Virus: Form and Function. *Annu Rev Virol* **3**, 429-451 (2016).
182. M. Nassal, The arginine-rich domain of the hepatitis B virus core protein is required for pregenome encapsidation and productive viral positive-strand DNA synthesis but not for virus assembly. *J Virol* **66**, 4107-4116 (1992).
183. S. H. Basagoudanavar, D. H. Perlman, J. Hu, Regulation of hepadnavirus reverse transcription by dynamic nucleocapsid phosphorylation. *J Virol* **81**, 1641-1649 (2007).
184. D. H. Perlman, E. A. Berg, B. O'Connor P, C. E. Costello, J. Hu, Reverse transcription-associated dephosphorylation of hepadnavirus nucleocapsids. *Proc Natl Acad Sci U S A* **102**, 9020-9025 (2005).
185. K. Liu, L. Ludgate, Z. Yuan, J. Hu, Regulation of multiple stages of hepadnavirus replication by the carboxyl-terminal domain of viral core protein in trans. *J Virol* **89**, 2918-2930 (2015).
186. H. J. Schlicht, R. Bartenschlager, H. Schaller, The duck hepatitis B virus core protein contains a highly phosphorylated C terminus that is essential for replication but not for RNA packaging. *J Virol* **63**, 2995-3000 (1989).
187. M. Yu, J. Summers, A domain of the hepadnavirus capsid protein is specifically required for DNA maturation and virus assembly. *J Virol* **65**, 2511-2517 (1991).
188. D. Ponsel, V. Bruss, Mapping of amino acid side chains on the surface of hepatitis B virus capsids required for envelopment and virion formation. *J Virol* **77**, 416-422 (2003).
189. L. Ludgate *et al.*, Cell-Free Hepatitis B Virus Capsid Assembly Dependent on the Core Protein C-Terminal Domain and Regulated by Phosphorylation. *J Virol* **90**, 5830-5844 (2016).
190. E. V. Gazina, J. E. Fielding, B. Lin, D. A. Anderson, Core protein phosphorylation modulates pregenomic RNA encapsidation to different extents in human and duck hepatitis B viruses. *J Virol* **74**, 4721-4728 (2000).
191. M. J. Roossinck, A. Siddiqui, In vivo phosphorylation and protein analysis of hepatitis B virus core antigen. *J Virol* **61**, 955-961 (1987).
192. C. T. Yeh, J. H. Ou, Phosphorylation of hepatitis B virus precore and core proteins. *J Virol* **65**, 2327-2331 (1991).

193.   Y. T. Lan, J. Li, W. Liao, J. Ou, Roles of the three major phosphorylation sites of hepatitis B virus core protein in viral replication. *Virology* **259**, 342-348 (1999).
194.   M. Yu, J. Summers, Multiple functions of capsid protein phosphorylation in duck hepatitis B virus replication. *J Virol* **68**, 4341-4348 (1994).
195.   H. C. Li *et al.*, Nuclear export and import of human hepatitis B virus capsid protein and particles. *PLoS Pathog* **6**, e1001162 (2010).
196.   C. C. Yang, E. Y. Huang, H. C. Li, P. Y. Su, C. Shih, Nuclear export of human hepatitis B virus core protein and pregenomic RNA depends on the cellular NXF1-p15 machinery. *PLoS One* **9**, e106683 (2014).
197.   X. Yu, L. Jin, J. Jih, C. Shih, Z. H. Zhou, 3.5A cryoEM structure of hepatitis B virus core assembled from full-length core protein. *PLoS One* **8**, e69729 (2013).
198.   S. A. Wynne, R. A. Crowther, A. G. Leslie, The crystal structure of the human hepatitis B virus capsid. *Mol Cell* **3**, 771-780 (1999).
199.   B. Bottcher, S. A. Wynne, R. A. Crowther, Determination of the fold of the core protein of hepatitis B virus by electron cryomicroscopy. *Nature* **386**, 88-91 (1997).
200.   J. F. Conway *et al.*, Visualization of a 4-helix bundle in the hepatitis B virus capsid by cryo-electron microscopy. *Nature* **386**, 91-94 (1997).
201.   A. Zlotnick *et al.*, Dimorphism of hepatitis B virus capsids is strongly influenced by the C-terminus of the capsid protein. *Biochemistry* **35**, 7412-7421 (1996).
202.   B. Bottcher, M. Nassal, Structure of Mutant Hepatitis B Core Protein Capsids with Premature Secretion Phenotype. *J Mol Biol* **430**, 4941-4954 (2018).
203.   J. C. Wang, M. S. Dhason, A. Zlotnick, Structural organization of pregenomic RNA and the carboxy-terminal domain of the capsid protein of hepatitis B virus. *PLoS Pathog* **8**, e1002919 (2012).
204.   S. Konig, G. Beterams, M. Nassal, Mapping of homologous interaction sites in the hepatitis B virus core protein. *J Virol* **72**, 4997-5005 (1998).
205.   M. Koschel, R. Thomssen, V. Bruss, Extensive mutagenesis of the hepatitis B virus core gene and mapping of mutations that allow capsid formation. *J Virol* **73**, 2153-2160 (1999).
206.   R. C. Oliver *et al.*, Assembly of Capsids from Hepatitis B Virus Core Protein Progresses through Highly Populated Intermediates in the Presence and Absence of RNA. *ACS Nano* **14**, 10226-10238 (2020).
207.   E. B. Lewellyn, D. D. Loeb, The arginine clusters of the carboxy-terminal domain of the core protein of hepatitis B virus make pleiotropic contributions to genome replication. *J Virol* **85**, 1298-1309 (2011).
208.   T. H. Chu, A. T. Liou, P. Y. Su, H. N. Wu, C. Shih, Nucleic acid chaperone activity associated with the arginine-rich domain of human hepatitis B virus core protein. *J Virol* **88**, 2530-2543 (2014).
209.   M. Newman, P. K. Chua, F. M. Tang, P. Y. Su, C. Shih, Testing an electrostatic interaction hypothesis of hepatitis B virus capsid stability by using an in vitro capsid disassembly/reassembly system. *J Virol* **83**, 10616-10626 (2009).
210.   K. Semrad, Proteins with RNA chaperone activity: a world of diverse proteins with a common task-impediment of RNA misfolding. *Biochem Res Int* **2011**, 532908 (2011).
211.   B. Beames, R. E. Lanford, Carboxy-terminal truncations of the HBV core protein affect capsid formation and the apparent size of encapsidated HBV RNA. *Virology* **194**, 597-607 (1993).
212.   S. Le Pogam, P. K. Chua, M. Newman, C. Shih, Exposure of RNA templates and encapsidation of spliced viral RNA are influenced by the arginine-rich domain of human hepatitis B virus core antigen (HBcAg 165-173). *J Virol* **79**, 1871-1887 (2005).
213.   P. Y. Su *et al.*, HBV maintains electrostatic homeostasis by modulating negative charges from phosphoserine and encapsidated nucleic acids. *Scientific reports* **6**, 38959 (2016).

214. C. K. Chong *et al.*, Role of hepatitis B core protein in HBV transcription and recruitment of histone acetyltransferases to cccDNA minichromosome. *Antiviral Res* **144**, 1-7 (2017).
215. Y. H. Guo, Y. N. Li, J. R. Zhao, J. Zhang, Z. Yan, HBc binds to the CpG islands of HBV cccDNA and promotes an epigenetic permissive state. *Epigenetics* **6**, 720-726 (2011).
216. J. A. Kwon, H. M. Rho, Hepatitis B viral core protein activates the hepatitis B viral enhancer II/pregenomic promoter through the nuclear factor kappaB binding site. *Biochem Cell Biol* **80**, 445-455 (2002).
217. R. E. Lanford, J. S. Butel, Construction and characterization of an SV40 mutant defective in nuclear transport of T antigen. *Cell* **37**, 801-813 (1984).
218. S. Nakielny, G. Dreyfuss, Transport of proteins and RNAs in and out of the nucleus. *Cell* **99**, 677-690 (1999).
219. A. Zlotnick, J. Z. Porterfield, J. C. Wang, To build a virus on a nucleic acid substrate. *Biophys J* **104**, 1595-1604 (2013).
220. H. Mabit, K. M. Breiner, A. Knaust, B. Zachmann-Brand, H. Schaller, Signals for bidirectional nucleocytoplasmic transport in the duck hepatitis B virus capsid protein. *J Virol* **75**, 1968-1977 (2001).
221. K. Weigand, A. Knaust, H. Schaller, Assembly and export determine the intracellular distribution of hepatitis B virus core protein subunits. *J Gen Virol* **91**, 59-67 (2010).
222. C. M. Chu, Y. F. Liaw, Intrahepatic distribution of hepatitis B surface and core antigens in chronic hepatitis B virus infection. Hepatocyte with cytoplasmic/membranous hepatitis B core antigen as a possible target for immune hepatocytolysis. *Gastroenterology* **92**, 220-225 (1987).
223. C. M. Chu, C. T. Yeh, I. S. Sheen, Y. F. Liaw, Subcellular localization of hepatitis B core antigen in relation to hepatocyte regeneration in chronic hepatitis B. *Gastroenterology* **109**, 1926-1932 (1995).
224. H. C. Hsu *et al.*, Biologic and prognostic significance of hepatocyte hepatitis B core antigen expressions in the natural course of chronic hepatitis B virus infection. *J Hepatol* **5**, 45-50 (1987).
225. S. Nair *et al.*, Use of a Fluorescent Analogue of a HBV Core Protein-Directed Drug To Interrogate an Antiviral Mechanism. *J Am Chem Soc* **140**, 15261-15269 (2018).
226. C. T. Yeh, S. W. Wong, Y. K. Fung, J. H. Ou, Cell cycle regulation of nuclear localization of hepatitis B virus core protein. *Proc Natl Acad Sci U S A* **90**, 6459-6463 (1993).
227. F. Pastor *et al.*, Direct interaction between the hepatitis B virus core and envelope proteins analyzed in a cellular context. *Scientific reports* **9**, 16178 (2019).
228. X. Ning *et al.*, Common and Distinct Capsid and Surface Protein Requirements for Secretion of Complete and Genome-Free Hepatitis B Virions. *J Virol* **92**, (2018).
229. A. Pairan, V. Bruss, Functional surfaces of the hepatitis B virus capsid. *J Virol* **83**, 11616-11623 (2009).
230. T. T. Yuan, G. K. Sahu, W. E. Whitehead, R. Greenberg, C. Shih, The mechanism of an immature secretion phenotype of a highly frequent naturally occurring missense mutation at codon 97 of human hepatitis B virus core antigen. *J Virol* **73**, 5731-5740 (1999).
231. L. Selzer, A. Zlotnick, Assembly and Release of Hepatitis B Virus. *Cold Spring Harb Perspect Med* **5**, (2015).
232. Z. Tan, M. L. Maguire, D. D. Loeb, A. Zlotnick, Genetically altering the thermodynamics and kinetics of hepatitis B virus capsid assembly has profound effects on virus replication in cell culture. *J Virol* **87**, 3208-3216 (2013).
233. C. R. Bourne, S. P. Katen, M. R. Fulz, C. Packianathan, A. Zlotnick, A mutant hepatitis B virus core protein mimics inhibitors of icosahedral capsid self-assembly. *Biochemistry* **48**, 1736-1742 (2009).

234. H. Y. Shim, X. Quan, Y. S. Yi, G. Jung, Heat shock protein 90 facilitates formation of the HBV capsid via interacting with the HBV core protein dimers. *Virology* **410**, 161-169 (2011).

235. S. J. Lee, H. Y. Shim, A. Hsieh, J. Y. Min, G. Jung, Hepatitis B virus core interacts with the host cell nucleolar protein, nucleophosmin 1. *J Microbiol* **47**, 746-752 (2009).

236. H. Jeong, M. H. Cho, S. G. Park, G. Jung, Interaction between nucleophosmin and HBV core protein increases HBV capsid assembly. *FEBS Lett* **588**, 851-858 (2014).

237. C. Hartmann-Stuhler, R. Prange, Hepatitis B virus large envelope protein interacts with gamma2-adaptin, a clathrin adaptor-related protein. *J Virol* **75**, 5343-5351 (2001).

238. M. Rost *et al.*, Gamma-adaptin, a novel ubiquitin-interacting adaptor, and Nedd4 ubiquitin ligase control hepatitis B virus maturation. *J Biol Chem* **281**, 29297-29308 (2006).

239. K. P. Lu, X. Z. Zhou, The prolyl isomerase PIN1: a pivotal new twist in phosphorylation signalling and disease. *Nat Rev Mol Cell Biol* **8**, 904-916 (2007).

240. M. Nishi *et al.*, Prolyl Isomerase Pin1 Regulates the Stability of Hepatitis B Virus Core Protein. *Front Cell Dev Biol* **8**, 26 (2020).

241. G. Qian *et al.*, NIRF, a novel ubiquitin ligase, interacts with hepatitis B virus core protein and promotes its degradation. *Biotechnol Lett* **34**, 29-36 (2012).

242. S. Y. Sohn, S. B. Kim, J. Kim, B. Y. Ahn, Negative regulation of hepatitis B virus replication by cellular Hsp40/DnaJ proteins through destabilization of viral core and X proteins. *J Gen Virol* **87**, 1883-1891 (2006).

243. Y. Li *et al.*, Mechanisms and Effects on HBV Replication of the Interaction between HBV Core Protein and Cellular Filamin B. *Virol Sin* **33**, 162-172 (2018).

244. E. C. Hsu *et al.*, Suppression of hepatitis B viral gene expression by protein-tyrosine phosphatase PTPN3. *J Biomed Sci* **14**, 731-744 (2007).

245. M. Genera *et al.*, Molecular basis of the interaction of the human tyrosine phosphatase PTPN3 with the hepatitis B virus core protein. *Scientific reports* **11**, 944 (2021).

246. H. Chabrolles *et al.*, Hepatitis B virus Core protein nuclear interactome identifies SRSF10 as a host RNA-binding protein restricting HBV RNA production. *PLoS Pathog* **16**, e1008593 (2020).

247. Y. Guo *et al.*, Hepatitis B viral core protein disrupts human host gene expression by binding to promoter regions. *BMC Genomics* **13**, 563 (2012).

248. A. Xiang *et al.*, The hepatitis B virus (HBV) core protein enhances the transcription activation of CRE via the CRE/CREB/CBP pathway. *Antiviral Res* **120**, 7-15 (2015).

249. J. Du *et al.*, Hepatitis B virus core protein inhibits TRAIL-induced apoptosis of hepatocytes by blocking DR5 expression. *Cell Death Differ* **16**, 219-229 (2009).

250. Y. L. Chung, T. Y. Tsai, Promyelocytic leukemia nuclear bodies link the DNA damage repair pathway with hepatitis B virus replication: implications for hepatitis B virus exacerbation during chemotherapy and radiotherapy. *Mol Cancer Res* **7**, 1672-1685 (2009).

251. X. Ning *et al.*, Capsid Phosphorylation State and Hepadnavirus Virion Secretion. *J Virol* **91**, (2017).

252. E. B. Lewellyn, D. D. Loeb, Serine phosphoacceptor sites within the core protein of hepatitis B virus contribute to genome replication pleiotropically. *PLoS One* **6**, e17202 (2011).

253. J. Jung *et al.*, Phosphoacceptors threonine 162 and serines 170 and 178 within the carboxyl-terminal RRRS/T motif of the hepatitis B virus core protein make multiple contributions to hepatitis B virus replication. *J Virol* **88**, 8754-8767 (2014).

254. B. Lubyova *et al.*, PRMT5: A novel regulator of Hepatitis B virus replication and an arginine methylase of HBV core. *PLoS One* **12**, e0186982 (2017).

255.   J. Heger-Stevic, P. Zimmermann, L. Lecoq, B. Bottcher, M. Nassal, Hepatitis B virus core protein phosphorylation: Identification of the SRPK1 target sites and impact of their occupancy on RNA binding and capsid structure. *PLoS Pathog* 14, e1007488 (2018).

256.   M. Kann, W. H. Gerlich, Effect of core protein phosphorylation by protein kinase C on encapsidation of RNA within core particles of hepatitis B virus. *J Virol* 68, 7993-8000 (1994).

257.   J. Pugh, A. Zweidler, J. Summers, Characterization of the major duck hepatitis B virus core particle protein. *J Virol* 63, 1371-1376 (1989).

258.   Q. Zhao *et al.*, Hepatitis B Virus Core Protein Dephosphorylation Occurs during Pregenomic RNA Encapsidation. *J Virol* 92, (2018).

259.   H. de Rocquigny *et al.*, Phosphorylation of the Arginine-Rich C-Terminal Domains of the Hepatitis B Virus (HBV) Core Protein as a Fine Regulator of the Interaction between HBc and Nucleic Acid. *Viruses* 12, (2020).

260.   L. Lott, B. Beames, L. Notvall, R. E. Lanford, Interaction between hepatitis B virus core protein and reverse transcriptase. *J Virol* 74, 11479-11489 (2000).

261.   N. Patel *et al.*, HBV RNA pre-genome encodes specific motifs that mediate interactions with the viral core protein that promote nucleocapsid assembly. *Nat Microbiol* 2, 17098 (2017).

262.   A. Diab *et al.*, Polo-like-kinase 1 is a proviral host factor for hepatitis B virus replication. *Hepatology* 66, 1750-1765 (2017).

263.   L. Ludgate *et al.*, Cyclin-dependent kinase 2 phosphorylates s/t-p sites in the hepadnavirus core protein C-terminal domain and is incorporated into viral capsids. *J Virol* 86, 12237-12250 (2012).

264.   H. Daub *et al.*, Identification of SRPK1 and SRPK2 as the major cellular protein kinases phosphorylating hepatitis B virus core protein. *J Virol* 76, 8124-8137 (2002).

265.   L. Wittkop *et al.*, Inhibition of protein kinase C phosphorylation of hepatitis B virus capsids inhibits virion formation and causes intracellular capsid accumulation. *Cell Microbiol* 12, 962-975 (2010).

266.   J. C. Duclos-Vallee, F. Capel, H. Mabit, M. A. Petit, Phosphorylation of the hepatitis B virus core protein by glyceraldehyde-3-phosphate dehydrogenase protein kinase activity. *J Gen Virol* 79 (Pt 7), 1665-1670 (1998).

267.   J. Xi, L. Luckenbaugh, J. Hu, Multiple roles of PP2A binding motif in hepatitis B virus core linker and PP2A in regulating core phosphorylation state and viral replication. *PLoS Pathog* 17, e1009230 (2021).

268.   Z. Hu *et al.*, Protein phosphatase 1 catalyzes HBV core protein dephosphorylation and is co-packaged with viral pregenomic RNA into nucleocapsids. *PLoS Pathog* 16, e1008669 (2020).

269.   M. L. Garcia, R. Byfield, M. D. Robek, Hepatitis B virus replication and release are independent of core lysine ubiquitination. *J Virol* 83, 4923-4933 (2009).

270.   H. Langerova *et al.*, Hepatitis B Core Protein Is Post-Translationally Modified through K29-Linked Ubiquitination. *Cells* 9, (2020).

271.   W. Zhang *et al.*, PRMT5 restricts hepatitis B virus replication through epigenetic repression of covalently closed circular DNA transcription and interference with pregenomic RNA encapsidation. *Hepatology* 66, 398-415 (2017).

272.   J. R. Gareau, C. D. Lima, The SUMO pathway: emerging mechanisms that shape specificity, conjugation and recognition. *Nat Rev Mol Cell Biol* 11, 861-871 (2010).

273.   Z. Hannoun, S. Greenhough, E. Jaffray, R. T. Hay, D. C. Hay, Post-translational modification by SUMO. *Toxicology* 278, 288-293 (2010).

274.   Y. C. Liang *et al.*, SUMO5, a Novel Poly-SUMO Isoform, Regulates PML Nuclear Bodies. *Scientific reports* 6, 26509 (2016).

275. H. Yuan *et al.*, Small ubiquitin-related modifier paralogs are indispensable but functionally redundant during early development of zebrafish. *Cell Res* **20**, 185-196 (2010).

276. M. H. Tatham *et al.*, Polymeric chains of SUMO-2 and SUMO-3 are conjugated to protein substrates by SAE1/SAE2 and Ubc9. *J Biol Chem* **276**, 35368-35374 (2001).

277. K. A. Wilkinson, J. M. Henley, Mechanisms, regulation and consequences of protein SUMOylation. *Biochem J* **428**, 133-145 (2010).

278. K. M. Bohren, V. Nadkarni, J. H. Song, K. H. Gabbay, D. Owerbach, A M55V polymorphism in a novel SUMO gene (SUMO-4) differentially activates heat shock transcription factors and is associated with susceptibility to type I diabetes mellitus. *J Biol Chem* **279**, 27233-27238 (2004).

279. P. Bayer *et al.*, Structure Determination of the Small Ubiquitin-related Modifier SUMO-1. *J Mol Biol* **280**, 275-286 (1998).

280. A. Verger, J. Perdomo, M. Crossley, Modification with SUMO. A role in transcriptional regulation. *EMBO Rep* **4**, 137-142 (2003).

281. G. Gill, SUMO and ubiquitin in the nucleus: different functions, similar mechanisms? *Genes Dev* **18**, 2046-2059 (2004).

282. D. Mukhopadhyay, M. Dasso, Modification in reverse: the SUMO proteases. *Trends Biochem Sci* **32**, 286-295 (2007).

283. R. T. Hay, SUMO: a history of modification. *Mol Cell* **18**, 1-12 (2005).

284. E. Van Damme, K. Laukens, T. H. Dang, X. Van Ostade, A manually curated network of the PML nuclear body interactome reveals an important role for PML-NBs in SUMOylation dynamics. *Int J Biol Sci* **6**, 51-67 (2010).

285. J. M. Desterro, J. Thomson, R. T. Hay, Ubch9 conjugates SUMO but not ubiquitin. *FEBS Lett* **417**, 297-300 (1997).

286. L. Gong, T. Kamitani, K. Fujise, L. S. Caskey, E. T. Yeh, Preferential interaction of sentrin with a ubiquitin-conjugating enzyme, Ubc9. *J Biol Chem* **272**, 28198-28201 (1997).

287. J. Xu *et al.*, A novel method for high accuracy sumoylation site prediction from protein sequences. *BMC Bioinformatics* **9**, 8 (2008).

288. C. B. Gocke, H. Yu, J. Kang, Systematic identification and analysis of mammalian small ubiquitin-like modifier substrates. *J Biol Chem* **280**, 5004-5012 (2005).

289. M. Yang, C. T. Hsu, C. Y. Ting, L. F. Liu, J. Hwang, Assembly of a polymeric chain of SUMO1 on human topoisomerase I in vitro. *J Biol Chem* **281**, 8264-8274 (2006).

290. O. Kerscher, SUMO junction-what's your function? New insights through SUMO-interacting motifs. *EMBO Rep* **8**, 550-555 (2007).

291. A. Minty, X. Dumont, M. Kaghad, D. Caput, Covalent modification of p73alpha by SUMO-1. Two-hybrid screening with p73 identifies novel SUMO-1-interacting proteins and a SUMO-1 interaction motif. *J Biol Chem* **275**, 36316-36323 (2000).

292. X. J. Yang, C. M. Chiang, Sumoylation in gene regulation, human disease, and therapeutic action. *F1000Prime Rep.* **5**, 45 (2013).

293. X. J. Yang, Multisite protein modification and intramolecular signaling. *Oncogene* **24**, 1653-1662 (2005).

294. X. Li *et al.*, SUMOylation of the transcriptional co-repressor KAP1 is regulated by the serine and threonine phosphatase PP1. *Sci Signal* **3**, ra32 (2010).

295. X. Li *et al.*, Role for KAP1 serine 824 phosphorylation and sumoylation/desumoylation switch in regulating KAP1-mediated transcriptional repression. *J Biol Chem* **282**, 36177-36189 (2007).

296. J. A. Tan, J. Song, Y. Chen, L. K. Durrin, Phosphorylation-dependent interaction of SATB1 and PIAS1 directs SUMO-regulated caspase cleavage of SATB1. *Mol Cell Biol* **30**, 2823-2836 (2010).

297. P. Stehmeier, S. Muller, Phospho-regulated SUMO interaction modules connect the SUMO system to CK2 signaling. *Mol Cell* **33**, 400-409 (2009).

298. P. Wimmer *et al.*, Cross-talk between phosphorylation and SUMOylation regulates transforming activities of an adenoviral oncoprotein. *Oncogene* **32**, 1626-1637 (2013).

299. C. Cubenas-Potts, M. J. Matunis, SUMO: a multifaceted modifier of chromatin structure and function. *Dev Cell* **24**, 1-12 (2013).

300. F. Golebiowski *et al.*, System-wide changes to SUMO modifications in response to heat shock. *Sci Signal* **2**, ra24 (2009).

301. T. Makhnevych *et al.*, Global map of SUMO function revealed by protein-protein interaction and genetic networks. *Mol Cell* **33**, 124-135 (2009).

302. R. S. Hilgarth *et al.*, Regulation and function of SUMO modification. *J Biol Chem* **279**, 53899-53902 (2004).

303. S. Muller, A. Ledl, D. Schmidt, SUMO: a regulator of gene expression and genome integrity. *Oncogene* **23**, 1998-2008 (2004).

304. E. S. Johnson, Protein modification by SUMO. *Annu Rev Biochem* **73**, 355-382 (2004).

305. U. Sahin *et al.*, Oxidative stress-induced assembly of PML nuclear bodies controls sumoylation of partner proteins. *J Cell Biol* **204**, 931-945 (2014).

306. U. Sahin, H. de The, V. Lallemand-Breitenbach, PML nuclear bodies: assembly and oxidative stress-sensitive sumoylation. *Nucleus* **5**, 499-507 (2014).

307. H. R. Chang *et al.*, The functional roles of PML nuclear bodies in genome maintenance. *Mutat Res* **809**, 99-107 (2018).

308. S. Osterwald *et al.*, PML induces compaction, TRF2 depletion and DNA damage signaling at telomeres and promotes their alternative lengthening. *J Cell Sci* **128**, 1887-1900 (2015).

309. V. Collin, A. Gravel, B. B. Kaufer, L. Flamand, The Promyelocytic Leukemia Protein facilitates human herpesvirus 6B chromosomal integration, immediate-early 1 protein multiSUMOylation and its localization at telomeres. *PLoS Pathog* **16**, e1008683 (2020).

310. C. Hoischen, S. Monajembashi, K. Weisshart, P. Hemmerich, Multimodal Light Microscopy Approaches to Reveal Structural and Functional Properties of Promyelocytic Leukemia Nuclear Bodies. *Front Oncol* **8**, 125 (2018).

311. A. Corpet *et al.*, PML nuclear bodies and chromatin dynamics: catch me if you can! *Nucleic acids research*, (2020).

312. N. Stuurman *et al.*, A monoclonal antibody recognizing nuclear matrix-associated nuclear bodies. *J Cell Sci* **101 (Pt 4)**, 773-784 (1992).

313. S. Nisole, M. A. Maroui, X. H. Mascle, M. Aubry, M. K. Chelbi-Alix, Differential Roles of PML Isoforms. *Front Oncol* **3**, 125 (2013).

314. J. Y. Chan *et al.*, Cell-cycle regulation of DNA damage-induced expression of the suppressor gene PML. *Biochem Biophys Res Commun* **240**, 640-646 (1997).

315. R. Bernardi, P. P. Pandolfi, Structure, dynamics and functions of promyelocytic leukaemia nuclear bodies. *Nat Rev Mol Cell Biol* **8**, 1006-1016 (2007).

316. M. Hodges, C. Tissot, K. Howe, D. Grimwade, P. S. Freemont, Structure, organization, and dynamics of promyelocytic leukemia protein nuclear bodies. *Am J Hum Genet* **63**, 297-304 (1998).

317. C. A. Ascoli, G. G. Maul, Identification of a novel nuclear domain. *J Cell Biol* **112**, 785-795 (1991).

318. G. Dellaire, D. P. Bazett-Jones, PML nuclear bodies: dynamic sensors of DNA damage and cellular stress. *Bioessays* **26**, 963-977 (2004).

319. H. de The *et al.*, The PML-RAR alpha fusion mRNA generated by the t(15;17) translocation in acute promyelocytic leukemia encodes a functionally altered RAR. *Cell* **66**, 675-684 (1991).

320. A. Kakizuka *et al.*, Chromosomal translocation t(15;17) in human acute promyelocytic leukemia fuses RAR alpha with a novel putative transcription factor, PML. *Cell* **66**, 663-674 (1991).

321. P. P. Pandolfi *et al.*, Structure and origin of the acute promyelocytic leukemia myl/RAR alpha cDNA and characterization of its retinoid-binding and transactivation properties. *Oncogene* **6**, 1285-1292 (1991).

322. P. Salomoni, P. P. Pandolfi, The role of PML in tumor suppression. *Cell* **108**, 165-170 (2002).

323. M. Mazza, P. G. Pelicci, Is PML a Tumor Suppressor? *Front Oncol* **3**, 174 (2013).

324. T. H. Shen, H. K. Lin, P. P. Scaglioni, T. M. Yung, P. P. Pandolfi, The mechanisms of PML-nuclear body formation. *Mol Cell* **24**, 331-339 (2006).

325. Y. A. Rivera-Molina, F. P. Martinez, Q. Tang, Nuclear domain 10 of the viral aspect. *World J Virol* **2**, 110-122 (2013).

326. K. Jensen, C. Shiels, P. S. Freemont, PML protein isoforms and the RBCC/TRIM motif. *Oncogene* **20**, 7223-7233 (2001).

327. M. Fagioli *et al.*, Alternative splicing of PML transcripts predicts coexpression of several carboxy-terminally different protein isoforms. *Oncogene* **7**, 1083-1091 (1992).

328. M. Alcalay *et al.*, Expression pattern of the RAR alpha-PML fusion gene in acute promyelocytic leukemia. *Proc Natl Acad Sci U S A* **89**, 4840-4844 (1992).

329. C. Li, Q. Peng, X. Wan, H. Sun, J. Tang, C-terminal motifs in promyelocytic leukemia protein isoforms critically regulate PML nuclear body formation. *J Cell Sci* **130**, 3496-3506 (2017).

330. H. de The, M. Le Bras, V. Lallemand-Breitenbach, The cell biology of disease: Acute promyelocytic leukemia, arsenic, and PML bodies. *J Cell Biol* **198**, 11-21 (2012).

331. T. Kamitani *et al.*, Identification of three major sentrinization sites in PML. *J Biol Chem* **273**, 26675-26682 (1998).

332. T. Sternsdorf, K. Jensen, H. Will, Evidence for covalent modification of the nuclear dot-associated proteins PML and Sp100 by PIC1/SUMO-1. *J Cell Biol* **139**, 1621-1634 (1997).

333. S. Muller, M. J. Matunis, A. Dejean, Conjugation with the ubiquitin-related modifier SUMO-1 regulates the partitioning of PML within the nucleus. *EMBO J* **17**, 61-70 (1998).

334. M. L. Schmitz, I. Grishina, Regulation of the tumor suppressor PML by sequential post-translational modifications. *Front Oncol* **2**, 204 (2012).

335. P. Brand, T. Lenser, P. Hemmerich, Assembly dynamics of PML nuclear bodies in living cells. *PMC Biophys.* **3**, (2010).

336. L. A. Nguyen *et al.*, Physical and functional link of the leukemia-associated factors AML1 and PML. *Blood* **105**, 292-300 (2005).

337. D. Cuchet-Lourenco, E. Vanni, M. Glass, A. Orr, R. D. Everett, Herpes simplex virus 1 ubiquitin ligase ICP0 interacts with PML isoform I and induces its SUMO-independent degradation. *J Virol* **86**, 11209-11222 (2012).

338. D. Cuchet *et al.*, PML isoforms I and II participate in PML-dependent restriction of HSV-1 replication. *J Cell Sci* **124**, 280-291 (2011).

339. A. Hoppe, S. J. Beech, J. Dimmock, K. N. Leppard, Interaction of the adenovirus type 5 E4 Orf3 protein with promyelocytic leukemia protein isoform II is required for ND10 disruption. *J Virol* **80**, 3042-3049 (2006).

340. K. N. Leppard, E. Emmott, M. S. Cortese, T. Rich, Adenovirus type 5 E4 Orf3 protein targets promyelocytic leukaemia (PML) protein nuclear domains for disruption via a sequence in PML isoform II that is predicted as a protein interaction site by bioinformatic analysis. *J Gen Virol* **90**, 95-104 (2009).

341. J. Berscheminski, P. Groitl, T. Dobner, P. Wimmer, S. Schreiner, The Adenoviral Oncogene E1A-13S Interacts with a Specific Isoform of the Tumor Suppressor PML To Enhance Viral Transcription. *J. Virol* **87**, 965-977 (2013).

342. Z. X. Xu, W. X. Zou, P. Lin, K. S. Chang, A role for PML3 in centrosome duplication and genome stability. *Mol Cell* **17**, 721-732 (2005).

343. Q. Wu *et al.*, PML3 Orchestrates the Nuclear Dynamics and Function of TIP60. *J Biol Chem* **284**, 8747-8759 (2009).

344. V. Fogal *et al.*, Regulation of p53 activity in nuclear bodies by a specific PML isoform. *EMBO J.* **19**, 6185-6195 (2000).

345. R. D. Everett, M. K. Chelbi-Alix, PML and PML nuclear bodies: implications in antiviral defence. *Biochimie* **89**, 819-830 (2007).

346. W. Oh *et al.*, PML-IV functions as a negative regulator of telomerase by interacting with TERT. *J Cell Sci* **122**, 2613-2622 (2009).

347. H. Yoshida *et al.*, PML-retinoic acid receptor alpha inhibits PML IV enhancement of PU.1-induced C/EBPepsilon expression in myeloid differentiation. *Mol Cell Biol* **27**, 5819-5834 (2007).

348. M. Pearson *et al.*, PML regulates p53 acetylation and premature senescence induced by oncogenic Ras. *Nature* **406**, 207-210 (2000).

349. A. Guo *et al.*, The function of PML in p53-dependent apoptosis. *Nat Cell Biol* **2**, 730-736 (2000).

350. O. Bischof *et al.*, Deconstructing PML-induced premature senescence. *EMBO J* **21**, 3358-3369 (2002).

351. M. Buschbeck *et al.*, PML4 induces differentiation by Myc destabilization. *Oncogene* **26**, 3415-3422 (2007).

352. M. A. Maroui, M. Pampin, M. K. Chelbi-Alix, Promyelocytic leukemia isoform IV confers resistance to encephalomyocarditis virus via the sequestration of 3D polymerase in nuclear bodies. *J Virol* **85**, 13164-13173 (2011).

353. M. Reichelt *et al.*, Entrapment of viral capsids in nuclear PML cages is an intrinsic antiviral host defense against varicella-zoster virus. *PLoS Pathog* **7**, e1001266 (2011).

354. D. Blondel, S. Kheddache, X. Lahaye, L. Dianoux, M. K. Chelbi-Alix, Resistance to rabies virus infection conferred by the PMLIV isoform. *J Virol* **84**, 10719-10726 (2010).

355. S. Weidtkamp-Peters *et al.*, Dynamics of component exchange at PML nuclear bodies. *J. Cell Sci.* **121**, 2731-2743 (2008).

356. Y. Geng *et al.*, Contribution of the C-terminal regions of promyelocytic leukemia protein (PML) isoforms II and V to PML nuclear body formation. *J Biol Chem* **287**, 30729-30742 (2012).

357. P. Wimmer *et al.*, PML isoforms IV and V contribute to adenovirus-mediated oncogenic transformation by functionally inhibiting the tumor-suppressor p53. *Oncogene* **35**, 69-82 (2016).

358. M. A. Maroui *et al.*, Requirement of PML SUMO interacting motif for RNF4- or arsenic trioxide-induced degradation of nuclear PML isoforms. *PLoS One* **7**, e44949 (2012).

359. V. Lallemand-Breitenbach, H. de The, PML nuclear bodies. *Cold Spring Harb Perspect Biol* **2**, a000661 (2010).

360. M. J. Matunis, X. D. Zhang, N. A. Ellis, SUMO: the glue that binds. *Dev Cell* **11**, 596-597 (2006).

361. A. Kentsis, R. E. Gordon, K. L. Borden, Control of biochemical reactions through supramolecular RING domain self-assembly. *Proc Natl Acad Sci U S A* **99**, 15404-15409 (2002).

362. R. Bernardi, A. Papa, P. P. Pandolfi, Regulation of apoptosis by PML and the PML-NBs. *Oncogene* **27**, 6299-6312 (2008).

363. E. Krieghoff-Henning, T. G. Hofmann, Role of nuclear bodies in apoptosis signalling. *Biochim Biophys Acta* **1783**, 2185-2194 (2008).

364.	M. C. Geoffroy, M. K. Chelbi-Alix, Role of promyelocytic leukemia protein in host antiviral defense. *J Interferon Cytokine Res* **31**, 145-158 (2011).

365.	A. Rabellino, P. P. Scaglioni, PML Degradation: Multiple Ways to Eliminate PML. *Front Oncol* **3**, 60 (2013).

366.	N. Stuurman *et al.*, The nuclear matrix from cells of different origin. Evidence for a common set of matrix proteins. *J Biol Chem* **265**, 5460-5465 (1990).

367.	A. Varadaraj *et al.*, Evidence for the receipt of DNA damage stimuli by PML nuclear domains. *J Pathol* **211**, 471-480 (2007).

368.	S. O. Boe *et al.*, Promyelocytic leukemia nuclear bodies are predetermined processing sites for damaged DNA. *J Cell Sci* **119**, 3284-3295 (2006).

369.	G. Dellaire *et al.*, Promyelocytic leukemia nuclear bodies behave as DNA damage sensors whose response to DNA double-strand breaks is regulated by NBS1 and the kinases ATM, Chk2, and ATR. *J Cell Biol* **175**, 55-66 (2006).

370.	K. L. Borden, Pondering the promyelocytic leukemia protein (PML) puzzle: possible functions for PML nuclear bodies. *Mol Cell Biol* **22**, 5259-5269 (2002).

371.	A. A. Hyman, C. A. Weber, F. Julicher, Liquid-liquid phase separation in biology. *Annu Rev Cell Dev Biol* **30**, 39-58 (2014).

372.	S. F. Banani *et al.*, Compositional Control of Phase-Separated Cellular Bodies. *Cell* **166**, 651-663 (2016).

373.	Y. Lin, D. S. Protter, M. K. Rosen, R. Parker, Formation and Maturation of Phase-Separated Liquid Droplets by RNA-Binding Proteins. *Mol Cell* **60**, 208-219 (2015).

374.	G. Dellaire, C. H. Eskiw, H. Dehghani, R. W. Ching, D. P. Bazett-Jones, Mitotic accumulations of PML protein contribute to the re-establishment of PML nuclear bodies in G1. *J Cell Sci* **119**, 1034-1042 (2006).

375.	R. D. Everett, P. Lomonte, T. Sternsdorf, R. van Driel, A. Orr, Cell cycle regulation of PML modification and ND10 composition. *J Cell Sci* **112 (Pt 24)**, 4581-4588 (1999).

376.	L. Cappadocia *et al.*, Structural and functional characterization of the phosphorylation-dependent interaction between PML and SUMO1. *Structure* **23**, 126-138 (2015).

377.	C. C. Chang *et al.*, Structural and functional roles of Daxx SIM phosphorylation in SUMO paralog-selective binding and apoptosis modulation. *Mol Cell* **42**, 62-74 (2011).

378.	O. Bischof *et al.*, Regulation and localization of the Bloom syndrome protein in response to DNA damage. *J Cell Biol* **153**, 367-380 (2001).

379.	R. Carbone, M. Pearson, S. Minucci, P. G. Pelicci, PML NBs associate with the hMre11 complex and p53 at sites of irradiation induced DNA damage. *Oncogene* **21**, 1633-1640 (2002).

380.	S. Vilotti *et al.*, The PML nuclear bodies-associated protein TTRAP regulates ribosome biogenesis in nucleolar cavities upon proteasome inhibition. *Cell Death Differ* **19**, 488-500 (2012).

381.	M. Miteva, K. Keusekotten, K. Hofmann, G. J. Praefcke, R. J. Dohmen, Sumoylation as a signal for polyubiquitylation and proteasomal degradation. *Subcell Biochem* **54**, 195-214 (2010).

382.	C. M. Hecker, M. Rabiller, K. Haglund, P. Bayer, I. Dikic, Specification of SUMO1- and SUMO2-interacting motifs. *J Biol Chem* **281**, 16117-16127 (2006).

383.	X. Xu *et al.*, SUMO-1 modification of FEN1 facilitates its interaction with Rad9-Rad1-Hus1 to counteract DNA replication stress. *J Mol Cell Biol* **10**, 460-474 (2018).

384.	Z. Guo *et al.*, Sequential posttranslational modifications program FEN1 degradation during cell-cycle progression. *Mol Cell* **47**, 444-456 (2012).

385.	T. Tammsalu *et al.*, Proteome-wide identification of SUMO2 modification sites. *Sci Signal* **7**, rs2 (2014).

386. N. Selak *et al.*, The Bloom's syndrome helicase (BLM) interacts physically and functionally with p12, the smallest subunit of human DNA polymerase delta. *Nucleic acids research* **36**, 5166-5179 (2008).

387. M. Moreno-Onate, A. M. Herrero-Ruiz, M. Garcia-Dominguez, F. Cortes-Ledesma, J. F. Ruiz, RanBP2-Mediated SUMOylation Promotes Human DNA Polymerase Lambda Nuclear Localization and DNA Repair. *J Mol Biol* **432**, 3965-3979 (2020).

388. P. Rallabhandi *et al.*, Sumoylation of topoisomerase I is involved in its partitioning between nucleoli and nucleoplasm and its clearing from nucleoli in response to camptothecin. *J Biol Chem* **277**, 40020-40026 (2002).

389. M. Agostinho *et al.*, Conjugation of human topoisomerase 2 alpha with small ubiquitin-like modifiers 2/3 in response to topoisomerase inhibitors: cell cycle stage and chromosome domain specificity. *Cancer Res* **68**, 2409-2418 (2008).

390. M. M. Yoshida, Y. Azuma, Mechanisms behind Topoisomerase II SUMOylation in chromosome segregation. *Cell Cycle* **15**, 3151-3152 (2016).

391. F. Impens, L. Radoshevich, P. Cossart, D. Ribet, Mapping of SUMO sites and analysis of SUMOylation changes induced by external stimuli. *Proc Natl Acad Sci U S A* **111**, 12432-12437 (2014).

392. G. Dellaire, R. W. Ching, H. Dehghani, Y. Ren, D. P. Bazett-Jones, The number of PML nuclear bodies increases in early S phase by a fission mechanism. *J Cell Sci* **119**, 1026-1033 (2006).

393. M. M. Kordon *et al.*, PML-like subnuclear bodies, containing XRCC1, juxtaposed to DNA replication-based single-strand breaks. *FASEB J* **33**, 2301-2313 (2019).

394. W. Q. Jiang *et al.*, Induction of alternative lengthening of telomeres-associated PML bodies by p53/p21 requires HP1 proteins. *J Cell Biol* **185**, 797-810 (2009).

395. D. Branzei, F. Vanoli, M. Foiani, SUMOylation regulates Rad18-mediated template switch. *Nature* **456**, 915-920 (2008).

396. E. Papouli *et al.*, Crosstalk between SUMO and ubiquitin on PCNA is mediated by recruitment of the helicase Srs2p. *Mol Cell* **19**, 123-133 (2005).

397. B. Pfander, G. L. Moldovan, M. Sacher, C. Hoege, S. Jentsch, SUMO-modified PCNA recruits Srs2 to prevent recombination during S phase. *Nature* **436**, 428-433 (2005).

398. S. Nagai, N. Davoodi, S. M. Gasser, Nuclear organization in genome stability: SUMO connections. *Cell Res* **21**, 474-485 (2011).

399. H. Zhang *et al.*, Nuclear body phase separation drives telomere clustering in ALT cancer cells. *Mol Biol Cell* **31**, 2048-2056 (2020).

400. H. Gali *et al.*, Role of SUMO modification of human PCNA at stalled replication fork. *Nucleic acids research* **40**, 6049-6059 (2012).

401. M. Li *et al.*, SUMO2 conjugation of PCNA facilitates chromatin remodeling to resolve transcription-replication conflicts. *Nat Commun* **9**, 2706 (2018).

402. M. K. Chelbi-Alix, F. Quignon, L. Pelicano, M. H. Koken, H. de The, Resistance to virus infection conferred by the interferon-induced promyelocytic leukemia protein. *J Virol* **72**, 1043-1051 (1998).

403. T. Regad, M. K. Chelbi-Alix, Role and fate of PML nuclear bodies in response to interferon and viral infections. *Oncogene* **20**, 7274-7286 (2001).

404. N. Tavalai, T. Stamminger, New insights into the role of the subnuclear structure ND10 for viral infection. *Biochim Biophys Acta* **1783**, 2207-2221 (2008).

405. S. Hofmann, M. Stubbe, J. Mai, S. Schreiner, Double-edged role of PML nuclear bodies during human adenovirus infection. *Virus Res* **295**, 198280 (2021).

406. R. D. Everett, DNA viruses and viral proteins that interact with PML nuclear bodies. *Oncogene* **20**, 7266-7273 (2001).

407. J. Choi *et al.*, Association of hepatitis B virus polymerase with promyelocytic leukemia nuclear bodies mediated by the S100 family protein p11. *Biochem Biophys Res Commun* **305**, 1049-1056 (2003).

408.   I. Sengupta, D. Das, S. P. Singh, R. Chakravarty, C. Das, Host transcription factor Speckled 110 kDa (Sp110), a nuclear body protein, is hijacked by hepatitis B virus protein X for viral persistence. *J Biol Chem* **292**, 20379-20393 (2017).

409.   W. H. Wang, L. L. Studach, O. M. Andrisani, Proteins ZNF198 and SUZ12 are down-regulated in hepatitis B virus (HBV) X protein-mediated hepatocyte transformation and in HBV replication. *Hepatology* **53**, 1137-1147 (2011).

410.   C. B. Gocke, H. Yu, ZNF198 stabilizes the LSD1-CoREST-HDAC1 complex on chromatin through its MYM-type zinc fingers. *PLoS One* **3**, e3255 (2008).

411.   R. Villa *et al.*, Role of the polycomb repressive complex 2 in acute promyelocytic leukemia. *Cancer Cell* **11**, 513-525 (2007).

412.   P. Kunapuli, C. S. Kasyapa, S. F. Chin, C. Caldas, J. K. Cowell, ZNF198, a zinc finger protein rearranged in myeloproliferative disease, localizes to the PML nuclear bodies and interacts with SUMO-1 and PML. *Exp Cell Res* **312**, 3739-3751 (2006).

413.   D. Pasini, A. P. Bracken, M. R. Jensen, E. Lazzerini Denchi, K. Helin, Suz12 is essential for mouse development and for EZH2 histone methyltransferase activity. *EMBO J* **23**, 4061-4071 (2004).

414.   C. Niu *et al.*, The Smc5/6 Complex Restricts HBV when Localized to ND10 without Inducing an Innate Immune Response and Is Counteracted by the HBV X Protein Shortly after Infection. *PLoS One* **12**, e0169648 (2017).

415.   J. Cheng *et al.*, Interferon Alpha Induces Multiple Cellular Proteins That Coordinately Suppress Hepadnaviral Covalently Closed Circular DNA Transcription. *J Virol* **94**, (2020).

416.   Y. L. Chung, M. L. Wu, Dual oncogenic and tumor suppressor roles of the promyelocytic leukemia gene in hepatocarcinogenesis associated with hepatitis B virus surface antigen. *Oncotarget* **7**, 28393-28407 (2016).

417.   Y. L. Chung, M. L. Wu, Promyelocytic leukaemia protein links DNA damage response and repair to hepatitis B virus-related hepatocarcinogenesis. *J Pathol* **230**, 377-387 (2013).

418.   F. Madeira *et al.*, The EMBL-EBI search and sequence analysis tools APIs in 2019. *Nucleic acids research*, (2019).

419.   J. Schindelin *et al.*, Fiji: an open-source platform for biological-image analysis. *Nature methods* **9**, 676-682 (2012).

420.   Q. Zhao *et al.*, GPS-SUMO: a tool for the prediction of sumoylation sites and SUMO-interaction motifs. *Nucleic acids research* **42**, W325-330 (2014).

421.   J. Hayer *et al.*, HBVdb: a knowledge database for Hepatitis B Virus. *Nucleic acids research* **41**, D566-570 (2013).

422.   A. Waterhouse *et al.*, SWISS-MODEL: homology modelling of protein structures and complexes. *Nucleic acids research* **46**, W296-W303 (2018).

423.   W. D. Humphrey, A.; Schulten, K., VMD - Visual Molecular Dynamics. *J. Molec. Graphics* **14**, 33-38 (1996).

424.   B. G. Pierce *et al.*, ZDOCK server: interactive docking prediction of protein-protein complexes and symmetric multimers. *Bioinformatics* **30**, 1771-1773 (2014).

425.   D. Hanahan, Studies on transformation of Escherichia coli with plasmids. *Journal of Molecular Biology* **166**, 557-580 (1983).

426.   P. Gripon *et al.*, Infection of a human hepatoma cell line by hepatitis B virus. *Proc Natl Acad Sci U S A* **99**, 15655-15660 (2002).

427.   R. B. DuBridge *et al.*, Analysis of mutation in human cells by using an Epstein-Barr virus shuttle system. *Mol Cell Biol* **7**, 379-387 (1987).

428.   E. Sloan *et al.*, Analysis of the SUMO2 Proteome during HSV-1 Infection. *PLoS pathogens* **11**, e1005059-e1005059 (2015).

429.   R. D. Everett *et al.*, PML contributes to a cellular mechanism of repression of herpes simplex virus type 1 infection that is inactivated by ICP0. *J Virol* **80**, 7995-8005 (2006).

430. W. R. Beyer, M. Westphal, W. Ostertag, D. von Laer, Oncoretrovirus and lentivirus vectors pseudotyped with lymphocytic choriomeningitis virus glycoprotein: generation, concentration, and broad host range. *J Virol* **76**, 1488-1495 (2002).

431. T. Dull *et al.*, A third-generation lentivirus vector with a conditional packaging system. *J Virol* **72**, 8463-8471 (1998).

432. T. Carvalho *et al.*, Targeting of adenovirus E1A and E4-ORF3 proteins to nuclear matrix-associated PML bodies. *J. Cell. Biol.* **131**, 45-56 (1995).

433. L. N. Shen, C. Dong, H. Liu, J. H. Naismith, R. T. Hay, The structure of SENP1-SUMO-2 complex suggests a structural basis for discrimination between SUMO paralogues during processing. *Biochem J* **397**, 279-288 (2006).

434. F. El-Asmi, B. El-Mchichi, M. A. Maroui, L. Dianoux, M. K. Chelbi-Alix, TGF-beta induces PML SUMOylation, degradation and PML nuclear body disruption. *Cytokine* **120**, 264-272 (2019).

435. J. Ren *et al.*, Systematic study of protein sumoylation: Development of a site-specific predictor of SUMOsp 2.0. *Proteomics* **9**, 3409-3412 (2009).

436. D. H. Janssens *et al.*, Automated in situ chromatin profiling efficiently resolves cell types and gene regulatory programs. *Epigenetics Chromatin* **11**, 74 (2018).

437. P. J. Skene, S. Henikoff, An efficient targeted nuclease strategy for high-resolution mapping of DNA binding sites. *Elife* **6**, (2017).

438. I. Fukuda *et al.*, Ginkgolic acid inhibits protein SUMOylation by blocking formation of the E1-SUMO intermediate. *Chem Biol* **16**, 133-140 (2009).

439. T. V. Sekar *et al.*, Molecular Imaging Biosensor Monitors p53 Sumoylation in Cells and Living Mice. *Anal Chem* **88**, 11420-11428 (2016).

440. H. Li *et al.*, Ginkgolic acid suppresses the invasion of HepG2 cells via downregulation of HGF/cMet signaling. *Oncol Rep* **41**, 369-376 (2019).

441. M. Stubbe *et al.*, Viral DNA Binding Protein SUMOylation Promotes PML Nuclear Body Localization Next to Viral Replication Centers. *mBio* **11**, (2020).

442. D. Ganem, H. E. Varmus, The molecular biology of the hepatitis B viruses. *Annu Rev Biochem* **56**, 651-693 (1987).

443. F. V. Chisari, C. Ferrari, Hepatitis B virus immunopathogenesis. *Annu Rev Immunol* **13**, 29-60 (1995).

444. C. Lambert, T. Doring, R. Prange, Hepatitis B virus maturation is sensitive to functional inhibition of ESCRT-III, Vps4, and gamma 2-adaptin. *J Virol* **81**, 9050-9060 (2007).

445. T. Li *et al.*, Human Hepatitis B Virus Core Protein Inhibits IFNalpha-Induced IFITM1 Expression by Interacting with BAF200. *Viruses* **11**, (2019).

446. H. Folz *et al.*, SUMOylation of the nuclear pore complex basket is involved in sensing cellular stresses. *J Cell Sci* **132**, (2019).

447. M. Koschel, D. Oed, T. Gerelsaikhan, R. Thomssen, V. Bruss, Hepatitis B virus core gene mutations which block nucleocapsid envelopment. *J Virol* **74**, 1-7 (2000).

448. A. Chakraborty *et al.*, Synchronised infection identifies early rate-limiting steps in the hepatitis B virus life cycle. *Cell Microbiol* **22**, e13250 (2020).

449. M. A. Maroui *et al.*, Promyelocytic Leukemia Protein (PML) Requirement for Interferon-induced Global Cellular SUMOylation. *Mol Cell Proteomics* **17**, 1196-1208 (2018).

450. Y. Ohsaki *et al.*, PML isoform II plays a critical role in nuclear lipid droplet formation. *J Cell Biol* **212**, 29-38 (2016).

451. A. Jul-Larsen, A. Grudic, R. Bjerkvig, S. O. Boe, Subcellular distribution of nuclear import-defective isoforms of the promyelocytic leukemia protein. *BMC Mol Biol* **11**, 89 (2010).

452. Y. Chen, J. Wright, X. Meng, K. N. Leppard, Promyelocytic Leukemia Protein Isoform II Promotes Transcription Factor Recruitment To Activate Interferon Beta and Interferon-Responsive Gene Expression. *Mol Cell Biol* **35**, 1660-1672 (2015).

453. Y. Liu *et al.*, Interferon-inducible ribonuclease ISG20 inhibits hepatitis B virus replication through directly binding to the epsilon stem-loop structure of viral RNA. *PLoS Pathog* **13**, e1006296 (2017).

454. W. Condemine *et al.*, Characterization of endogenous human promyelocytic leukemia isoforms. *Cancer Res* **66**, 6192-6198 (2006).

455. A. D. Goddard *et al.*, Cloning of the murine homolog of the leukemia-associated PML gene. *Mamm Genome* **6**, 732-737 (1995).

456. L. G. Guidotti, V. Martinez, Y. T. Loh, C. E. Rogler, F. V. Chisari, Hepatitis B virus nucleocapsid particles do not cross the hepatocyte nuclear membrane in transgenic mice. *J Virol* **68**, 5469-5475 (1994).

457. H. Li *et al.*, HBV life cycle is restricted in mouse hepatocytes expressing human NTCP. *Cell Mol Immunol* **11**, 175-183 (2014).

458. M. Suzawa *et al.*, A gene-expression screen identifies a non-toxic sumoylation inhibitor that mimics SUMO-less human LRH-1 in liver. *Elife* **4**, (2015).

459. J. Gerstmeier *et al.*, Ginkgolic Acid is a Multi-Target Inhibitor of Key Enzymes in Pro-Inflammatory Lipid Mediator Biosynthesis. *Front Pharmacol* **10**, 797 (2019).

460. J. S. Schneekloth, Jr., Drug discovery: Controlling protein SUMOylation. *Nat Chem Biol* **13**, 1141-1142 (2017).

461. M. D. Demarque *et al.*, Sumoylation by Ubc9 regulates the stem cell compartment and structure and function of the intestinal epithelium in mice. *Gastroenterology* **140**, 286-296 (2011).

Acknowledgements

Publications and presentations

Publications in peer-reviewed journals

Ai J, Wörmann SM, Görgülü K, Vallespinos M, Zagorac S, Alcala S, Wu N, Kabacaoglu D, Berninger A, Navarro D, Kaya-Aksoy E, Ruess DA, Ciecielski KJ, Kowalska M, Demir EI, Ceyhan GO, Heid I, Braren R, Riemann M, Schreiner S, **Hofmann S**, Kutschke M, Jastroch M, Slotta-Huspenina J, Muckenhuber A, Schlitter AM, Schmid RM, Steiger K, Diakopoulos KN, Lesina M, Sainz B Jr, Algül H.
BCL3 couples cancer stem cell enrichment with pancreatic cancer molecular subtypes
Gastroenterology, doi: 10.1053/j.gastro.2021.03.051 (Impact factor 2020: 17.37)

Hofmann S, Stubbe M, Mai J, Schreiner S.
Double-edged role of PML nuclear bodies during human adenovirus infection.
Virus Research, doi: 10.1016/j.virusres.2020.198280 (Impact factor 2019: 2,93)

Hofmann S, Mai J, Masser S, Groitl P, Herrmann A, Sternsford T, Brack-Werner R, Schreiner S
ATO (Arsenic Trioxide) effects on PML nuclear bodies reveals antiviral intervention capacity
Advanced Science, doi: 10.1002/advs.201902130 (Impact factor 2019: 15.84)

Stubbe M, Mai J, Paulus C, Stubbe HC, Berscheminski J, Karimi M, **Hofmann S**, Weber E, Hadian K, Hay RT, Groitl P, Nevels M, Dobner T, Schreiner S.
HAdV E2A SUMOylation prevents antiviral response promoted by host PML-NB components.
mBio, doi: 10.1128/mBio.00049-20 (Impact factor 2019: 6.50)

Hofmann S, Plank V, Groitl P, Skvorc N, Ko C, Zimmerman P, Bruss V, Stadler D, Rezk S, Nassal M, Protzer U, Schreiner S.
HBV core SUMOylation represents a novel functional switch to promote HBV cccDNA conversion at PML nuclear bodies
Manuscript in preparation

Patents

Hofmann S, Schreiner S

Inhibition of Human Adenovirus (HAdV) and other pathogenic DNA viruses by ATO (Arsenic Trioxide) treatment

Europäische Patentanmeldung Nr. 19 205 530.9

Presentations at international conferences

24.-26.03.2021: 30th Annual Meeting of the Society of Virology

Hofmann S, Plank V, Groitl P, Skvorc N, Ko C, Zimmerman P, Bruss V, Stadler D, Rezk S, Nassal M, Protzer U, Schreiner S.

HBV core protein SUMOylation promotes PML association and productive HBV infection (Presentation)

01.-05.10.2019: 2019 International HBV Meeting

Hofmann S, Plank V, Groitl P, Ko C, Nassal M, Stadler D, Protzer U, Schreiner S

HBV core protein SUMOylation promotes PML association and productive HBV infection (Presentation)

20.-23.03.2019: 29th Annual Meeting of the Society of Virology

Hofmann S, Plank V, Groitl P, Ko C, Nassal M, Stadler D, Protzer U, Schreiner S

HBV core protein SUMOylation promotes PML association and chronic infection (Presentation)

03.-06.10.2018: 2018 International HBV Meeting

Hofmann S; Plank V, Groitl P, Ko C, Nassal M, Protzer U, Schreiner S

HBV core protein SUMOylation and PML association (Poster)

14.-17.03.2018: 28th Annual Meeting of the Society of Virology

Hofmann S, Weiß C, Groitl P, Schreiner S

Generation and phenotypic characterization of novel cloning systems for Human Adenovirus types D26, D48 and B35 (Poster)